“In vitro analysis of the influences of a formaldehyde treatment on neural progenitor cells carrying a heterozygous *BRCA2* mutation in 2D and 3D culture”

„In-vitro Untersuchung der Auswirkungen einer Formaldehydbehandlung auf neuronale Vorläuferzellen mit heterozygoter *BRCA2* Mutation in 2D- und 3D-Kulturen“

Dissertation
Zur Erlangung des Grades
Doktor der Naturwissenschaften

Am Fachbereich Biologie
Der Johannes Gutenberg-Universität Mainz

Ann-Sophie Pabst
geb. am 01.05.1993 in Freising

Mainz, 2026

Dekan: Prof. Dr. Eckhard Thines
1. Berichterstatter: [redacted]
2. Berichterstatter: [redacted]
Tag der mündlichen Prüfung: 11.05.2026

Zusammenfassung

Heterozygote *BRCA2* Mutation wurden bisher primär mit Krebs in Verbindung gebracht, während bekannt ist, dass homozygote *BRCA2* Mutationen zu Fanconi Anämie führen, welche oft mit neurologischen Entwicklungssymptomen einhergeht. *BRCA2* spielt eine Hauptrolle in der homologen Rekombination (HR) und ist essenziell für die Neurogenese zu verschiedenen Zeitpunkten im Zellzyklus. Formaldehyd kann DNA-Doppelstrangbrüche (DSBs) induzieren und BRCA2 durch Haploinsuffizienz direkt hemmen oder abbauen. Darauf basiert die Hypothese, dass Formaldehyd induzierter Stress einen anderen Einfluss auf Zellen mit *BRCA2* Mutation hat als auf wildtypische Zelle.

In der vorliegenden Studie wurden die Auswirkungen einer Formaldehydbehandlung auf neuronale Vorläuferzellen mit *BRCA2* Mutation untersucht, wobei der Schwerpunkt der Experimente auf den Auswirkungen auf die *BRCA1* und *BRCA2* Expression, auf Doppelstrangbrüche, Zellzyklusveränderungen und Zellproliferation lag.

Aus einer Hautstanzen einer *BRCA2* Patientin wurden Fibroblasten isoliert und zu induzierten pluripotenten Stammzellen (iPSCs) reprogrammiert. In Kontroll-iPSCs wurden passende isogene Kontrollen via CRIPSER/Cas9 hergestellt und alle Zelllinien in neuronale Vorläuferzellen (NPCs) differenziert. Zusätzlich wurden 3D-Kulturen, Neurospheres, generiert und untersucht. Fibroblasten, NPCs und Neurospheres wurde anschließend mit Formaldehyd behandelt und analysiert.

Die Ergebnisse zeigten, dass Formaldehyd die BRCA2 Protein- und RNA-Level in beiden Genotypen reduzierte und zu signifikant niedrigeren BRCA2 RNA- und Protein-Leveln in heterozygoten *BRCA2* NPCs führte. Unabhängig vom Genotyp wurde durch die Formaldehydbehandlung die Anzahl der Doppelstrangbrüche in beiden Zelllinien erhöht, während sich die Proliferation verringerte. Außerdem veränderte die Behandlung die Verteilung der Zellen während des Zellzyklus. Formaldehyd führte zu einer Anhäufung von Zellen in der G2-Phase und reduzierte die Proliferationsrate. Im Gegensatz dazu führte die *BRCA2* Mutation dazu, dass mehr Zellen in der S-Phase und weniger in der G1-Phase waren. In 3D Neurospheres, welche aus NPCs mit hoher Passage hergestellt wurden, führten beide Faktoren, Formaldehyd plus *BRCA2* Mutation, zusammen zu einer geringeren Größe, ergo weniger Proliferation.

Diese Ergebnisse zeigen eine spezifische Sensitivität (alter) neuronaler Vorläuferzellen mit *BRCA2* Mutation gegenüber Formaldehyd, was auf einen Zusammenhang zwischen Stress, Formaldehyd und Alterung hindeutet. Die Ergebnisse bilden die Basis für zukünftige Studien zur Aldehydtoxizität, den Auswirkungen des Alterns und dem Einfluss von *BRCA2* (Mutationen) auf die neuronale Entwicklung, mit potenziellen Implikationen für die genetische Beratung von *BRCA2* Patienten.

Abstract

Heterozygous mutations in the *BRCA2* gene have mostly been associated with cancer, while homozygous/compound heterozygous mutations lead to Fanconi Anemia often with neurodevelopmental symptoms. *BRCA2* plays a key role in homologous recombination (HR) throughout the whole cell cycle and is essential for neurogenesis. Since formaldehyde can induce DNA double-strand breaks (DSBs) and directly inhibit or deplete *BRCA2* via haploinsufficiency, formaldehyde-induced stress may differentially affect cells carrying *BRCA2* mutations.

This study investigated the effects of formaldehyde exposure on neuronal cells derived from *BRCA2* mutation carriers, focusing on its effects on *BRCA2* expression, DSBs, and cell proliferation. Patient-derived fibroblasts were reprogrammed into induced pluripotent stem cells (iPSCs), from which isogenic controls via CRISPR/Cas9 were generated, and which were differentiated into neural progenitor cells (NPCs) and neurospheres to compare wildtype and heterozygous *BRCA2* genotypes. Those cells were treated with formaldehyde.

The results showed that formaldehyde reduced BRCA2 protein and RNA levels in both genotypes and led to significantly lower levels of *BRCA2* RNA and protein in heterozygous *BRCA2* NPCs. Furthermore, formaldehyde exposure increased the number of double-strand breaks and decreased proliferation independent of genotype. It moreover, altered cell cycle distribution, inducing G2-phase arrest and reducing proliferation rates. Contrarily, *BRCA2* mutations caused S-phase accumulation and decreased the time spent in the G1-phase. In 3D neurospheres generated from aged NPCs, both factors formaldehyde treatment and *BRCA2* heterozygosity together led to reduced proliferation.

These findings show a specific sensitivity of *BRCA2*-deficient neuronal cells to formaldehyde, indicating a connection between stress, formaldehyde, and ageing. The results provide a fundament for future studies on aldehyde toxicity, implications of aging, and *BRCA2*-related neurogenetic risk, with potential implications for genetic counseling in *BRCA2* mutation carriers.

Table of contents

1 Introduction

1.1 *BRCA2* and its functions/ involvement

1.1.1 The *BRCA2* gene and its involvement in genetic disorders

Breast Cancer Susceptibility Gene 2 (*BRCA2*) is an essential player in maintaining genomic stability and preventing tumorigenesis. It was first described in 1994 by Wooster and colleagues (Wooster et al., 1994) and was found to be located on the long arm of Chromosome 13 (13q12-q13). The coding sequence of *BRCA2* consists of 11,385 base pairs, which translates into a protein of 3,418 amino acids (Tavtigian et al., 1996). The gene is composed of 27 exons, with exon 11 being the longest exon with 1643 amino acids (Andreassen et al., 2021; Tavtigian et al., 1996) and showing some highly conserved sequences. Different types of mutations in the *BRCA2* gene are associated with several genetic disorders.

Heterozygous or monoallelic loss of *BRCA2* has been associated with several types of cancer. It is primarily associated with an increased susceptibility to hereditary breast and ovarian cancer, also known as HBOC. The specific type of cancer can vary based on the mutation site but is not restricted to that specific site. In 1997, Gayther and colleagues idlentified the Ovarian Cancer Cluster Region (OCCR) (Gayther et al., 1997; Neuhausen et al., 1998; Thompson & Easton, 2001) in exon 11 of the gene, which leads to different types of cancers, including ovarian, colorectal, stomach, pancreatic, and prostate cancer, when mutated (Risch et al., 2001). Breast cancer, on the other hand, is suggested to be associated with mutations outside of the OCCR (Risch et al., 2001) and mainly in the breast cancer cluster regions (BCCR) (Hollis et al., 2017). Prostate cancer in males has an increased probability to develop when *BRCA2* is mutated (Edwards et al., 2003; Giusti et al., 2003), especially in the prostate cancer cluster region (PrCCR) (Nyberg et al., 2020). In 2023 even a pancreas cancer cluster region (PcCCR) has been identified in the *BRCA2* gene, which lies outside the OCCR (Chian et al., 2023).

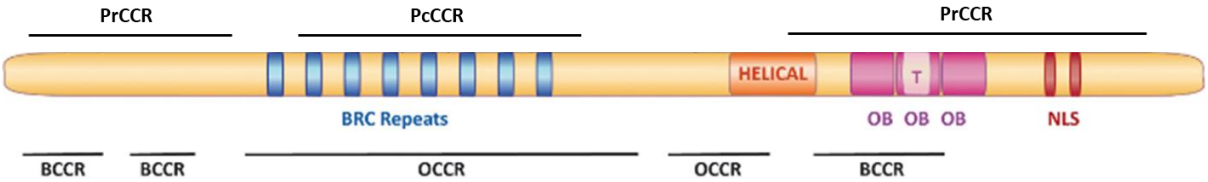

Figure 1 Overview of the cancer cluster regions, modified from (Stella et al., 2022)

However, it is important to note that not all individuals carrying *BRCA2* mutations necessarily will develop cancer during their lifetime. The lifetime risk of developing breast cancer is estimated to be around 45 -85%, while it is only 10-27% for ovarian cancer, depending on the study reporting and their cohort (Breast Cancer Study Group, 2000; Evans et al., 2008; Kurian et al., 2017; Torres et al., 2017). The lifetime risks of being diagnosed with breast or ovarian cancer in individuals not carrying any *BRCA* mutation are 13% and 1.1%, respectively (The website of the National Cancer Institute, 2023).

In 1971 Alfred G. Knudson introduced a hypothesis regarding cancer and its relation to tumor suppressor genes such as *BRCA2*. He postulated that if a tumor suppressor gene is heterozygously mutated,, e.g., due to genetic inheritance, it can still function properly. But if a second hit (somatic event in the second allele) in the same gene leads to homozygous or compound heterozygous mutations and therefore an inactivation of both alleles, it would show a loss of function of the protein. This loss of function would lead to cancer, as the DNA damage could no longer be repaired properly. (Chernoff, 2021; Knudson, 1971). A second hit can come

from various factors. Examples are ionized radiation, epigenetic alterations, or failed DNA replication events (compare 1.5). Until today, there are studies supporting the hypothesis postulated more than 50 years ago (Y.-P. Li et al., 2022).

Homozygous/ compound heterozygous mutations or biallelic loss in the *BRCA2* gene have been associated with Fanconi anemia (Howlett et al., 2002). This disorder, occurring with a frequency of approximately 0.4% in the population (Schroeder et al., 1964), is characterized by a diversity of symptoms that can vary in severeness depending on the position of the mutations within the *BRCA2* gene (Radulovic et al., 2021). The symptoms of Fanconi anemia include anemia, neurodevelopmental delays, skeletal aberrations (Schroeder et al., 1964), café-au-lait spots (Weinberg-Shukron et al., 2018), high rates of leukemia, and specific solid tumors (Alter et al., 2007). Interestingly, microcephaly (Rump et al., 2016; Weinberg-Shukron et al., 2018) and intellectual disability (Rump et al., 2016) have been described as symptoms. Additionally, in 2005, Kennedy and D'Andrea described that cells from patients with Fanconi anemia are hypersensitive to DNA interstrand crosslinking agents (Kennedy & D'Andrea, 2005).

A loss of *BRCA2* causes genome instability due to chromosome breakage (Tutt et al., 1999) and chromosomal abnormalities (Gretarsdottir et al., 1998).

BRCA2-deficient cells display genetic instability (Venkitaraman, 2003), and it has also been seen that haploinsufficiency of *BRCA2*, without complete loss of the wild-type allele, might be enough to increase levels of DNA damage (Karaayvaz-Yildirim et al., 2020).

Most of the mutations in the *BRCA2* gene that have been described are nonsense or frameshift mutations leading to truncated protein products (Connor et al., 1997; Friedman et al., 1997; Tavtigian et al., 1996; Weber, 1996; Wooster et al., 1995), and if there is a nonfunctional *BRCA2* mutant, it cannot translocate into the nucleus (Spain et al., 1999). Many of the mutations in the *BRCA2* gene lead to alternative splicing, especially when occurring at highly conserved domains of the protein ((Acedo et al., 2012; Easton et al., 2007; Fackenthal et al., 2016; Miki et al., 1996; Xiping et al., 2017) and could also end in exon skipping (Caputo et al., 2018; Fackenthal et al., 2002; Pensabene et al., 2009).

Data from mice expands the picture of *BRCA2* and its potential loss. In mice *Brca2* is located on Chromosome 5 and translates into a protein with 3328 amino acids, being 90 amino acids shorter than the human BRCA2 protein. The overall identity between the murine and the human protein is 59% and shows a similarity of 72%, while on a nucleotide level the homology is 74%. (Sharan & Bradley, 1997)

If the *Brca2* gene is heterozygously mutated in mice, the mice show a phenotype resembling the one of the wildtype mice, not showing an increased risk to develop cancer. But when both alleles are mutated and show a loss of function, the mice are strongly affected (Ludwig et al., 1997). Suzuki and colleagues showed in 1997 that mice carrying homozygous mutations in *Brca2* show embryonic lethality before E.8.5 and defective cellular proliferation, even though apoptosis was normal in those mice (Suzuki, De La Pompa, et al., 1997). Hakem and colleagues could confirm those results one year later (Hakem et al., 1998). Mice with a conditional knockout of *Brca2* in the central nervous system (*Brca2*$^{LoxP/LoxP}$*;Nestin-cre*) display microcephaly with neurogenesis defects, particularly in the cerebellar development (Frappart et al., 2007a). Therefore, *Brca2* is essential for normal neurogenesis and the prevention of the generation of medulloblastoma brain tumors, which had been found in *Brca2*$^{Nes\text{-}cre}$*;p53*$^{-/-}$ but not in *p53*$^{-/-}$ mice (Frappart et al., 2007b; Frappart & McKinnon, 2007).

1.1.2 BRCA2 and the cell cycle

BRCA2 has several functions and roles, heavily depending on the cell cycle phase.

The cell cycle in general is a precisely regulated process consisting of G1-, S-, G2-, and M-phases with which the cell regulates its maintenance, growth, and proliferation. In the G1-phase, right after cell division, the cell grows. In S-phase, following G1-phase, the DNA is replicated, while in the upcoming G2-phase, the cell continues to grow and prepares itself for the division, which is happening during mitosis (M-phase). G1-, S-, and G2-phases together form the so-called interphase.

It has been observed that in *BRCA2* heterozygously mutated cells, more cells are in the G2/ M- (Patel et al., 1998a; Warren et al., 2003), and G1-phases (Patel et al., 1998b) compared to wildtype cells. Fridlich and colleagues in 2015 showed that *BRCA2* heterozygous cells, when treated with hydrogen peroxide, accumulate in S-phase, as this compound induces DSB (Fridlich et al., 2015a). This data suggests that cells with a *BRCA2* mutation cannot repair the increased number (due to the hydrogen peroxide) of DSB as efficiently and fast as wildtype cells, which makes them accumulate in S-phase, where DNA repair takes place.

To achieve their proliferative capacity, proliferating neural progenitors have a shortened cell cycle. During the cell cycle of these cells, miRNA-4673 has been shown to silence the transcription of *BRCA2*, relaxing the G1/S cell cycle checkpoint. This leads to an approximately 2.5-fold acceleration of the interphase and amplifies the proliferative capacity. Therefore, a delay in the differentiation of human neural progenitors can be observed (Farahani et al., 2019).

BRCA2 is also responsible for normal cell cycle progression in the cleavage process. A loss of *BRCA2* delays and prevents the cell division, thus extending the cell (Daniels et al., 2004).

Senescence is a cellular state in which proliferation is stopped. It is a mechanism for the cell to stop proliferation, e.g., if too much damage has happened to the cell. Senescence mainly occurs in the G1-phase of the cell cycle, but it can also occur in the G2-phase (Gire & Dulić, 2015). Depletion of BRCA2 has been associated with cellular senescence. (Carlos et al., 2013)

The expression of *BRCA2* is regulated in a cell cycle-dependent manner, peaking at the boundary between G1- and S-phase (Rajan et al., 1996).

Depending on the phase of the cell cycle and the number of chromatids available in each phase, the cell chooses different pathways to repair its double-strand breaks (DSB). Those DSB need to be repaired, as it otherwise leads to genome instability and potential tumorigenesis (Krenning et al., 2019a). How DSBs occur is described in 1.5.

There are two different pathways for the cell to choose from to repair the DSB: the error-free homology-directed repair (HR) and the error-prone non-homologous end joining (NHEJ), which often leads to sequence alterations.

The cell can only do HR if it has a matching DNA sequence, specifically a sister chromatid. Otherwise, it will use NHEJ. (X. Zhao et al., 2017) A sister chromatid is only available after the DNA has been replicated in S-phase. Therefore, HR primarily occurs during late S- and G2-phase (Mao et al., 2008b; Shibata et al., 2011; Wei et al., 2015). Accordingly, HR factors, like *BRCA2* and *RAD51*, are down-regulated by miRNAs during the G1-phase (Choi et al., 2014), which facilitates NHEJ repair of DSB in this phase. Furthermore, *BRCA1* inhibits *BRCA2* during the G1- phase (Orthwein et al., 2015).

In accordance with this inhibition, HR-deficient cells show a stronger sensitivity to DSB-inducing agents in late S/G2-phase compared to G1-phase (Rothkamm et al., 2003). And DSBs can initiate a (reversible) cell cycle arrest in G1- and G2-phases (Krenning et al., 2019a).

NHEJ, on the other hand, is not restricted to the G1-phase but can be used during the whole cell cycle (X. Zhao et al., 2017).

1.1.3 *BRCA2* and homologous recombination

BRCA2 plays a major role in HR during the S-phase of the cell cycle (Xia et al., 2001). The regulation of HR is complex and requires several proteins interacting in a specific manner with each other, with *BRCA2* playing a key role in the orchestration (compare Figure 2).

After a DSB occurs, it is detected by a complex of MRE11, RAD50, and NBS1. Next ATM phosphorylates γH2AX, MDC1, and RNF8, which then trigger the complex formation of BRCA1 with RAP80 and ABRAXAS. After BRCA1 has located to the site of DSB, it forms a big complex with MRE11, RAD50, NBS1 and CtIP to induce the 5'- end resection of the DSB. For the strand inversion, BRCA1 gets phosphorylated by CHK2 and forms a complex with PALB2 and BRCA2. (Sadeghi et al., 2020) BRCA2, as a dimer, interacts with two oppositely oriented sets of RAD51 (Moynahan et al., 2001; Shahid et al., 2014). USP21, PLK, and Cyclin D1 support the formation of the binding of RAD51 to BRCA2, while A-CDK2 via a phosphorylation of Ser3291 in the C-terminus of the BRCA2 inhibits the formation (Esashi et al., 2005; Sadeghi et al., 2020). BRCA2 binds the still monomeric RAD51 through its BRC repeats (Galkin et al., 2005; M. Lee et al., 2004) and facilitates and stabilizes the oligomerization of RAD51 via its C-terminal domain (Ambjørn et al., 2021; Esashi et al., 2005). Once the strand inversion took place, RAD51 is loaded onto the nascent DNA strands, a process again controlled by BRCA2 (Shahid et al., 2014). With the DNA homolog, the DSB can be repaired, and an unwinding of strands can happen. Therefore, a DNA lesion has been repaired in a high-fidelity manner, and genome integrity can be ensured (Thorslund & West, 2007).

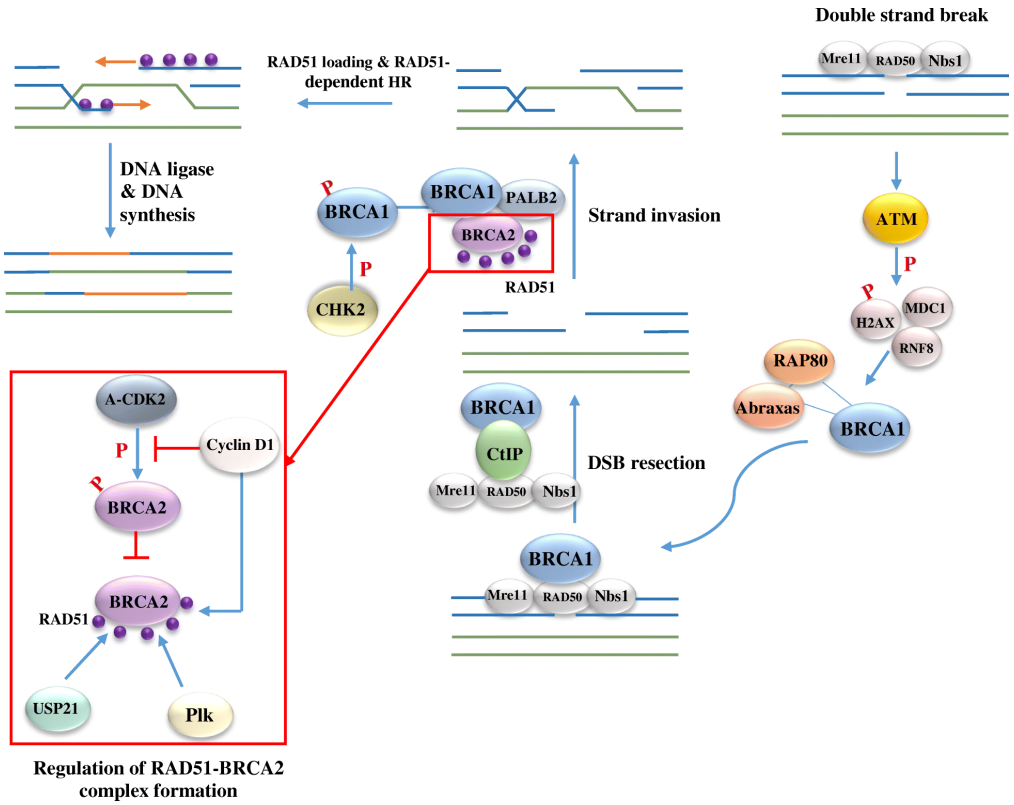

Figure 2 The pathway of HR- directed repair from Sadeghi et al., 2020

Homologous recombination does not only take place during HR but also during the Fanconi anemia pathway, which the cell relies on when an interstrand crosslink (ICL) happens. Also here, BRCA2 is important to resolve the DNA lesion during the homologous recombination (Fradet-Turcotte et al., 2016).

Furthermore, BRCA2 plays an essential role in protecting stalled replication forks. A replication fork is stalled in its progression whenever there is an obstacle in its way. An obstacle can be caused by template damage, slow-moving or paused transcription complexes with covalent protein-DNA complexes, and non-B-form DNA structures, like unrelieved positive superhelical tension (Gupta et al., 2013). Whenever the replication fork is stalled and replication is paused, it is highly vulnerable to collapsing. To ensure that the cell can protect the replication fork, different mechanisms come into play: the single-stranded DNA is protected via RPA, mediated fork reversal is inhibited by RAD51, and nucleolytic fork degradation is suppressed (Liao et al., 2018). As long as the stalled replication fork is protected, fork degradation or reversal does not happen, and the replication fork can recover and restart the DNA replication again.
In this scenario, BRCA2 protects the newly formed, nascent DNA (Lomonosov et al., 2003) from degradation via MRE11 nuclease at stalled replication forks (Schlacher et al., 2011a). It also stabilizes RAD51 nucleoprotein filaments (Liao et al., 2018), preventing fork reversal (Lomonosov et al., 2003). This function of BRCA2 in protecting stalled replication forks is necessary to promote proper DNA synthesis. Furthermore, DSB can happen during the stalling or collapsing of the replication fork. Also here, HR and *BRCA2* come into play for the repair. (Ait Saada et al., 2018)

1.1.4 Other functions of *BRCA2*

Beyond its roles in DNA replication and repair during S-phase, *BRCA2* has been associated with various processes throughout the whole cell cycle (Futamura et al., 2000; Martinez et al., 2015). It has been shown that *BRCA2* has transcriptional activation potential (Milner et al., 1997) in the G1- phase and that it functions in the regulation of R-loop metabolism (Bhatia et al., 2014) in the G1- and S-phases. Additionally, there is the already described HR-repair and the replication fork stabilization in S-phase as well as telomere maintenance in S-phase. G2/M checkpoint maintenance happens at the border of the G2- and M-phases and is mediated via BRCA2 interacting with PALB2 (Menzel et al., 2011; Simhadri et al., 2018). During mitosis, BRCA2 functions as a scaffold protein for proper spindle assembly checkpoint (SAC) activation (Martinez et al., 2015), assuring proper segregation of chromosomes through acetylation of B4BR1. Furthermore, it serves as a scaffold protein in the cytokinetic midbody, ensuring proper cytokinesis (Daniels et al., 2004).
Finally, BRCA2 also plays a fundamental role during meiosis. Due to the interaction with DMC1, it creates genetic variability through reciprocal crossovers, facilitating random combinations of alleles and traits (Thorslund & West, 2007).
Figure 2 gives an overview and summary of the functions of *BRCA2* during the cell cycle.

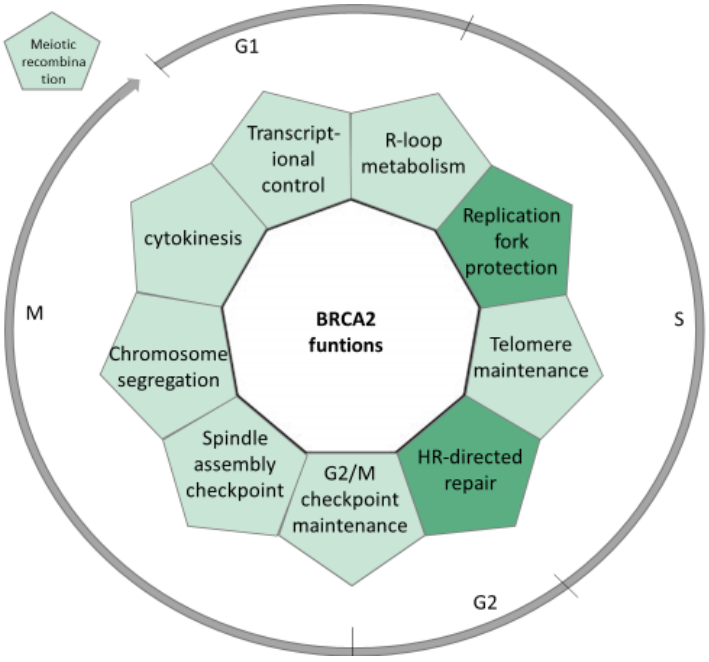

Figure 3 Functions of BRCA2 depending on the cell cycle. The functions of BRCA2 can be grouped together into three main aspects during the cell cycle: replication fork protection, HR-directed repair, and mitotic cell division. Figure relays on Martinez et al., 2015.

On a cellular level, *BRCA2* has a strong influence on the number of cells in specific contexts, as it can influence proliferation and apoptosis. The highest expression of *BRCA2* can be found in rapidly proliferating cells (Chodosh, 1998; Orii et al., 2006; Rajan et al., 1996) as well as during brain development (Petryszak et al., 2016). A link between highly proliferating cells in breast cancer and high *BRCA2* expression has been found (Satyananda et al., 2021). And during the early proliferation phase in embryogenesis, DSBs are repaired by HR to conserve the genetic information. If this cannot happen, embryonic lethality at early stages of development is observed. (Huang et al., 2012)

If cells carry a truncated BRCA2 protein, a proliferation impediment can be observed, which worsens with successive aging /passaging of the cells (Patel et al., 1998a).

On the other hand, *BRCA2* suppresses the proliferation via stabilizing MAGE-D1 and inhibits tumor cell proliferation in vitro and tumor growth in vivo (Tian et al., 2005; S.-C. Wang et al., 2002). In hereditary tumors cell proliferation did not differ significantly between BRCA1- and BRCA2-associated tumors. Furthermore, apoptosis was not different comparing hereditary and sporadic tumors. (Levine et al., 2002). In a study investigating the in vitro and in vivosensitivity of cancer cells towards TRAIL-R-mediated apoptosis, *BRCA2* mutations led to a strongly increased susceptibility (De Toni et al., 2016). Furthermore, it could be observed that a loss of *Brca2* increases the likelihood of a mouse T-lineage cell to show chromosomal aberrations and a deregulation of apoptosis in the absence of p53 (Cheung et al., 2002). Going along with an impairment of the DNA damage repair, *BRCA2* inactivation leads to cell death (Heijink et al., 2019).

1.2 Human neurogenesis

Neurogenesis is the generation of neurons. During neurogenesis progenitor cells proliferate and produce neurons, which migrate, differentiate, and integrate into the existing network (Braun & Jessberger, 2014). Several factors can influence neurogenesis. To those belong external factors, like growth factors and neurotransmitters, as well as internal factors like transcription factors (e.g., *BRCA2*) and epigenetic modulators (DNA/histone modifications) (H. Liu & Song, 2016; Yao et al., 2016).

Neurogenesis occurs during embryonic and early postnatal development and probably also during adulthood (compare later in the text). Several different cell lines emerge during neurogenesis, including neurons, glia cells, and astrocytes. (Mira & Morante, 2020)

A review from Zhang and colleagues from 2023 was the source for the following description of neurogenesis (compare also Figure 4): During the embryonic development neurulation takes place, which is the transformation of the neural plate into the neural tube, where later the brain and the spinal cord develop from. The neural tube consists of three different regions: the prosencephalon, mesencephalon, and rhombencephalon. The prosencephalon is again divided into the diencephalon and telencephalon. In the telencephalon symmetrically dividing neuroepithelia (NE) cells can be found, which form the ventricular zone (VZ). During initiation of neurogenesis initiation NE cells go through distinct morphological, molecular, and mitotic changes, which transform them into apical RG (aRG) cells, also called ventricular radial glia (vRG) cells. Those cells are highly polarized with their cell body in the VZ, while extensions reach into the ventricular and pial surfaces. Those aRGs generate neurons in small amounts but mainly produce basal progenitors (BPs). Those BPs form the subventricular zone (SVZ) and produce neurons. The SVZ is divided into two layers, the inner and the outer SVZ (ISVZ and OSVZ, respectively).

The BPs in the SVZ consist of two types of cells: the outer radial glia (oRG) cells and the basal intermediate progenitors (bIP), both being highly proliferating. oRG cells show both division modes: symmetrically (producing two oRGs) or asymmetrically, producing one daughter oRG cell and either one bIP or one neuron. bIPs divide several times before they produce postmitotic neurons.

Later during the embryogenesis, around gestational week (GW) 17, the vRGs transform into truncated radial glia (tRG) cells via losing contact with the pial surface and continue only with processes contacting the ventricular surface. As, therefore, the migration scaffold for the neurons is lost, the oRGs serve as a new scaffold for migration into the cortical plate (CP).

Next to the VZ at the beginning of the neurogenesis there is also the preplate (PP), which is located between the VZ and the pial surface. This preplate contains different types of early-born neurons, like the predecessor neurons, Cajal-Retzius (CR) cells, and subplate (SP) cells.

After the CP appeares and neurons from the CP migrate into the PP, the PP divides into the marginal zone (SZ) and subplate (SP). This happens around 17-18 GW. The MZ lies above the CP and will eventually form layer I of the mature cortex. The SP is located between the CP and the intermediate zone (IZ) in the developing cortex and is a transient zone. It is moreover, important for axon guidance and the formation of neural circuits.

The neurons generated in the VZ and SVZ migrated radially through the SP into the CP. As neurons are generated sequentially, different layers of the cortex appear. First, deep-layer (DL) neurons are generated, which will build layers 5 and 6. Second, layer 4 neurons are produced. Third, upper-layer (UL) neurons for layers 2 and 3 are mainly produced from oRGs.

As soon as the neurons reach their distinct layer during their migration, they receive a signal to start differentiating, which means extension and elaboration of dendrites and formation of synaptic connections.
Gliogenesis follows the neurogenic period, but both processes happen in parallel for a while. The generation of oligodendrocyte precursor cells (OPCs) and astrocytes from RG cells happens after neurogenesis and continues also postnatally.

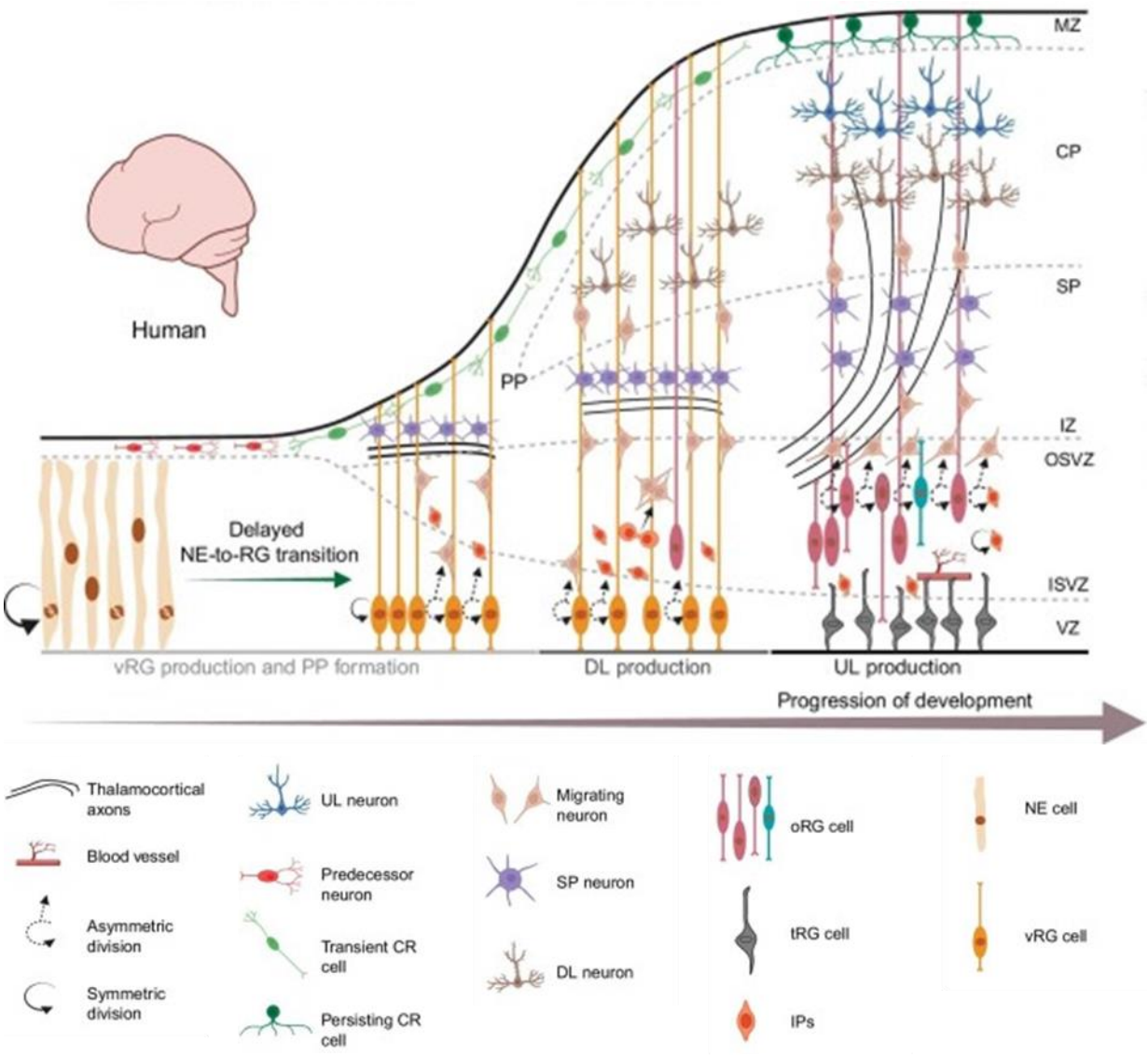

Figure 4 Overview of human neurogenesis in the progression of development from Zhang et al., 2023**.** A description of the process can be found in the text above, the abbreviations are: neuroepithelial (NE) cells, radial glial (RG) cells, ventricular zone (VZ), intermediate progenitors (IPs), outer subventricular zone (OSVZ), inner subventricular zone *(ISVZ)*, outer radial glia (oRG) cell, upper-layer (UL) neuron, ventricular radial glia (vRG) cells, truncated radial glia (tRG), deep-layer (DL), subplate (SP), Cajal-Retzius (CR), intermediate zone*(IZ), cortical plate (*CP*)*, marginal zone *(MZ)*, preplate *(PP)*

If neurogenesis still occurs during adulthood was and, in small parts, still is under discussion. Recent literature states that adult neurogenesis cannot be found in humans (Duque et al., 2021), but only in mice and rats. In humans, hippocampal neurogenesis is almost undetectable after it already drops significantly in childhood (Sorrells et al., 2018). It is also suggested that the methods that are currently used to investigate the question have their limitations and would

need more critical regulations to answer the question (Moreno-Jiménez et al., 2021). The investigation of adult neurogenesis can only be done postmortem and there are systematic limitations. Often information about the living conditions, like drug usage, physical activity, sleep pattern, medication, diet, and potential comorbidities of the donor, which could be an influence on the tissue, is not given. Furthermore, often the regular procedures of storing the brains at brain banks, with formalin and paraffin-embedding or flash-freezing, are different from what would be needed for experiments regarding adult neurogenesis. Moreover, fixation procedure and duration might differ between different brain banks, which makes it harder to reach homogeneity between the samples. And last but not least, it needs special training of the researchers to be able to detect the right brain region, detect falsely negative or positive signals, and distinguish high autofluorescence and nonspecific staining, which characterizes aged human brain tissue, from proper signals. (Moreno-Jiménez et al., 2021)
Some studies, on the other hand, state that neurogenesis also occurs postnatally and throughout adulthood in predominantly two brain regions: the subgranular zone of the hippocampal dentate gyrus and the SVZ lining the lateral ventricles. Those regions are called neurogenic niches. NSCs that can be found in those regions can renew themselves and differentiate into neurons, astrocytes, and oligodendrocytes (Reynolds & Weiss, 1992; Richards et al., 1992). Additionally, recent publications follow this hypothesis, as, for example, Kempermann and colleagues stated in 2018 that there is "no reason to abandon the idea that adult-generated neurons make important functional contributions to neural plasticity and cognition across the human lifespan" (Kempermann et al., 2018). Evidence on how adult neurogenesis takes place has also been studied (Mira & Morante, 2020).
Furthermore, some groups already draw the connection between adult neurogenesis and human brain diseases like Alzheimer's, Parkinson's, Huntington's, and brain tumors (Braun & Jessberger, 2014; H. Liu & Song, 2016; C. Zhao et al., 2008). One study found that adult neural stem/progenitor cells and /or newborn neurons migrate chemokine-guided to the region of brain lesions,, e.g., after a stroke or neurodegenerative diseases like Parkinsons's disease (Braun & Jessberger, 2014; M. Li et al., 2012). Another study saw that in postmortem brains of Huntington's patients, an increased number of proliferating cells in the SVZ correlated with the degree of the disease's severity and the number of CAG repeats. Furthermore, those proliferating cells were expressing the cannabinoid CB1 receptor, which is preferentially lost in HD patients. (H. Liu & Song, 2016)
Regarding Alzheimer's disease, there are some contradicting results in several studies regarding an increase or a decrease in neurogenesis. But commonly it could be shown that microglial activity in postmortem AD brains is increased, pointing towards adult hippocampal neurogenesis. (Gemma & Bachstetter, 2013; H. Liu & Song, 2016)

However, studies on human neurogenesis are limited, but neurogenesis can also be modelled in vitro. iPSCs can be reprogrammed from,, e.g., fibroblasts, and further differentiated into either 2D or 3D structures. If neurogenesis should be investigated in 2D culture, iPSCs can be differentiated into NPCs, which still have the capacity to proliferate and can also further be differentiated into glia cells, astrocytes, or neurons. Those neurons can migrate and mature until they resemble all layers of the cortical brain. (Käseberg, 2023)
Proliferation and migration in neuronal tissues can also be analyzed in 3D culture. A simpler way is to work with neurospheres, 3D structures generated from NPCs. Those can be used for proliferation and migration analysis in a more brain-like structure and a short procedure of a maximum of five days until the first analysis time point. (Zhou et al., 2016)

A more advanced model to study brain-like structures is organoids. Depending on the brain region of interest, different organoids, like forebrain or hindbrain organoids, can be generated. Those models have the benefit that they can be generated in the lab from iPSCs but still resemble important structures of the human brain, like ventricular structures or XX. Additionally, they recapitulate major developmental processes during neurogenesis. They first mimic early neurogenesis with a diverse stem cell pool, later form several types of neurons, and resemble all stratified cortical layers. And afterwards they perform gliogenesis with astrocytes specific for humans. (Yang et al., 2022)
Moreover, they can also model diseases and neurodegenerative disorders and resemble disease-specific phenotypes if genetically modified. And they could be used for drug screening, deciphering environmental from genetic causes for diseases, and the analysis of the influence of specific genes during neurodevelopment. (C. T. Lee et al., 2017; Yang et al., 2022)
Currently there are still several limitations of brain organoid research. One is the growing of brain organoids over a long time period without the development of a necrotic core within the organoids themselves. Another one is the lack of high-fidelity cell types, meaning that not all cell types of the brain,, e.g., vascular cells, immune cells, and other non-neural cells, and the vascular system, usually present in the brain, can be mimicked in the organoids leading to an atypical microenvironment. Additionally, typical regions of the brain, like the hypothalamus, are not present in organoids, so there is a lack of arealization. (Andrews & Kriegstein, 2022; Qian et al., 2019)
Furthermore, brain organoids resemble the embryonic brain in its development, but not the mature brain. Until the organoids reach a point where they are more mature and suitable for some experiments, they cost a lot of resources. Up-speeding processes are currently under investigation. (Qian et al., 2019)
Some studies are already reporting the investigation of interaction between the brain and other tissues like the vascular system (Cakir & Park, 2022), but a very complex system with several different tissues cannot be generated at the moment.

1.3 *BRCA2* and the brain

BRCA2 is required for neurogenesis. In studies with mice, it has been shown that *Brca2* nullizygous mice only survive until E8.5 (Ludwig et al., 1997), and cellular proliferation is impaired in *Brca2* mutants (missing exons 10 and 11 homozygously) in vivo and in vitro (Suzuki, De La Pompa, et al., 1997). Mice with a conditional knockout of *Brca2* in the brain displayed microcephaly, as well as callosal agenesis and hippocampal hypoplasia (Keil et al., 2020).
Brca2 is not only required for normal neurogenesis but also for the prevention of medulloblastoma brain tumors (Frappart et al., 2007b; Frappart & McKinnon, 2007). In 2010, it could be shown that defective DSB repair causes enhanced tumorigenesis and chromosomal instability in *p27*-deficient mice. P27 interacts with Cdk, and Cdk activity can be directly linked to DNA repair and BRCA2 (Ratner et al., 2019; See et al., 2010). CDK mediates the phosphorylation of Ser3291 in the C-terminus of BRCA2 and therefore blocks the interaction between BRCA2 and RAD51. This inhibits RAD51-mediated DNA repair. (Esashi et al., 2005) Compare 1.1.3.
Also, in humans it has been seen that ovarian cancer patients with a heterozygous *BRCA2* mutation have an increased risk of developing brain metastasis compared to patients without a *BRCA2* mutation (Ratner et al., 2019). Furthermore, patients with *BRCA2* mutations seem to

show poorer survival when developing astrocytomas, the most common brain tumor, compared to patients without a BRCA2 mutation. (Sousa et al., 2017, 2020)

1.4 *BRCA2* and neurodevelopmental/ -psychiatric disorders

The brain is constantly working, and during these cellular processes, it is in constant need of energy and oxygen. Oxygen is supplied in the form of reactive oxygen species (ROS) and is produced by mitochondria. ROS is important for normal function of neuronal tissues, as it helps with synaptic plasticity, memory, neuronal differentiation and polarization, axon outgrowth, neurotransmission in mature neurons, and homeostasis in neuronal processes (Biswas et al., 2022; Massaad & Klann, 2011; Oswald et al., 2018). However, ROS can also have detrimental effects. If there is an overproduction of ROS in neuronal mitochondria, it can lead to an increase in surface levels of α-amino-3-hydroxy-5-methyl-4-isoxazolepropionic acid (AMPA) and N-methyl-D-aspartate (NMDA) receptors containing GluA1 and NR2B subunits, which leads to impaired glutamatergic signaling, calcium overload, and excitotoxicity. Due to the alteration in glutamatergic signaling, it contributes to the progression of frontotemporal dementia (Esteras et al., 2022). Increased levels of ROS are also linked to proliferation and lineage specification (Adusumilli et al., 2021). In NPCs, ROS levels are dependent on the NPCs' specific cell state. When NPCs are in quiescence, they show elevated levels of ROS, but as they are active in proliferation and differentiation, lower levels of ROS can be found (Adusumilli et al., 2021).
On a molecular level, ROS leads to DSBs, which need to be repaired,, e.g., by BRCA2 (Fridlich et al., 2015a) and BRCA1 (Gorodetska et al., 2019a). High levels of ROS, especially accumulated in neurons, lead to DNA damage and impaired DNA damage repair.
Impaired DNA damage repair has been associated with neurodegeneration (Madabhushi et al., 2014), (neuro-) psychiatric disorders, and intellectual disability (Raza et al., 2016; Shiwaku & Okazawa, 2015; Suberbielle et al., 2013). A neurodegenerative disorder, which has been connected to accumulated DSBs in neuronal tissues, is Alzheimer's disease (Alt et al., 2017; Alt & Schwer, 2018; Shanbhag et al., 2019).
As already mentioned before, *BRCA2* plays a pivotal role in DNA damage repair. Especially in the brain, it is highly important to sustain genome stability and prevent neurodegeneration (Mckinnon, 2013; McKinnon, 2017). If DNA damage accumulates over time, it can lead to ultimate neuronal loss and has been connected to neural deterioration (Harman, 1981).
Bipolar disorder and autism spectrum disorder (ASD) are two common neuropsychiatric disorders. Both have been associated with mutations in the *BRCA2* gene in computational approaches. In a genome-wide association study (GWAS), SNPs in *BRCA2* and *PALB2* were significantly associated with bipolar disorder, suggesting that altered DNA repair in neuronal tissue might be responsible for the pathophysiology of bipolar disorder (Tesli et al., 2010). Also, in ASD, two *de novo* missense mutations in the *BRCA2* gene have been associated with ASD. ASD patients and their parents had been sequenced to find a potential genetic cause for ASD. *BRCA2* showed two *de novo* mutations (Neale et al., 2012b), indicating a potential connection between *BRCA2* and neuropsychiatric disorders.

1.5 DNA damage

The term "DNA damage" describes any kind of alteration of DNA structure that impairs normal functioning. To the group of DNA damage belong several different types of damages, including single- and double-strand breaks (Galano et al., 2018; Morimoto et al., 2019), adduct formations, ICLs, intrastrand crosslinks or DNA-protein crosslinks, and the loss of a purine or pyrimidine base. Furthermore, alkylation, deamination, methylation, and hydrolysis of bases

are also DNA damages, as well as damage of the sugar/backbone (Ahmad et al., 2015). Also, oxidative damages via ROS belong to this group (Poetsch, 2020). (Chatterjee & Walker, 2017) DNA damage can be induced by a diverse variety of exogenous and endogenous factors. Exogenous sources of DNA damage are external agents and behaviors that can influence DNA. Ionizing radiation (IR), e.g., at medical procedures as well as from sunlight or radioactive elements, can harm DNA. Various further environmental sources (Burgio et al., 2018; Nurul et al., 2019) like smoking, a common habit, have been linked to DNA damage (Yamaguchi, 2019). Furthermore, effects of alcohol abuse on DNA damage have been studied as well (Garaycoechea et al., 2018; Mulderrig et al., 2021). Chronic stress, an overall factor in modern life, can also lead to DNA damage (Flint & Bovbjerg, 2012). And finally, chemical agents, like industrial pollutants, heavy metals, and toxins, as well as anti-cancer chemotherapeutic agents, can pose a significant threat to DNA stability (Pizzino et al., 2017).

Endogenous sources of DNA damage, arising internally within our cells, are equally diverse. Reactive oxygen species (ROS), generated during normal cellular metabolism, can lead to DNA damage (Galano et al., 2018; Morimoto et al., 2019; Pizzino et al., 2017). Failed DNA replication events that can happen almost any time in the cell can introduce errors and damage (Kunkel & Erie, 2015). The juxtaposition of repair events, where repair mechanisms intersect with one another, has also been connected to DNA damage. Furthermore, DNA damage can arise as natural intermediates during V(D)J recombination, a critical process in the development of lymphocytes.

Concluding, several different factors can lead to DNA damage, which has various effects on the cell, its metabolism, and its function (compare Figure 5).

DNA damage can be repaired with several different pathways (compare Figure 5), in the so-called DNA damage response (DDR). Which pathway is chosen by cells depends mostly on the kind of damage and the current cell cycle stage. The main pathways for lesions on the base level are either base excision repair (BER) or mismatch repair (MMR). In BER a damaged base is repaired, which could, if not repaired, lead to mispairing or breaks in replicating DNA. With MMR, a mismatch of two bases can be repaired. Those mismatches appear,, e.g., during replication when a base is accidentally inserted or deleted in a repetitive DNA sequence. Some papers also mention a repair pathway called direct reversal of DNA damage, which works by easily reversing a (e.g., UV-induced) damaged base. (Hakem, 2008)

For multiple damages or bulky base damages, the cell uses the nucleotide excision repair (NER) pathway. NER is chosen when bulky DNA adducts are present either throughout the genome or in actively transcribed genes. Two different sub-pathways are used: global genome NER (G-NER) and transcription-coupled NER (TC-NER), respectively. (Hakem, 2008)

Furthermore, breaks build a group of DNA damage. There are single- and double-strand breaks. Single-strand breaks (SSB) can lead to replication or transcription breakdown and can be repaired via three different sub-pathways: direct SSB, indirect SSB, or TOP1-SSB. DSBs are either repaired by NHEJ or HR, already described in 1.1. In the previous chapter the involvement of BRCA2 in DSB repair has already been described, as well as in replication fork protections, which also play a role when there is a DSB (compare Figure 5). (Chatterjee & Walker, 2017; Hakem, 2008; Tiwari & Wilson, 2019)

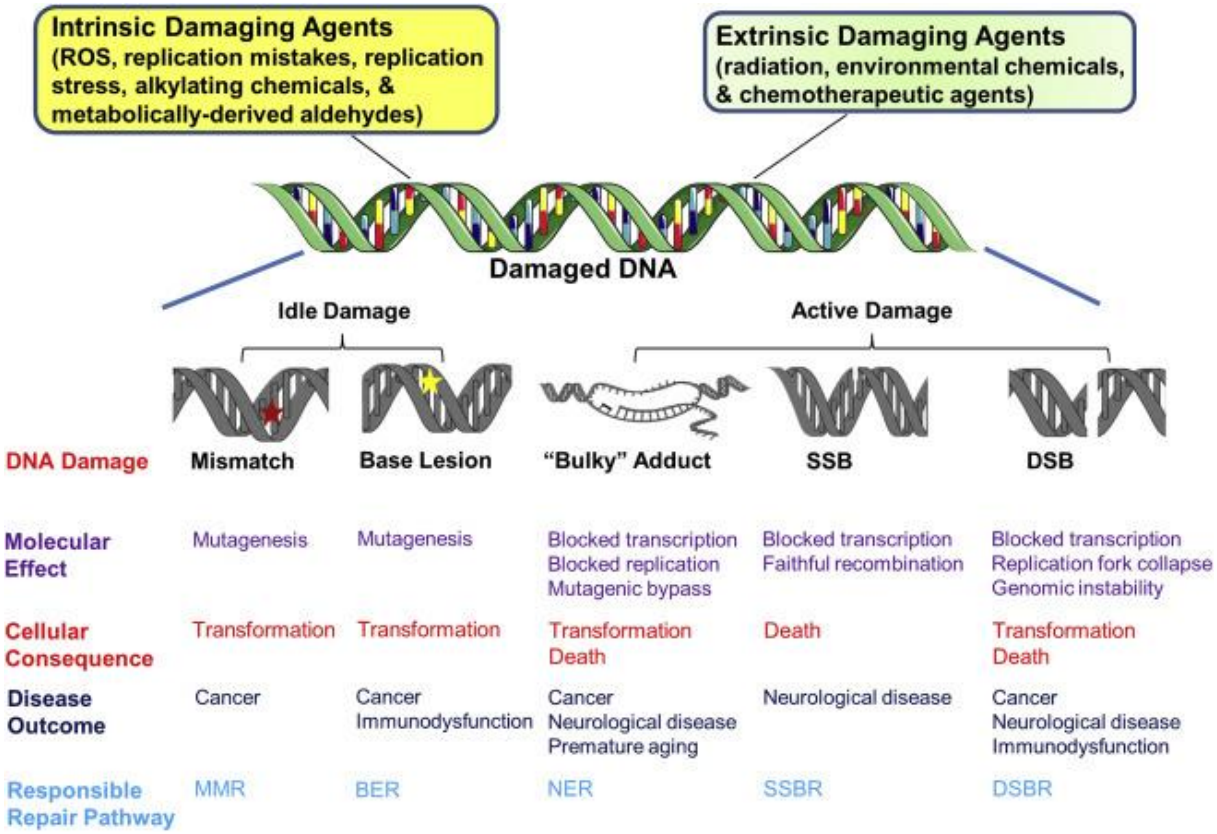

Figure 5 Overview of DNA damage with its causes and consequences from Tiwari & Wilson, 2019. The focus during this work is on DSBs and the involvement of *BRCA2* during DNA repair and replication fork protection. The link between DNA damage and neurological diseases is also displayed in this figure.

There are two more types of repair pathways, which are missing in the figure. Those are DNA crosslinks, either inter-, intra-, or DNA-protein crosslinks and translesion synthesis (TLS) pathway. Crosslinks are always covalent bindings either between two nucleotides on the same strand, between two strands, or between DNA and proteins. Those crosslinks can be resolved by the proteins, inter alia *BRCA2*, of the Fanconi anemia pathway via HR (Fradet-Turcotte et al., 2016). (Chatterjee & Walker, 2017)
With the translesion synthesis (TLS) pathway, the cell can continue its replication even though the DNA is still damaged. It's a tolerance pathway, where low-fidelity polymerases continue the replication in regions of DNA damage and (mis)incorporate some nucleotides. (Chatterjee & Walker, 2017; Vaisman et al., 2012)

1.6 Formaldehyde

Formaldehyde, chemically known as methanal (CH_2O), is a simple but highly reactive aldehyde (Kalapos, 1999). It can ubiquitously be found in the environment as a metabolic product of,, e.g., tobacco smoke, motor vehicles, cosmetics, industrial emissions, and methanol (Bernardini et al., 2020). Formaldehyde can be taken up via ingestion, inhalation, and absorption (Tulpule & Dringen, 2013). Additionally, it is also an endogenous product of cellular metabolism, like histone demethylation, methanol oxidation, and the oxidative deamination of methylamine (Cloos et al., 2008; Kou et al., 2022; O'Sullivan et al., 2004; P. H. Yu et al., 2003). It can be found in every cell type of the human body (Tyihák et al., 1998), and due to its water solubility and reactivity, it can easily diffuse into many organs and tissues (Leng et al., 2019; Q. Liu et al., 2018). Formaldehyde can also accumulate in certain tissues like the brain, which is important in regard to tissue-specific toxicity. Formaldehyde can result from the oxidation of

methanol by catalase and alcohol dehydrogenase 1 (ADH1) via a non-enzymatic reaction of methanol with hydroxyl radicals (Harris et al., 2003; Lees-Murdock & Walsh, 2008; MacAllister et al., 2011). Usually, formaldehyde is further metabolized in cells into formate, which can be fragmented into CO_2 and water (Kalász, 2003; Tyihák et al., 1998), compare Figure 6, or it can be released from the body as a sodium salt in urine (Friedenson, 2011).

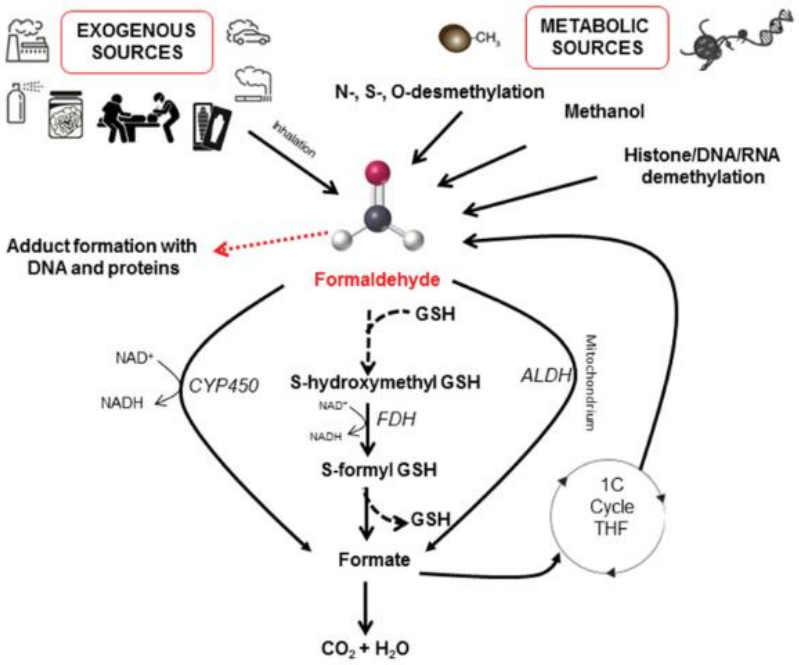

Figure 6 from Bernardini et al., 2020 ***describing the formaldehyde metabolism with its main exogenous and endogenous sources and catabolic reactions in humans***

Formaldehyde acts in a dose-dependent manner. It has been shown that low doses (0.5-0.1mM) of formaldehyde reduce apoptotic activity and enhance cell proliferation, while 1mM leads to an increase in apoptosis and reduced mitotic activity (Mo & He, 2017; Nadalutti et al., 2020). A high dose of 10mM caused necrotic cell death (Szende & Tyihák, 2010), while necrosis also depends on cell density (Mo & He, 2017). Furthermore, the cell cycle is affected by formaldehyde. Low doses suffice to deplete S-phase, so less time is spent in S-phase. Additionally, formaldehyde-treated cells show an arrest in the G2/M phase of the cell cycle, while controls show an undisturbed cell cycle. (Nadalutti et al., 2020; Ortega-Atienza et al., 2015)

Formaldehyde has several influences on the cell and can cause several DNA lesions (Cheng et al., 2003). It can inhibit chromosome assembly (D. Chen et al., 2017) and introduce cross-links. Pontel and colleagues found that formaldehyde can introduce interstrand crosslinks between adjacent purine bases (Chaw et al., 1980), which can be repaired by alcohol dehydrogenase 5 (Pontel et al., 2015). Grafstrom and colleagues furthermore found that there are also crosslinks between DNA and proteins (Grafstrom et al., 1983), DPCs (DNA-protein crosslinks). Those DPCs can cause stalled replication forks and can introduce DSBs. It has been shown that cells from Fanconi anemia patients are hypersensitive to DNA interstrand crosslinking agents, like formaldehyde (Kennedy & D'Andrea, 2005). And it is likely that homologous recombination-deficient cells (e.g., *BRCA2*) are hypersensitive to formaldehyde because of those DPCs (Ridpath et al., 2007).

Formaldehyde can stall the replication fork (Tan et al., 2017) and can induce DSB (Kumari et al., 2012; Tan et al., 2017). Even in mitochondria, formaldehyde can induce DSB (Nadalutti et al., 2020). It can also cause single-strand breaks in DNA, which lead to genomic instability and mutations, and inhibit resealing of single-strand breaks produced by ionizing radiation. (Grafstrom et al., 1983)
Formaldehyde can induce oxidation of specific RNA transcripts, which is often an early process in carcinogenesis analogous to oxidative events in early stages of neurodegenerative diseases (Gonzalez-Rivera et al., 2020a).
Taken together, formaldehyde is an endogenous and exogenous factor that can induce DNA damage via several ways to harm the cell.
In a study in 2018, an RNAi screen for pathways that decrease cellular formaldehyde toxicity was performed. Four inter-related pathways, which are homologous recombination, DSB repair, ionizing radiation response, and DNA replication, were found (Juarez et al., 2018). Ionizing radiation can lead to DSBs, and HR is part of DSB repair; therefore those pathways are related. Furthermore, BRCA2 plays a role in HR and helps to protect DNA replication forks (as already described in 1.1) and is therefore involved in all of the mentioned pathways. It could potentially help to mitigate the effect of formaldehyde, even though *BRCA2* was not explicitly found as a gene to mitigate the effect of formaldehyde.
Finally, adverse effects between formaldehyde and reproduction and development have been detected. Mostly in males a positive association between formaldehyde exposure and reproductive toxicity was found. Potential underlying reasons are DNA damage, oxidative stress, and altered levels and function of enzymes, hormones, and proteins, as well as apoptosis. (Duong et al., 2011) Additionally, during pregnancy, C-14 formaldehyde can cross the placenta through diffusion and enter fetal tissue (Thrasher & Kilburn, 2001), where it can accumulate (Pidoux et al., 2015) and impair the fetal defense against allergic stimuli and infectious agents. (Maiellaro et al., 2014; Silva Ibrahim et al., 2015)

1.7 Formaldehyde in the Brain

Formaldehyde can easily enter the brain through the blood-brain barrier (BBB) (Bernardini et al., 2020) and it has been proposed that formaldehyde is produced locally in the brain, as astrocytes and neurons have the potential to generate and oxidize formaldehyde (Tulpule et al., 2013; Tulpule & Dringen, 2012).
The concentration of formaldehyde in brains of healthy adult humans, mice, and rats has been shown to be 0.2- 0.4mM, while it is around 0.1mM in blood (Heck et al., 1982; Tong et al., 2011a; Tong, Han, Luo, Wang, et al., 2013a). Moderate levels of formaldehyde can be extinguished and metabolized quickly. In vitro even an acute exposure of high concentrations (up to 1mM) of formaldehyde for up to 3h does not lead to severe toxicity in astrocytes or neurons (Tulpule et al., 2013; Tulpule & Dringen, 2012). Brain cells might be able to tolerate acute exposures to formaldehyde due to rapid metabolism of formaldehyde to formate, which is less harmful (Oyama et al., 2002). In humans, high levels of formaldehyde lead to neurotoxicity, where the effect depends on the concentration and duration of formaldehyde exposure (Kilburn, Seidman, et al., 1985; Kilburn, Warshaw, et al., 1985; Songur et al., 2008, 2010). Additionally, neuronal cells are more sensitive to the toxicity of formaldehyde compared to other cell types (Mo & He, 2017).
Formaldehyde is the most important carcinogen in outdoor air pollutants (Zhu et al., 2017), and those are causing factors for neurodevelopmental (like ASD) and neurodegenerative (like Alzheimer) disorders (Costa et al., 2017). Furthermore, an impairment of adult neurogenesis

even due to only an acute exposure to a high concentration (250–300 µg/m^3 for 6 h) of air pollution has been found (Costa et al., 2017).
As formaldehyde at a certain concentration can induce apoptosis in cells, it has been linked to neurodegenerative processes (Szende & Tyihák, 2010).
Formaldehyde has also been linked to cognitive decline in humans (Kilburn et al., 1987; Tong et al., 2011a), and it even has been shown that accumulated aging-associated formaldehyde contributes to cognitive decline during aging in rats (Heck et al., 1982; Tong, Han, Luo, Li, et al., 2013), as well as that "excess endogenous formaldehyde is a critical factor in memory loss in age-related memory-deteriorating diseases" (Tong, Han, Luo, Wang, et al., 2013a). A bioinformatic approach by Rana and colleagues supports the link between formaldehyde and brain diseases and tumors (Rana et al., 2021). Some studies investigating the effect of formaldehyde on the aged brain have also already been published. It has been described that formaldehyde gradually accumulates in brains of mice in their aging process from six to 24 months (Kou et al., 2022; Tong, Han, Luo, Wang, et al., 2013b). And if formaldehyde is injected intraperitoneally or intrahippocampally into healthy rats, it resembles the age-related memory decline in old rats (Tong, Han, Luo, Li, et al., 2013). Excessive formaldehyde in the brain has been shown to lead to cognitive decline via inhibition of NMDA receptors (Kou et al., 2022). In humans, formaldehyde levels in the urine, which are highly elevated among the 70-year-old probands, can be associated with cognitive decline (Tong et al., 2017; J. Yu et al., 2014).
Another study working with a knockout mouse model of the aldehyde dehydrogenase-2 (ALDH2) knockout saw that formaldehyde accumulation due to the knockout of ALDH2 impairs memory. This is consistent with observations of patients with Alzheimer's disease (AD). (Ai et al., 2019) Furthermore, urine levels in AD patients show an increase in formaldehyde, which positively correlates with the degree of dementia observed in those patients (Heck et al., 1982; Tong et al., 2011b).
Finally, it needs to be mentioned that other aldehydes also have an influence on the brain, primarily acetaldehyde through the uptake of alcohol. Acetaldehyde is a metabolic product of ethanol and chemically similar to formaldehyde. Tan and colleagues could show that acetaldehyde has the same effects on heterozygous *BRCA2* cells as formaldehyde (Tan et al., 2017) (compare 1.8).
Moderate intake of alcohol seems to have a neuroprotective effect on the brain via improved vasculature (Kotsopoulos et al., 2021). If alcohol is consumed in high doses during pregnancy, this can lead to fetal alcohol syndrome (FAS) (Nutt et al., 2021). FAS is the most common non-heritable cause for intellectual disability and comes along with prenatal and/or postnatal growth retardation, facial dysmorphology, abnormal brain growth with microcephaly, central nervous system dysfunctions, and neurobehavioral disabilities (Denny et al., 2017; Mattson et al., 2019; Niccols, 2007). The alcohol consumed by the mother reduces the transport of taurine, which is essential for proper developmental neurogenesis (Lui et al., 2014). When rats were exposed to alcohol during their in-utero development, this led to significant changes in neurogenesis and synaptic formation in the adult rats (Singh et al., 2009).

1.8 *BRCA2* and formaldehyde

BRCA2 and formaldehyde have several connection points. Formaldehyde, as already elucidated in 1.6, can induce DNA damage in the form of DSB, ICL, and DPCs. Those types of damage require repair; otherwise, there remains a big threat to the DNA. If mutations persist due to DSB and ICLs, this leads to cancer via genome instability (Hashimoto et al., 2016) or to disturbance of chromatic transactions like replication and transcription if DPC are not resolved (Stingele et

al., 2016; H. Zhang et al., 2020). Homology-directed repair, where *BRCA2* is involved, as well as NER helps to eliminate those damages (Williams et al., 2013; H. Zhang et al., 2020).
Furthermore, within one study it has been shown that there are four pathways that decrease the toxicity of formaldehyde in cells. Those are homologous recombination, DSB repair, ionizing radiation response, and DNA replication (Juarez et al., 2018), and *BRCA2* plays a role in all of those pathways (compare 1.6).
Fifteen years ago, it was also shown that formaldehyde has an adverse effect on mutant chicken DT40 carrying a mutation in the *BRCA2* gene. The cells showed an increase of DPCs induced by formaldehyde. They showed hypersensitivity to formaldehyde going along with a reduced survival under exposure to formaldehyde. (Ridpath et al., 2007) And *BRCA2*-deficient cells, biallelic and heterozygously mutated, are more susceptible to myeloid leukemia, induced by formaldehyde, compared to healthy cells. (Friedenson, 2011)
Furthermore, formaldehyde can stall the replication fork (see 1.6). BRCA2 helps to protect stalled replication forks (compare 1.1.3). Another important factor is that formaldehyde can selectively deplete BRCA2 via proteasomal degradation (Tan et al., 2017). This induces BRCA2 haploinsufficiency. Interestingly, Tan and colleagues could also show that heterozygous *BRCA2* cells have an even increased sensitivity for *BRCA2* haploinsufficiency introduced by formaldehyde. The haploinsufficiency of BRCA2 leads to replication fork stalling and unplanned RNA-DNA hybrids (R-loops), which promote genome instability through MRE-dependent degradation of nascent DNA. They furthermore showed that heterozygous *BRCA2* cells were sensitive to acetaldehyde, another chemical compound of aldehydes. (Tan et al., 2017)
The sensitivity of *BRCA2*-deficient cells to acetaldehyde has also been detected by Tacconi and colleagues and goes along with stalled replication forks and increased DNA damage with G2/M arrest and cell death in those cells (Tacconi et al., 2017).
Until now, it has not been investigated which effect formaldehyde has on neuronal cells carrying a *BRCA2* mutation.

1.9 *BRCA1* in the story

Breast cancer susceptibility gene 1 (BRCA1) is located on the long arm of chromosome 17 at q.21.31 and is translated into a protein with 1,863 amino acids and around 210kDa. Eight different isoforms are known. Like *BRCA2*, *BRCA1* is a tumor suppressor gene and has several different functions. In all its functions and different roles, *BRCA1* very often closely accompanies *BRCA2*. Both expression patterns are strikingly similar (Connor et al., 1997); their spatial and temporal expression patterns are virtually indistinguishable during embryonic development (Chodosh, 1998), and both have been found to be expressed in proliferating cells in mice (Blackshear et al., 1998). They are often regulated (Rajan et al., 1996), colocalizing (Garcia-Higuera et al., 2001), and functioning together, as both play a role in HR-directed repair. DSBs can also occur during a replication fork stalling or collapsing and could be repaired by HR, where *BRCA1* is involved. (Ait Saada et al., 2018; Noordermeer & van Attikum, 2019). Different than *BRCA2*, *BRCA1* is additionally involved in NHEJ.
BRCA1 was shown to be essential for cell proliferation during embryogenesis, as a full knockout of *BRCA1* is lethal (Hakem et al., 1998), while embryos carrying a heterozygous conditional knockout of *BRCA1* develop normally (Shapiro et al., 2016).
In 2009, it has been shown that *BRCA1* is necessary for the development of the mouse cerebral cortex. *BRCA1* could prevent apoptosis in early neural progenitors and therefore ensure normal brain size during embryonic neurogenesis. (Pulvers & Huttner, 2009). Further studies also

revealed the involvement of *BRCA1* in brain development. (Pao et al., 2014). Further, it has been shown that the transplantation of overexpressed *BRCA1* into an ischemic stroke in NSCs facilitates functional recovery and cell survival after transplantation (Xu et al., 2019). Patients carrying a BRCA1 germline mutation show an increased risk of developing brain metastasis from breast cancer compared to patients without a BRCA1 mutation.
A depletion of *BRCA1*, implying reduced DNA repair capabilities, has been associated with the neurological disorder Alzheimer's Disease (Wezyk et al., 2018) via increased DNA double-strand breaks, neuronal shrinkage, and synaptic plasticity impairments. This led to learning and memory deficits. (Suberbielle et al., 2015) Furthermore, an upregulation of *BRCA1* in postmortem AD brains could be found, going along with a hypomethylation of the gene. Those effects could also be found in AD mice (Mano et al., 2017). (Wezyk & Zekanowski, 2018)
And widening the picture, BRCA1 with its cytosolic mislocalization could be associated with the pathogenesis of several tauopathies, not only AD (Nakamura et al., 2020).

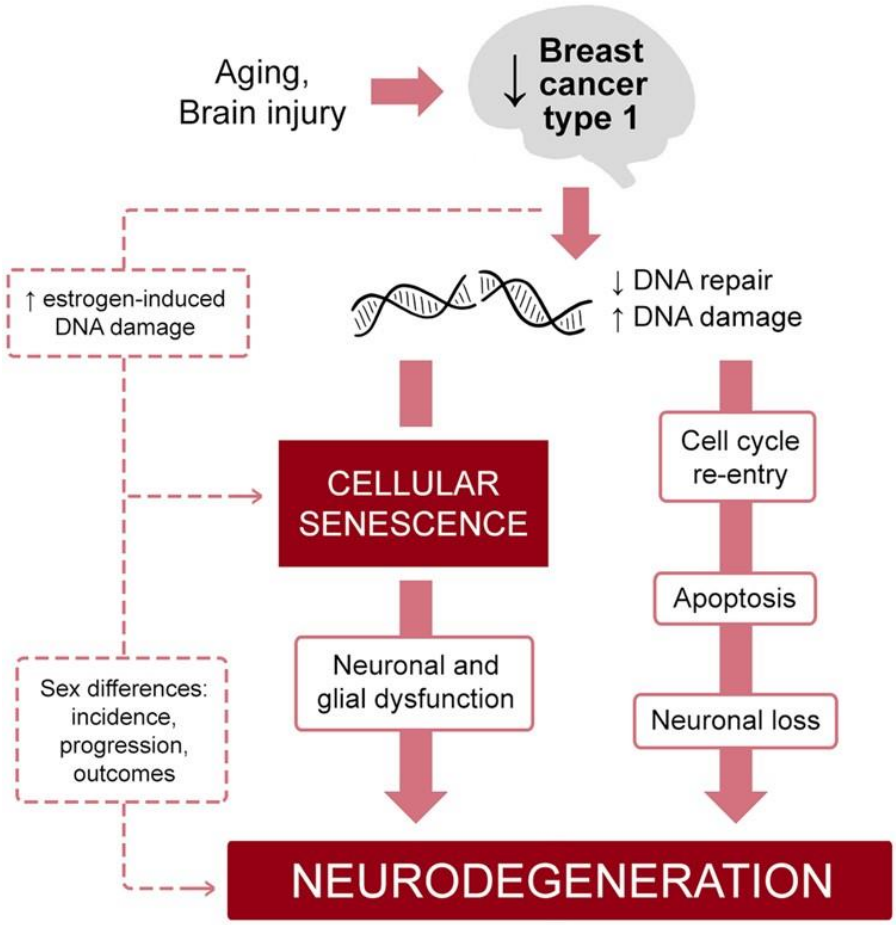

Figure 7 LEUNG 2021 shows the involvement of BRCA1 in neurodegeneration primarily via cellular senescence. BRCA1 is one example of DNA repair genes and a depletion of *BRCA2* has also already been associated with senescence (Carlos et al., 2013).

An association between formaldehyde and *BRCA1* has also already been investigated. Tan and colleagues determined whether formaldehyde also depletes BRCA1 and leads to a haploinsufficiency, as it does with *BRCA2* (compare 1.8). But cells carrying a *BRCA1* mutation were not affected by formaldehyde. (Tan et al., 2017) Those results, also already elucidated in 1.8, are supported by another study from 2017, only finding a relation between acetaldehyde-induced effects and *BRCA2* deletion, but not *BRCA1*-deficient cells (Tacconi et al., 2017).

Interestingly, ethanol, the metabolic precursor of acetaldehyde, induced an ROS-mediated depletion of *BRCA1* (Drake & Wells, 2021). And when mice carrying a heterozygous conditional knockout of *BRCA1* are treated with ethanoln they show more oxidatively damaged DNA and embryopathies compared to wildtype littermates (Shapiro et al., 2016).

1.10 Diagnostics: 3 out of a cohort of 161 patients with developmental disorders carry a *BRCA2* mutation

In the diagnostics of the human genetics department in Mainz, 161 patients presented with developmental delay, mild to moderate intellectual disability, or behavioral anomalies. To find a genetic cause for their disease, the exomes of those 161 patients were sequenced by NGS. Surprisingly, three out of those 161 patients carried heterozygous *BRCA2* mutations that were predicted to be pathogenic. All three presented with learning difficulties as well as behavioral abnormalities, and none had a family history of *BRCA2*-associated cancer. Those heterozygous mutations are predicted to lead to a loss of function of *BRCA2*. Three out of 161 is 1.8%, which is significantly higher (one-sample t-test, $p<0.0001$) than the population frequency of *BRCA2* mutations of max. 0.51% (depending on population) (Maxwell et al., 2016). Interestingly, those 3 patients presented with unfavorable social backgrounds, including substantial stress exposure during pregnancy.

From one of the three patients, it was possible to receive a skin biopsy, which could be used for this project. The heterozygous mutation of this patient was an insertion of an adenine at position 4631 in exon 11 of the BRCA2 gene (c.4631delA).

At the time point of skin biopsy, the female patient was nine years old and presented with a severe delay in speech development, mild intellectual disability, attention deficit disorder, and memory problems. Furthermore, she had an impaired visuomotor integration. She did not show any aggression, nor were her social features impaired.

2 Aim of the study

Until now, heterozygous mutations in the *BRCA2* gene have mostly been associated with cancer, while homozygous/compound heterozygous mutations lead to Fanconi Anemia with symptoms like microcephaly, neurodevelopmental delay, and intellectual disability. *BRCA2* usually functions throughout the whole cell cycle, is very important for proliferating cells, and also affects the cell cycle itself. In the brain, *BRCA2* is essential for neurogenesis and has already been associated with neurodevelopmental disorders, like ASD and bipolar disorder.
BRCA2 also plays a major role in HR-directed repair and replication fork protection. Therefore, *BRCA2* is heavily involved in the repair of DNA damage induced by various external and internal stressors. One of those stressors is formaldehyde, which can lead to DSBs and stop replication forks. Furthermore, formaldehyde has a direct effect on BRCA2 by inhibiting BRCA2 as well as selectively depleting BRCA2, which leads to haploinsufficiency. Additionally, heterozygously mutated *BRCA2* cell lines are even more sensitive to formaldehyde.
In the diagnostics of the human genetics department, it has been found that three out of a cohort of 161 patients with developmental disorders carry a *BRCA2* mutation leading to a loss of function of protein. In at least one of those patients, external stress during pregnancy has been attested.
Taken all those facts together, the hypothesis of this study is that proliferating, neuronal, heterozygous *BRCA2* cells are more sensitive to a formaldehyde treatment compared to wildtype cells.

In order to prove the hypothesis, the first aim of this study was to generate and characterize necessary cell lines. Those were fibroblasts from male and female wildtype cells as well as cells isolated from a patient's skin biopsy. The patients' fibroblasts were reprogrammed into iPSCs, and the wildtype iPSCs were genome-edited via CRISPR/Cas9 to generate isogenic controls. Those cell lines were further differentiated into NPCs and neurospheres to generate neuronal 2D and 3D models, respectively.
An important factor in the characterization of the cell lines was the analysis of RNA and protein levels of BRCA2 and BRCA1 in all cell lines to find out if *BRCA2* is differentially expressed between wildtype and heterozygously mutated *BRCA2* cells.
In order to see if BRCA2 RNA and protein levels change due to a formaldehyde treatment and if BRCA2 gets depleted by formaldehyde, the next aim was the establishment of a proper formaldehyde concentration to treat the cells with. This was first established and tested in fibroblasts and subsequently transferred to NPCs. After potential alterations in RNA and protein levels due to treatment were analyzed, further effects were examined.
The third aim of the study was to investigate molecular effects of formaldehyde. Two effects were analyzed: the amount of DSBs after formaldehyde treatment and alteration in cell cycle. DSBs were analyzed to see if formaldehyde induces DSBs in treated cells, as it has already been described before. And to see if there is a difference in the amount of DSBs in *BRCA2*-mutated cell lines compared to wildtype, as the protein amount is reduced by half due to the mutation. The cell cycle was analyzed to see if it is altered due to formaldehyde and if *BRCA2*-mutated cells would be affected differently. The cell cycle was of interest, as it has already been shown that there are more cells in G2/M-phase in *BRCA2* mutation cell lines and that cells get arrested in G2/M-phase due to a formaldehyde treatment.
As a last aim, cellular effects in 2D and 3D were analyzed, focusing on proliferation and migration to see if the molecular alterations lead to any cellular changes.

3 Material and Methods

3.1 Material

3.1.1 Equipment and software

Table 1 Overview of equipment used in this work. Standard laboratory equipment (e.g. centrifuges, PCR cycler) is not included.

Name	Manufacturer	Model
4D-Nucleofector	Lonza	AAF-1002B + AAF-1002X
Trans-Blot Turbo Transfer System	Bio-Rad	# 1704150
Fusion FX	Vilber	Fusion FX
Nanodrop™ One^{C} Spectrophotometer	Thermo Fisher Scientific	ND-ONEC-W
Revolve Microscope	Echo	Revolve
StepOnePlus™ System	Thermo Fisher Scientific	4376600

Table 2 Overview of software used in this work

Name	Manufacturer
BioEdit	mBio
Crispr.mit.edu	Zhang Lab
Fiji	ImageJ
FlowJo v.10.9.0	BD Biosciences
Fusion FX	Vilber
Leica Application Suite X	Leica Microsystems
Office	Microsoft
Primer3	GitHub
Prism	GraphPad

3.1.2 Chemicals and cell culture media and supplements

Table 3 Overview of chemicals used in this work

Name	Manufacturer
Acrylamide	Carl Roth
Agar	Carl Roth
Agarose	AppliChem
Ampicillin	AppliChem
APS	Sigma
Aqua-Poly/Mount	Tebu Bio
Boric acid	Carl Roth
Bromophenol blue	Carl Roth
BSA	Carl Roth
$CaCl_2$	Carl Roth
EDTA	AppliChem
Ethidium bromide	Carl Roth
Fluoromount-G, withDAPI	eBioscience

Name	Manufacturer
Formaldehyde	Thermo Scientific™
Glycerin	Carl Roth
Glycine	Carl Roth
HEPES	Carl Roth
Isopropanol	Carl Roth
Kanamycin	AppliChem
Milk powder	Carl Roth
Na_2HPO_4	Carl Roth
NaCl	Carl Roth
NaOH	Carl Roth
PFA	Carl Roth
PhosStop	Roche
Protease inhibitor	Roche
Proteinase K	AppliChem
SDS	Carl Roth
Sodium bicarbonate	Sigma
TEMED	Invitrogen
Tris	Carl Roth
Triton X 100	Carl Roth
Tryptone	Carl Roth
Tween20	Carl Roth
Urea	Carl Roth
Yeast extract	Carl Roth
β-mercaptoethanol	Carl Roth

Table 4 Overview of cell culture media and supplements used in this work. Certain compositions are given in the methods part.

Name	Manufacturer	Ordering Number
Accutase	Thermo Fisher Scientific	A1110501
Advanced DMEM	Gibco Life Technologies	12634
B27+ VitA-supplement	Gibco Life Technologies	17504001
B27-supplement	Gibco Life Technologies	12587010
bFGF	Gibco Life Technologies	PHG0264
CloneR™ 10X Cloning Supplement	Stemcell Technologies	5889
DMEM	Gibco Life Technologies	41966-029
DMEM with GlutaMAX™	Gibco Life Technologies	10569-010
DMEM/F-12	Gibco Life Technologies	11320033
DMEM/F-12 GlutaMAX™	Gibco Life Technologies	31331-028
DMSO	Carl Roth	175223617
DPBS	Gibco Life Technologies	14190-169
ESC-qualified FBS	Gibco Life Technologies	16141-079
FBS	Gibco Life Technologies	10270-106

Name	Manufacturer	Ordering Number
FGF	Stemgent	130095863
Gelatin	Sigma	61393-100ML
Geltrex	Gibco Life Technologies	A1413301
GlutaMax™	Life Technologies	35050-038
HBSS	Sigma	H6648-1l
Heparin	Biogen Scientifica	13256029
IMDM	Gibco Life Technologies	12440-053
Insulin	Sigma	I9278-5ml
KOSR	Gibco Life Technologies	10828-028
Laminin	Sigma	L2020-1mg
Matrigel	Corning	356234
mTeSR™1	Stemcell Technologies	85851 + 05827
N2-supplement	Gibco Life Technologies	17502048
NEAA	Gibco Life Technologies	11140-050
Neural Induction Supplement	Gibco Life Technologies	A1647801
Neurobasal	Gibco Life Technologies	21103049
Opti-MEM	Gibco Life Technologies	51702490
PBS	Gibco Life Technologies	14190-094
Pen/Strep	Gibco Life Technologies	15140-122
Poly-Ornithine	Sigma	P3655-50mg
Recombinant Murine EGF	Peprotech GmbH	315-09-100
Rock Inhibitor	Stemcell Technologies	72302
RPMI 1640	Gibco Life Technologies	51254487
TrypLE™Express (Trypsin)	Gibco Life Technologies	12604-013

3.1.3 Kits and enzymes

Table 5 Overview of kits used in this work

Name	Manufacturer	Ordering number
Click-iT™ EdU Alexa Fluor™ 647 Flow Cytometry Assay Kit	Invitrogen™	C10419
CytoTune™-iPS 2.0 Sendai Reprogramming Kit	Thermo Fisher Scientific	A16517
EndoFree Plasmid Maxi Kit	QIAGEN	12362
High Pure RNA Isolation Kit	Roche	11828665001
Trans-Blot Turbo RTA Midi 0.2 µm Nitrocellulose Transfer Kit	Biorad	1704271
P3 Primary Cell 4D-Nucleofector™ X Kit L	Lonza	V4XP-3024
PSC Neural Induction Kit	Thermo Fisher Scientific	A1647801
QuickExtract DNA Extraction	Lucigen	QE09050
Western Lightning® Plus-ECL, Enhanced Chemiluminescence Substrate	PerkinElmer	NEL 103001EA

Table 6 Overview of enzymes used in this work

Name	Manufacturer	Ordering number
AflII	NEB	R0520S
Exonuclease I	NEB	M0293S
FastStart™ Taq DNA Polymerase	Roche	12032953001
Gibson Assembly® Master Mix	NEB	E2611S
Phusion Polymerase	NEB	M0530S
PrimeScript™ RT Master Mix	TaKaRa	RR036Q
Shrimp alkaline phophatase (SAP)	NEB	M0371S
SYBR® Premix Ex Taq™ II	TaKaRa	RR820L

3.1.4 Primers

Table 7 Overview of primers used in this work senescence.

All primers were ordered at Sigma-Aldrich and diluted 1:10 before use.

Name	Sequence
DNA	
BRCA1_indel5_F	GCCAGTCATTTGCTCCGTTT
BRCA1_indel5_R	TCCCATTTCTCTTTCAGGTGACA
BRCA2_indel2_F	TGAAAGAAAGTGTCCCAGTTGGT
BRCA2_indel2_R	CACAGCTGCCCCAAAGTGTA
qPCR	
BRCA1_hinterMut_F	GAGTCTGGGCCACACGATTT
BRCA1_hinterMut_R	TGAAGACAGAGCCCCAGAGT
BRCA2_hinterMut_F	CAAAAACAACTCCAATCAAGCA
BRCA2_hinterMut_R	AGAAGAAACAAAGGCAACGC
GAPDH_f	CCACATCGCTCAGACACCAT
GAPDH_r	AAATCCGTTGACTCCGACCTT
KLF4_f	CCCACATGAAGCGACTTCCC
KLF4_r	CAGGTCCAGGAGATCGTTGAA
NANOG_f	AAGGTCCCGGTCAAGAAACAG
NANOG_r	CTTCTGCGTCACACCATTGC
NESTIN_f	CCAGATCGCTCAGGTCCTG
NESTIN_r	AGCTGAGGGAAGTCTTGGAG
OCT4_f	GTGTTCAGCCAAAAGACCATCT
OCT4_r	GGCCTGCATGAGGGTTTCT
PAX6_f	ACCCAAGAGCAAATTGAGGC
PAX6_r	CCATTTGGCCCTTCGATTAGA
SOX2_f	TGGACAGTTACGCGCACAT
SOX2_r	CGAGTAGGACATGCTGTAGGT

3.1.5 Plasmid and gRNA constructs

Table 8 Plasmids used in this work

Name	Manufacturer	Ordering number
Cas9-GFP	Ralf Kühn	
gRNA cloning vector	Addgene	41824

Table 9 gRNAs used in this work

Name	Sequence
BRCA2_indel2	CCAGGGACAACCCGAACGTGATG
BRCA1_indel5	AAAGTGGTGGTATACGATAT

3.1.6 Antibodies

Table 10 Overview of primary antibodies used in this work

Protein	Host	Manufacturer	Ordering number
BRCA1	mouse	Merck/ Sigma	OP92
BRCA2		Merck/ Sigma	OP95
NESTIN		Merck	MAB5326
TRA-1-60		Millipore	4360
yH2AX		Merck	05-636
ACTIN	rabbit	Sigma	A2066-200UL
NANOG		R&D Systems	AF1997
PAX6		BioLegend	901301
SERPINH1		Sigma-Aldrich	S5950
SOX2		Abcam	ab137385

Table 11 Overview of secondary antibodies used in this work

Name	Manufacturer
Goat anti-mouse IgG Alexa Fluor488	Invitrogen
Goat anti-mouse IgG HRP	Jackson
Goat anti-rabbit IgG Alexa Fluor594	Invitrogen
Goat anti-rabbit IgG HRP	Jackson

3.1.7 Media

All media were warmed up to 37°C before use.

3.1.8 Coatings

Fibroblasts during its isolation, iPSCs in regular culturing, during reprogramming and in differentiation to NPCs as well as NPCs and neurospheres in migration experiment needed a special coating of the plastic ware for proper growing of cells. As neurospheres in the proliferation stage were cultured in low-attachment U-bottom-shaped 96-well plates, they did not need a coating for plasticware.

3.1.8.1 Gelatin coating

Plates needed to be coated with gelatin for the isolation of fibroblasts from skin biopsies. Therefore, gelatin was warmed up at 37°C and diluted to 0.1% gelatin in DBPS. After an incubation of 30-60min at 37°C, plates were ready for use.

3.1.8.2 MEF culture dish

Mouse embryonic fibroblasts (MEF) culture plates, so-called feeder cells, were used during the reprogramming of fibroblasts into iPSCs. Therefore, MEFs were thawed in 1ml of DMEM with 10% ESC-qualified FBS, 1% NEAA, and 0.1% β-mercaptoethanol. Once cells were thawed, they were counted, and 2.5 x 105 cells per well of a 6-well plate were seeded. One full six-well plate per reprogrammed cell line was prepared and could be used two days later.

3.1.8.3 Geltrex

A Geltrex coating is needed for regular culturing of iPSCs and in the first weeks of differentiation into NPCs. Therefore, Geltrex is thawed in 1 ml of DMEM-F12 + Glutamax. Once thawed, the 1 ml is mixed with another 11ml of DMEM-F12 + Glutamax, and 2 ml were plated into one well of a six-well plate. After incubation of at least 1h at 37°C, coated plates could be used.

3.1.8.4 Poly-Ornithine-Laminin-Coating (PL)

PL-coated plates were used for standard culturing of NPCs, during all experiments with NPCs, and for neurospheres in migration experiments. Therefore, 50mg poly-L-ornithine is dissolved in 100ml of H_2O, and 5.5ml of this was mixed with 45ml of boric acid (4,6g boric acid in 500ml H_2O, pH 8.35 (adjusted with NaOH)). 1.5ml per one well of a six-well plate were coated, and plates were incubated at 37°C overnight. On the next day, the plates were washed thrice with 2ml of HBSS per well and covered with 1.5ml of laminin. Therefore, 1mg laminin was diluted in 200ml HBSS. After a cool-down phase of circa 3h in the fridge, the plates could be frozen at -20°C. For using the plates, they were placed into the incubator to warm up for at least 30min until they were ready for use.

3.1.8.5 Coverslips

To stain cells, they needed to grow on coverslips with the appropriate coating for each cell line. Therefore, coverslips were moved in 70% ethanol until completely covered and placed vertically into a 12-well plate, one coverslip per well. Under UV-light exposure for at least 30min, coverslips were dried and could be tipped to fall horizontally into the wells. Afterwards they could be covered with the desired coating.

3.1.9 Cells

Table 12 Overview of cells used in this work

Patient	Donor age	Sex	Cells	Cell type	Mutation	BRCA	Abbreviation (for thesis)
1263/16	26 years	Male	1263/16	Fibroblasts	-	BRCA2/1 (+/+)	♂_BRCA2$^{(+/+)}$
			1263/16 S21	iPSCs			
			1263/16 S21 NPCs	NPCs			
			1263/16 S21 BRCA2 53	iPSCs	c.4524_4525insA	BRCA2 (+/-)	♂_BRCA2$^{(+/-)}$
			1263/16 S21 BRCA2 53 NPCs	NPCs			
			1263/16 S21 BRCA2 62	iPSCs	c.[4523_4524insA]; [4518_4523delCCAGGG]	BRCA2 (-/-)	♂_BRCA2$^{(-/-)}$
			1263/16 S21 BRCA2 62 NPCs	NPCs			
			1263/16 S21 BRCA1 11	iPSCs	c.2030_2045delTTTTACAAAACCCATA	BRCA1 (+/-)	♂_BRCA1$^{(+/-)}$
			1263/16 S21 BRCA1 11 NPCs	NPCs			
1262/16	26 years	Female	1262/16	Fibroblasts	-	BRCA2/1 (+/+)	♀_BRCA2$^{(+/+)}$
			1262/16 J11	iPSCs			
			1262/16 J11 NPCs	NPCs			
			1262/16 J11 BRCA2 22	iPSCs	c.[4524_4526delinsGC]	BRCA2 (+/-)	♀_BRCA2$^{(+/-)}$
			1262/16 J11 BRCA2 22 NPCs	NPCs			
369/20	9 years	Female	396/20	Fibroblasts	c.4631_4631delA	BRCA2 (+/-)	♀p_BRCA2$^{(+/-)}$

Table 13 Overview of cells used in each experiment

Experiment	♂_**BRCA2**$^{(+/+)}$	♂_**BRCA2**$^{(+/-)}$	♂_**BRCA2**$^{(-/-)}$	♂_**BRCA1**$^{(+/-)}$	♀_**BRCA2**$^{(+/+)}$	♀_**BRCA2**$^{(+/-)}$	♀**p_BRCA2**$^{(+/-)}$
Characterization	+	+	+	+	+	+	+
BRCA1 / 2 expression	+	+	+	+	+ (only RNA)	+ (only RNA)	
Formaldehyde establishment in fibroblasts					+		+
Formaldehyde treatment in fibroblasts	+ (only RNA)				+		+
Formaldehyde treatment in NPCs	+	+					
2D proliferation assay	+	+			+	+	
2D proliferation assay - recovery	+	+					
Cell cycle	+	+			+	+	
yH2AX - FACS	+	+					
yH2AX - Staining	+	+					
Neurospheres - over time	+	+			+	+	
Neurospheres - 5h formaldehyde					+	+	
Neurospheres - 24h formaldehyde low passage	+	+					
Neurospheres - 24h formaldehyde high passage	+	+	+	+			

3.1.10 Media

Table 14 Overview of media used for different cell types and culturing steps

fibroblasts			
isolation from skin biospy	fibroblast extraction media	DMEM	
		FBS	20%
		Pen/Strep	1%
feed	fibroblast media	IMDM	
		FBS	15%
		Pen/Strep	1%
freeze	fibroblast media +DMSO	DMSO	10%
iPSCs			
during reprogramming	reprogramming fibroblast media	DMEM	
		ESC-qualified FBS	10%
		NEAA	1%
		β-mercaptoethanol	0.1%
	iPSC media	DMEM/F- 12	
		KOSR	20%
		NEAA	1%
		β-mercaptoethanol	0.1%
		Pen/Strep	1%
		bFGF	0.04%
		β-mercaptoethanol	0.1%
feed	mTeSR	mTeSR	
		Pen/Strep	1%
wash	wash media	DMEM F12+GlutaMAX	
split	PBS/EDTA	0.9g NaCl and 250µl 1M EDTA in 500ml PBS, steril filtered	
freeze	iPSC freezing media	mTeSR	65%
		KOSR	25%
		DMSO	10%
NPCs			
basic	NM	DMEM F12+ GlutaMAX	1/2
		Neurobasal	1/2
		N2-Supplement	1%
		B27	2%
		Pen/Strep	1%
feed	NM+FGF	FGF	1:1000
split	NM+KOSR	KOSR	20%
freeze	NM+KOSR+DMSO	DMSO	10%

Neurospheres			
proliferation	NS media	DMEM F12+ GlutaMax	1/2
		Neurosbasal	1/2
		N2-Supplement	1%
		B27	2%
		GlutaMax	2mM
		NEAA	1%
		bFGF	10ng/ml
		EGF	10ng/ml
		Pen/Strep	1%
migration	Neurobasal +	DMEM/F-12,	
		N2-Supplement	1%
		B27 + VitaminA	2%
		Pen/Strep	1%
NPC differentiation			
1st week of NPC differentiation	Neural Induction media (NIM)	Advanced DMEM	1/2
		Neurobasal	1/2
		N2-Supplement	1%
		B27	2%
		Pen/Strep	1%
after 1st week until switch to PL-coated plates	Neural Expansion Media (NEM)	Neurobasal	
		N2-Supplement	1%
		B27	2%
		Pen/Strep	1%

3.2 Methods

3.2.1 Workflow

An overview of the performed experiments and the workflow can be understood in Figure 8.

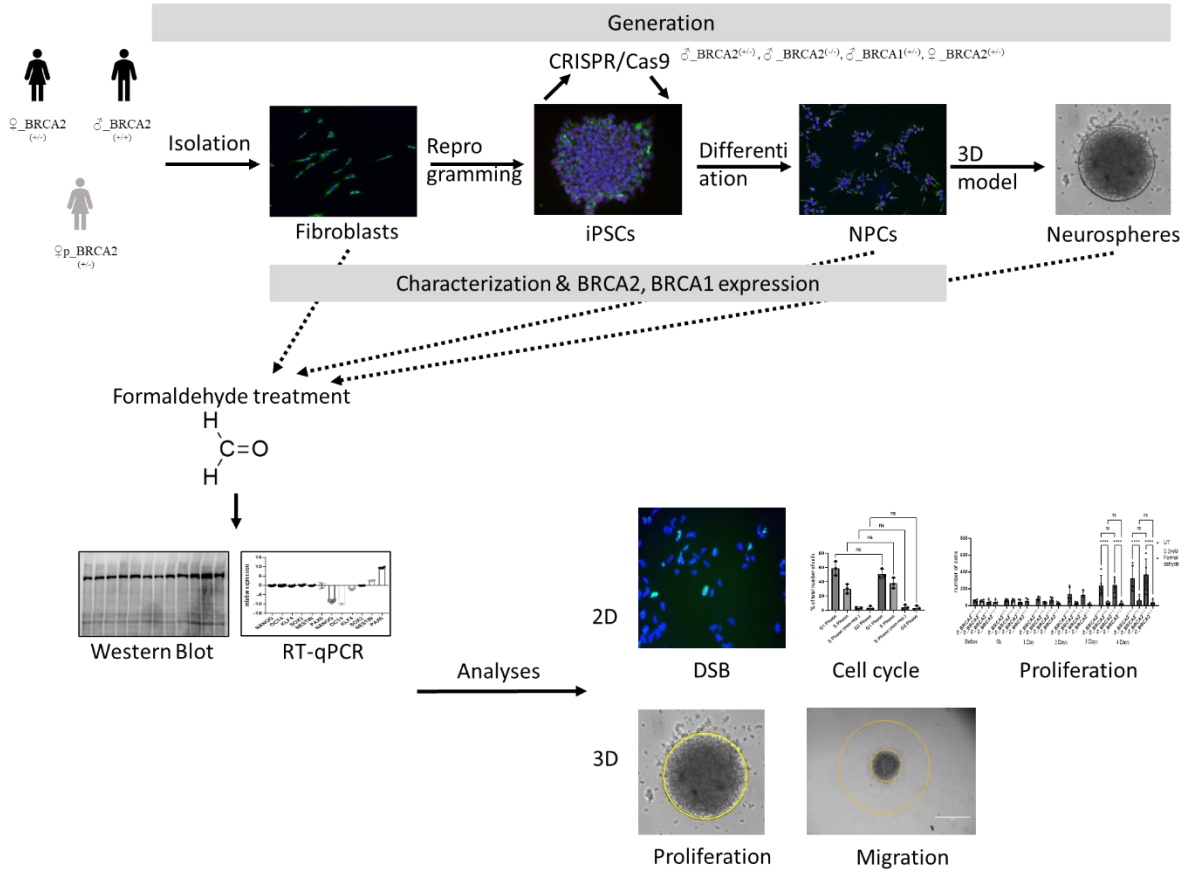

Figure 8 Overview of the workflow during this project senescence. Fibroblasts of a male and a female wildtype person had already been reprogrammed before, while fibroblasts of a person carrying a BRCA2 mutation were reprogrammed into iPSCs during this project. The wildtype iPSCs were genome-edited to introduce a mutation in the BRCA2 or BRCA1 gene. All generated iPSCs were differentiated into NPCs, and neurospheres were generated as a 3D model. Fibroblasts, iPSCs, and NPCs were characterized, and BRCA2 and BRCA1 protein and RNA expression were determined. Fibroblasts, NPCs, and neurospheres were treated with formaldehyde, and again BRCA2 and BRCA1 protein and RNA levels were analyzed. Additionally, the influence of BRCA2 mutation and formaldehyde on the number of double-strand breaks (DSB), cell cycle, and proliferation rate in NPCs were analyzed. Neurospheres were investigated regarding proliferation and migration.

3.2.2 Cell culture

3.2.2.1 Pellets

From cell pellets it is possible to isolate DNA, RNA, or protein. Oftentimes cells were treated with formaldehyde before, and pellets were stored until further processing. DNA and RNA isolation was performed after pellets were stored at -80°C to, e.g., isolate all replicates for the same experiment at the same time. Protein was isolated directly.

Cells were washed twice with DPBS to remove all residual media, and DPBS was added again. Cell scrapers were used to scratch the cells from the well/petri dish, and more DPBS was added to collect the cells in a 15ml Falcon. Fibroblasts and iPSCs were centrifuged at 200g for 4min, while NPCs were centrifuged at 300g for 4min. The supernatant was discarded, and the cell pellet was resuspended in 1ml of DPBS to transfer the cells into a 1.5ml tube. After another centrifugation at 450g for 5min, the supernatant was discarded again, and the pellet was stored at -80°C as fast as possible.

3.2.2.2 Counting

It is necessary to count the cells if a certain number of cells is needed. For example, when seeding or freezing a certain number of cells or for a proliferation assay (described in detail here 0)

For counting cells, they need to be detached from the surface and in suspension. For every cell type, the first steps of splitting (compare methods of each cell type) until resuspension of the cells in 1ml media after centrifugation are performed. 10µl of this cell suspension was put into a Neubauer Zählkammer (counting chamber), and cells are counted. Cells on the upper and right borders of the area counted were taken, while the lower and left borders were not counted. The equation to calculate the cells per microliter is the following:

$$\frac{Number\ of\ cells\ counted}{counted\ area\ (mm2) * chamber\ depth\ (mm) * dilution} = cell\ per\ \mu l$$

The required number of cells was used.

3.2.2.3 PFA fixation

A PFA fixation of cells was necessary to fix cells at a certain time point in their proliferation. Cells for fixation can either be in suspension or on coverslips, to later be able to stain them with the antibodies of interest.

Here the fixation of cells on coverslips is described. For the description of the fixation of cells in suspension, see 3.2.2.10.

For fixation and subsequent staining of cells, the cells were seeded on coverslips in 12-well plates with appropriate coating (3.1.10) per cell type. Once the cells reach a confluency of 80-90%, the media is removed, and cells are washed with DPBS and incubated with 4% PFA for 15-20min at room temperature. Afterwards, cells were washed thrice with DPBS for 5-10min at room temperature and stored at 4°C until further processing. Storing is possible for up to a maximum of 6 months in plates with a sufficient volume of DPBS and sealed with parafilm.

3.2.2.4 Morphology

The morphology of all used cells was checked every time before dealing with the cells. If the morphology was as supposed to be, work was continued; if not, cells were either discarded or cleaned, depending on the cell type.

3.2.2.5 Fibroblasts

Fibroblasts were used from a female patient carrying a BRCA2 mutation and from a female and a male control. Those cells were used to establish some experiments and were also reprogrammed into iPSCs, whose genomes were further edited to repair or introduce the heterozygous *BRCA2* mutation.

3.2.2.5.1 Isolation

Fibroblasts were isolated from skin biopsies from the patient and control cell lines. Control cell lines were already generated before, so only the patient cell line was isolated for this project. For the fibroblast isolation, the protocol from Vangipuram and colleagues (Vangipuram et al., 2013) was followed with slight modifications.

In a petri dish under the microscope and laminar hood, the skin biopsy was cut into 15-20 pieces containing all skin layers. Those pieces were equally distributed into a 6-well plate coated with gelatin (3.1.8.1) and filled with 800µl of fibroblast extraction media. Every second day 200µl

of media were added to compensate for media loss through evaporation. After one week, the medium was increased to 2ml per well and thereafter changed every other day completely. After 3-4 weeks, the fibroblasts reached 80% confluency in the well and were split into two 175cm^2 flasks as described in 3.2.2.5.4. After 2-3 days, fibroblasts reached confluency again and were split into three 175cm^2 flasks. When reaching confluency again, cells were frozen with 1 million cells per vial following the protocol described in 3.2.2.5.5 and using fibroblast extraction media containing 10% DMSO.

3.2.2.5.2 Thawing

To thaw cells, the vials were brought from -80°C or liquid nitrogen to the cell culture and warmed quickly between the palms. Once all ice was melted, cells were taken up in 5ml of fibroblast media and transferred into a 15ml falcon. After centrifugation, the supernatant was discarded, and the pellet was resuspended in 1ml of culturing media as well as transferred into a 25cm^2 flask.

3.2.2.5.3 Culturing

The fibroblasts were regularly cultured in 25cm^2 flasks at 37°C with 5% CO_2. Media was completely changed every fourth day. Fibroblasts were used until passage 10.

3.2.2.5.4 Splitting

Fibroblasts were usually split once they reached 100% confluency and looked packed, but at the latest after 10days of culturing on the same ground. For splitting fibroblasts, cells were washed first once with 10ml of DPBS. Three milliliters of trypsin were added to the flask to cover the whole surface, and flasks were incubated at 37°C for 5min. By slightly tapping the flask, cells were detached from the surface and resuspended in 7ml of media. All cells were collected in a 15ml falcon and spun at 200g for 4min to pellet cells. After centrifugation, cells were resuspended in fibroblast media (amount depending on number of cells), and the wanted amount of cell suspension was seeded into new flasks or petri dishes already filled with 8ml of media.

For taking pellets, cells were usually split 1:3 on two petri dishes and back in one flask. For formaldehyde treatment, cells were usually split 1:5 on four petri dishes (two dishes for protein and two for RNA isolation, treated and untreated cells each) and back in one flask for the continuation of culturing.

3.2.2.5.5 Freezing

The process for freezing cells was similar to splitting cells with washing with DPBS once and detaching with trypsin for 5min at 37°C. After collecting the cells with media in a 15ml Falcon and centrifugating for 4min at 200g, the pellet was resuspended in fibroblast media. Via counting, the suspension was diluted to 1 million cells per ml, and DMSO was added to reach a concentration of 10% DMSO in the media. One million cells per vial were frozen in labeled freezing vials and transferred to -80°C in freezing containers as fast as possible. For long-term storage, cells were transferred to liquid nitrogen.

3.2.2.6 iPSCs

Induced pluripotent stem cells were reprogrammed from fibroblasts and used in this work to either repair patient cells or introduce a heterozygous, out-of-frame mutation into wildtype control cells via CRISPR/Cas9. Having two cell lines only differing in one mutation is called

an isogenic pair and lets you relate your differences between the cell lines to the mutation difference. (Kyrousi et al., 2021) Those cells were then further differentiated into NPCs.

3.2.2.6.1 Reprogramming

For the reprogramming of fibroblasts into iPSCs, the CytoTune™-iPS 2.0 Sendai Reprogramming Kit from Thermo Fisher Scientific and the protocol for reprogramming fibroblasts in a feeder-dependent way was followed with slight modifications here described briefly: Two days before the planned transduction of fibroblasts with the viruses, the fibroblasts were split following the usual protocol (3.2.2.5.4) and seeded in two 6-well plates with 200-220-240-260-280-300*10^3 cells per well. On the day of transduction, the cells of one well, which was 30-60% confluent, were harvested by washing with DPBS, trypsinizing for 5min at 37°C and collecting all cells with fibroblast media. These cells were counted and used for determining the current number of cells in the parallel well (on the other 6-well plate) and calculating the volume of virus needed. This equation is necessary to calculate the volume of viruses:

$$\frac{MOI\ \left(\frac{CIU}{cell}\right) * number\ of\ cells}{titer\ of\ virus\ \left(\frac{CIU}{mL}\right) * 10\text{^}(-3)(\frac{mL}{\mu L})} = volume\ of\ virus[\mu l]$$

MOI is the multiplicity of infection, meaning the ratio of virus to cell. The MOIs suggested by the protocol were used (KOS / hc-Myc MOI=5, hKlf4 MOI=3) and the titters of the viruses were KOS / hKlf4=130.000.000 and hc-Myc= 110.000.000.
The volumes of viruses were added to 1ml warm fibroblast media and mixed thoroughly. The media of the parallel well was removed, and prepared virus media was added. After an overnight incubation with the viruses, the media was changed completely. Media was changed completely every second day while culturing for another 6 days. One or two days before passaging the transduced fibroblasts, the 6-well MEF culture plate was prepared. On day 7 after transduction, fibroblasts were split using the usual splitting procedure (3.2.2.5.4) and seeded as a gradient in 5-10-20-40-80-100*10^3 cells per well in the MEF culture dish. After an overnight incubation at 37°C, the media was changed to iPSC medium and thereafter changed every second day completely. From day 8 on, cells were monitored daily to determine the appropriate time point to transfer the emerging colonies into 12-well plates. After 3-4 weeks, the colonies were big enough to be transferred to 12-well plates and were manually scratched from the MEF culture plate with a 200µl tip and placed into the new well. Only one colony per well in order to guarantee a homogenous population. As the colony grew bigger, differentiated cells were manually removed by cleaning the cells (see 3.2.2.6.6), and homogenous, not-differentiated-looking clones were expanded onto Geltrex-six-well plates. At this stage, cells were characterized and frozen and treated to get virus-free. To get cells virus-free they were kept at 39°C for 24h, and a PCR (3.2.4.1.4) was run afterwards to prove that all viruses disappeared. As soon as the characterization showed healthy, normal, virus-free iPSCs, cells could be continued to work with.

3.2.2.6.2 Thawing

iPSCs were thawed as described before (3.2.2.5.2) using wash media to collect the cells in a 15ml falcon and mTeSR to resuspend and seed the cells after centrifugation.

3.2.2.6.3 Culturing

iPSCs were regularly cultured on Geltrex-coated plates at 37°C with 5% CO_2. Daily, the media was fully changed with 2ml of wash media per well of a 6-well plate to wash the spent media away and directly after changed again with 2ml of fresh and warm mTeSR per well. iPSCs were used until passage 40, with genome editing starting around passage 17.

3.2.2.6.4 Splitting

At the latest after 7 days or when an 80-90% confluence was reached, the cells were split. For splitting cells, each well was washed twice with 1ml of PBS+EDTA before being incubated with 1ml of PBS+EDTA for 2min at room temperature. PBS+EDTA was removed and 1ml of mTeSR was added to each split well. With the help of a cell scraper, cells were detached from the plate. After adding another 2.5ml of mTeSR, the cell colonies were broken apart by pipetting the suspension up and down 5 times. The usual splitting ratio was 1:6 or 1:12 into fresh Geltrex-coated plates already filled with 2ml mTeSR per well. Media was changed only two days after splitting.

3.2.2.6.5 Picking

Picking of a single colony is necessary during reprogramming as well as during normal iPSC culture to expand cells from one good-looking colony without differentiation. For picking, the colony was slightly scratched and detached from the surface using a cell scraper and transferred into a new Geltrex-coated well with the help of a 200µl pipette. Depending on the size of the colony, it was broken apart or left as one piece to grow bigger.

3.2.2.6.6 Cleaning (removal of differentiated cells)

Cleaning of iPSCs means the removal of wrongly differentiated cells within one well of iPSCs to maintain a homogenous population of iPSCs. Therefore, a Pasteur pipette was formed with a Bunsen burner into a certain structure looking like a bent finger. The thin glass part was heated and pulled apart to generate a very thin piece. This piece was melted into a bulb. Roughly 2cm behind the bulb, the glass was bent into a 45° angle and again in a 90° angle after 4-5cm. After every use the front bulb was heat sterilized.

The cleaning procedure was performed under a microscope placed in the laminar hood. All wrongly differentiated colonies were manually removed by scratching them away with the glass tool. The differentiation can appear white or black under the microscope or as colonies looking heterogenous or frayed at the borders.

The whole procedure for one full plate was maximally performed within 30min; otherwise, cells were dying due to being at room temperature for too long. After cleaning, cells were washed and fed with fresh mTeSR.

3.2.2.6.7 Freezing

For freezing iPSCs, cells were detached from the plate as described in the splitting procedure (3.2.2.6.4), but wash media was used to collect the cells in a 15ml Falcon. After centrifugation, the number of freezing vials was determined by assessing the cell pellet size. The pellet was resuspended in an appropriate volume of freezing media (3.1.10), and 1ml of the suspension was frozen per vial. Vials in freezing containers were directly stored at -80°C. For long-term storage the cells were transferred to liquid nitrogen the day after.

3.2.2.6.8 Genome Editing with FACS sorting

The genome editing process consists of two steps. First electroporation of iPSCs with gRNA-vector and Cas9-plasmid and after two days sorting of one single cell per well of a 96-well plate via FACS, which is possible because of GFP in the Cas9 plasmid.

For the electroporation, cells with a passage below 20 were seeded in one 6-well plate well. As soon as they reached an 80-90% confluency and looked healthy, they were fed in the morning with 3ml of fresh media, and the electroporation procedure was carried out in the afternoon. Therefore, cells were washed twice with DPBS and incubated with 1ml of trypsin for 6min at 37°C. For the resuspension of cells and the collection of all cells in a 15ml Falcon, 1ml of DPBS was added and the cells were first in the well, and again in the 15ml Falcon resuspended. Not too harsh, but harsh enough to break the colonies apart and generate a single cell suspension. Single-cell status was checked while counting the cells. If they were not single cells yet, they were resuspended again. 800.00 cells per electroporation/ gRNA +10% were transferred into a fresh 15ml Falcon and centrifuged at 300g for 5min. Resuspension and counting of cells were not supposed to take longer than 10min to decrease the probability of cells dying.

After centrifugation, cells were resuspended in 100µl per gRNA + 10% electroporation buffer (82µl of P3 + 18µl of supplement). 100µl of the cell suspension was transferred to tubes already prepared with 2.5µg Cas9 plasmid + 2.5µg gRNA. After pipetting up and down once, the whole suspension was transferred into electroporation cuvettes, tapped on the bench once to remove any air bubbles, and electroporated in the Lonza 4D-Nucleofector™ X Unit with the program CB-150.

Afterwards, 100µl of warm RPI media was added to the cells, and they were incubated for 8min at 37°C. 500µl of mTeSR+ Rock inhibitor (1:1000) was added to the cells, and the full volume was transferred into a prepared 6-well plate well with 2ml of mTeSR+ Rock inhibitor. After 24h, the media was fully changed to first the wash media and second to mTeSR. After another 24h, cells could be sorted.

For FACS sorting of single cells into a 96-well plate, the Geltrex-coated plate was prepared with 100µl of mTeSR + 10% CloneR and kept until usage at 37°C. Cells were washed twice with DBPS and incubated again with 1ml of trypsin at 37°C for 5min. 1-3ml of DPBS were used to collect all cells in a 15ml Falcon and cells were resuspended in a falcon via pipetting against the wall of the falcon to generate a single-cell suspension. The status of the cells was checked again in a Neubauer counting chamber. If the cells were single-cells, they were centrifuged at 300g for 4min, if not, they were pipetted again against the wall until they reached single-cell status. After centrifugation, the supernatant was removed, and cells were resuspended in 200µl of mTeSR+ 10% CloneR and transferred into FACS tubes.

During FACS sorting, which was performed at the Flow Cytometry Core Facility 911 by [redacted] using a “FACS Aria”, one single, GFP-positive cell was sorted in one well of a 96-well plate, and afterwards the plate was kept at 37°C for 48h. After those 48h, the media was completely change with 100µl of mTeSR + 10% CloneR and after another 48h, the media was fully changed to 100µl of mTeSR. Cells were kept on the 96-well plate for a maximum of 10days or until the well reached a 80-90% confluence. During this time, the media was changed every second day and meanwhile adapted in the volume of mTeSR depending on the consumption/ color of media in the well.

Cells were split from one well of a 96-well plate to one well of a 12-well plate. Therefore, cells were washed with 200µl of DPBS and incubated with 100µl of trypsin for 5min at 37°C. The reaction was stopped with 100µl of wash media, and with a 200µl pipette, the colony was detached from the plate and transferred into a 15ml Falcon prepared with 3ml of wash media. After a centrifugation of 300g for 5min, the supernatant was removed. The pellet was

resuspended in 200µl of mTeSR + 10% CloneR and 10-20µl were pipetted into a 1.5ml tube, while the rest was plated into the 12-well plate well containing 1ml of mTeSR + 10% CloneR. After 48h, the media was fully changed to mTeSR. While being on the 12-well plate, the sequence of the colony was determined to see if the cells carry the mutation of interest. If so, they were expanded, frozen, characterized, and continued to work with. If not, the cells were discarded.
For sequencing, the 1.5ml tube with 10-20µlof cell suspension was used. 50µl of QuickExtract DNA extraction solution was added to the 1.5ml tube. The tube was vortexed for 15sec followed by an incubation of 6min at 65°C. After another vortexing of 15sec, the tube was again incubated for 2min at 98°C and then the DNA was stored at 4°C for short-term storage or at -20°C for long-term storage until sequencing (3.2.4.1.5).

3.2.2.7 NPCs

Neural progenitor cells (NPCs) are used in this work to be able to investigate proliferation and cell cycle of neuronal, proliferating cells being treated with/without FA. Furthermore, they were used to investigate a 3D model, neurospheres, generated from NPCs to explore proliferation and migration. Mainly the male control cell line and its isogenic counterpart with a heterozygous mutation in the *BRCA2* gene were used.

3.2.2.7.1 Differentiation

iPSCs were differentiated into NPCs following the protocol "Induction of Neural Stem Cells from Human Pluripotent Stem Cells Using Gibco PSC Neural Induction Medium" from Thermo Fisher Scientific, here described quickly.
As soon as a healthy, homogenous-looking well of iPSCs reached a 70-80%, it was split following the regular protocol (3.2.2.6.4), and cells were plated as a gradient with 200-300-400-500-700-1000µl per well. After 24h, the media was changed completely to 2.5ml of NIM (neural induction media) per well. After 48h, the media was changed completely with 2.5ml fresh NIM per well. After another 48h, the media of wells that might be split later, was changed with fresh NIM in a volume depending on the cell density in the well. The more cells, the more media was given. After 24h, one day before splitting, the media of the chosen wells was changed completely again, giving as much media as needed to not starve the cells until the next day. On day 7 one well of differentiated cells was split from P-1 to P0. The well with the best-looking morphology and confluency was chosen. The splitting procedure was as described here: cells were washed with DPBS and afterwards incubated with 1ml pre-warmed Accutase for 5-8min at 37°C until almost all cells detached. For detaching the rest of the cells 1ml of DPBS was added to the well, and the whole volume was pipetted up and down in the well. Cells were passed through a 100µm cell strainer and transferred into a 15ml Falcon. After a centrifugation step of 300g for 4min, the supernatant was discarded. The cell pellet was resuspended again in 5ml of DPBS and spun again for 4min at 300g. After discarding the supernatant, the cell pellet was resuspended in 1ml of NEM (neural expansion media) + Rock inhibitor (final concentration of 5µM) and counted. A gradient of 200-300-400-500-700-1000*10^3 cells was seeded into a Geltrex-coated, 6-well plate already prepared with 2ml of warm NEM. After 24h, the media was changed completely with 2ml of NEM media. Every second day, the media was fully changed with a volume so the cells would not starve. After 6-7 days, cells in the wells reach confluency and were ready to be split again. For the first 3-4 passages, the appendix B protocol was used to split the cells, as a lot of wrongly differentiated cells needed to be removed. For this splitting, cells are washed with DPBS and incubated with 1ml of Accutase for 3-4min at

room temperature to detach all wrongly differentiated cells. Accutase was removed, and cells were washed with DPBS and incubated again with 1ml of Accutase at 37°C for 3-4min. Afterwards, the procedure already described above for splitting from P-1 to P0 was followed.
As soon as the cells looked homogenous on the Geltrex plate, cells were split onto PL-coated plates, following NPCs splitting procedure (3.2.2.7.4), and expanded from there on. After characterization via RT-qPCR and staining, cells were ready to be used for further experiments.

3.2.2.7.2 Thawing

Cells were thawed as described before (3.2.2.5.2), and 5ml of NM + KOSR media was used to take up the cells. After centrifugation, cells were resuspended in 1ml of NM +FGF and seeded in a PL-coated plate already prepared with 2ml NM+FGF.

3.2.2.7.3 Culturing

NPCs were regularly cultured at 37°C with 5% CO_2 on PL-coated plates. A full media change with 2.5ml of NM + FGF was performed every other day. NPCs were used until passage 20.

3.2.2.7.4 Splitting

Splitting of NPCs was following the same procedure as already described for fibroblasts (3.2.2.5.4) but using NM+KOSR to stop the trypsin reaction after incubation. To plate cells, the pellet was resuspended after centrifugation in NM+ FGF and counted (3.2.2.1). Usually 150-200k cells were seeded per one well of a six-well plate, depending on the exact cell line and its proliferation speed. Regularly, the aim was to have a densely confluent well after 7days.

3.2.2.7.5 Freezing

For freezing NPCs, the splitting procedure was followed until the counting step. Via counting, the total number of cells was determined, and after another centrifugation at 300g for 4min, cells were resuspended and diluted in NPC freezing media to a concentration of 1 million cells per milliliter. One milliliter was aliquoted per vial and directly frozen at -80°C in a freezing container. For long-term storage, cells were transferred to liquid nitrogen.

3.2.2.8 Formaldehyde treatment

Formaldehyde treatment was first established in fibroblasts and later translated to NPCs. For formaldehyde treatment, cells were cultured until they reached confluency but would still proliferate. In the afternoon before treatment, cells were fed again so they would not starve overnight. On the next morning the media was removed, and fresh media with either 0mM or 0.2mM formaldehyde was added. After an incubation of 5h at 37°C, cells were washed once with DPBS and proceeded depending on the experiment. Either cell pellets (3.2.2.1) were taken, cells were fixed (3.2.2.3) for staining (3.2.4.3.3) or cell cycle analysis (3.2.2.10) or counted (3.2.2.1) for the proliferation assay (3.2.2.9).
For establishing the treatment 5h incubations of formaldehyde with concentrations of 0, 0.1, 0.2 and 0.3mM were tested, and the concentration was chosen, where the BRCA2 protein concentration in *BRCA2*$^{(+/-)}$ cells in a western blot had almost completely vanished, while it was still clearly detectable in *BRCA2*$^{(+/+)}$ cells. This concentration was 0.2mM and was continued to work with in all further experiments. (Furthermore, this concentration is still in the range of naturally occurring concentrations of formaldehyde in the brain.)
Fibroblasts were treated in 10cm dishes, while NPCs were treated in a 6- or 24-well plate. The number of dishes and wells per condition depended on the performed experiment.

The regular treatment of NPCS plus subsequent analysis via RT-qPCR and western blot was performed by [redacted] for her medical PhD under my supervision.

3.2.2.9 Analysis of DSB in NPCS with γ H2AX staining w/o subsequent FACS analysis

Analysis of DNA double-strand breaks in NPCS with and without formaldehyde treatment was performed to see if there is an increase in *BRCA2*$^{(+/-)}$ cells compared to *BRCA2*$^{(+/+)}$ cells due to formaldehyde treatment. This was done in two ways: first, to see the amount of damage in different conditions and second, to investigate the number of foci per nuclei in each condition.
For the first experiment, cells were treated with and without formaldehyde, stained with a γH2AX antibody, and median fluorescence intensity of the cell population was measured via FACS.
One million cells per well were seeded 48h before treatment. On the day of treatment, media was exchanged for fresh media without or with a concentration of 0.2mM formaldehyde. After incubating for 5h at 37°C, cells were washed once with DPBS and then fixed as already described in 3.2.2.10, and stored overnight at 4°C.
On the next day, the pellet was resuspended in 750µl of 0.1% saponin +5% FCS in PBS (PERM) and incubated for 30min at 4°C for permeabilization. Cells were centrifuged at 300g for 4min and resuspended in 100µl with the γH2AX antibody (1:250). After incubating for 20 min at 37°C in a water bath, cells were spun again at 300g for 4min and washed once in 600µl PERM. The pellet was resuspended in 100µl of AlexaFluor647 Gt-Anti-ms (1:400) and incubated for 20min at 37°C in a water bath in the dark. Cells were spun, washed with 600µl PERM, and incubated with DAPI in PBS (1:1000) for 20min at room temperature. After pelleting the cells once, they were washed with PBS once and resuspended in 300µl of PBS for FACS analysis.
FACS analysis was performed by the Flow Cytometry Core Facility 911 with [redacted]. A "FACS Aria" was used to measure the samples, while data analysis was performed with FlowJo and the help of [redacted].
For statistical data analysis, the Prism software was used. If comparing only two conditions, an unpaired, two-tailed t-test was performed, and if comparing more groups, a one-way ANOVA with multiple comparisons comparing the mean of a column with the mean of every other column.
For the second analysis, cells were also treated with and without formaldehyde and stained with γH2AX, but then analyzed microscopically. The intensity of γH2AX foci was determined with a program from [redacted].
Therefore, 250,000 cells per well were seeded in a 12-well PL-coated plate with coverslips. On the next day, the media was changed, and cells were treated for 5h at 37°C without and with 0.2mM of formaldehyde. After treatment, cells were fixed, as already described in 3.2.2.3. Cells were then stained with ms-anti- γH2AX (1:500) and alexaFlour488-Anti-ms (1:400) as described in 3.2.4.3.3. Pictures of at least 300 nuclei of each condition were taken with an ECHO Revolve microscope, and 300 nuclei were analyzed in Fiji with a modified script from [redacted]:

```
image = getTitle();
roiManager("reset");
run("Clear Results");
run("Split Channels");
selectWindow(image + " (blue)");
waitForUser("Please adjust brightness and contrast");
run("Median...", "radius=10");
setAutoThreshold("Mean dark");
run("Convert to Mask");
run("Watershed");
run("Analyze Particles...", "size=50-Infinity display exclude clear add");
selectWindow(image + " (green)");
run("Set Measurements...", "area integrated redirect=None decimal=3");
run("Clear Results");
roiManager("deselect");
roiManager("Measure");
waitForUser("Please copy data from the result table for gammaH2AX intensity");

run("Close All");
print("finish analyzing "+image);
```

3.2.2.10 Cell cycle analysis with subsequent analysis by FACS in NPCs

Cell cycle analysis was performed to compare cell cycle stages between *BRCA2*$^{(+/+)}$ and *BRCA2*$^{(+/-)}$ NPCs without and after formaldehyde treatment. Therefore, the Click-iT™ EdU kit from Invitrogen™ was used.

Once cells reached confluence in the 6-well plate, media was discarded, and fresh media w/o formaldehyde (0.2mM) and with EdU (10µM) was added for an incubation of 5h at 37°C. Afterwards, cells were washed with DPBS, trypsinized for 5min at 37°C and the reaction was stopped with 1% BSA in PBS. Cells were collected via centrifugation at 300g for 4min, and resuspended in 0.5ml of 4% PFA for fixation. After incubating for 15min at room temperature, cells were spun again at 300g for 4min, and the PFA was discarded. Cells were washed once with 1%BSA in PBS, and after centrifugation, cells were stored covered with 0.5ml 1%BSA in PBS at 4°C overnight.

On the next day, supernatant was removed, and the pellet was resuspended in 1ml o 0.5% Triton in PBS for permeabilization and incubated for 15min at room temperature. After a centrifugation of 300g for 4min, the supernatant was removed and the pellet was washed once with 0.5ml of 1% BSA in PBS. In the meantime, the Click reaction buffer was prepared following the instructions from the kit. For the Click-iT reaction, 0.5ml buffer was added to the cells and mixed well. After an incubation of 30min at room temperature in the dark, the pellet was washed with 0.5% Triton in PBS and spun again at 300g for 4min to remove the supernatant. For the DAPI staining, the cell pellet was resuspended in 300µl DAPI (0.1µg/ml) in PBS and incubated for 15min at room temperature in the dark. The pellet was washed twice with PBS, resuspended in 300µl PBS and brought to the Flow Cytometry Core Facility 911 to [redacted]. Using a “FACS Aria”, the measurement of the samples was performed, while the data analysis was done with FlowJo and the help of [redacted].

For the statistical data analysis, the Prism software was used. If comparing only two conditions, an unpaired, two-tailed t-test was performed, and if comparing more groups, a one-way

ANOVA with multiple comparisons comparing the mean of a column with the mean of every other column.

3.2.2.11 Proliferation assay in NPCs (counting)

The proliferation assay is based on the number of cells within wells at given time points before and after a potential treatment. *BRCA2*$^{(+/+)}$ and *BRCA2*$^{(+/-)}$ cells with and without formaldehyde treatment can be compared.

Therefore, 200,000 NPCs were seeded in each well of a PL-coated 24-well plate. After 48h, when cells were confluent, wells were washed with DBPS, and the first timepoint was harvested by trypsinization and collected with DMEM F12+ GlutaMAX and a 1ml pipette in a 2ml tube. The well was washed again with DMEM F12+ GlutaMAX and 1ml pipette. During a centrifugation of cells from the first time point at 300g for 4min, media of the rest of the wells is changed to fresh media with 0.2mM formaldehyde or without FA. Plates were incubated at 37°C for 5h. The supernatant of the centrifuged cells was discarded, and the pellet was resuspended in 100µl DPBS and counted (see 3.2.2.1).

At the other time points were directly after the end of the formaldehyde treatment, 1, 2, 3 and 4 days after formaldehyde treatment. Cells were harvested and counted, as just described for time point 1.

For each time point, two wells were harvested and counted to take the average of those wells. For statistical analysis, more groups were compared using a one-way ANOVA with multiple comparisons, comparing the mean of a column with the mean of every other column.

3.2.2.12 Neurospheres

For the generation of neurospheres, a published protocol (Zhou et al., 2016) was followed, which is described shortly. In order to generate neurospheres, NPCs were cultured until they reached 100% confluency in the well. Cells were washed with 2ml DPBS per well and trypsinized with 1ml per well for 5min at 37°C. The trypsinization reaction was stopped with 2ml of NM +KOSR and cells were collected in a 15ml falcon. After a centrifugation of 4min at 300rpm, the supernatant was removed, and the cell pellet resuspended in 1ml of neurospheres media. Cells were counted, and 120,000 cells in 120µl media were seeded in 1 well of a 96-well plate. With this method it is possible to analyze two aspects: proliferation of neurospheres and migration of cells away from neurospheres. For proliferation, neurospheres were just cultured in a 96-well plate with 100µl of media being added on day 5.

For the migration assay, on day 3, neurospheres were transferred with a cut 200µl tip to a PL-coated 6-well plate with 500µl of neurobasal media and spread equally across the surface. The neurospheres were covered with media but were not floating, so they could attach to the surface, and cells could migrate out from the neurosphere. If necessary, neurobasal media was added on day 4, 5, and 8.

Pictures for the analyses were taken on day 5, day 8, and day 10. For proliferation a 10x magnification was used, while for migration a 4x magnification was sufficient.

The analysis of the pictures was performed with the software Fiji. For the proliferation analysis, a code was used to run a batch analysis:

```
run("Duplicate...", " ");
run("16-bit");
run("Threshold...");
setThreshold(0,X);
setOption("Blackbackground", false);
run("Convert to Mask");
run("Close");
run("Set Measurements...", "werea Feret's redirect=None decimal=3");
run("Set Scale...", "distance=1.1025 known=1 unit=[ Î¼m] global");
run("Analyze Particles...", "size=100000-Infinity circularity=0.1-1.00 show=Outlines display");
```

The threshold (X) was manually adapted, depending on the brightness of pictures. If pictures could not be analyzed automatically, a circle was drawn manually around the neurospheres. For comparisons, the Feret diameter of neurospheres was used. If comparing only two conditions, an unpaired, two-tailed t-test was performed, and if comparing more groups, a one-way ANOVA with multiple comparisons comparing the mean of a column with the mean of every other column.
When using NPCs, they were between passage P7 and P20. Below P14, they were categorized as young, while P17-P20, they were handled as old NPCs.
When treating neurospheres with FA, two cell lines were compared in each batch. Both cell lines were pipetted into the same 96-well plate, so 48 wells of the plate were filled with each cell line. Two 96-well plates were used for one batch. Therefore, one plate could be treated with FA, while the other one did not encounter formaldehyde at all.
Formaldehyde treatment took place on day 3 of neurosphere generation. Therefore, 120µl with 0.4mM formaldehyde were added into each well to reach a concentration of 0.2mM formaldehyde in the well. For the untreated group, media without any formaldehyde was added. After 5h or 24h of treatment, the whole media was removed from the well, and 100µl of fresh, warm media were added per well. During the 24h treatment, plates were sealed with parafilm to inhibit evaporation.
Batches of neurospheres were generated under the same conditions and later taken together for analysis.
Cell lines used to generate neurospheres were the male control NPCs with their isogenic counterparts carrying a heterozygous mutation in either the *BCRA2* or the *BRCA1* gene or having gone through the genome editing process but coming out wild type.

3.2.3 Bacterial culture

Bacterial culture was necessary for generating gRNAs for genome editing. Those gRNAs were generated from primers (designed and chosen with the software CRISPOR), cloned into vectors, and transfected into E. coli for multiplication. The E. coli culture needed to be harvested, and DNA needed to be prepared and purified from the E. coli culture.

3.2.3.1 Cloning

Cloning of gRNAs into vectors consists of several steps, namely “vector linearization”, “annealing” of oligos to gRNA primers, and “Gibson assembly” using the Gibson Master Mix. For vector linearization, meaning cutting the vector, the following mixture was incubated for 15min at 37°C, followed by 20min at 65°C for inactivating the enzyme.

Table 15 Overview of ingredients and their volume/ amount for vector linearization

Ingredient	**Volume/ Amount**
Restriction Enzyme Afl II.	1µl
gRNA cloning vector	1µg
Cut Smart Buffer	5µl
H_2O	43µl
Σ:	50µl

For oligo annealing, annealing of proper overhangs to gRNAs to fit in the vector, the following mix was incubated after 30sec at 95°C, for 10min at 72°C.

Table 16 Ingredients and their volume for oligo annealing

Ingredients	**Volume**
5* High Fidelity Phusion Buffer	4µl
dNTPs	0.4µl
Primer forward	1µl
Primer reverse	1µl
High Fidelity Phusion Polymerase	0.2µl
H_2O	13.4µl
Σ:	20µl

Afterwards, the samples and the linearization of the vector were checked in an agarose gel. If everything worked, vector and gRNAs could be annealed with the Gibson Assembly MasterMix for 60min at 50°C.

Table 17 Ingredients and their volume for Gibson assembly

Ingredients	**Volume**
Linearized vector	3µl
Anneald gRNAs	7µl
Gibson MasterMix	10µl
Σ:	20µl

After the assembly, a transformation of the complete vector into E. coli took place (3.2.3.2).

3.2.3.2 Transformation

Transformation of constructs into E. coli is used to multiply the amount of DNA. This was either used for freshly prepared vectors with inserted gRNAs or as a retransformation for multiple existing constructs like the Cas9 vector. For a retransformation, a lower amount of construct is needed. Different constructs carry different antibiotic resistances, like kanamycin or ampicillin, which needed to be paid attention to.

For the transformation, 5µl of gRNA-vector or 1µl of Cas9-construct, were added to 250µl of competent E. coli; the tube was flicked once, and incubated for 30min on ice. After a heat shock of 90sec at 42°C in a water bath, the tube was put on ice again for 2min. 300µl of warm LB media were added to the tube, and it was shaken for 30min at 37°C. 250µl of gRNA- E. coli and 100µl of Cas9- E. coli were plated onto LB plates containing kanamycin and ampicillin remittances, respectively. The plates were kept at 37°C overnight.

Until the next day, colonies emerged on the plates, and colony PCRs were run to amplify the region of interest. In this case, the potentially inserted gRNAs and Cas9 constructs. Colony PCRs are standard PCRs, described here in 3.2.4.1.4, but parts of the colonies were used for the

PCR reaction instead of DNA. Therefore, the colony was taken up from the plate with a 200µl tip, swirled in the PCR tube, and released in a pre-culture tube filled with 3ml of LB media+ appropriate antibiotics for further incubation. If the gel revealed the insertion of a gRNA into the vector, the pre-culture tube was shaken overnight at 30rpm and 37°C to multiply the number of E. coli.
On the next day, DNA isolation of DNA in E. coli was performed using the miniprep system without columns.

3.2.3.3 Miniprep

For the miniprep, the buffers from the Maxiprep kit were used.
For the miniprep, 1.5ml of the E. coli culture was decanted into a 1.5ml tube. The other half of the culture was stored at 4°C for inoculating a maxiprep later. A maxiprep was performed in case the gRNAs/ Cas9 of interest was in the DNA and furthermore, inserted into the right direction into the vector.
The 1.5ml tube was centrifuged for 5min at 6000rpm and the supernatant was discarded by drying the tube upside down on a paper tissue. The pellet was dissolved in 100µl of P1 buffer. 100µl of P2 buffer were added, and the tube was inverted several times to mix liquids. After an incubation of 5min at room temperature, 100µl of P3 buffer was added, and the tube was vortexed to mix everything. After another incubation of 5min at room temperature, the tube was centrifuged for 10min at 14.000rpm. The supernatant was transferred with a pipette into a fresh tube filled with 1ml of 100% ethanol, not touching any of the cell debris. The tube was centrifuged at 14.000rpm for 10min and the supernatant was decanted. The DNA pellet was washed with 150µl of 70% ethanol and centrifuged for 5min at 14.000rpm. The supernatant was removed making sure as much as possible of the ethanol was removed. The pellet was dried at 50°C and resuspended in 50µl of distilled water.
The DNA was sent for sequencing (see 3.2.4.1.5) to see if the desired insert was there in the correct direction.

3.2.3.4 Maxiprep

A maxiprep was used to amplify the desired construct in huge amounts. Therefore, 1.5ml of the pre-culture that was still left was poured into 300ml of LB media + appropriate resistance and was shaken overnight at 37°C at 30rpm. After 16h, the protocol for the kit "Endofree Plasmid Maxi Kit" from Qiagen was followed to perform the Maxiprep. Only slight modifications were made, which are mentioned here. All 300ml of starting culture were used, and the centrifugations were performed at 5000rpm for 1h at 4°C. At the end the concentration of the DNA was determined with the Nanodrop (3.2.4.1.3) and diluted to 1µg/µl.

3.2.4 Molecular Methods

3.2.4.1 DNA

3.2.4.1.1 Karyotyping: iPSCs

A karyogram of iPSCs was performed to see if there were any major structural or numerical aberrations in cells after reprogramming and genome editing, as those processes could lead to big changes in chromosomes. The karyogram was performed by the cytogenetic department of the human genetics institute in Mainz. As a preparation for that, cells were split in 2 wells of a 6-well plate and cultured until 70-80% confluent and then handed to [redacted]. Dividing cells were stopped with colcemid in their metaphase. Afterwards it is possible to analyze

metaphases of cells and determine if there were any chromosomal, numerical, or structural aberrations in the cells.
It was only continued to work with the cells if no aberrations were found.

3.2.4.1.2 DNA isolation

DNA often needs to be isolated to see if there are any changes in the DNA sequence, e.g., after willingly introducing a mutation by genome editing or vector generation. A protocol that was established in the lab was followed and is described here in detail.
After thawing a cell pellet (3.2.2.1), it was resuspended in 200µl SE-Buffer and aliquoted into three parts containing 10%, 20% and 50% of the suspension. It was continued to work with all three aliquots, since at the beginning it was not sure which aliquot had the right number of cells to give the best result. After filling up each aliquot to 200µl again, 20µl of 10%SDS and 20µl of proteinase K were added, and the tube was incubated at 50°C and 350rpm for 1h. Thereafter, 60µl of 6M NaCl were added, and the sample was vortexed for 15sec to then be centrifuged for 15min at 6000rpm at room temperature. The supernatant, containing DNA, was transferred into a fresh tube, and 600µl of 100% ethanol were added. Due to shaking the tube carefully, DNA precipitated and could be collected at the bottom of the tube by centrifuging for 20min at 14000rpm at room temperature. After the supernatant was discarded, the pellet was washed with 1000µl of 70% ethanol and spun for 5min at 14.000rpm at room temperature. The supernatant was discarded. The wash step was repeated once. The pellet was left to air-dry with an open lid for around 30min at 37°C, until the pellet was dry and all ethanol evaporated. DNA was solved in 20µl of sterile H_2O while incubating at 37°C for 30min. The concentration could then be determined with a nanodrop (3.2.4.1.3).

3.2.4.1.3 Nanodrop measurement

After RNA, DNA, or protein isolation, the concentration of each sample was determined using a Nanodrop device. In the Nanodrop software, it was chosen which concentration should be determined, and the instructions of the device were followed. After choosing the right measurement, 1µl of blank solution, the solution in which the RNA, DNA, and protein were eluted into, was added on the Nanodrop. Afterwards, the samples were measured one after the other using again 1µl. The concentration in the sample was given by the device and, if necessary, diluted to the needed concentration.

3.2.4.1.4 PCR

With the help of a polymerase chain reaction (PCR), it is possible to amplify certain, targeted parts in the DNA. In every reaction step the product is doubled and can at the end be used for subsequent analyses. Standard PCR protocol was followed and is not described here in detail.
The primers were usually designed to give a product of 300-500bp with the targeted mutation in the middle and to have a melting temperature of 60°C. Primers were designed using the software Primer3.
A negative and a positive control, if possible, were always taken along to control the experiment.

Table 18 Overview of regularly used ingredients and their amounts for one PCR reaction

Ingredient	**Amount [µl]**
PCR buffer	2.5µl
dNTPs	0.5µl
Primer F+R (10nM)	1 µl
Taq (FastStart)	0.2µl
H_2O	Up to 25 µl
DNA	100ng
∑:	25 µl

Table 19 Regularly used cycling steps for PCR reaction

Step 1	95°C	5min
Step 2	95°C	30sec
Step 3	60°C	30sec
Step 4	72°C	40sec
Go back to Step 2 for 34 more times		
Step 5	72°C	10min
Step 6	12°C	∞

After PCR the product was checked using standard agarose gel electrophorese. Therefore, 5µl of PCR product and 2µl of DNA staining dye (OrangeG) were loaded into a pocket of a gel, and current was applied at 100-180Watt for 10 - 40min. Afterwards, the gel was analyzed using UV light.

3.2.4.1.5 Sequencing

At several points in this work, it was necessary to analyze the DNA sequence of a product, e.g., after genome editing or gRNA generation. A standard Sanger sequencing was performed at Starseq, a company at the JGU.
After a cleanup of the PCR product via Exo-Sap digestion, the sample was sent to Starseq, and the results were analyzed using the software BioEdit.
For Exo-Sap digestion, the following reaction was used and incubated for 15min at 37°C and 15min at 90°C. The tube could be kept at 12°C afterwards if necessary.

Table 20 Ingredients and their volume for one Exo-Sap digestion reaction

Ingredients	**Amount**
H_2O	4.875µl
Ex1	0.225µl
SAP	0.9µl
PCR-Product	25µl

For the sequencing 1µl of cleaned-up PCR product, 1µl of forward or reversed primer and 5µl of H_2O were mixed and sent for sequencing.

3.2.4.2 RNA

3.2.4.2.1 RNA isolation

RNA isolation was performed with the High Pure RNA Isolation Kit from Roche following the slightly modified protocol of the manufacturer. Here described shortly.
The cell pellet was resuspended in 200µl of DPBS, 400µl of Lysis/-Binding Buffer were added, and the sample was vortexed for exactly 15s. After transferring the sample into the High Filter

Tube, inserted into the Collection Tube, the sample was centrifuged for 30s at 8000g. 90µl of DNase Incubation Buffer and 10µl of DNase I were mixed and added on the glass filter fleece of the High Filter Tube. After an incubation of exactly 15min at RT, the flowthrough was discarded, and 500µl of Wash Buffer I were added to the Filter Tube. The flowthrough was again discarded after a centrifugation of 30sat 8000g, and 500µl of Wash Buffer II were added. Again, a centrifugation of the sample for 30s at 8000g was performed, and the flowthrough was discarded. 200µl of Wash Buffer II were added again, and a centrifugation for 2min at 13.000g was run to remove any residual wash buffer. The Filter Tube was then transferred into a labeled 1.5ml Eppendorf tube and 30µl of elution buffer were added directly on the glass fleece. After an incubation of 1min, the sample was spun for 1min at 8000g, so RNA would be collected in the Eppendorf tube.

3.2.4.2.2 cDNA synthesis

For cDNA synthesis, RNA is reverse transcribed into cDNA and can then be used in, e.g., RT-qPCR. Therefore, RNA is diluted to a concentration of 100-500ng/µl; otherwise volumes that need to be pipetted would be too small and more prone to error.

PrimeScript™ One Step RT-PCR Kit, Ver.2 from TaKaRa Bio was used to transcribe RNA into cDNA. For one reaction, a maximum of 500ng of RNA could be used. RNA is diluted with water to a concentration of 500ng in 8µl, and 2µl of TaKaRa solution were added. The sample was incubated in a PCR cycler for 15min at 37°C and for 5s at 85°C. It could be stored at 4°C for short-term storage, at -20°C for long-term storage, or directly be diluted to 5ng/µl and used for RT-qPCR.

3.2.4.2.3 RT- qPCR

RT-qPCR is the abbreviation for reverse transcriptase quantitative polymerase chain reaction and is built on the main principle that SYBR green, a fluorescing dye, can intercalate into the minor groove of cDNA, which is doubling in every PCR cycle. With every cycle the amount of cDNA is doubled, the double amount of dye can intercalate, and the fluorescent intensity is doubled. A threshold is set for the intensity of the fluorescence, and the cycle at which the intensity is reached can be determined. Therefore, the expression level of the gene of interest in the sample can be determined.

With RT-qPCR, it is possible to analyze several genes at the same time, always relating them to a housekeeping gene that is constantly expressed in all tissues. In this project GAPDH was used as a housekeeping gene.

First, one master mix per gene was pipetted with 0.4µl of the primer, forward and reverse combined and diluted to 10µM, 5.2µl of TaKaRa solution, and 2.4µl of H_2O per reaction. Next, a transparent 96-well plate was put on a cooling block, and 2µl of cDNA with a concentration of 5ng/µl were pipetted at the bottom of the wells without touching other parts of the well. For each gene, triplicates of the sample were pipetted into a 96-well plate.

Eight microliters of the master mix were pipetted at the upper border of each well, without touching the cDNA.

After plating all samples with all master mixes for all genes and the negative controls (only master mix, no cDNA), the plate was sealed with a transparent foil, spun to collect all liquid at the bottom of the wells, and placed into the plate reader.

The program of the plate reader started with a holding stage at 95°C for 15min. Afterwards, 40 cycles were run with 95°C for 15sec, 60°C for 30sec and 72°C for 40sec. Data was collected at 72°C. Subsequently, a melt curve was run with 60°C for 1min and up to 95°C for 15sec with 0.3°C per step.

The analysis of the run was performed manually by transferring the raw data into an Excel file. For each gene, the ΔCt values given by the device were used and divided by the mean of the control sample to generate the ΔΔCt values. Those values were then used for statistical analysis and the presentation of results via Prism, different for each experiment.

3.2.4.3 Protein

Proteins of interest were investigated within three different methods in this work. First, proteins were isolated from cell pellets right after harvesting cell pellets and were used for western blot analyses to quantify the protein amount of a protein of interest in certain cells. Second, cells could also be fixed on coverslips and stained with primary and secondary antibodies for proteins of interest. And third, cells could be fixed in suspension and stained for proteins of interest that could be quantified via FACS.

3.2.4.3.1 Protein isolation

Cell pellets (compare 3.2.2.1) were generated from the sample of interest, but instead of transferring the pellet into a 1.5ml tube, it was resuspended in an appropriate volume of Magic Mix and pipetted up and down to be fully resuspended; if the suspension was too viscous, more Magic Mix was added. The whole suspension was transferred into spin columns and centrifuged at 12.000rpm for 2min. The flowthrough containing proteins was transferred into a fresh 1.5ml tube and stored at -80°C until further processing.

3.2.4.3.2 SDS gel-electrophoresis and western blot

SDS gel electrophoresis and the subsequent western blot are used to quantify the amount of a protein of interest in a sample.

Via SDS gel electrophoresis it is possible to separate proteins within a sample, after protein isolation (3.2.4.3.1), by size. Therefore, all samples are diluted with H_2O to the same concentration and mixed with loading dye (Magic Mix + bromophenol blue) in a 2:1 (protein: loading dye) ratio. After a denaturation at 95°C for 2min, samples plus markers (HiMark for big proteins and PAGE ruler for small proteins) were loaded in the prepared gel. The gel consisted of two parts, stacking and separating gel. Samples were loaded into the stacking gel, which collects all samples at the border to the separating gel, in which they were separated by size. Usually, a 6% separating gel for BRCA1 and BRCA2 proteins were used as well as a 10% separating gel for the housekeeping protein ACTIN. Gels were run for 60min at 200V within a running buffer (3g Tris, 14.4g Glycin, 1g SDS for 1L) and transferred onto nitrocellulose membranes with a TurboBlot device, a semi-dry method using the Trans-Blot Turbo RTA Midi 0.2 µm Nitrocellulose Transfer Kit from Biorad. Therefore, a stack of paper, membrane, gel and paper was built and put into the device. The whole stack was wet carefully with blotting buffer. The chosen program of the device was the high molecular weight program, which provides blotting conditions of 1.3A, 25V for 10min. A Ponceau staining was performed to check that the blotting of proteins onto the membrane worked as expected. Afterwards the membrane was blocked with 5% milk powder in DPBS for 60min at room temperature while rolling on a roller in a 50min Falcon. Membranes were washed three times for 5min at room temperature with PBST (2 PBS tablets, 1ml Tween for 1L) and incubated overnight at 4°C with the target antibodies. On the next day, the membrane was washed again three times for 5min at room temperature with PBST and thereafter incubated with the secondary antibody for 60min at room temperature.

After another washing for three times 5min at room temperature with PBST, proteins were detected using the ECL kit (based on the HRP principle) in the Fusion FX device from Vilber.

Subsequent analysis and quantification of proteins was performed with Fiji. Therefore, pictures for AKTIN, BRCA1, and BRCA2 were opened at the same time. A box, which fitted all bands, was drawn and put around every band. Several lanes could be marked, and all lanes of one blot could be plotted as curves. The background of the blot/ the part below the curve, was subtracted from the curve, and the area under the curve was determined. With those areas, statistics were performed afterwards. Therefore, the area of the BRCA1 and BRCA2 bands was normalized against the area of AKTIN. Afterwards they were set into relation with the control sample within the blot, and subsequently statistics were calculated.

Table 21 Recipe for 10% and 6% separating gel and

Ingredients:	**1 gel / 10%**	**1 gel / 6%**
H_2O	1.9ml	4.2ml
1.5 M Tris pH 8.8	1.3ml	2ml
30% Acrylamide	1.7ml	1.6ml
10% SDS	50µl	80µl
10% APS	50µl	80µl
TEMED	2µl	8µl

for stacking gel

Ingredients:	**1 gel**
H_2O	1.4ml
0.5 M Tris pH 6.8	250µl
30% Acrylamide	330µl
10% SDS	20µl
10% APS	20µl
TEMED	2µl

3.2.4.3.3 Staining (Fibroblasts, iPSCs, NPCs)

For staining, cells need to be fixed on coverslips and washed thrice with DPBS. DPBS was removed, and 1ml of blocking solution (5% BSA, 0.3% Triton X100 in DPBS) was added per well. After an incubation of 30- 60min at room temperature, the supernatant was removed, and coverslips were put upside down on 50µl of primary antibody on a 12-well plate covered with parafilm. After incubating overnight at 4°C in a Styrofoam box with wet tissues, coverslips were placed back into the 12-well plated cells facing upwards and washed thrice for 5min at room temperature with 1ml of wash buffer (0.3% TritonX 100 in DBPS). For incubating the secondary antibody, coverslips were again put onto the parafilm-covered 12-well plate with 50µl of secondary antibody. After an incubation for 60min at room temperature in the dark, coverslips were put back into the 12-well plate and washed again thrice with wash buffer. For mounting two coverslips on one slide, coverslips were taken out from the 12-well plate, dried on a tissue, and placed upside down onto 10µl of Fluoromount on slides. After a hardening phase of 24h at 4°C, it was possible to take pictures of the cells. The microscope for taking pictures was the revolve from ECHO.

4 Results

4.1 Cell line generation and characterization

Before performing any experiment with the cell lines, it was necessary to confirm that the cells showed the typical cell type-specific morphology and expression pattern. Otherwise, potential observed differences between cell lines could be caused by mutation or by abnormal characteristics of the cell line. An overview of all cell lines can be found in Table 12.

4.1.1 Fibroblasts

In this project, three different fibroblast lines were used. A male and a female control cell line, both having *BRCA2* and *BRCA1* wildtype alleles, and an additional cell line derived from a female patient carrying a heterozygous mutation in the *BRCA2* gene.

4.1.1.1 Morphology

All three cell lines showed an elongated cell morphology and grew in monolayers (Figure 9) with a steady growth rate that is typical for fibroblasts.

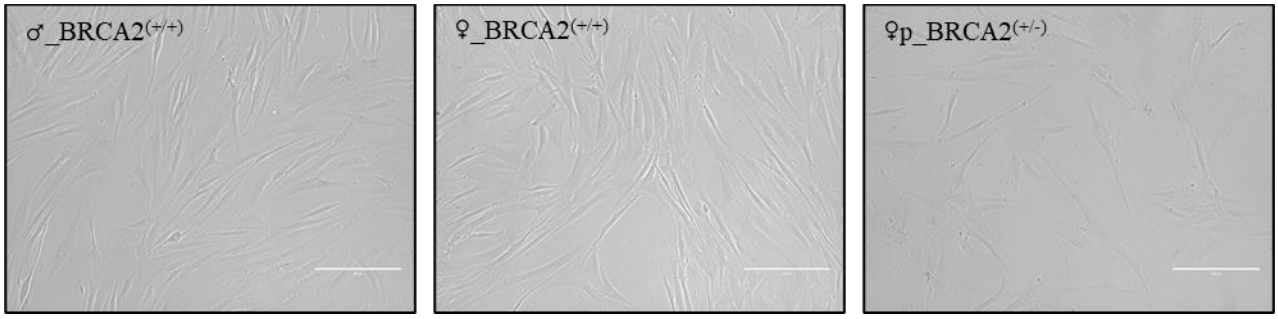

Figure 9 Morphology of three fibroblast cell lines. Bright-field pictures of fibroblasts with an elongated morphology. The picture of ♀p_BRCA2$^{(+/-)}$ shows fewer cells compared to the wildtype samples as this picture was taken two days after splitting, while the other two pictures were taken four days after splitting. The scale bar has a length of 200µm.

4.1.1.2 Immunofluorescent staining

All three fibroblast lines were stained for SERPINH1 (Figure 10), a protein binding specifically to collagen. Both skin fibroblasts and SERPINH1 play an important role in the generation of collagen. The key protein SERPINH1 functions as an essential chaperone for efficient folding of collagen triple helices in the endoplasmic reticulum (ER). Therefore, SERPINH1 can be used as a marker for fibroblasts. SERPINH1 is located in the cytoplasm.

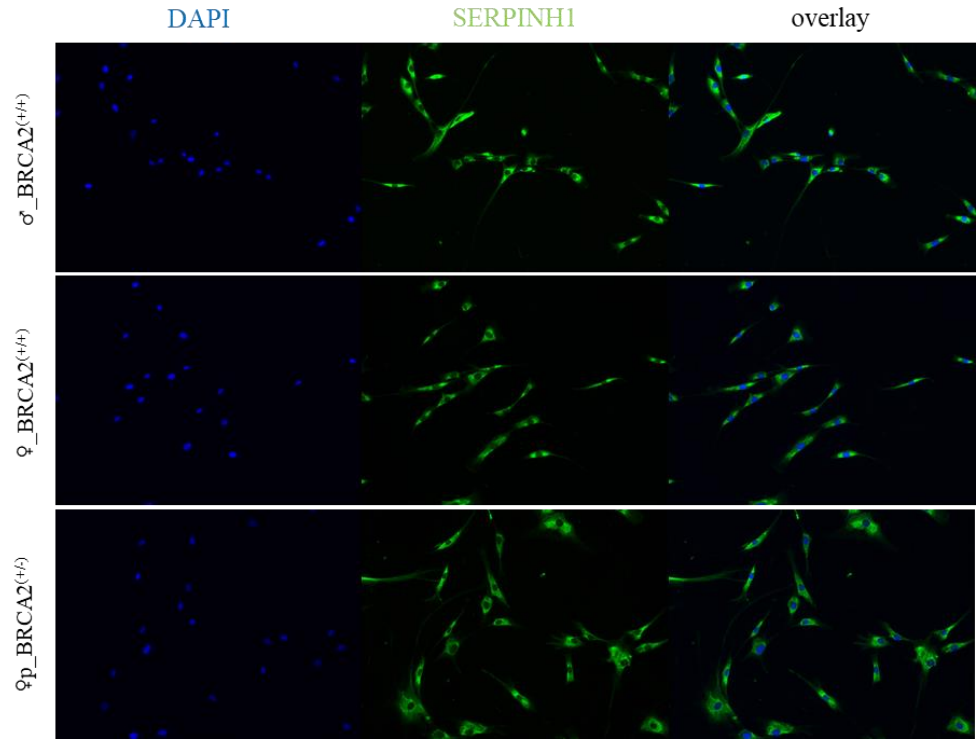

Figure 10 Immunofluorescent staining for SERPINH1 in the three fibroblast cell lines. All three cell lines show SERPINH1 expression in their cytoplasm. DAPI is staining the nucleus of each cell. The magnification in these pictures is 10x.

4.1.2 iPSCs

In this project six different iPSC lines were used. The male and female fibroblast cell lines described above had already been reprogrammed by [redacted] to generate iPSC lines for another project. Those cell lines were used as control cell lines, and their genomes were additionally edited via CRISPR/Cas9. From the male cell line, three different isogenic cell lines were generated, while from the female cell line, one isogenic cell line was generated.

4.1.2.1 Genome editing

Four genome-edited cell lines were generated via CRISPR/Cas9. For the male cell lines, the wildtype cell line ♂_*BRCA2*$^{(+/+)}$ was used for genome editing. ♂_*BRCA2*$^{(+/-)}$ was a male cell line carrying a heterozygous mutation (c.[4524_4525insA]) in the *BRCA2* gene. The cell line ♂_*BRCA2*$^{(-/-)}$ carried two compound heterozygous mutations in the *BRCA2* gene: c.[4523_4524insA]; [4518_4523delCCAGGG]. One heterozygous mutation in the *BRCA1* gene, c.[2030_2045delTTTTACAAAACCCATA], could be found in the ♂_*BRCA1*$^{(+/-)}$ cell line.

In the female wildtype cell line, ♀_*BRCA2*$^{(+/+)}$, a heterozygous mutation (c.[4524_4526delinsGC]) was inserted into the *BRCA2* gene, generating the cell line ♀_*BRCA2*$^{(+/-)}$.

The mutations in *BRCA2* were inserted in exon 11 of the *BRCA2* gene, in close proximity to the mutation of the patient fibroblast cell line. The mutation in the *BRCA1* gene was also inserted in exon 11, which is the largest exon of the *BRCA1* gene and with its structure, binding domains, and size, similar to exon 11 in the *BRCA2* gene; compare Figure 11.

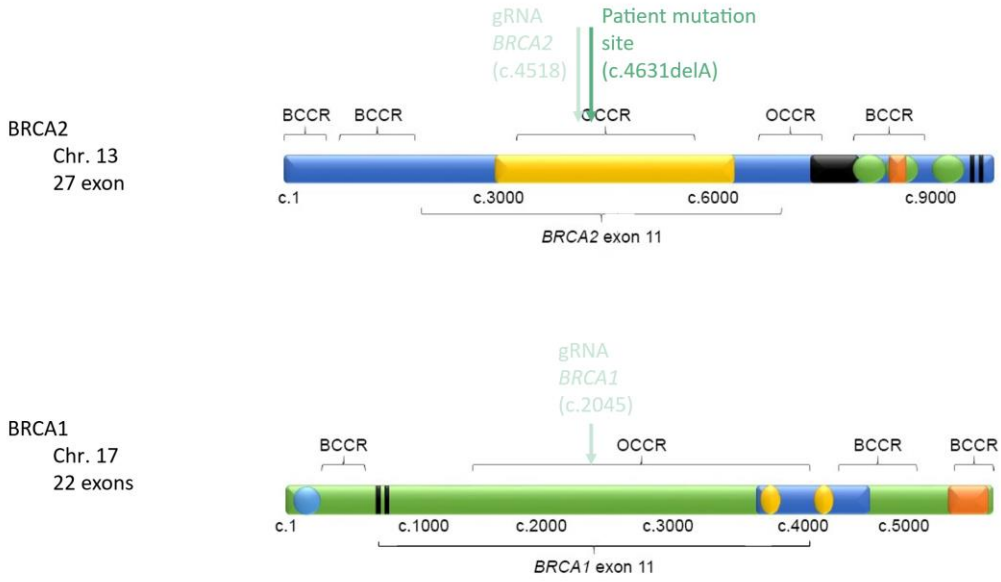

Figure 11 Scheme of BRCA2 and BRCA1 gene . Depicted are the main structural elements, exon 11 as the biggest exon in both genes, and the target sites for the gRNAs, as well as the site of the patient's mutation in the *BRCA2* gene.

In both cell lines, male and female, the same gRNA targeting the *BRCA2* gene was used. For editing *BRCA1*, a different gRNA was used.

Sequencing chromatograms of those four cell lines are depicted in Figure 12 .

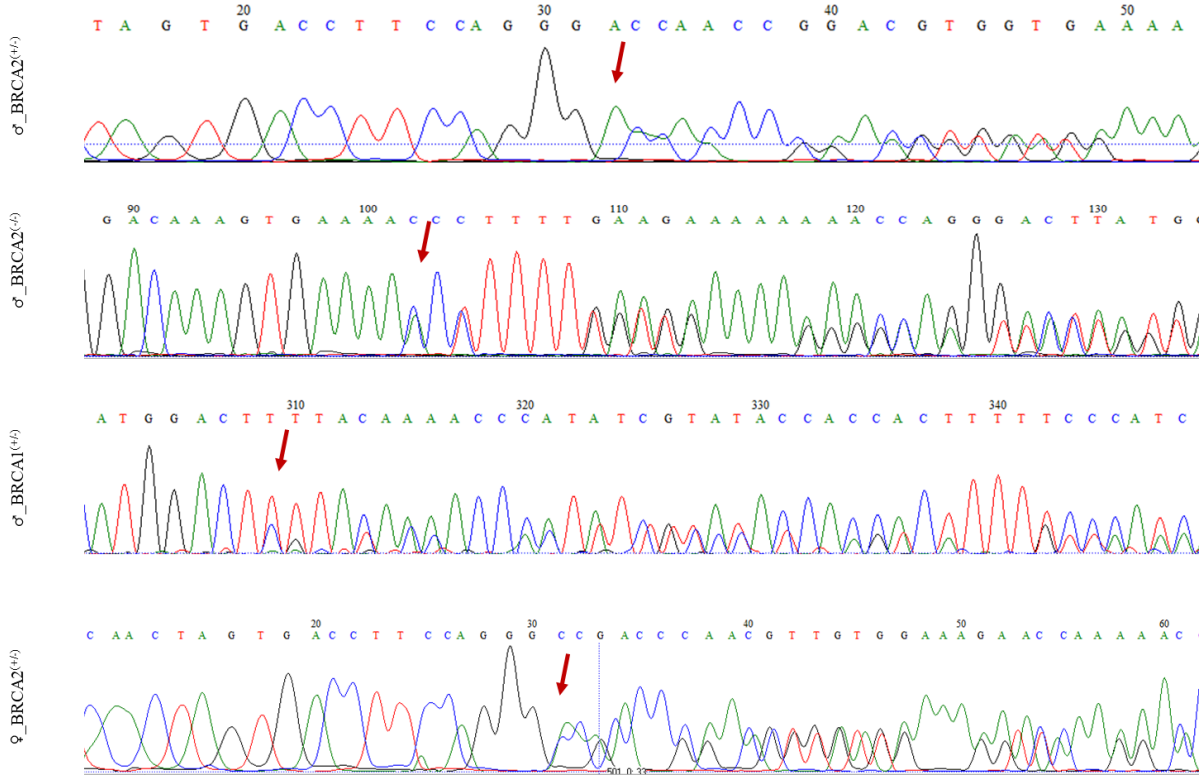

Figure 12 Sequencing chromatograms of the genetically modified cell lines ♂_BRCA2$^{(+/-)}$, ♂_BRCA2$^{(-/-)}$, ♂_BRCA1$^{(+/-)}$ and ♀_BRCA2$^{(+/-)}$. Red arrows indicate the mutation site in each chromatogram. ♂_*BRCA2*$^{(+/-)}$ and ♀_*BRCA2*$^{(+/-)}$ were sequenced with a forward primer for *BRCA2*, while ♂_*BRCA2*$^{(-/-)}$ was sequenced with a reverse primer.

4.1.2.2 Karyotype

The karyotype of each cell line was analyzed in the diagnostics department of the Institute of Human Genetics at the University Medical Center in Mainz.

All male cell lines showed a 46, XY karyotype, while both female cell lines showed a 46, XX karyotype. Numerical or structural aberrations could not be detected in any of the cell lines (Figure 13).

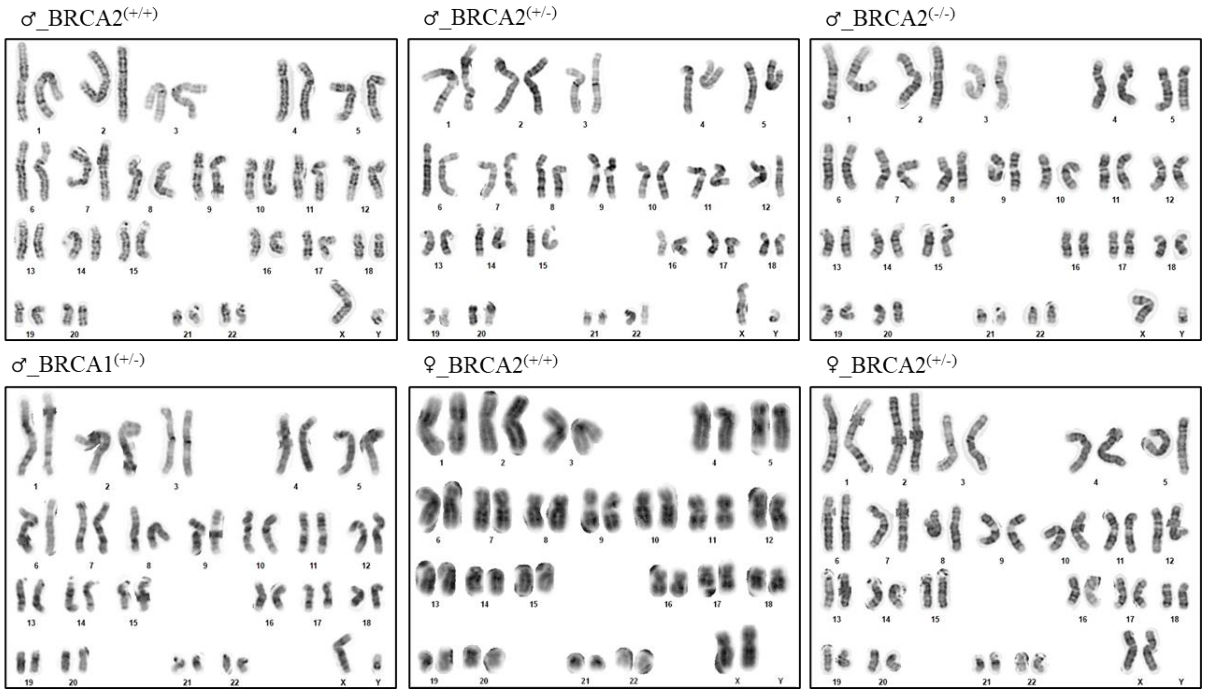

Figure 13 Karyotypes of all iPS cell lines. All karyotypes show regular karyotypes for the male cell lines with 46, XY and the female cell lines with 46, XX without any numerical or structural aberrations.

4.1.2.3 Morphology

Bright-field pictures of iPSCs show cells in compact colonies with sharp borders and in monolayers (Figure 14). Cells have a round shape and prominent nuclei, accounting for around 90% of total cell volume. Cells showed a steady growth rate.

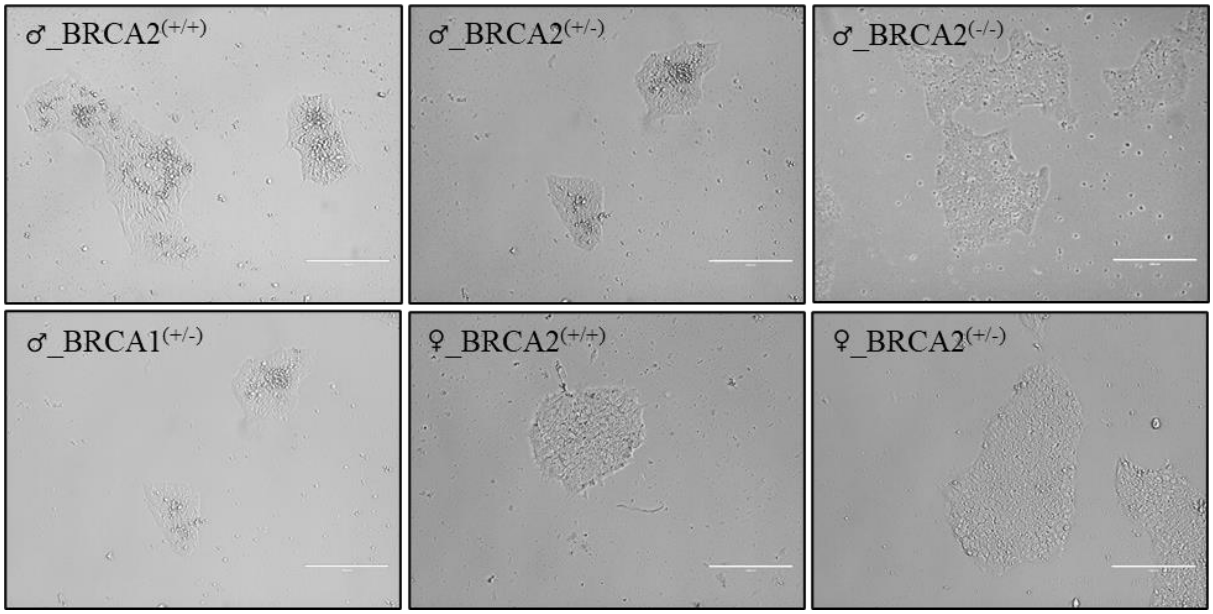

Figure 14 Morphology of all iPSC lines. Bright-field pictures show compact iPSC colonies in monolayers with sharp borders, round single cells, and prominent nuclei within cells. The scale bar has a length of 200µm.

4.1.2.4 Immunofluorescent staining

iPSCs were stained with antibodies against the pluripotency markers NANOG and TRA-1-60 (Figure 15). NANOG is a transcription factor controlling stem cell proliferation, renewal, and pluripotency and is localized in the cell's nucleus, therefore overlaying with a DAPI staining (Gong et al., 2015). TRA-1-60 is also a marker for pluripotent stem cells but localizes on the cell surface (Neganova et al., 2016). A negative control staining in iPSCs without the primary antibody controlled for non-specific binding of the secondary antibody and background fluorescence in the cells. Positive controls with cells that had already been characterized as iPSCs were always taken along.

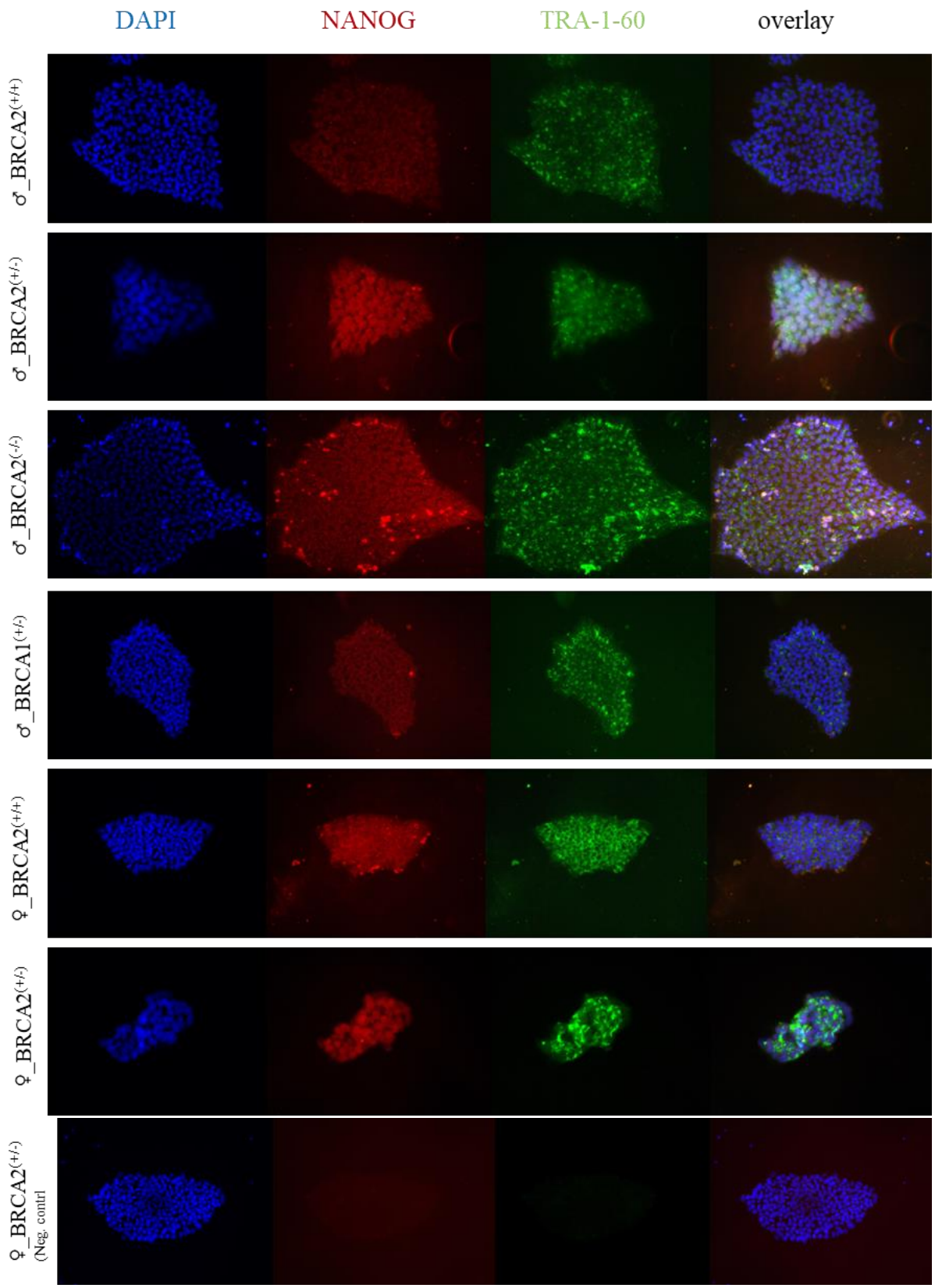

Figure 15 Immunofluorescent staining of all iPS cell lines. The staining showed that all cell lines expressed the pluripotency markers NANOG and TRA-1-60. For the negative control, cells were not stained with the primary antibody. All other steps of the staining protocol remained the same. Magnification in these pictures is 10x.

A close-up of the cells of each cell line is depicted in Figure 16. The close-up showed merged staining of DAPI, NANOG, and TRA-1-60.

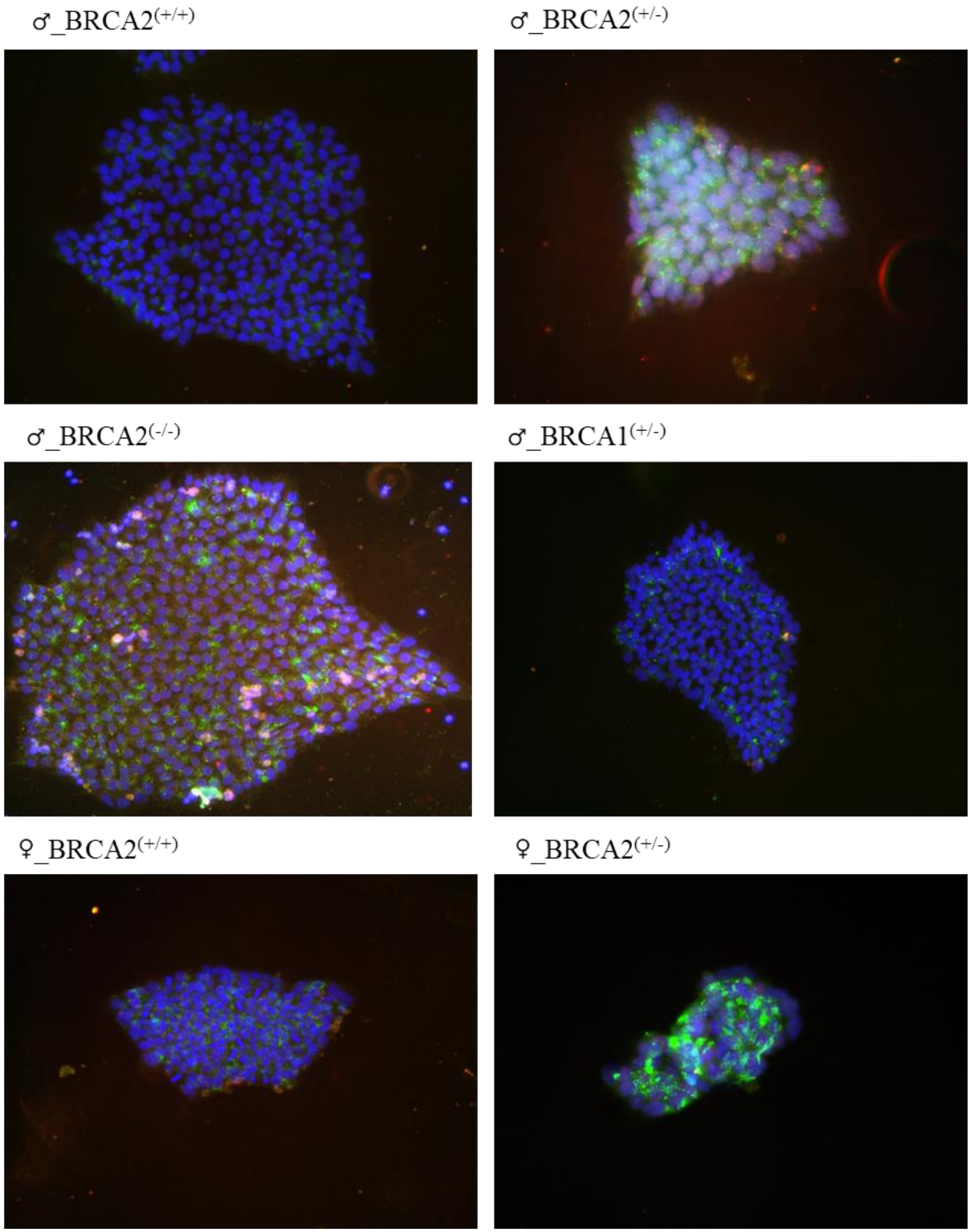

Figure 16 Close-ups of merged staining pictures of all iPSC lines. The expressions of DAPI, NANONG, and TRA-1-60 could be observed in every cell line. The magnification of cells is 10x.

4.1.3 NPCs

Neural progenitor cells (NPCs) were used in this work to investigate the effect of formaldehyde on RNA and protein levels, proliferation, quantity of DSB, and cell cycle analysis. In addition,

neurospheres were generated from these cells to investigate the effect of formaldehyde on proliferation and migration in a 3D model. NPCs from six different iPSC lines were used. Male and female wildtype NPCs had already been generated before by [redacted]. Genome-edited NPCs carrying mutations in either the *BRCA2* or *BRCA1* gene were generated for this project. Cells were cultured until passage 20.

4.1.3.1 Morphology

All NPCs grew in monolayers, as expected. They showed slightly elongated structures. Most cells showed a regular phenotype and no axon-like structures, which would point towards spontaneous differentiation. Growth rate was consistent over time within the same cell line and similar for all cell lines.

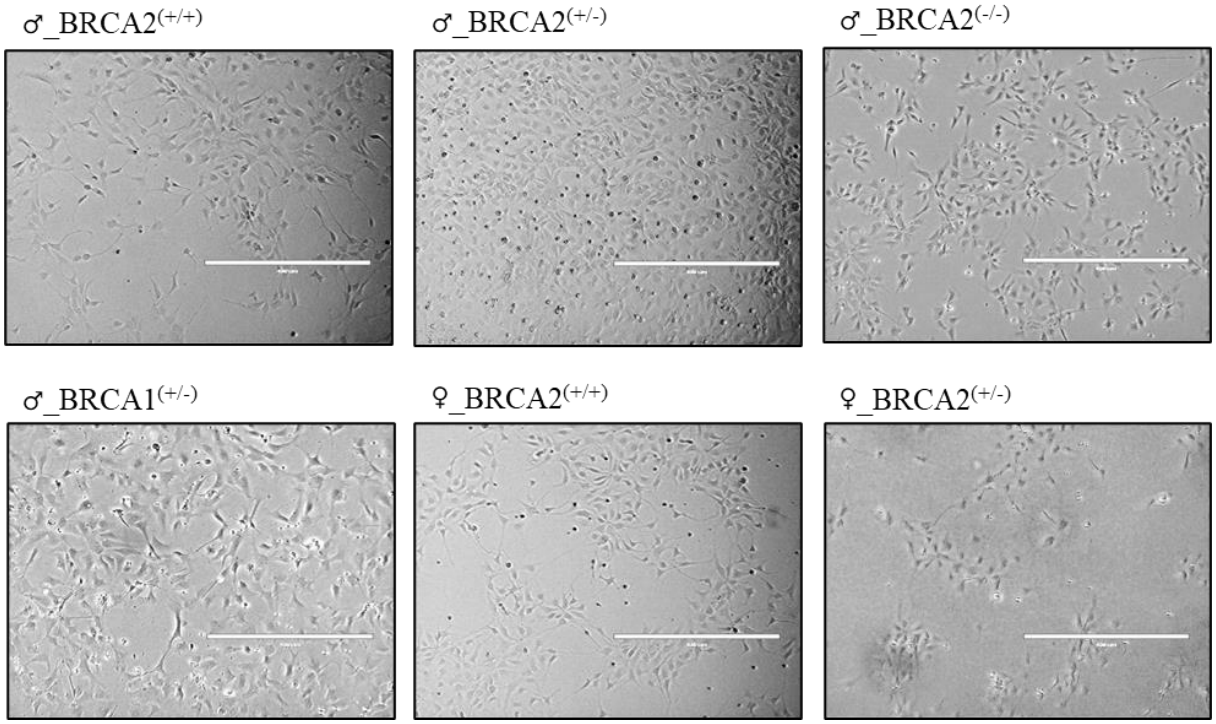

Figure 17 Morphology of all NPC lines. Bright-field pictures show NPCs growing in monolayers. Single cells partly display elongated structures. The scale bar has a length of 400µm.

4.1.3.2 Immunofluorescent staining

NPCs were further characterized by immunofluorescent staining of the markers SOX2, PAX6, and NESTIN. All cell lines stained positively for the three markers. As expected, transcription factors SOX2 and PAX6 co-localized with DAPI in the nucleus. The intermediate filament protein NESTIN could be detected in the cytoplasm of the cells. A negative control staining in NPCs without the primary antibody controlled for non-specific binding of the secondary antibody and background fluorescence in the cells. SOX2 is a transcription factor, which is essential for stem cell self-renewal and cellular reprogramming (Avilion et al., 2003; S. Zhang et al., 2020). It is expressed in iPSCs and NPCs. PAX6 is also a transcription factor and is expressed in multiple cell types during development and maintenance of the CNS (Ochi et al., 2022). It is only expressed in NPCs but not in iPSCs. NESTIN is an intermediate filament and strongly expressed in NPCs (Bott et al., 2019).

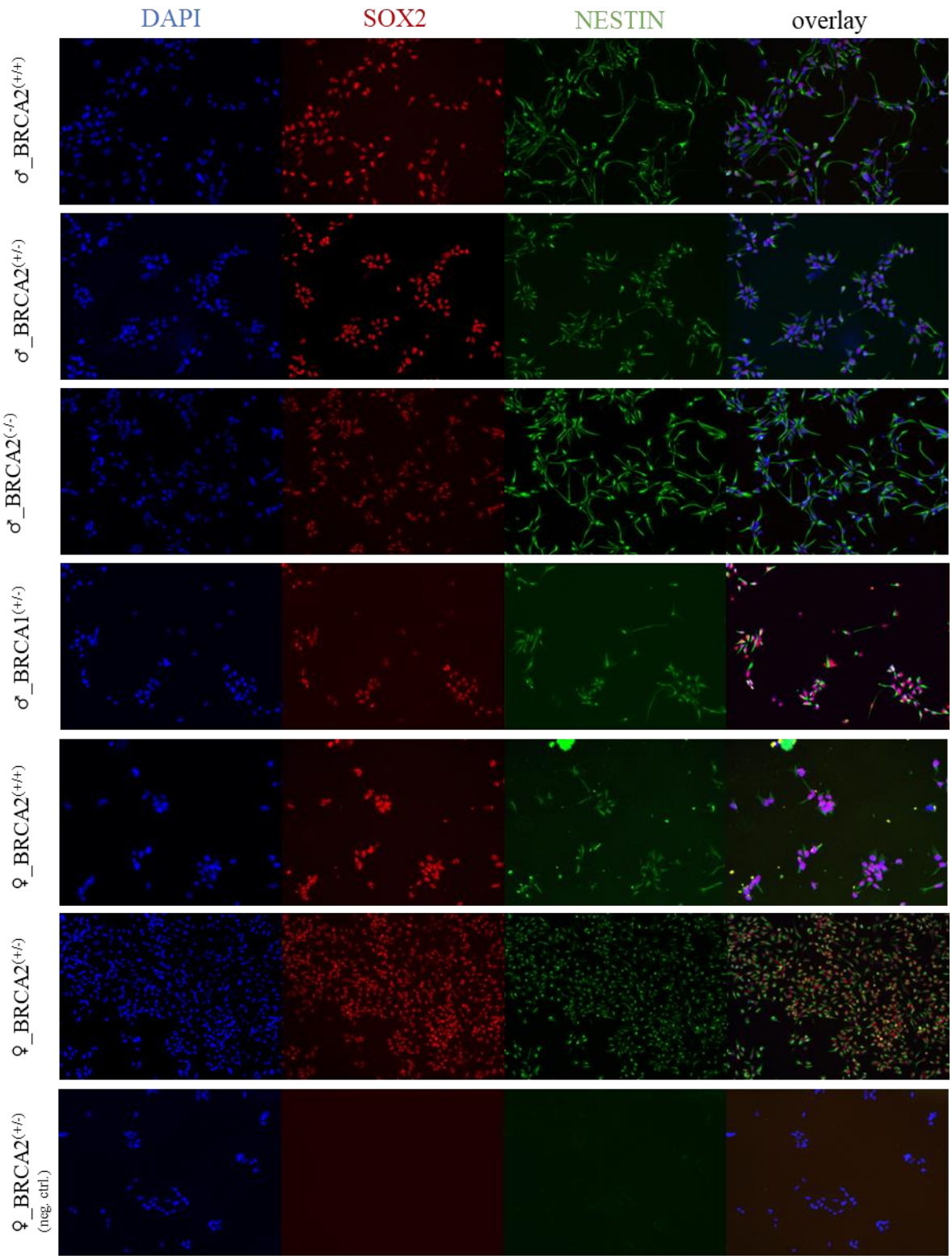

Figure 18 Immunofluorescent staining of SOX2 and NESTIN in all NPC lines. The staining showed that all cell lines expressed the markers SOX2 and NESTIN. For the negative control, cells were not stained with the primary antibody. All other steps of the staining protocol remained the same. The magnification in these pictures, besides ♀_BRCA2$^{(+/-)}$, is 10x. For ♀_BRCA2$^{(+/-)}$ it is a magnification of 4x.

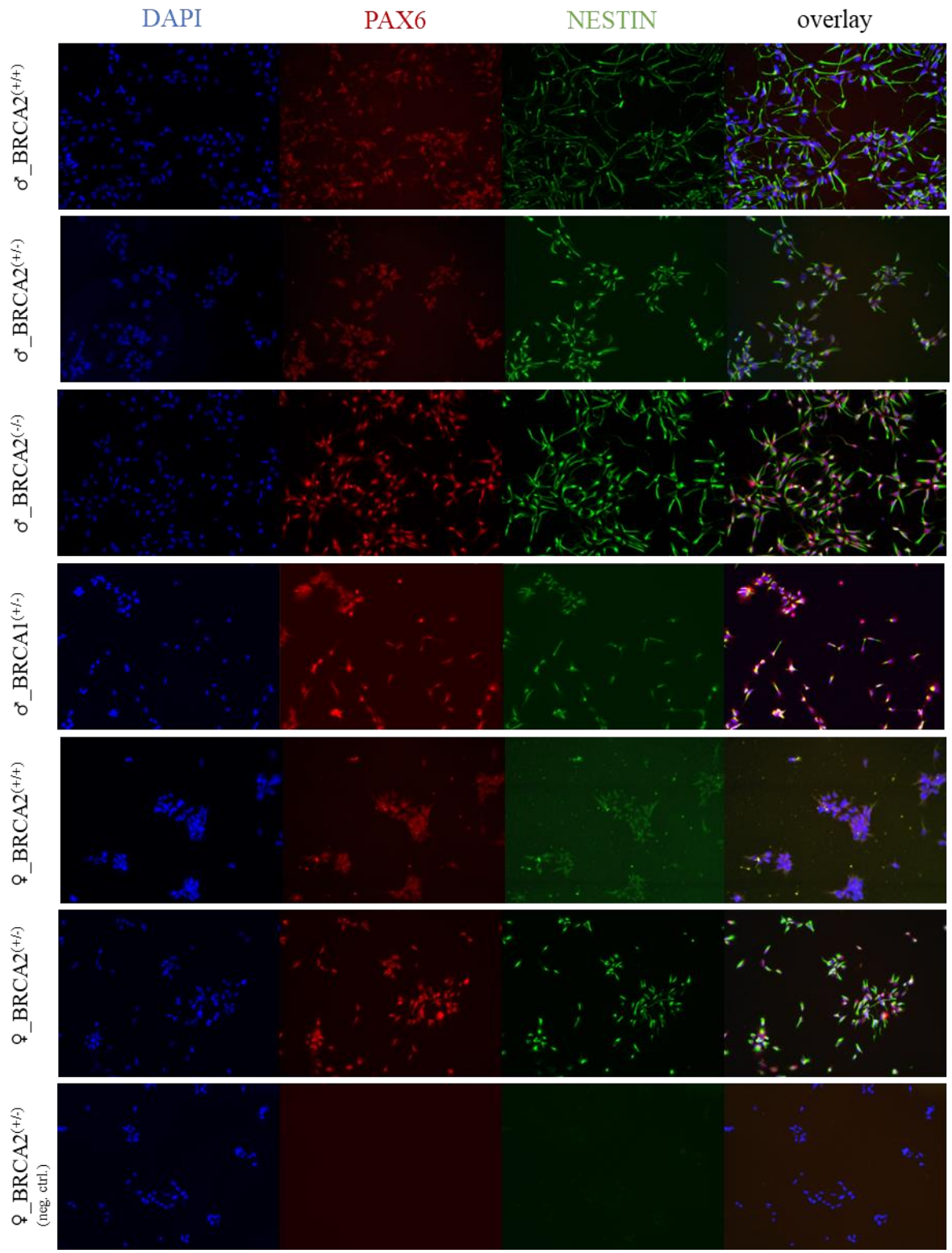

Figure 19 Immunofluorescent staining of PAX6 and NESTIN in all NPC lines. The staining showed that all cell lines expressed the markers PAX6 and NESTIN. For the negative control, cells were not stained with the primary antibody. All other steps of the staining protocol remained the same. The magnification in these pictures is 10x.

4.1.3.3 RT- qPCR

NPCs were also characterized via RT-qPCR to check if markers for pluripotency, stem cells, and NPCs are expressed at expected levels. Four biological replicates were used, and the ΔΔct-method was applied for the analysis. First, ct-values of the genes of interest of each NPC and iPSC line were normalized against *GAPDH* expression of the same cell lines. This generated

Δct-values. Second, Δct-values of the NPCs were normalized against the mean of the Δct-values of iPSCs. This produced ΔΔct-values, which were plotted in the graph.
As can be observed in Figure 20, the pluripotency markers *NANOG* and *OCT4* in NPCs were downregulated between 5- and 10-fold on the log2 scale compared to iPSCs. The stem cell marker *SOX2* was similarly expressed in NPCs compared to iPSCs, which is as expected, as it is a general marker for stem cells. As expected, NPC markers *NESTIN* and *PAX6* were upregulated 5- to 10-fold on a log2 scale in all cell lines compared to iPSCs. *KLF4* was downregulated in ♂_*BRCA2*$^{(-/-)}$ and ♀_*BRCA2*$^{(+/-)}$ cells, which is as expected. In ♂_*BRCA2*$^{(+/-)}$ cells *KLF4* was equally expressed in NPCs compared to iPSCs, while it was upregulated in ♂_*BRCA1*$^{(+/-)}$ NPCs compared to iPSCs.

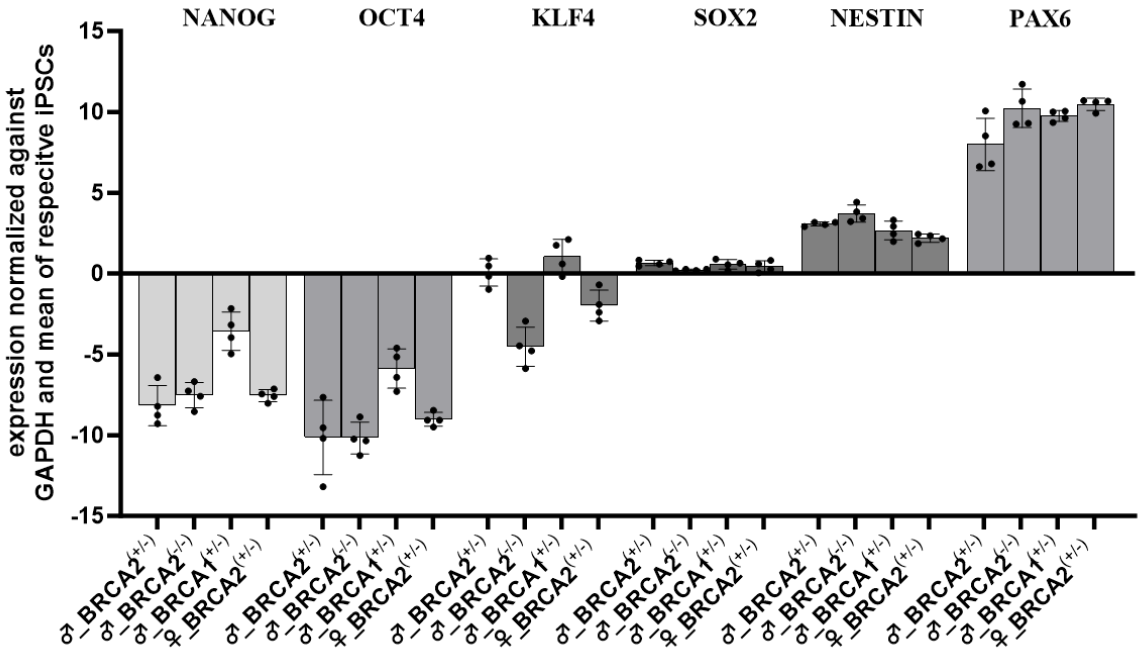

Figure 20 RT-qPCR results for the characterization of NPCs. RNA expression was analyzed via RT-qPCR, and ct-values were normalized against *GAPDH* and the mean of the normalized ct-values of the wildtype iPSCs. Each dot resembles one biological replicate of the cell line. Statistics were not applied. RT-qPCR results showed that in all cell lines the pluripotency markers *NANOG and OCT4* were downregulated compared to the expression in iPSCs, while the stem cell marker *SOX2* showed similar levels and NPC markers *PAX6* and *NESTIN* were upregulated. *KLF4* was inconsistent between cell lines.

A hypothesis is that ♂_*BRCA1*$^{(+/-)}$ cells might be less differentiated compared to the other cell lines. They showed higher ΔΔct-values of *NANOG* and *OCT4* levels and even positive ΔΔct-values for *KLF4* compared to the other cell lines. As the expression of *SOX2*, *NESTIN* and *PAX6*, the staining (4.1.3.2), and the morphological analysis (4.1.3.1) were regular and as expected, work continued with these cells.
As the analysis was only qualitative, but not quantitative, no statistics were applied, and the cell lines were not compared with each other. The question of this experiment was not to compare the different cell lines with each other but to compare expression levels of certain markers between different cell types within each cell line.
The control cell lines were not characterized via RT-qPCR, as those had been analyzed before and were not necessary as controls for the edited cell lines in this analysis. Controls were always internal within one cell line: NPCs relative to iPSCs.

4.2 *BRCA2* and *BRCA1* RNA and protein expression in all cell types

In order to investigate if and how RNA and protein expression was influenced by the introduced mutations in the different cell lines and cell types, RNA and protein expression levels of BRCA1 and BRCA2 in fibroblasts, iPSCs, and NPCs were examined. With this information on changes in RNA and protein levels due to a mutation, it is possible to link further results to those mutations.

For this experiment, characterized cell lines, introduced in 3.1.9, were used. Those cell lines were male wildtype and female patient fibroblasts, as well as male wildtype iPSCs and NPCs with their isogenic cell lines; compare Table 12.

4.2.1 RNA

RNA expression levels of all cell types of all cell lines were determined by RT-qPCR. The ΔΔct method was applied for the analysis. First, ct-values of the genes of interest were normalized against *GAPDH* expression in each cell line, for each cell type, and for each replicate. This led to Δct-values. Then, Δct-values were normalized against the mean of Δct-values of iPSCs. So, fibroblasts and NPCs against the mean of iPSCs. And Δct-values of iPSCs against their own mean. This produced ΔΔct-values, which were plotted in a graph.

For comparisons within each cell type, the mean of ΔΔct-values of each sample was calculated and set into relation to the mean of ΔΔct-values of the respective wildtype sample (Table 22). Therefore, the average *BRCA1* and *BRCA2* expression of each cell type could be depicted. For example, in NPCs, *BRCA1* expression in the wildtype sample was set to 100%. *BRCA1* expression was 84% in the ♂*_BRCA1*$^{(+/-)}$ NPC sample, and it could be stated that there was a reduction of averagely 16% of *BRCA1* RNA level in the ♂*_BRCA1*$^{(+/-)}$ sample compared to the wildtype sample. In the ♂*_BRCA2*$^{(+/-)}$ sample, *BRCA1* expression was 102%. No reduction could be observed, which is as expected, as there is no mutation in the *BRCA1* gene in this cell line.

Table 22 Means of ΔΔct-values of all biological replicates within one cell type of each cell line for the BRCA1 and BRCA2 genes

Cell type	Cell line	*BRCA2* [%]	*BRCA1* [%]
fibroblasts	♂_BRCA2$^{(+/+)}$	100	100
	♀p_BRCA2$^{(+/-)}$	34	56
iPSCs	♂_BRCA2$^{(+/+)}$	100	100
	♂_BRCA2$^{(+/-)}$	80	107
	♂_BRCA2$^{(-/-)}$	48	110
	♂_BRCA1$^{(+/-)}$	94	113
NPCs	♂_BRCA2$^{(+/+)}$	100	100
	♂_BRCA2$^{(+/-)}$	61	102
	♂_BRCA2$^{(-/-)}$	54	105
	♂_BRCA1$^{(+/-)}$	74	84

For *BRCA2* RNA expression, very low levels could be found in fibroblasts compared to iPSCs (Figure 21). In the ♀p_*BRCA2*$^{(+/-)}$ cell line, *BRCA2* expression was reduced by 66% (100% (♂_BRCA2$^{(+/+)}$) - 34% (♀p_BRCA2$^{(+/-)}$) = 66%) compared to the male wildtype fibroblast cell line (compare Table 22).

In iPSCs, *BRCA2* levels were reduced by 20% in the ♂_*BRCA2*$^{(+/-)}$ and by 52% in the ♂_*BRCA2*$^{(-/-)}$ cell lines compared to the ♂_*BRCA2*$^{(+/+)}$ cell line. In the ♂_*BRCA1*$^{(+/-)}$ cell line, *BRCA2* expression was averagely reduced by 6%.

In NPCs, a similar picture could be observed with average reductions of 39% (♂_BRCA2$^{(+/-)}$) and 46% (♂_BRCA2$^{(-/-)}$) for the mutated BRCA2 cell lines and 26% for the ♂_*BRCA1*$^{(+/-)}$ cell line.

Statistically, a one-way ANOVA with multiple comparisons was performed. Comparisons of RNA expression were between all fibroblast cell lines. In iPSCs and NPCs, all cells carrying a mutation were compared to wildtype cells. None of the comparisons revealed any significant differences.

Results are shown in Figure 21.

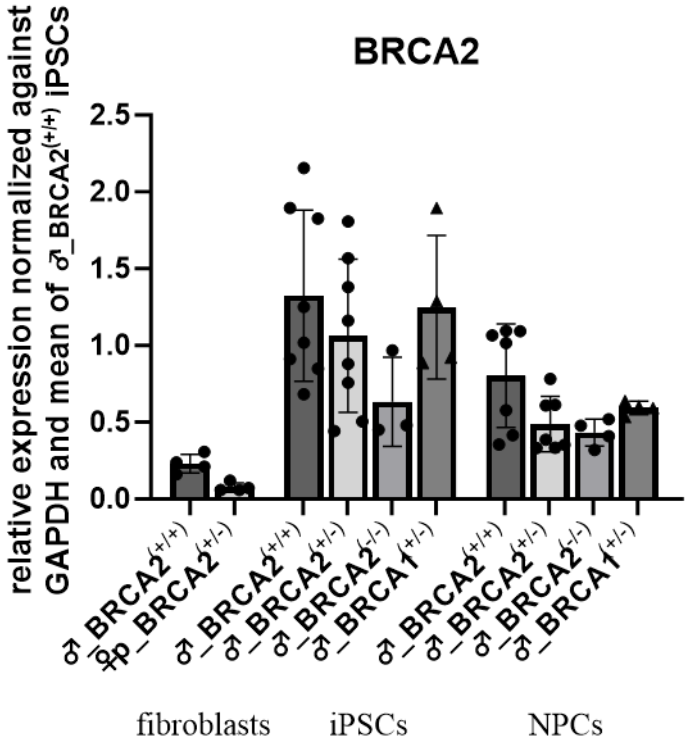

Figure 21 RNA expression of BRCA2 in male cell lines and the patient fibroblast cell line. *BRCA2* RNA expression was analyzed via RT-qPCR, and ct-values were normalized against *GAPDH* and the mean of the normalized ct-values of the wildtype iPSCs. Each dot and arrow resembles one biological replicate of the cell line. *BRCA2* RNA expression decreased in *BRCA2*-mutated samples compared to wildtype samples in fibroblasts, iPSCs, and NPCs. Even though those differences were statistically not significant.

Furthermore, *BRCA1* RNA levels (Table 22 and Figure 22) were determined in those samples. NPCs showed the highest *BRCA1* levels, which were lower in iPSCs and lowest in fibroblasts; compare Figure 22. In ♂_*BRCA2*$^{(+/-)}$ fibroblasts, *BRCA1* levels were reduced by 44% compared to ♂_*BRCA2*$^{(+/+)}$ fibroblasts.

In iPSCs, similar *BRCA1* expression levels were found in all cell lines tested. The difference between *BRCA1* expression levels was maximally 13% on average. Those 13% were found by comparing the ♂_*BRCA1*$^{(+/-)}$ cell line to the wildtype sample, with higher levels in the ♂_*BRCA1*$^{(+/-)}$ cell line.

In NPCs, *BRCA1* expression was reduced by 16% in the ♂_*BRCA1*$^{(+/-)}$ cell line compared to the wildtype sample. The other cell lines showed similar BRCA1 expression levels.

Statistically, a one-way ANOVA with multiple comparisons was performed. Comparisons of RNA expression were between fibroblast cell lines. And in iPSCs and NPCs, comparing all cells carrying a mutation to the wildtype cells. None of the comparisons revealed any significant differences.

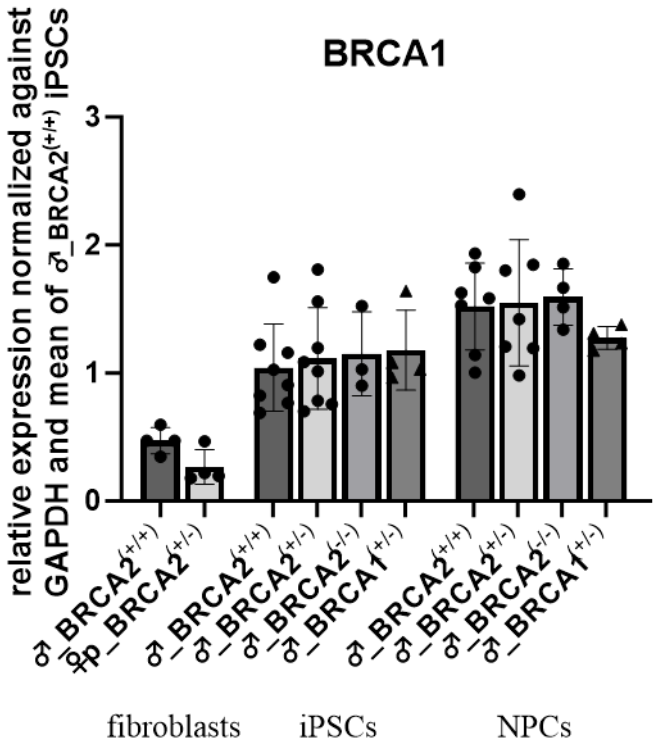

Figure 22 RNA expression of BRCA1 in all male cell lines and the patient fibroblast cell line. *BRCA1* RNA expression was analyzed via RT-qPCR and ct-values were normalized against *GAPDH* and the mean of the normalized ct-values of the wildtype iPSCs. Each dot and arrow resembles one biological replicate of the cell line. *BRCA1* RNA expression is lower in fibroblasts and higher in NPCs compared to iPSCs.

4.2.2 Protein

BRCA1 and BRCA2 Protein expressions were measured via western blot, normalized against ACTIN protein expression, and the relative expression of each sample was calculated against the mean of ♂_*BRCA2*$^{(+/+)}$ iPSCs. It was normalized against the iPSCs wildtype sample, as the BRCA2 expression was highest in this wildtype sample: iPSCs show the highest BRCA2 protein expression compared to fibroblasts and NPCs and the analysis should be similar to the RNA analysis. For the comparison within each cell type (Table 23), average means of the samples were calculated in the same way as it had already been described for RNA levels (compare Table 22 and Table 23).

Table 23 BRCA1 and BRCA2 protein levels in all cell lines relative to corresponding levels in wildtype cell lines.

Cell type	**Cell line**	***BRCA2* [%]**	***BRCA1* [%]**
fibroblasts	♂_BRCA2$^{(+/+)}$	100	100
	♀p_BRCA2$^{(+/-)}$	48	81
iPSCs	♂_BRCA2$^{(+/+)}$	100	100
	♂_BRCA2$^{(+/-)}$	49	75
	♂_BRCA2$^{(-/-)}$	50	112
	♂_BRCA1$^{(+/-)}$	70	107
NPCs	♂_BRCA2$^{(+/+)}$	100	100
	♂_BRCA2$^{(+/-)}$	57	111
	♂_BRCA2$^{(-/-)}$	91	142
	♂_BRCA1$^{(+/-)}$	101	145

The western blot (compare Figure 23) showed differences in band intensity of BRCA2 and BRCA1 depending on cell type and cell line. ACTIN and Ponceau staining revealed little differences in protein loading. The BRCA2 band can be found at a size of approximately 380kDa, while BRCA1 has a size of approximately 220kDA and ACTIN of approximately 45kDA. BRCA2 and BRCA1 bands show the expected size and a lower intensity in cell lines with mutations in the respective gene compared to wildtype cells.

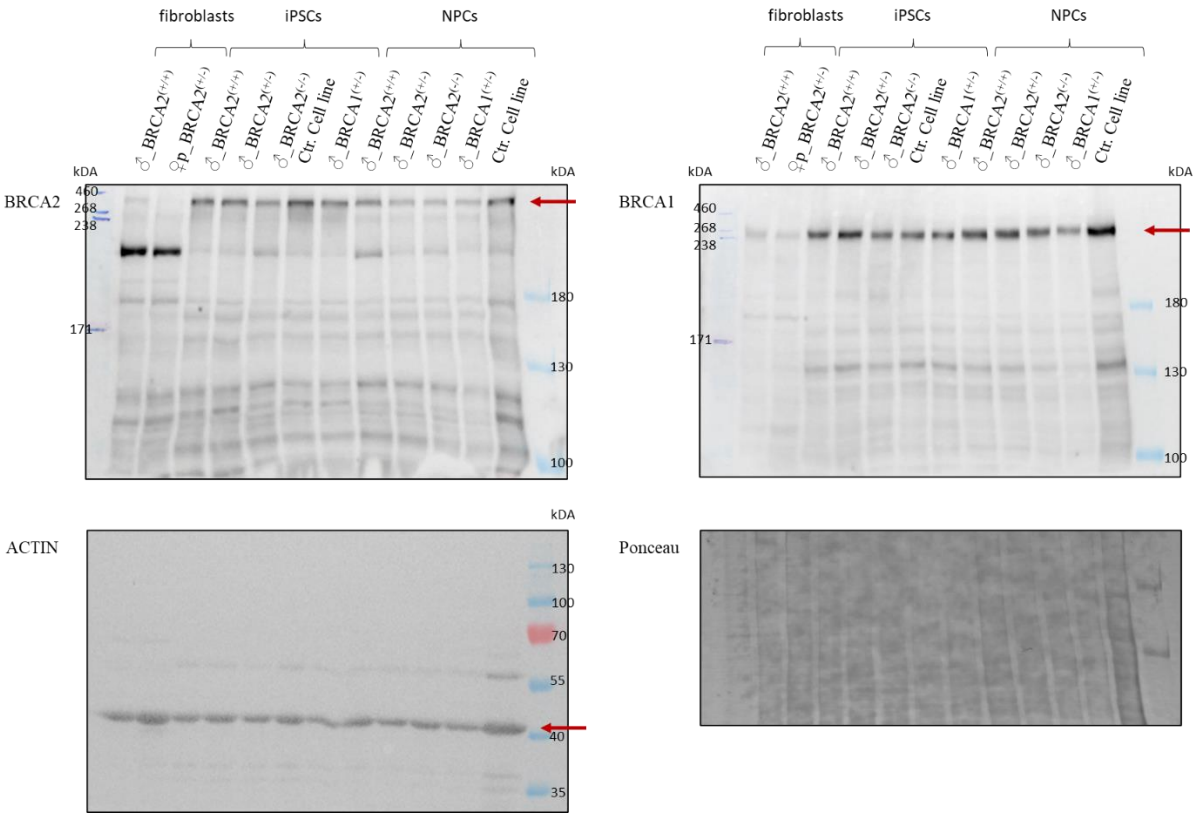

Figure 23 Representative Western blot of BRCA2, BRCA1, and ACTIN expression in all male samples and the patient sample. BRCA2 and BRCA1 blots were normalized against the same ACTIN blot. Two control samples, wildtype iPSC proteins from a different project, were taken along on all blots to serve as an optional additional loading control, which was not needed for the analysis. The ponceau staining is also shown. The bands show differences due to cell type and cell line. The red arrows indicate the bands of interest. At a size of approximately 380kDa, the BRCA2 band can be found; between 238 and 268kDa, the BRCA1 band is visible, and shortly above 40kDa, the band for ACTIN can be observed. The BRCA2 band showed lower intensity for BRCA2-mutated samples, and the BRCA1 band showed a lower intensity for BRCA1 mutated samples.

BRCA2 protein expression was lowest in fibroblasts, higher in NPCs, and highest in iPSCs; see Figure 24.

As can be seen in Table 23, BRCA2 protein expression was reduced by 52% in ♂*_BRCA2*$^{(+/-)}$ fibroblasts. In iPSCs, BRCA2 protein expression in mutated BRCA2 cell lines was reduced by 51% and 50% for ♂*_BRCA2*$^{(+/-)}$ and ♂*_BRCA2*$^{(-/-)}$, respectively. The ♂*_BRCA1*$^{(+/-)}$ cell line showed an average reduction in BRCA2 protein expression of 30%.

In NPCs, results were similar for the ♂*_BRCA2*$^{(+/-)}$ cell line, with BRCA2 being reduced by 43% compared to the wildtype sample, but only a 9% decrease in BRCA2 expression could be measured in the ♂*_BRCA2*$^{(-/-)}$ cell line compared to the wildtype sample.

For ♂*_BRCA1*$^{(+/-)}$ NPCs, no difference in BRCA2 expression compared to wildtype NPCs could be detected.

Statistically, a one-way ANOVA with multiple comparisons was performed. Comparisons of protein expression were between all fibroblast cell lines and in iPSCs and NPCs, where all cells carrying a mutation were compared to wildtype cells. In iPSCs the protein expression of ♂*_BRCA2*$^{(+/-)}$ was significantly lower compared to ♂*_BRCA2*$^{(+/+)}$, all other comparisons were not significantly different (see Figure 24).

Different from western blots (Figure 23), the table (Table 23) shows protein expression of all biological replicates together and not just one biological replicate.

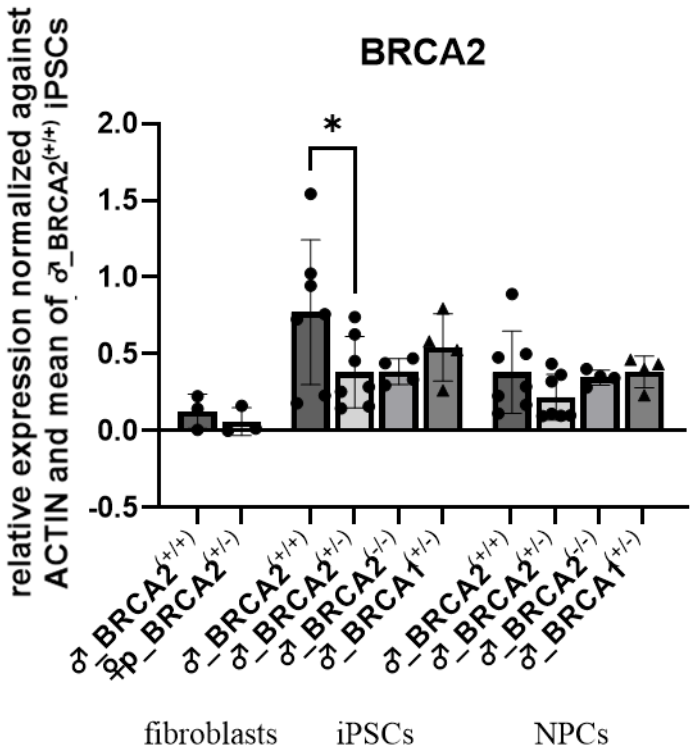

Figure 24 Protein expression of BRCA2 in all male samples and the patient fibroblast cell line. BRCA2 protein expression was analyzed via western blot, and protein expression was first normalized against the housekeeping gene, ACTIN, and second against the mean of the normalized protein expression of the wildtype iPSCs. Each dot and arrow resembles one biological replicate of the cell line. Fibroblasts, iPSCs, and NPCs were depicted with BRCA2 protein expression having been decreased around 50% in *BRCA2*-mutated samples (except ♂_BRCA2$^{(-/-)}$ NPCs). In iPSCs, protein expression of ♂*_BRCA2*$^{(+/-)}$ was significantly lower compared to ♂*_BRCA2*$^{(+/+)}$.

Also, BRCA1 protein levels were determined in all cell lines; compare Figure 25 and Table 23. Fibroblasts showed the lowest expression levels compared to iPSCs and NPCs. In iPSCs and NPCs protein expression showed very high differences between biological replicates within cell lines.

Mathematically, cell lines can be compared as follows; biologically the data is widely spread, so no statement can be made about differences in expression.

In fibroblasts, an average reduction in BRCA1 protein expression of 19% could be detected in the ♂*_BRCA2*$^{(+/-)}$ cell line compared to ♂*_BRCA2*$^{(+/+)}$.

In iPSCs, BRCA1 protein levels were averagely decreased by 25% in ♂*_BRCA2*$^{(+/-)}$ cells compared to wildtype cells. In ♂*_BRCA2*$^{(-/-)}$ and ♂*_BRCA1*$^{(+/-)}$ cell lines, increases of BRCA1 protein levels of 12% and 7%, respectively, were found.

In NPCs, all isogenic cell lines showed a higher average expression of BRCA1 compared to the wildtype cell line: 11% for ♂*_BRCA2*$^{(+/-)}$ cells and 42% and 45% for ♂*_BRCA2*$^{(-/-)}$ and ♂*_BRCA1*$^{(+/-)}$ cells, respectively.

Statistically, a one-way ANOVA with multiple comparisons was performed. Comparisons of protein expression were between all fibroblast cell lines and in iPSCs and NPCs, where all cells carrying a mutation were compared to wildtype cells. None of the comparisons revealed any significant differences.

The spread of data of the biological replicates was very wide.

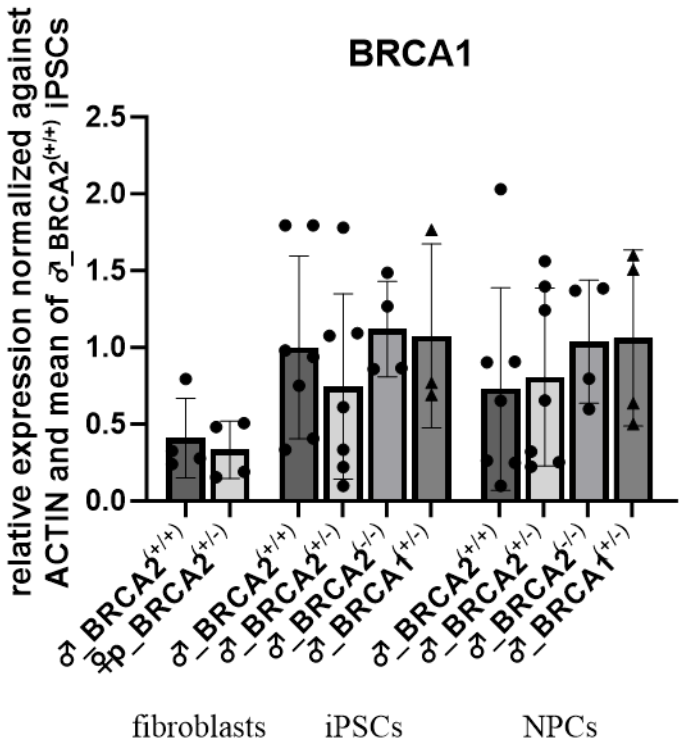

Figure 25 Protein expression of BRCA1 in all male samples and the patient fibroblast cell line. BRCA1 protein expression was analyzed via western blot, and the protein expression was first normalized against the housekeeping gene, ACTIN, and second against the mean of the normalized protein expression of the wildtype iPSCs. Each dot and arrow resembles one biological replicate of the cell line. BRCA1 protein expression was very variable between the biological replicates within each sample.

4.3 Establishment of formaldehyde treatment on all cell lines in fibroblasts and NPCs and investigation of its effects

It is hypothesized that cells carrying a heterozygous *BRCA2* mutation were more sensitive to formaldehyde treatment than wildtype cells. It has been shown that formaldehyde selectively depletes BRCA2 protein via proteasomal degradation. In cells that already have reduced BRCA2 levels due to heterozygous mutations, this further depletion makes them more susceptible to formaldehyde-induced haploinsufficiency. Furthermore, the hypothesis is that formaldehyde has an influence on BRCA2 protein levels, while BRCA1 protein levels are supposed to not be affected. Those effects have already been observed in 2017 by Tan and colleagues (Tan et al., 2017); see 1.8.

To test if formaldehyde has an influence on the expression of BRCA2 and BRCA1, their RNA and protein expression was analyzed after formaldehyde treatment. Therefore, the optimal formaldehyde concentration for treatment had to be figured out first. The optimal concentration was found when BRCA2 protein levels were decreased to undetectable levels in western blot in ♀p_*BRCA2*$^{(+/-)}$ cells but not in ♀_*BRCA2*$^{(+/+)}$ cells. The establishment of treatment was first performed in fibroblasts and subsequently adapted to NPCs and neurospheres.

4.3.1 Determining the formaldehyde concentration for treatment

To find the optimal formaldehyde concentration, fibroblasts were treated with different formaldehyde concentrations for five hours at 37°C. The concentrations were 0mM, 0.1mM, 0.2mM, and 0.3mM. Those concentrations resemble the naturally occurring concentrations in the brain (whole brain and hippocampus from mouse, rat, and human) of up to 0.4mM (Heck

et al., 1982; Tong et al., 2011b; Tong, Han, Luo, Wang, et al., 2013a). Additionally, previous studies already used a concentration of 0.2mM formaldehyde to treat their cells with (Kumari et al., 2012; Tan et al., 2017). After treatment, cells were pelleted, and protein lysates were prepared and analyzed by western blotting. For each western blot, protein concentrations were determined via Nanodrop. To control for equal loading, Ponceau staining was performed, and in addition, levels of the housekeeping protein ACTIN were determined by incubating the membrane with specific antibodies.

Increasing formaldehyde concentrations reduced BRCA2 protein levels in both the ♀p_*BRCA2*$^{(+/-)}$ and the ♀_*BRCA2*$^{(+/+)}$ cell lines. As expected, BRCA2 protein levels were lower in the formaldehyde-treated ♀p_*BRCA2*$^{(+/-)}$ cell line than in the ♀_*BRCA2*$^{(+/+)}$ cell line. Ponceau staining as well as ACTIN staining revealed equal loading. A formaldehyde concentration of 0.2mM was chosen for further treatment because this concentration reduced BRCA2 protein levels strongly in ♀p_BRCA2$^{(+/-)}$ cells but not in ♀_*BRCA2*$^{(+/+)}$ cells (Figure 26).

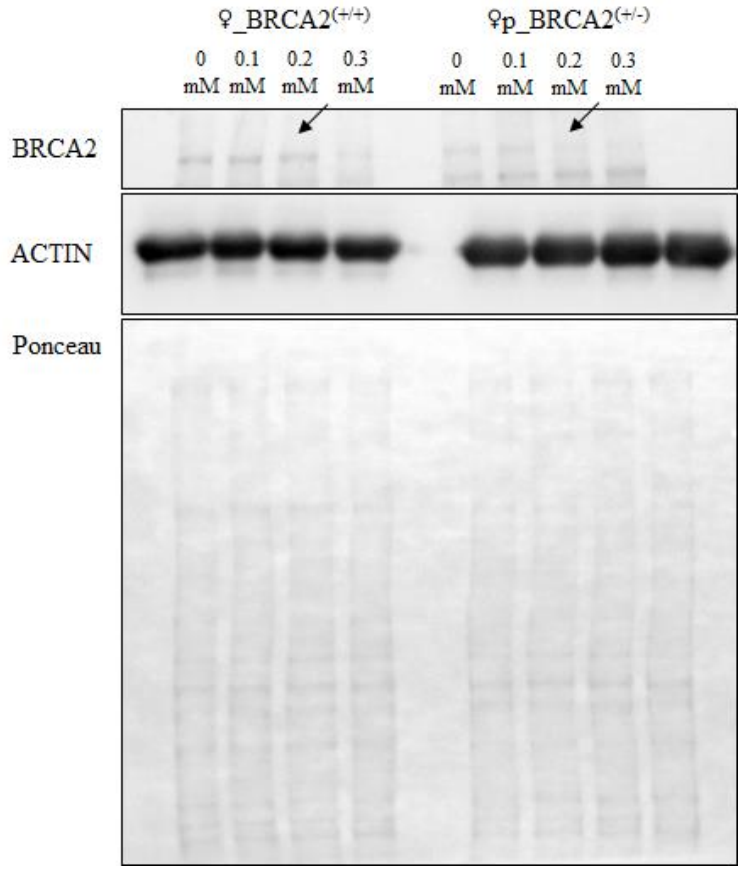

Figure 26 Western blot of fibroblasts (♀_BRCA2$^{(+/+)}$ and ♀p_ BRCA2$^{(+/-)}$) treated with different concentrations of formaldehyde. ♀_*BRCA2*$^{(+/+)}$ as well as ♀p_*BRCA2*$^{(+/-)}$ fibroblasts were treated with formaldehyde concentrations of 0mM to 0.3mM for 5h at 37°C. At a concentration of 0.2mM formaldehyde, the BRCA2 band was still visible in ♀_*BRCA2*$^{(+/+)}$ cells, while the BRCA2 band was not detectable anymore in ♀p_BRCA2$^{(+/-)}$ cells.

The experiment was performed once for the establishment and eight times in a final quantifying experiment; see 4.3.2.

4.3.2 Effects on BRCA2 and BRCA1 RNA and protein level of formaldehyde treatment in fibroblasts

To test if formaldehyde has an influence on the expression of BRCA2 and BRCA1, their RNA and protein expression was analyzed after formaldehyde treatment.

RNA levels were determined via RT-qPCR, while protein levels were determined via western blot with subsequent quantification. For RT-qPCR, the ΔΔCT method was applied, and values were normalized against *GAPDH*. For western blot, relative expression was generated by normalizing against ACTIN. Because it was not possible to generate all biological replicates at the same time and use the same 96-well plate (qPCR) or load them on the same gel (western blot), a normalization to control for differences between runs was used in addition. Therefore, within each RT-qPCR and western blot run, all values were normalized against the mean value of the untreated ♀_*BRCA2*$^{(+/+)}$ sample. For both experiments, one-way ANOVA testing with multiple comparisons was performed. Comparisons of interest were between both untreated samples, to determine the effect of the mutation; between the untreated and the treated sample within each cell line, to determine the effect of formaldehyde; and between both treated samples, to determine the effect of formaldehyde and mutation together.
Those differences were also calculated as percentages by using means of the biological replicates and are also displayed in the graphs; compare Figure 27 and Figure 29.
The experiment was performed in the female fibroblast lines, namely ♀_*BRCA2*$^{(+/+)}$ and ♀p_*BRCA2*$^{(+/-)}$.
Without treatment, the baseline expression of *BRCA2* RNA (compare Figure 27) was significantly lower (reduced by 56%; p-value <0.0001) in the ♀p_*BRCA2*$^{(+/-)}$ cell line compared to the ♀_*BRCA2*$^{(+/+)}$ cell line. Upon formaldehyde treatment, *BRCA2* RNA expression was reduced in both cell lines: In the ♀_*BRCA2*$^{(+/+)}$ cell line it was reduced by 59% (p<0.0001) and in the ♀p_*BRCA2*$^{(+/-)}$ cell line by 53% (p=0.0001) when compared to the respective untreated cell lines. This suggests that formaldehyde treatment reduces *BRCA2* expression in both. the wildtype cell line (♀_*BRCA2*$^{(+/+)}$) and in the cell line carrying the patient mutation (♀p_*BRCA2*$^{(+/-)}$). Of note, *BRCA2* RNA expression in formaldehyde-treated ♀p_*BRCA2*$^{(+/-)}$ cells was further reduced by 49% (p=0.0003) when compared to ♀_*BRCA2*$^{(+/+)}$ cells. This indicates that formaldehyde reduces BRCA2 expression to a much lower level in cells carrying a mutation in the *BRCA2* gene and therefore already showing a lower baseline *BRCA2* expression than in wildtype cells.
When studying RNA levels of *BRCA1,* similar results could be observed. The difference between the untreated ♀p_*BRCA2*$^{(+/-)}$ and untreated ♀_*BRCA2*$^{(+/+)}$ cell lines was significant (p<0.0001), with ♀p_*BRCA2*$^{(+/-)}$ cells having 40% less *BRCA1* RNA. This suggests that a mutation in the BRCA2 gene influences BRCA1 expression. Additionally, significantly lower *BRCA1* RNA levels could be detected in treated compared to untreated conditions (40% (p<0.0001) for the wildtype cell line and 43% (p=0.0016) for the patient sample), suggesting that formaldehyde leads to a reduction of *BRCA1* RNA. Moreover, the 43% reduction of the treated ♀p_*BRCA2*$^{(+/-)}$ sample compared to the treated ♀_*BRCA2*$^{(+/+)}$ sample was also significant (p=0.0007). This indicates that formaldehyde also reduces *BRCA1* RNA levels in cells already showing a lower baseline expression of *BRCA1* in an untreated condition.
The results in the untreated condition were expected, as *BRCA2* and *BRCA1* are often co-regulated, but the effect of formaldehyde had so far only been published on the protein level.

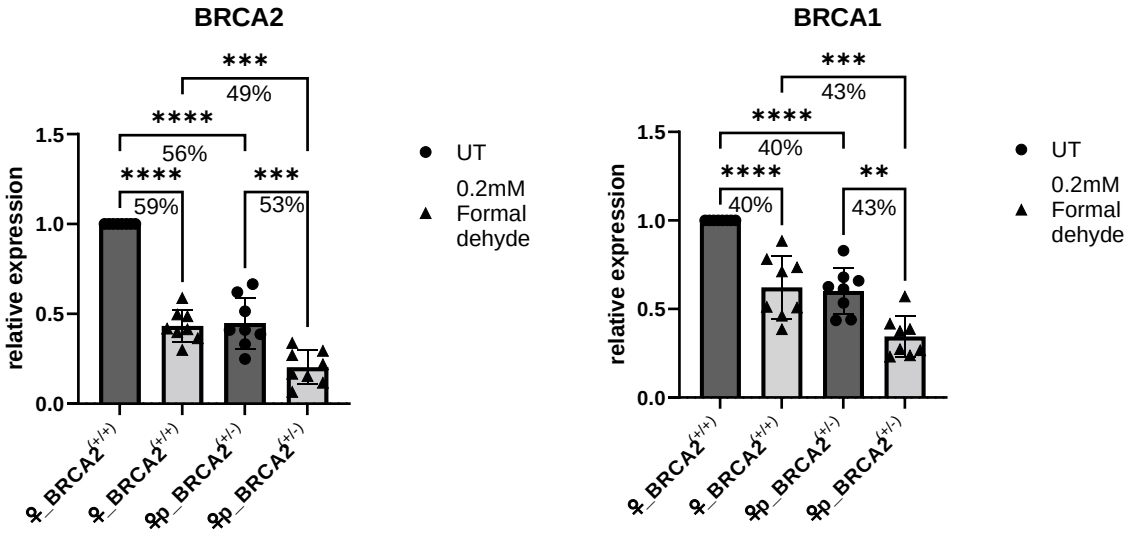

Figure 27 RNA levels of BRCA2 and BRCA1 in untreated (UT) and formaldehyde-treated (0.2mM) fibroblasts. RNA expression was analyzed via RT-qPCR and normalized against GAPDH and untreated ♀_*BRCA2*$^{(+/+)}$. Each circle and arrowhead represents one biological replicate of the respective cell line. Mean ± SD, one-way ANOVA with multiple comparisons, **p<0.01, ***p<0.001, ****p<0.0001. The percentages indicate the mean difference between both samples. For both genes, similar expression patterns in the samples can be observed. The untreated ♀p_BRCA2$^{(+/-)}$ cell line had lower baseline levels of *BRCA1* and *BRCA2* compared to the untreated wildtype cell line. Formaldehyde decreased *BRCA2* and *BRCA1* RNA levels in both treated samples, and treated ♀p_BRCA2$^{(+/-)}$ samples showed the lowest *BRCA2* and *BRCA1* expression compared to the other samples.

Moreover, BRCA2 and BRCA1 protein levels after formaldehyde treatment were analyzed and compared to untreated samples. Proteins are the primary functional molecules in cells, so changes in protein level potentially induced by formaldehyde (Tan et al., 2017) could affect cellular processes and activities. In Figure 28, two representative samples of the western blot can be seen. Ponceau staining as well as the ACTIN band showed a consistent loading between all samples. The BRCA1 band also looked consistent in intensity between all samples, while BRCA2 bands appeared weaker in the ♀p_*BRCA2*$^{(+/-)}$ samples and in the formaldehyde-treated ♀_*BRCA2*$^{(+/+)}$ sample compared to the untreated ♀_*BRCA2*$^{(+/+)}$ sample.

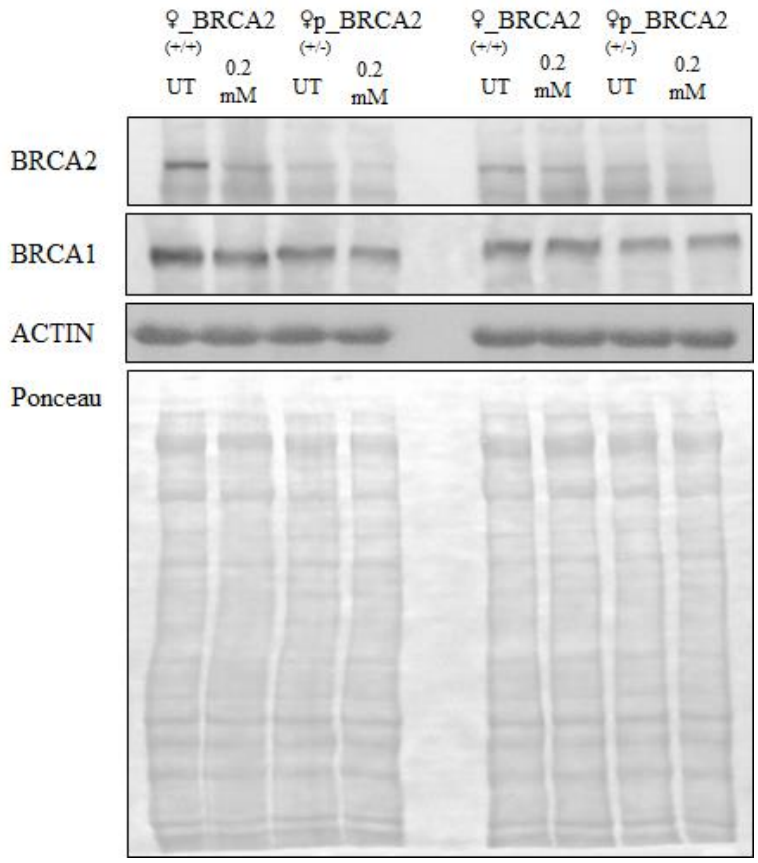

Figure 28 Western blot for the quantification of formaldehyde treatment in fibroblasts. Two representative biological replicates of ♀_BRCA2$^{(+/+)}$ and ♀p_BRCA2$^{(+/-)}$ cell lines, untreated or treated with 0.2mM formaldehyde for 5h at 37°C.

Observations from western blot pictures could be confirmed after quantifying the bands; see Figure 29. BRCA2 protein levels differed significantly between both untreated samples, with a reduction of 61% in the untreated ♀p_*BRCA2*$^{(+/-)}$ sample (p=0.0217). The difference between both formaldehyde-treated samples was 74%, but as the BRCA2 expression itself was not that high in both samples and the biological replicates in the ♀_*BRCA2*$^{(+/+)}$ sample showed a wider spread, this difference was statistically not significant (p=0.9176). This also accounted for the comparison between untreated and treated ♀p_*BRCA2*$^{(+/-)}$ samples. The difference was 82%, but it was not statistically significant with a p-value of p=0.3037. The comparison of untreated and treated samples within the ♀_*BRCA2*$^{(+/+)}$ cell line showed a difference of 72%, which was statistically significantly different (p=0.0071). In contrast to BRCA2, BRCA1 protein expression was similar in all samples.

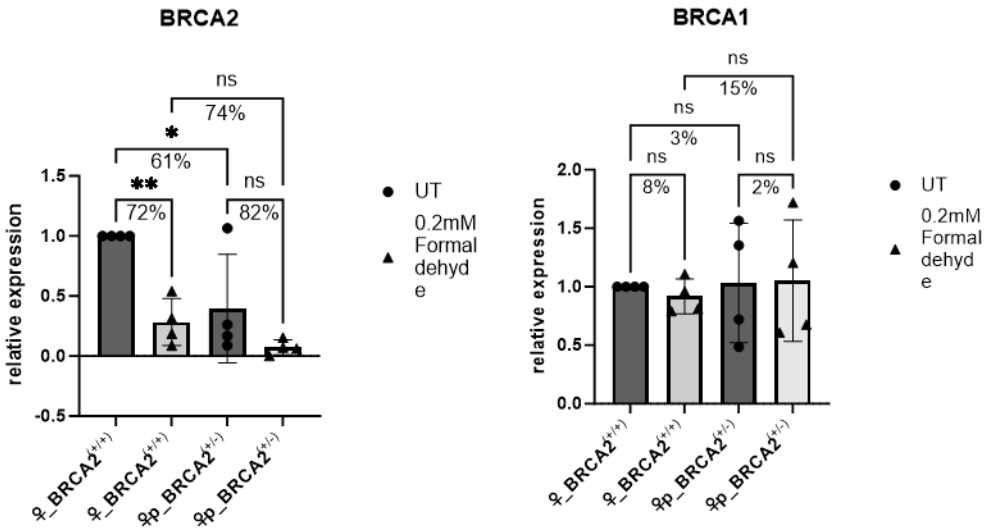

Figure 29 Quantification of protein levels of BRCA2 and BRCA1 in untreated (UT) and formaldehyde-treated (0.2mM) fibroblasts. Protein expression was analyzed via western blot and normalized against the housekeeping gene ACTIN, and untreated ♀_*BRCA2*$^{(+/+)}$. Each circle and arrowhead represents one biological replicate of the respective cell line. Mean ± SD, one-way ANOVA with multiple comparisons, *p<0.05, **p<0.01. The percentages indicate the mean difference between both samples. BRCA1 levels are not significantly different between any of the samples, while BRCA2 levels are lower in ♀p_BRCA2$^{(+/-)}$ samples and in the formaldehyde-treated ♀_*BRCA2*$^{(+/+)}$ sample compared to the untreated ♀_*BRCA2*$^{(+/+)}$ sample.

Differences between RNA and protein levels within fibroblasts could be observed. But expression differences between samples due to mutation or formaldehyde treatment were similar between BRCA2 RNA and protein expression. Reduced BRCA2 RNA and protein baseline expression could be found in untreated samples, suggesting a reduction due to the mutation. Also, formaldehyde reduced BRCA2 RNA and protein levels in wildtype and heterozygously mutated BRCA2 cells, leading to very low levels in ♂_*BRCA2*$^{(+/-)}$ cells.
BRCA1 expression levels were not similar when comparing RNA and protein expression. On the RNA level influences of the *BRCA2* mutation and formaldehyde could be observed on *BRCA1* RNA expression, while on the protein level no differences between samples could be observed.
Those results suggest that *BRCA2* and *BRCA1* RNA are co-regulated in these cells and that formaldehyde can influence both RNAs. Furthermore, the previous observation by TAN and colleagues (Tan et al., 2017) that formaldehyde influences only BRCA2 but not BRCA1 protein expression could be confirmed.

The results in untreated samples on RNA and protein levels in BRCA2 and BRCA1 resembled the results already observed in the BRCA2 and BRCA1 expression analyses (compare 4.2).

4.3.3 Effects of formaldehyde treatment on BRCA2 and BRCA1 RNA and protein levels in NPCs

After formaldehyde treatment had been established in fibroblasts, the optimal formaldehyde concentration of 0.2mM was also used for NPC samples. The sample collection, quantification of RNA (via RT-qPCR) and protein levels (via western blot), and data analyses were performed by [redacted], a medical student working on this project. Methods and analyses were the same as already described for fibroblasts in 4.3.2

In untreated ♂_BRCA2$^{(+/-)}$ NPCs, baseline RNA levels were 45% lower than in untreated ♂_BRCA2$^{(+/+)}$ NPCs. Upon formaldehyde treatment, BRCA2 RNA levels dropped significantly by 77% in ♂_BRCA2(+/+) samples and by 74% in ♂_BRCA2(+/-) samples compared to untreated controls ($p<0.0001$ for both). This suggests that formaldehyde, as already seen in fibroblasts, reduces the levels in both cell lines to a strong degree. The difference between both treated samples was 39%, but statistically not significant ($p=0.1727$). Similarly, BRCA1 RNA levels decreased significantly in treated samples compared to untreated ones. The reductions were 68% for ♂_BRCA2$^{(+/+)}$ ($p<0.0001$) and 69% for ♂_BRCA2$^{(+/-)}$ ($p<0.0001$), suggesting that formaldehyde has a strong influence on both samples.

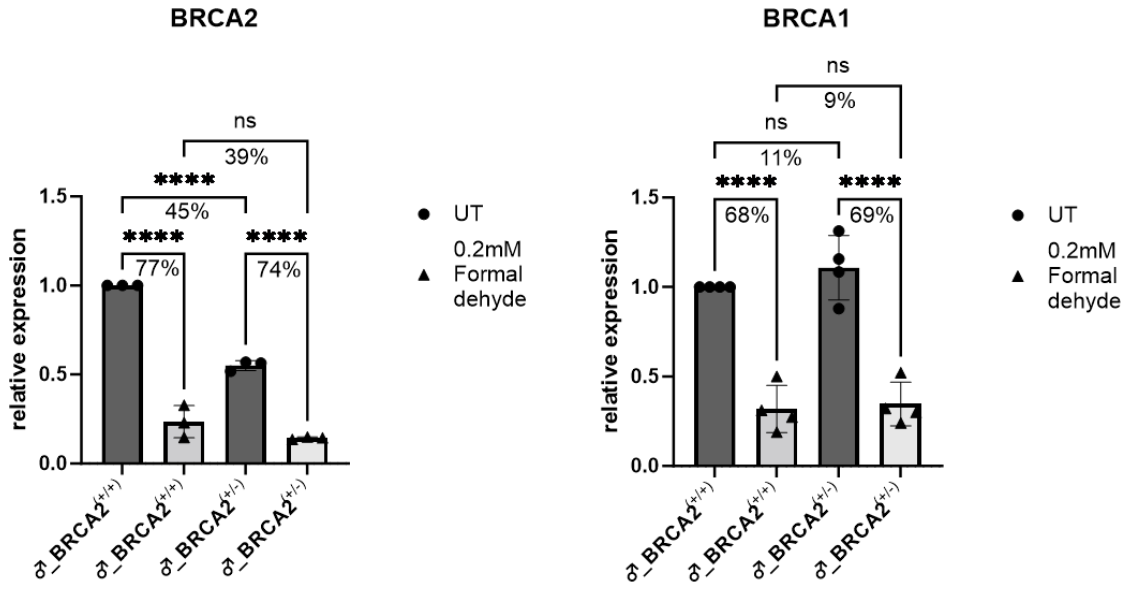

Figure 30 RNA levels of BRCA2 and BRCA1 in untreated (UT) and formaldehyde-treated (0.2mM) NPCs. RNA expression was analyzed via RT-qPCR and normalized against GAPDH and untreated ♂_*BRCA2*$^{(+/+)}$. Each dot and arrow resembles one biological replicate of the cell line. Mean ± SD, one-way ANOVA with multiple comparisons, ****$p<0.0001$. The percentages indicate the mean percentual difference between both samples. *BRCA2* and *BRCA1* RNA levels were significantly lower in treated samples compared to untreated counterparts. Only *BRCA2* RNA levels, but not *BRCA1*, showed a lower RNA baseline in ♂_BRCA2$^{(+/-)}$ compared to ♂_BRCA2$^{(+/+)}$ NPCs.

Significant differences in BRCA2 protein levels were observed across all comparisons. BRCA2 protein levels in untreated ♂_BRCA2$^{(+/-)}$ NPCs showed 54% lower protein levels compared to untreated ♂_BRCA2$^{(+/+)}$ NPCs ($p<0.0001$).

In both cell lines, treated samples exhibited notably lower protein levels. Specifically, in ♂_BRCA2$^{(+/+)}$ samples, treated cells showed a 46% reduction in BRCA2 protein levels compared to untreated cells, which was statistically significant ($p=0.0004$). Similarly, in ♂_BRCA2$^{(+/-)}$ samples, treated cells had a 56% reduction in BRCA2 protein levels compared to untreated cells, also statistically significant ($p=0.0086$). This suggests that formaldehyde also has a strong influence on protein levels and not only RNA levels.

Additionally, treated ♂_BRCA2$^{(+/-)}$ NPCs exhibited a 62% reduction in BRCA2 protein levels compared to treated ♂_BRCA2$^{(+/+)}$ NPCs, with this difference being statistically significant ($p=0.0458$). Suggesting that formaldehyde reduces the levels even more in cells already showing lower baseline levels.

In BRCA1 protein levels no significant differences between any samples could be found.

These findings indicate that while BRCA2 protein levels were significantly affected by treatments, BRCA1 protein levels remained relatively stable across the different sample groups.

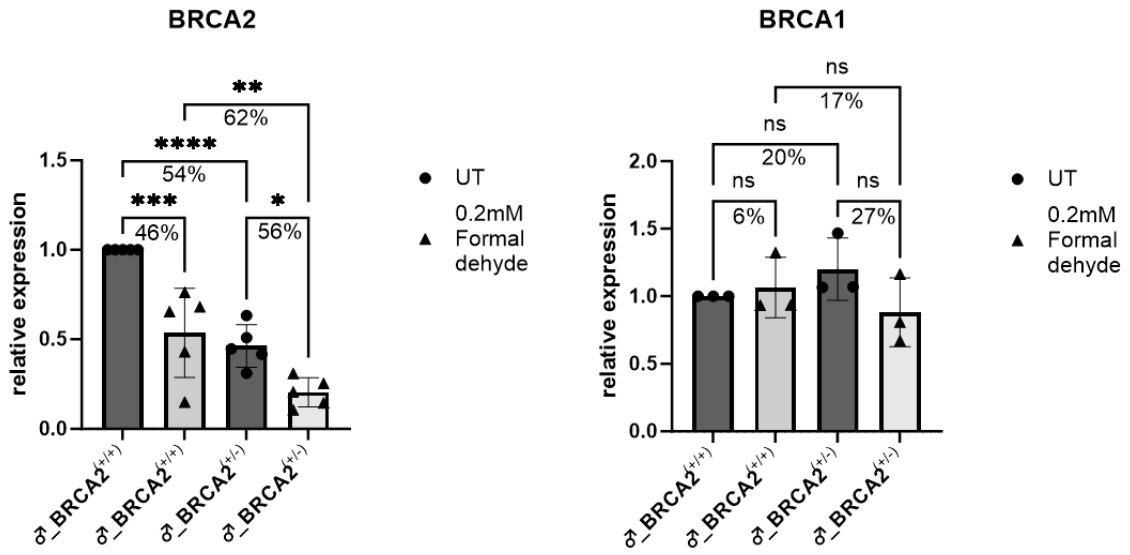

Figure 31 Protein levels of BRCA2 and BRCA1 in untreated (UT) and formaldehyde-treated (0.2mM) NPCs. Protein expression was analyzed via western blot and normalized against the housekeeping gene, ACTIN, and untreated ♂_*BRCA2*$^{(+/+)}$. Each dot and arrow resembles one biological replicate of the cell line. Mean ± SD, one-way ANOVA with multiple comparisons, *p<0.05, **p<0.01, ***p<0.001, ****p<0.0001. The percentages indicate the mean percentual difference between both samples. In all comparisons within BRCA2 protein levels, significant differences could be found. BRCA1 protein levels did not differ significantly, neither between different treatment conditions nor between cell lines.

There were notable differences comparing BRCA1 and BRCA2 RNA and protein levels in NPCs. Expression patterns of BRCA2 RNA and protein were similar, both showing decreased levels due to mutation or formaldehyde treatment. Specifically, untreated ♂_BRCA2$^{(+/-)}$ NPCs had approximately 50% less BRCA2 RNA and protein expression compared to ♂_BRCA2$^{(+/+)}$. Formaldehyde treatment further decreased BRCA2 expression in both mutant and wild-type samples.
In contrast, BRCA1 expression levels showed different patterns for RNA and protein. BRCA1 RNA levels decreased significantly following formaldehyde treatment, whereas BRCA1 protein levels did not exhibit significant changes compared to untreated samples.

When comparing NPCs to fibroblasts, BRCA2 RNA and protein expression levels were similar in both cell types.
Untreated ♂_BRCA2$^{(+/-)}$ samples showed a roughly 50% reduction in BRCA2 RNA and protein expression in both NPCs and fibroblasts. Formaldehyde treatment led to a decrease in BRCA2 RNA and protein levels in both cell types.
Regarding BRCA1 protein levels, no significant differences were observed between samples in either NPCs or fibroblasts. However, BRCA1 RNA levels differed between fibroblasts and NPCs. In untreated ♂_BRCA2$^{(+/-)}$ NPCs, BRCA1 RNA levels were similar to those in ♂_BRCA2$^{(+/+)}$ NPCs. In contrast, fibroblasts showed a 40% decrease in BRCA1 RNA levels in ♂_BRCA2$^{(+/-)}$ compared to ♂_BRCA2$^{(+/+)}$. Formaldehyde treatment decreased BRCA1 RNA levels in both cell types: approximately 70% in NPCs and 40% in fibroblasts.
These results highlight the differential impact of mutation and formaldehyde treatment on BRCA1 and BRCA2 expression at both RNA and protein levels in NPCs and fibroblasts.

4.4 Experiments in 2D culture

4.4.1 Analysis of DNA double-strand breaks in NPCS with γH2AX staining via FACS

Formaldehyde induces DNA DSBs, which can lead to changes in the cell cycle, potentially affecting cell proliferation. If and how strong the effect of formaldehyde in the cells of this experiment was, should be determined. DSBs induced by formaldehyde might be the cause of other potential effects.

Those DSBs can be marked with a γH2AX antibody, binding DSBs specifically. Two cell lines were used for this experiment: ♂_*BRCA2*$^{(+/+)}$ and ♂_*BRCA2*$^{(+/-)}$ NPCs. Those cell lines were used, as the main focus in this work was on the male cell lines, comparing wildtype cells and cells carrying a heterozygous mutation in the *BRCA2* gene.

Those cells were either untreated or treated with 0.2mM formaldehyde for 5h and subsequently fixed, stained with a γH2AX antibody, and labeled with the fluorescent antibody Alexa Fluor488. With a flow cytometry analysis, median fluorescent intensity (MIF) of the γH2AX-positive cells was determined and compared between samples with a one-way ANOVA with multiple comparisons. The FACS run was performed with the help of [redacted] from the Flow Cytometry Core Facility 911, University Medical Center Mainz, and the analysis was performed with the FlowJo software.

To measure γH2AX-positive cells, cells were gated in the following way: Initially, all cells were gated, followed by gating for single cells and cleaning to remove any debris. Then, γH2AX-positive cells were gated by plotting counts on the y-axis against fluorescent dye (Comp Alexa Fluor 647A) on the x-axis. Compare Figure 32.

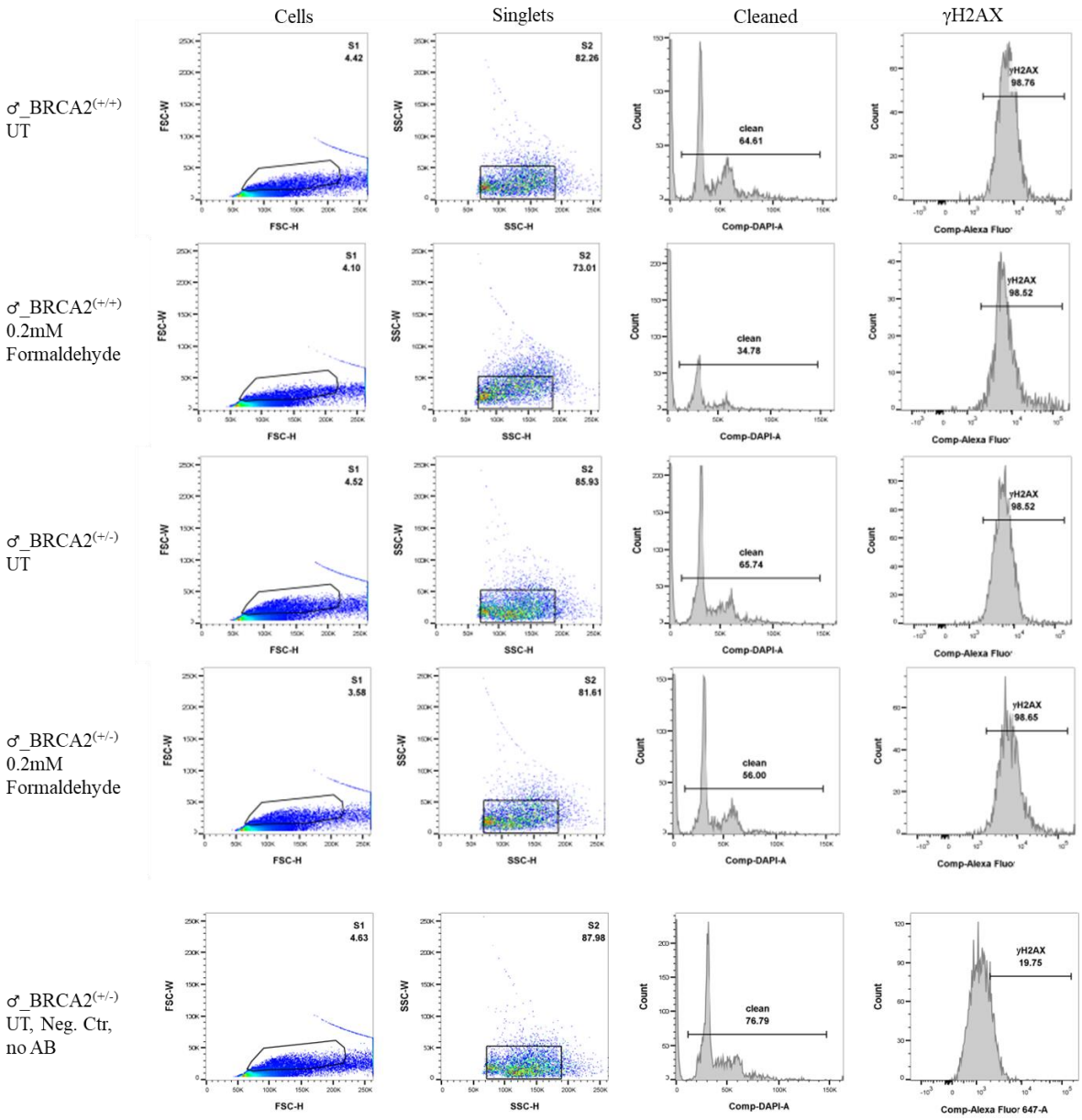

Figure 32 FACS analysis of γH2AX staining. To identify γH2AX-positive cells, cells were stained with a primary antibody against γH2AX and a secondary antibody AlexaFluor488, as well as with DAPI. The gating strategy included gating on cells (left column), subsequently gating for single cells (second column), gating on live cells by excluding dead cells (third column), and gating on γH2AX-positive cells (right column). One representative sample for each experimental condition and a negative control without γH2AX-staining are depicted. Numbers represent cell percentages in indicated gates. The samples had at least four independent biological replicates per experimental condition and did not differ significantly.

From these cells, median fluorescent intensity (MIF) was calculated with the FlowJo software. All samples were analyzed in the same way. No significant differences between the means of MIFs could be observed (Figure 33), suggesting that neither mutation nor formaldehyde treatment has an influence on the amount of DSBs in the cells.

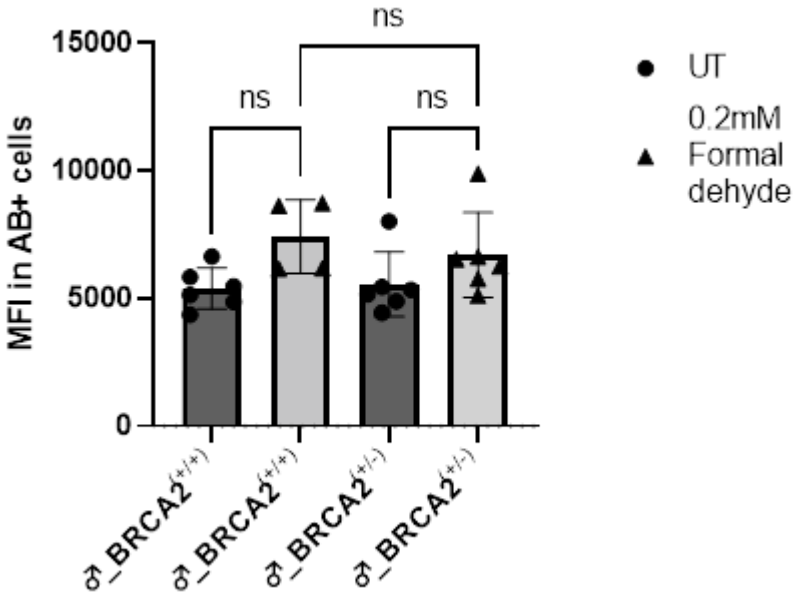

Figure 33 Median fluorescent intensity (MFI) of antibody-positive cells in untreated and formaldehyde-treated cells (0.2mM). At least four biological replicates per sample were analyzed via FACS after staining with γH2AX, AlexaFluor488 and DAPI. Mean ± SD, one-way ANOVA with multiple comparisons. There was neither a significant difference in MFI of γH2AX-positive cells comparing treated to untreated samples of both cell lines nor a significant difference comparing both treated samples.

4.4.2 Analysis of DNA double-strand breaks in NPCS with γH2AX staining via microscopy

To analyze DNA double-strand breaks with a second approach, a γH2AX staining with subsequent analysis via fluorescent microscopy was performed: This time cells were seeded on coverslips, treated, fixed, and stained with a primary γH2AX antibody and a secondary AlexaFluor488. Therefore, the fluorescence microscope Revolve from ECHO with a 10x magnification was used. Pictures were analyzed with a slightly modified script from [redacted], a PhD student from the collaborator's lab. In this script, the area of 300 nuclei per sample and its γH2AX staining intensity are determined automatically. Each experimental sample consisted of three biological replicates with 300 analyzed nuclei. Afterwards, a manual calculation of the fluorescent intensity per area was performed. Data was statistically analyzed with a one-way ANOVA with multiple comparisons.

In the immunofluorescent staining it could be seen that DAPI was detectable in all cell lines in the nucleus. The staining of γH2AX was detectable in both treated samples but not in the untreated samples. A substantial difference between both treated samples was not visible in the pictures; compare Figure 34 and Figure 35.

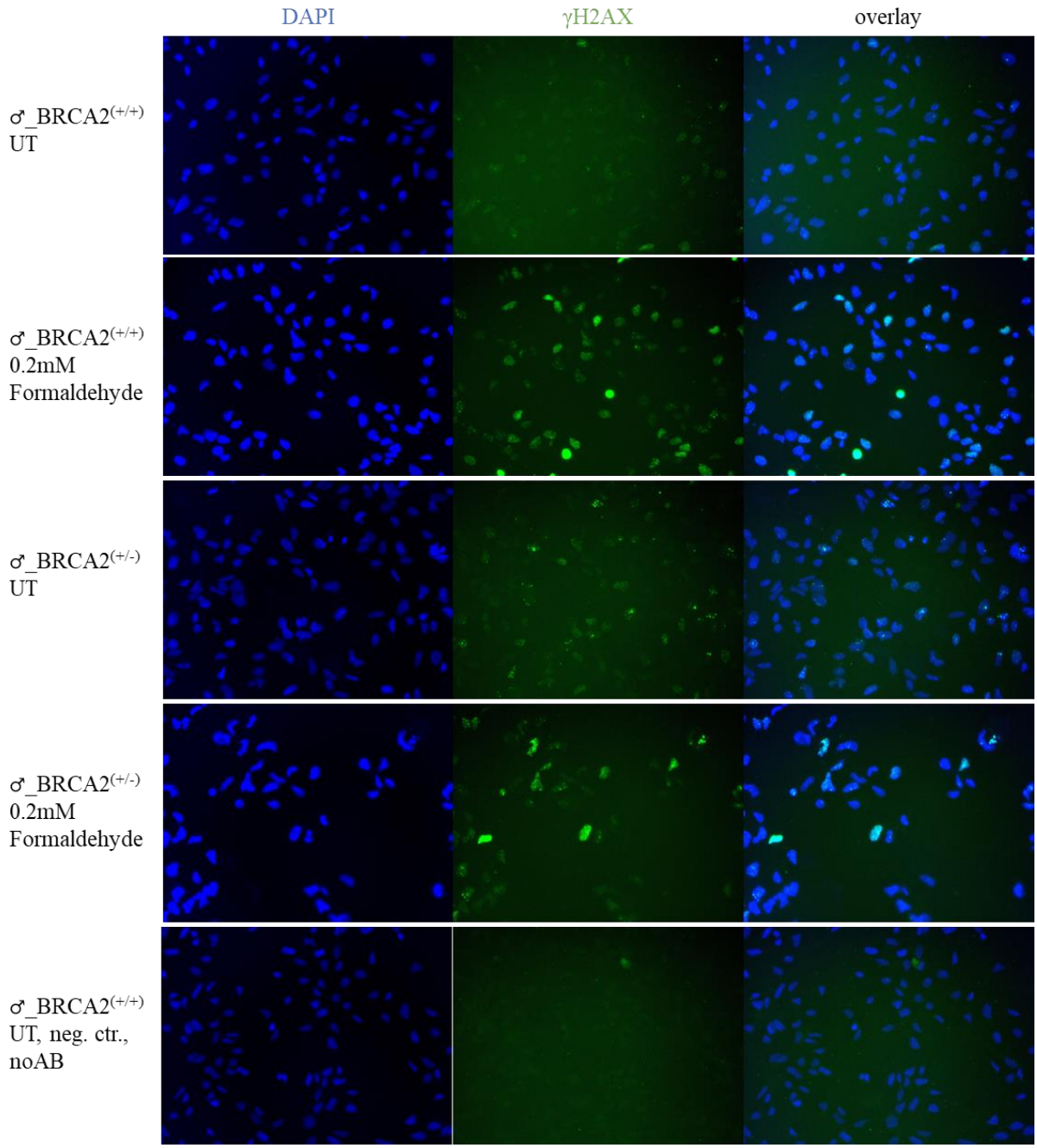

Figure 34 Representative immunofluorescent staining of γH2AX and DAPI in untreated and formaldehyde-treated (0.2mM) NPC and a negative control without γH2AX staining. After a treatment with and without formaldehyde (0.2mM) for 5h at 37°C, cells were fixed and stained with γH2AX, labeled with Alexa Fluor488, and DNA was stained with DAPI. The staining showed that in treated samples, γH2AX staining was detectable, while only slightly present in untreated samples. Magnification in these pictures is 10x.

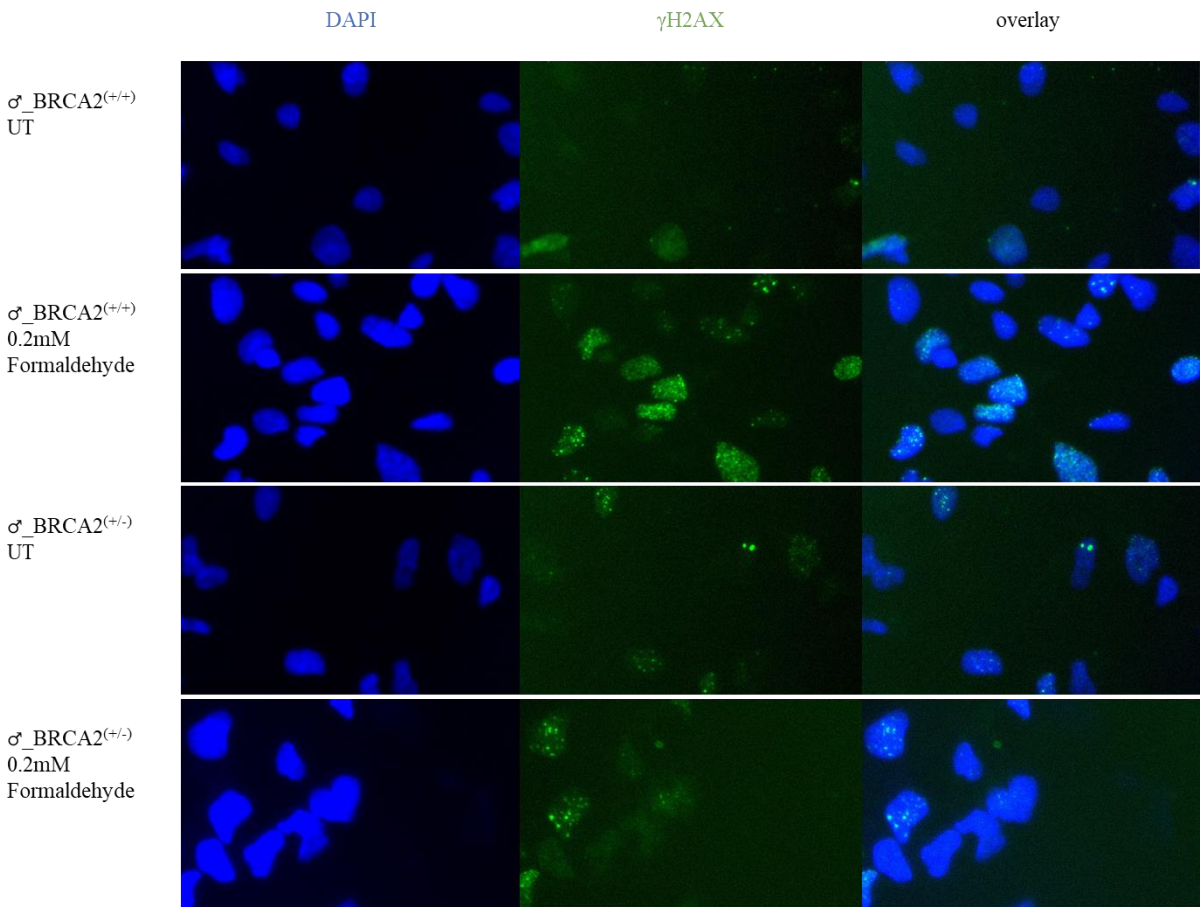

Figure 35 Close-up of immunofluorescent staining of γH2AX and DAPI in untreated and formaldehyde-treated (0.2mM) ♂_BRCA2(+/+) and ♂_BRCA2(+/-) samples

The mean fluorescent intensity per area was 42.79 for the ♂_*BRCA2*$^{(+/+)}$ sample and 39.69 for the ♂_*BRCA2*$^{(+/-)}$ sample. Both untreated samples did not differ significantly, indicating that the *BRCA2* mutation is not increasing the number of DSBs. For the treated ♂_*BRCA2*$^{(+/+)}$ sample, the mean fluorescent intensity per area was 63.28, while it was 55.66 for the treated ♂_*BRCA2*$^{(+/-)}$ sample. Statistically significant differences ($p<0.0001$) could be observed between untreated and treated samples in each cell line, suggesting that formaldehyde increases the amount of DSBs in both cell lines. According to statistics, the treated ♂_*BRCA2*$^{(+/-)}$ sample shows a significantly lower mean fluorescent intensity per area compared to the ♂_*BRCA2*$^{(+/+)}$ sample. This means that there are fewer DSBs in those cells. The difference itself, however, was not big (63.28 and 55.66 mean fluorescent intensity per area), but due to the high number of nuclei analyzed, statistics revealed the difference as significant.

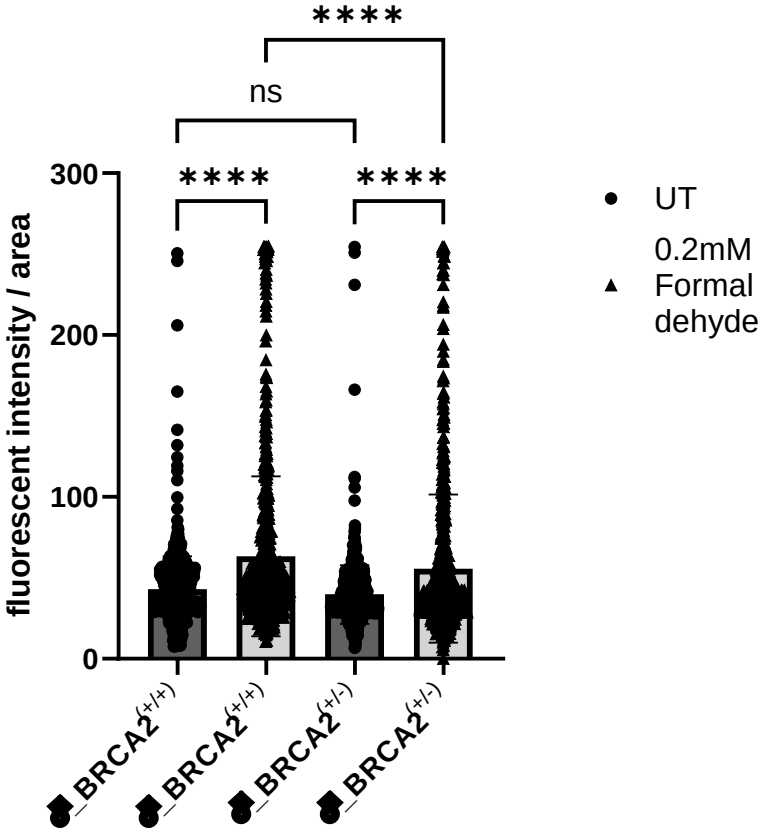

Figure 36 γH2AX fluorescent intensity per area of untreated and formaldehyde-treated cells (0.2mM). γH2AX fluorescent intensity and area per nuclei were determined after γH2AX staining with an automated script. Manually, the intensity was divided by area. 300 nuclei per biological replicate were analyzed. Three biological replicates per experimental sample were generated. Mean ± SD, one-way ANOVA with multiple comparisons, ****p<0.0001. Significant differences could be observed between untreated and treated samples in each cell line, as well as between both treated samples.

The results of the FACS analysis and the staining of DSBs differ in their message. The FACS analysis indicates no difference between samples, neither due to mutation nor due to formaldehyde treatment. The staining of γH2AX-positive cells reveals significant differences due to formaldehyde treatment. Staining is a more sensitive tool for the analysis of DSBs compared to FACS. The reasons for this are, first, a higher specificity of fluorescence microscopy, as the discrimination between background and true DSBs is better. And second, it is easier to detect low levels of DNA damage in fluorescent microscopy, as also single DSBs are highlighted, while with FACS the average signal across the nucleus is measured. (Durdik et al., 2021)
As the differences between the samples are highly significant in the fluorescent analysis and the FACS analysis is less sensitive, it could be assumed that formaldehyde leads to an increase of DSBs.

4.4.3 Cell cycle analysis in NPCs via FACS

As both BRCA2 and formaldehyde are associated with the cell cycle, it is analyzed within this project. DSBs and differences in RNA and protein expression due to a *BRCA2* mutation or a formaldehyde treatment could lead to changes in the cell cycle. Those changes in the cell cycle might influence proliferation of the cells, which should be analyzed in this work.
BRCA2 expression and function heavily depend on the cell cycle, with cells carrying a heterozygous mutation in the *BRCA2* gene accumulating more in the G2/M-phase and G1-phase compared to wildtype cells. Interestingly, a loss of *BRCA2* extends the cell cycle as it impairs

the completion of cell division by cytokinesis (Daniels et al., 2004); compare 1.1. Low doses of formaldehyde are already enough to shorten the S-phase, so less time is spent in the S-phase. Additionally, treated cells show an arrest in the G2/M phase of the cell cycle, while controls show an undisturbed cell cycle (Nadalutti et al., 2020; Ortega-Atienza et al., 2015).
Furthermore, DSBs, e.g. induced by formaldehyde or not repaired properly due to a mutation in the *BRCA2* gene, can initiate a (reversible) cell cycle arrest in the G1- and G2- phases (Krenning et al., 2019).

4.4.3.1 Analysis of cell cycle after formaldehyde treatment in male isogenic pair

The cell cycle of untreated and 0.2mM formaldehyde-treated ♂_*BRCA2*$^{(+/+)}$ and ♂_*BRCA2*$^{(+/-)}$ NPCs was analyzed. The G1-, S-, and G2-phases of the cell cycle were investigated, which leads to a lot of comparisons statistically. To focus on the comparisons of interest and not lose power due to p-value adjustments, first, untreated samples were compared. Second, both treated samples and third, the treated sample were compared to the untreated sample within each cell line. Those comparisons were statistically analyzed with a one-way ANOVA. In an explorative manner of the experiment, further t-tests were performed. In both cell lines each single phase of the cell cycle was compared between treated and untreated samples.
The Click-iT™ EdU kit was used, where an EdU-labeled thymidine analog is incorporated into replicating DNA. With a click reaction, the EdU analog gets fluorescently labeled with AlexaFluor647A. In the FACS run, which was performed with the help of [redacted], DAPI and AlexaFluor647A can be detected and analyzed. The analysis was performed with the FlowJo software, and the G1-, S- and G2-phases were investigated.
Comparing Figure 37, samples were gated for cells, and this set was subsequently gated for single cells and again cleaned by excluding any debris. By plotting DAPI against the fluorescent dye (AlexaFluor647A) different cell cycle phases could be gated (defined by the black rectangles). The chosen cell cycle phases were the usual G1-, S- and G2-phases, as well as G1+. G1 is the cell population with one copy of DNA and no inserted EdU, so not replicating. G2-phase is the set of cells with the double amount of DNA and no EdU, as they are not replicating. S-phase is the group of cells with inserted EdU, as those cells are replicating and incorporating modified nucleotides, and brings the cells from haploidy to diploidy. Furthermore, there was a group of cells (G1+) with inserted EdU and haploid status. Those cells are also in G1 phase, but as the treatment lasted for 5h they entered the G1-phase after having been in S-phase, so after incorporating EdU. For the analysis, G1 and G1+ cells were taken together as G1.

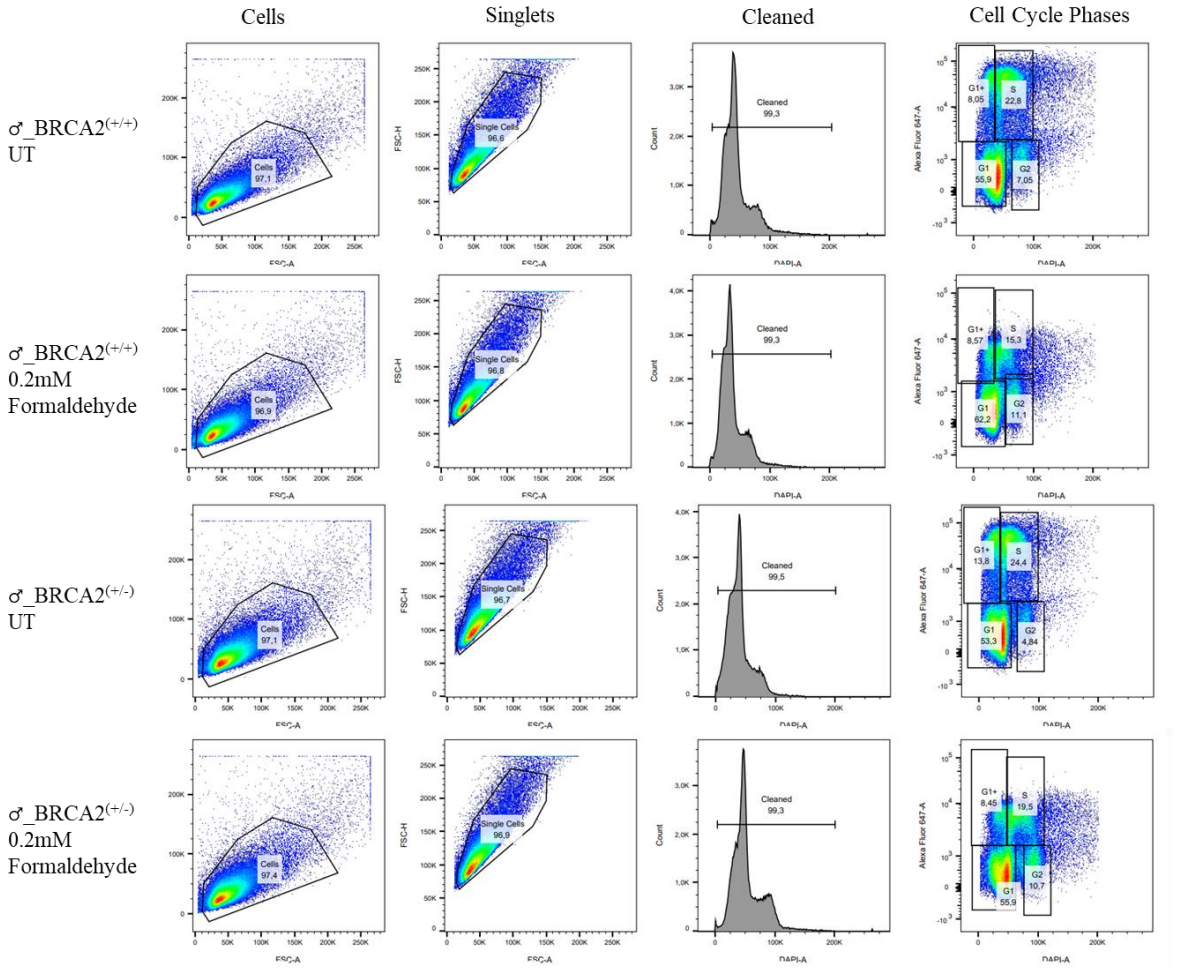

Figure 37 FACS analysis of the cell cycle phases cells. Gating strategy included gating on cells (left column), subsequently gating for single cells (second column), gating on live cells by excluding dead cells (third column), and gating on different cell cycle phases (right column). Numbers indicate the percentage of cells in each gate. Gated cell cycle phases were G1-, S- and G2-phase, as well as G1+. G1+ and G1 were taken together for the analysis. One representative sample for each experimental sample is depicted.

The mean percentage of the total number of cells of all male samples is depicted in Table 24. In the untreated ♂*_BRCA2*$^{(+/+)}$ sample, 69.21% of all cells could be found in G1-phase, 22.26% in S-phase, and 3.96% in G2-phase. Those percentages add up to 95.43%; the remaining 4.57% were excluded in the gating process, as those cells were not single cells or were counted as debris.

Table 24 Mean percentage of the number of cells per cell cycle phase in untreated and 0.2mM formaldehyde-treated ♂_BRCA2$^{(+/+)}$ and ♂_BRCA2$^{(+/-)}$ NPCs

		UT	0.2mM Formaldehyde
♂_BRCA2(+/+)	G1-phase	69.21	68.94
	S-phase	22.26	16.60
	G2-phase	3.96	9.18
♂_BRCA2(+/-)	G1-phase	58.18	63.75
	S-phase	34.89	23.67
	G2-phase	3.45	7.71

When first the untreated samples of both cell lines, ♂_*BRCA2*$^{(+/+)}$ and ♂_*BRCA2*$^{(+/-)}$, were compared, differences in the cell distribution could be observed. For the *BRCA2*$^{(+/-)}$ cell line, significantly (p=0.0039) fewer cells could be found in G1-phase, but significantly (p=0.0009) more in S-phase. The G2 phase showed no difference in cell number between the two cell lines when analyzed with a one-way ANOVA with multiple comparisons.

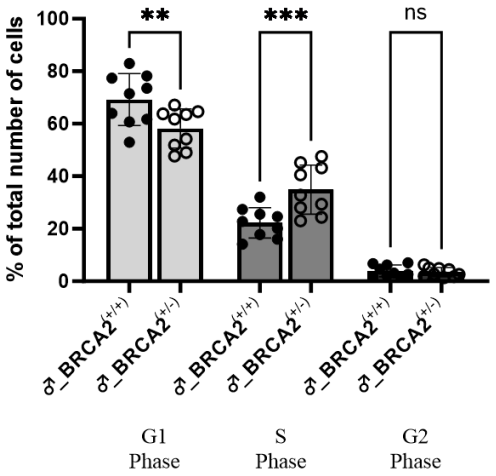

Figure 38 Cell cycle with its G1-, S-, and G2 phases comparing untreated ♂_BRCA2$^{(+/+)}$ and ♂_BRCA2$^{(+/-)}$ samples. The percentage of the total number of cells per cell cycle phase is plotted. The cell cycle of nine biological replicates per experimental sample was analyzed with the Click-iT™ EdU kit and FACS analysis. Mean ± SD, one-way ANOVA with multiple comparisons, **p<0.01, ***p<0.001. The ♂_*BRCA2*$^{(+/-)}$ sample showed significantly fewer cells in the G1-phase, while there were significantly more cells in the S-phase compared to wildtype cells.

Both cell lines were also treated with formaldehyde, with a concentration of 0.2mM for 5h, and analyzed in the same way as the untreated samples.
The treated ♂_*BRCA2*$^{(+/-)}$ sample showed significantly (p=0.0198) more cells in S-phase compared to the treated ♂_*BRCA2*$^{(+/+)}$ sample.

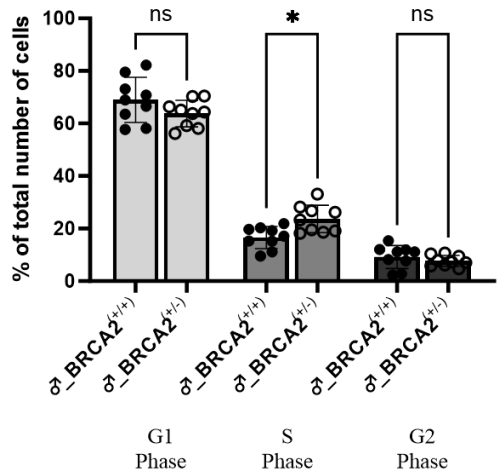

Figure 39 Cell cycle with its G1-, S-, and G2 phases comparing formaldehyde (0.2mM)-treated ♂_BRCA2$^{(+/+)}$ and ♂_BRCA2$^{(+/-)}$ samples. The percentage of the total number of cells per cell cycle phase is plotted. The cell cycle of nine biological replicates per experimental sample was analyzed with the Click-iT™ EdU kit and FACS analysis. Mean ± SD, one-way ANOVA with multiple comparisons, *p<0.05. The ♂_*BRCA2*$^{(+/-)}$ sample showed significantly more cells in the S-phase compared to wildtype cells. The G1- and G2-phase did not differ significantly between both treated samples.

Another comparison drawn was the analysis between treatment conditions within one cell line. The analysis was performed with a one-way ANOVA with multiple comparisons.

In the ♂_*BRCA2*$^{(+/+)}$ cell line no differences in the number of cells of the several phases comparing untreated and treated samples could be observed. In the ♂_*BRCA2*$^{(+/-)}$ cell line S-phase showed significantly (p=0.0005) fewer cells in the treated sample compared to the untreated sample.

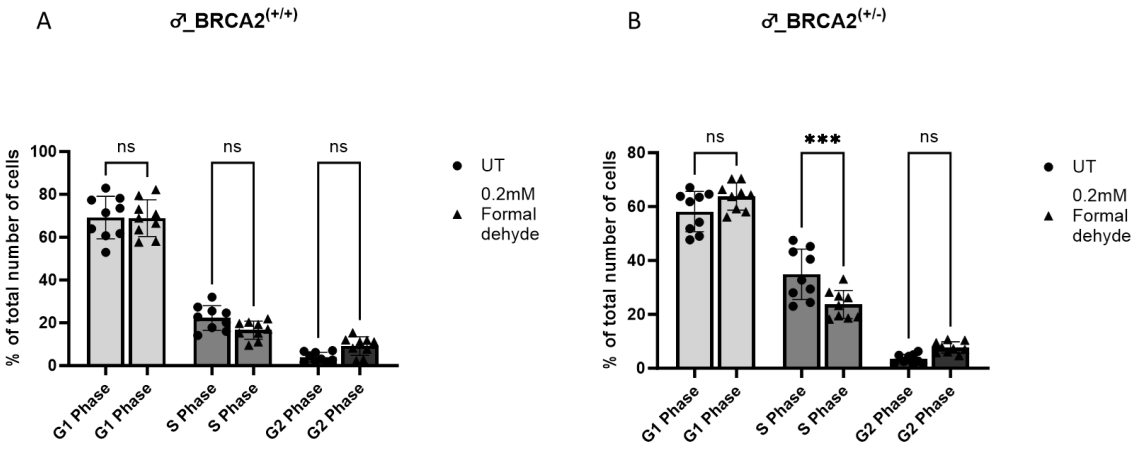

Figure 40 Cell cycle with its G1-, S-, and G2 phases in untreated and treated ♂_BRCA2$^{(+/+)}$ (A) and ♂_BRCA2$^{(+/-)}$ (B) samples. Percentage of the total number of cells per cell cycle phase is plotted. The cell cycle of nine biological replicates per experimental sample were analyzed with Click-iT™ EdU kit and FACS analysis. Mean ± SD, one-way ANOVA with multiple comparisons, ***p<0.001. The S-phase had significantly fewer cells in the treated ♂_*BRCA2*$^{(+/-)}$ sample compared to the untreated sample. All other comparisons did not reveal any differences between the samples.

A further analysis approach was tested to get another view on the data, as the starting hypothesis only said that there are changes in the cell cycle but did not specify those changes. Therefore, the analysis was further extended by comparing each single phase of the cell cycle within each cell line between treated and untreated samples with a t-test.
In the ♂_*BRCA2*$^{(+/+)}$ cell line, the number of cells in G1-phase was not significantly different between the untreated and treated samples. And while there were significantly (p=0.0305) fewer cells in the S-phase, there were significantly (p=0.0056) more cells in the G2- phase of the treated compared to the untreated sample.

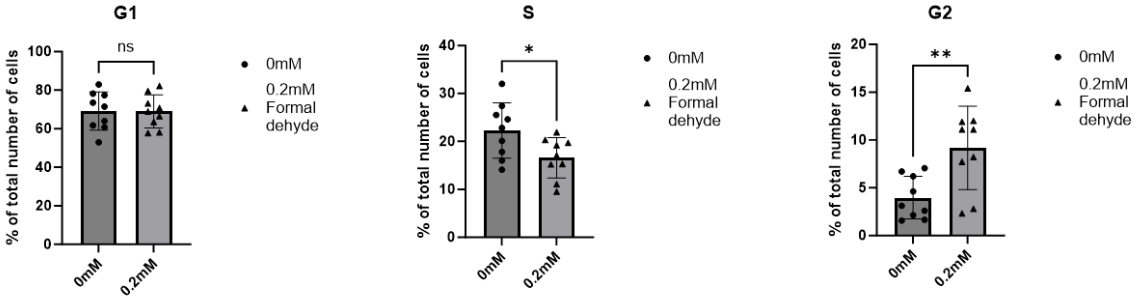

Figure 41 Analysis with t-tests of G1-, S-, and G2 phases in untreated and treated BRCA2$^{(+/+)}$ samples. The percentage of the total number of cells per cell cycle phase is plotted. The cell cycle of nine biological replicates per experimental sample was analyzed with the Click-iT™ EdU kit and FACS analysis. Mean ± SD, unpaired t-test, two-tailed, *p<0.05, **p<0.01. S-phase had significantly less and G2-phase significantly more cells in the treated sample compared to the untreated sample. The percentage of cells in the G1-phase did not differ between the untreated and treated samples.

In the ♂_*BRCA2*$^{(+/-)}$ cell line, similar results as in the ♂_*BRCA2*$^{(+/+)}$ cell line were obtained, with significantly (p=0.0063) fewer cells in the S-phase and significantly (p=0.0002) more cells in the G2-phase in treated compared to untreated samples.

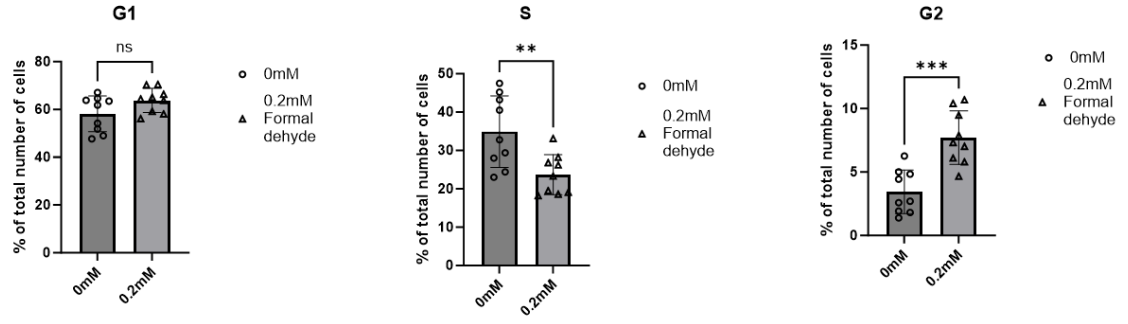

Figure 42 Analysis with t-tests of G1-, S-, and G2 phases in untreated and treated ♂_BRCA2$^{(+/-)}$ samples. The percentage of the total number of cells per cell cycle phase is plotted. The cell cycle of nine biological replicates per experimental sample was analyzed with the Click-iT™ EdU kit and FACS analysis. Mean ± SD, unpaired t-test, two-tailed, *p<0.05, **p<0.01. The S-phase had significantly fewer and the G2-phase significantly more cells in the treated sample compared to the untreated sample.

4.4.3.2 Analysis of cell cycle after formaldehyde treatment in female isogenic pair

Also, in the female isogenic pair, ♀_*BRCA2*$^{(+/+)}$ and ♀_*BRCA2*$^{(+/-)}$ NPCs, the cell cycle was analyzed. This time only two biological replicates of each cell line and treatment condition could be analyzed. Regarding statistics, several groups would need to be compared, similar to the procedure in male cells. In the male cells, this was done with one-way ANOVAs with multiple comparisons. A one-way ANOVA is a parametric test, requiring a normal distribution of data, which cannot be determined by two replicates only. In order to still be able to compare the results from the male and the female cells, the same statistical analysis strategy needs to be applied. To change the one-way ANOVA in the male cells to a nonparametric test would lead to less accurate results. Therefore, no one-way ANOVAs were used in the female samples, and only t-tests were performed in this data set comparing the single phases of the cell cycle.
The experimental procedure with the FACS gating strategy and cell cycle phases was the same as for the male isogenic pair; compare 4.4.3.1.

The mean percentage of the total cell number of all female samples is depicted in Table 25Table 24, similar to Table 24 in the experiment with male cells.

Table 25 Mean percentage of cell number per cell cycle phase in untreated and 0.2mM formaldehyde-treated ♀_BRCA2$^{(+/+)}$ and ♀_BRCA2$^{(+/-)}$ NPCs

		UT	0.2mM Formaldehyde
♂_BRCA2(+/+)	G1-phase	53.18	56.12
	S-phase	27.15	20.25
	G2-phase	10.12	15.90
♂_BRCA2(+/-)	G1-phase	45.13	47.60
	S-phase	34.70	24.65
	G2-phase	9.80	15.25

As in the male cell line, there were on average more cells in S-phase, as well as fewer cells in the G1-phase in the untreated ♀_*BRCA2*$^{(+/-)}$ cell line compared to the ♀_*BRCA2*$^{(+/+)}$ cell line. No difference could be seen in the G2-phase.

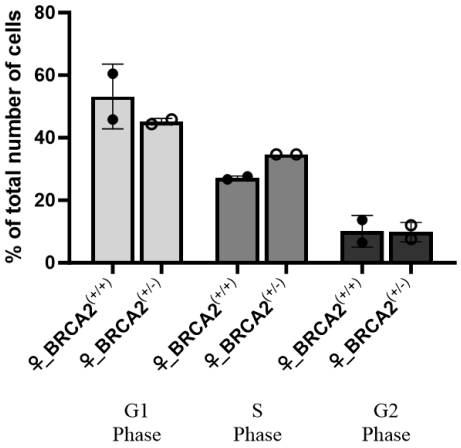

Figure 43 Cell cycle with its G1-, S-, and G2 phases comparing untreated ♀_BRCA2(+/+) and ♀_BRCA2$^{(+/-)}$ samples. The percentage of the total number of cells per cell cycle phase is plotted. The cell cycle of two biological replicates per experimental sample was analyzed with the Click-iT™ EdU kit and FACS analysis. No statistics were performed; mean ± SD is displayed. The *BRCA2*$^{(+/-)}$ sample showed fewer cells in the G1- phase, while there were more cells in the S-phase compared to wildtype cells.

When analyzing the treated samples, more cells in S-phase, as well as fewer cells in G1-phase were found in the treated ♀_*BRCA2*$^{(+/-)}$ cell line compared to the ♀_*BRCA2*$^{(+/+)}$ cell line. In the male samples (Figure 39), similar results in S-phase in the ♂_*BRCA2*$^{(+/-)}$ cell line were seen.

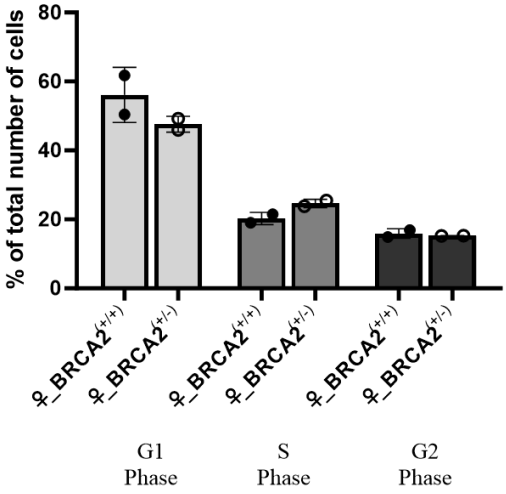

Figure 44 Cell cycle with its G1-, S-, and G2 phases comparing formaldehyde (0.2mM)-treated ♀_BRCA2$^{(+/+)}$ and ♀_BRCA2$^{(+/-)}$ samples. The percentage of the total number of cells per cell cycle phase is plotted. The cell cycle of two biological replicates per experimental sample was analyzed with the Click-iT™ EdU kit and FACS analysis. No statistics were performed; mean ± SD is displayed. The *BRCA2*$^{(+/-)}$ sample showed fewer cells in the G1- phase, while there were more cells in the S-phase compared to wildtype cells.

In the female cell lines, the analysis within each cell line comparing untreated to treated samples was performed. In the ♀_*BRCA2*$^{(+/+)}$ cell line there were no differences between untreated and treated cells in any of the cell cycle phases. In the treated samples of ♀_*BRCA2*$^{(+/-)}$, there were significantly fewer cells in S-phase compared to the untreated samples.
Those results resemble the ones already found in the male cell lines.

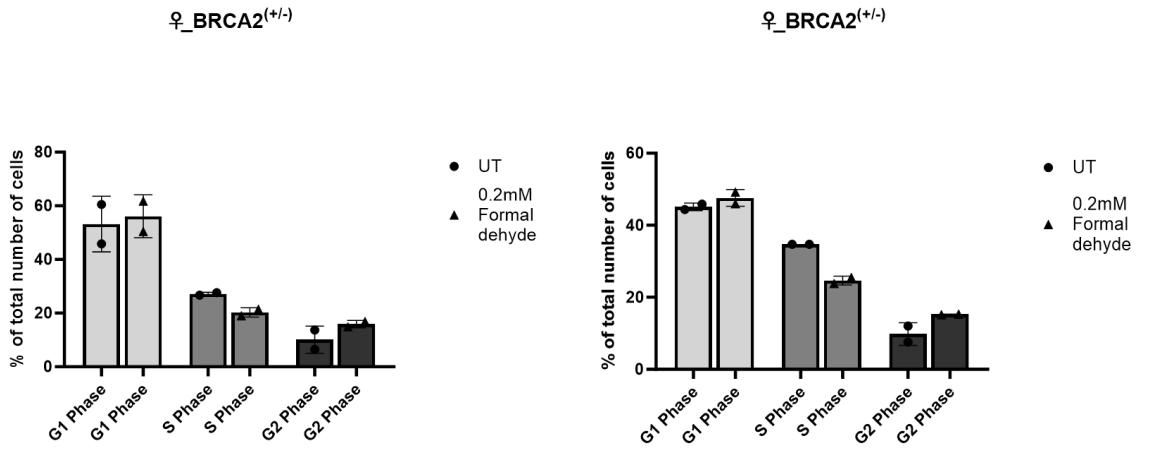

Figure 45 Cell cycle with its G1-, S-, and G2 phases in untreated and treated ♀_BRCA2(+/+) and ♀_BRCA2(+/-) samples. The percentage of the total number of cells per cell cycle phase is plotted. The cell cycle of two biological replicates per experimental sample was analyzed with the Click-iT™ EdU kit and FACS analysis. No statistical test was performed; mean ± SD is displayed. The strongest difference could be observed in the S-phase of the ♂_*BRCA2*$^{(+/-)}$ sample showing fewer cells in the treated compared to the untreated sample.

As for the male lines, cell cycle phases of the female samples were analyzed separately with a t-test comparing treated and untreated samples within each cell line.
For both cell lines, significantly fewer cells in treated samples compared to untreated samples in S-phase could be found. The p-value for the wildtype sample was p=0.0351 and p=0.0071 for the ♀_*BRCA2*$^{(+/-)}$ sample. In the G2-phase, more cells in the treated samples compared to the untreated ones could be seen, even though no statistically significant differences could be observed. Those results also resemble the findings of the male cell lines.

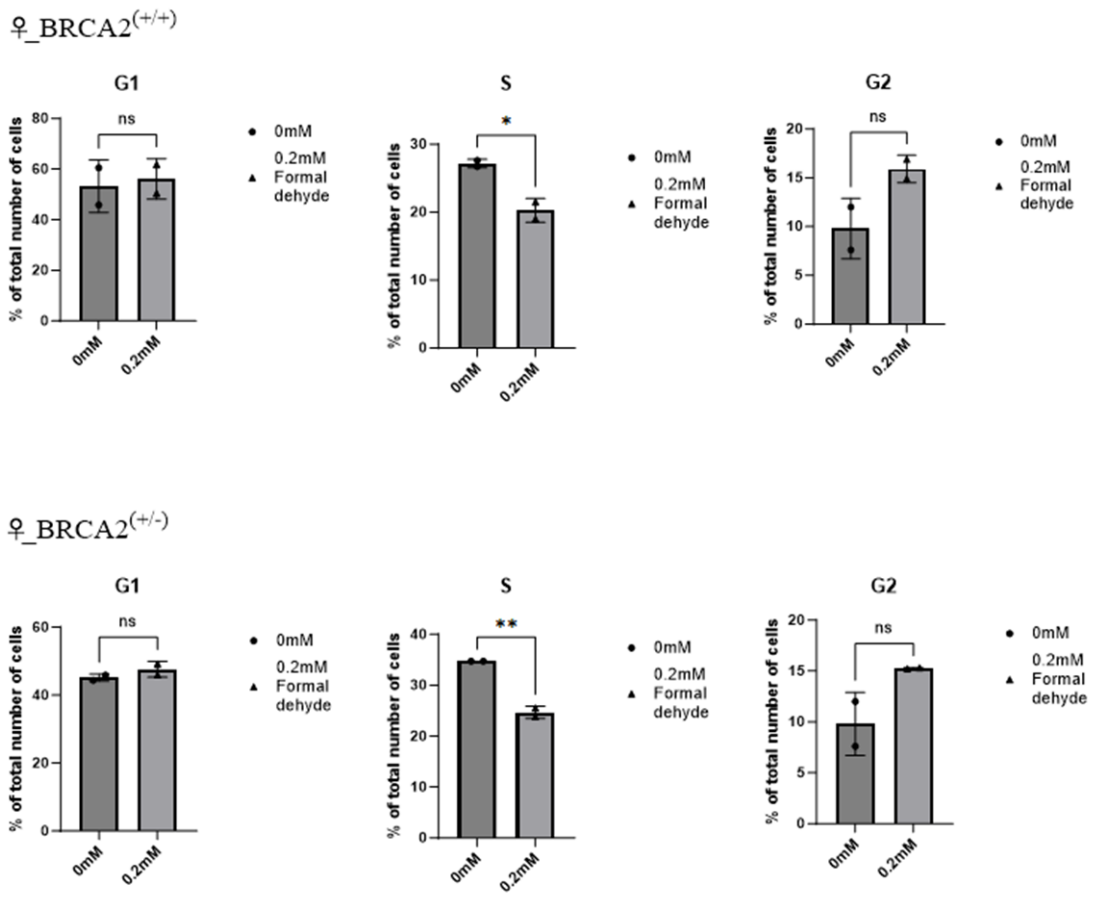

Figure 46 Analysis with t-tests of G1-, S-, and G2 phases in untreated and treated ♀_BRCA2$^{(+/+)}$ and ♀_BRCA2$^{(+/-)}$ samples. The percentage of the total number of cells per cell cycle phase is plotted. The cell cycle of two biological replicates per experimental sample was analyzed with the Click-iT™ EdU kit and FACS analysis. Mean ± SD, unpaired t-test, two-tailed, *p<0.05, **p<0.01. S-phase had significantly fewer cells in the treated samples compared to the untreated samples. The percentage of cells in the G1-phase and G2-phase did not differ between the untreated and treated samples.

The results suggest that there are two effects that influenced the cell cycle: one is due to the *BRCA2* mutation, and the other one is caused by the formaldehyde treatment. In ♀_*BRCA2*$^{(+/-)}$ samples more cells were in S-phase and fewer in G1-phase compared to wildtype cells. Moreover, in formaldehyde-treated samples the number of cells in S-phase was decreased, but the number of cells in G2-phase was increased. The results were significant in male cells and similar in female cell lines, which only had two biological replicates per cell line.

4.4.4 Proliferation assay in NPCs

Proliferation assays in the male isogenic pair and female isogenic pair in NPCs were performed to investigate a potential difference in the proliferation rate between samples due to the *BRCA2* mutation. Furthermore, cell lines were treated with 0.2mM formaldehyde and compared to their untreated counterparts to see if the treatment had an influence on cell proliferation in 2D culture. The number of cells per sample was counted manually with a counting chamber over several days depending on the experiment.

4.4.4.1 Analysis of proliferation in 2D after formaldehyde treatment in NPCs

To analyze the influence of a formaldehyde treatment on proliferating NPCs, cells were untreated or treated with 0.2mM formaldehyde. The number of cells was manually counted right before and after (0h) treatment and on four following days at the same time; compare Figure 47 and Figure 48. Over time it could be seen that untreated NPCs of ♂_*BRCA2*$^{(+/+)}$ and

♂_*BRCA2*$^{(+/-)}$ cells proliferated continuously, while formaldehyde-treated samples barely proliferated. No significant differences in the number of cells between untreated ♂_*BRCA2*$^{(+/-)}$ and ♂_*BRCA2*$^{(+/+)}$ NPCs could be found in any of the experiments.
On days 3 and 4 after treatment, significant differences in cell number between untreated and treated samples were observed, with treated samples showing significantly fewer cells. No difference could be seen between both treated samples on any of the days. Formaldehyde-treated samples did not increase in cell number during the days after formaldehyde treatment.
A one-way ANOVA with multiple comparisons, comparing all four samples within each day, was performed, but only the comparisons of day 3 and day 4 are displayed in the graphs. As only those comparisons showed differences between samples, while the comparisons on the other days did not show differences.

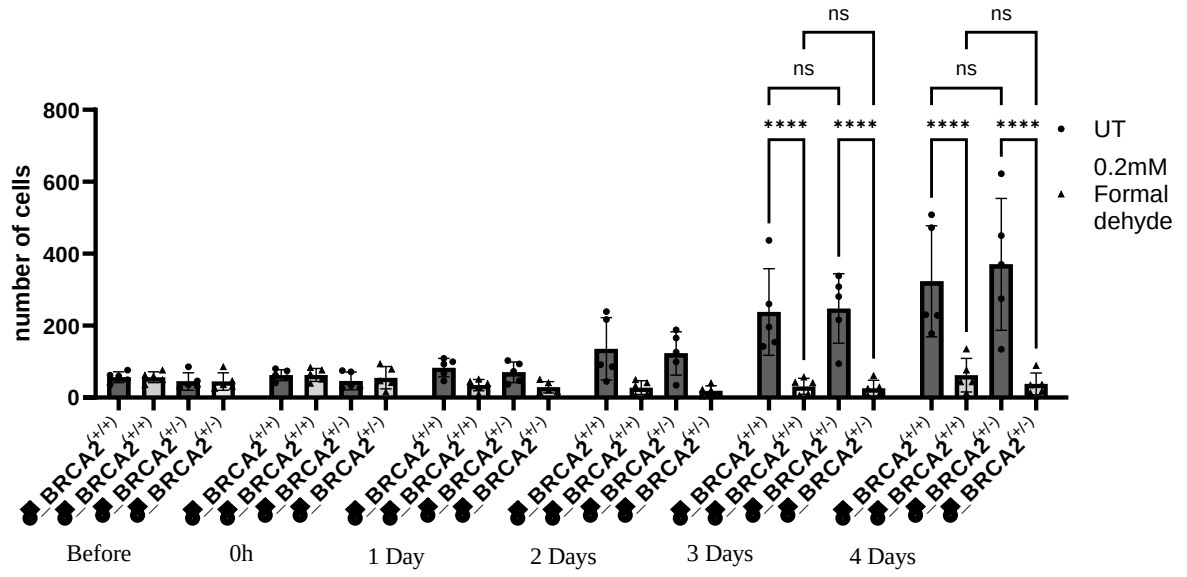

Figure 47 Proliferation assay in untreated and 0.2mM formaldehyde-treated male NPCs. ♂_*BRCA2*$^{(+/+)}$ and ♂_*BRCA2*$^{(+/-)}$ cells were used with five biological replicates per sample. The number of cells was manually counted with a counting chamber right before and after (0h) the treatment and on the four following days. Mean ± SD, one-way ANOVA with multiple comparisons, ****p<0.0001. Significant differences could be found 3 days and 4 days after treatment comparing the untreated to the treated samples within each cell line. There is no difference comparing both cell lines, neither in their untreated nor in their treated conditions on day 3 and day 4. As well as no significant differences between any of the samples at other time points.

The results were similar for both isogenic pairs (males and females). The only difference was the strength of the treatment effect on day 3 between male and female cell lines, with the male cell lines showing a stronger decrease in proliferation rate due to formaldehyde treatment (p<0.0001) than the female cell lines. In the female cell lines, the p-values for the comparison on day 3 were p=0.0191 for the ♀_*BRCA2*$^{(+/+)}$ sample and p=0.0056 for the ♀_*BRCA2*$^{(+/-)}$ sample. On day 4 it was p<0.0001. The formaldehyde-treated samples increased slightly in cell number during the days after formaldehyde treatment.
Three biological replicates for the female isogenic pair were used, while there were five biological replicates for the male isogenic pair.

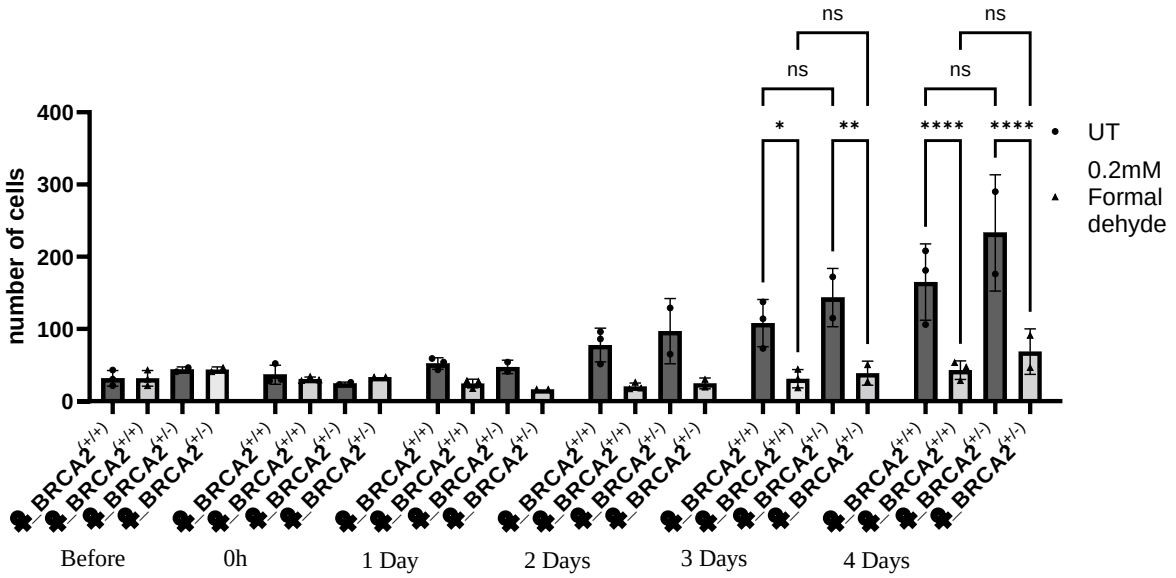

Figure 48 Proliferation assay in untreated and 0.2mM formaldehyde-treated female NPCs. ♀*_BRCA2(+/+)* and ♀*_BRCA2(+/-)* cells were used with three biological replicates per sample. The number of cells was manually counted with a counting chamber right before and after (0h) treatment and on four following days. Mean ± SD, one-way ANOVA with multiple comparisons, *p<0.05, **p<0.01, ****p<0.0001. Significant differences could be found 3 days and 4 days after treatment, comparing untreated to treated samples within each cell line. There is no difference comparing both cell lines, neither in their untreated nor in their treated conditions.

4.4.4.2 Long-term analysis after treatment

The reason to perform a long-term analysis was to analyze if the number of cells in formaldehyde-treated samples would increase again over time, as within four days after treatment the number of cells did not increase; compare 4.4.4.1.

The male isogenic pair was used for this experiment, and the number of cells was determined before and 1, 2, 4, 7, and 9 days after the 5h treatment with 0.2mM formaldehyde.

Figure 49 shows that in both cell lines, ♂*_BRCA2(+/+)* and ♂*_BRCA2(+/-)*, the number of cells in both untreated and treated samples increased over time. The increase of cells in the untreated samples started already 2 days after formaldehyde treatment, while in the treated samples only 7 days after treatment did the number of cells increase.

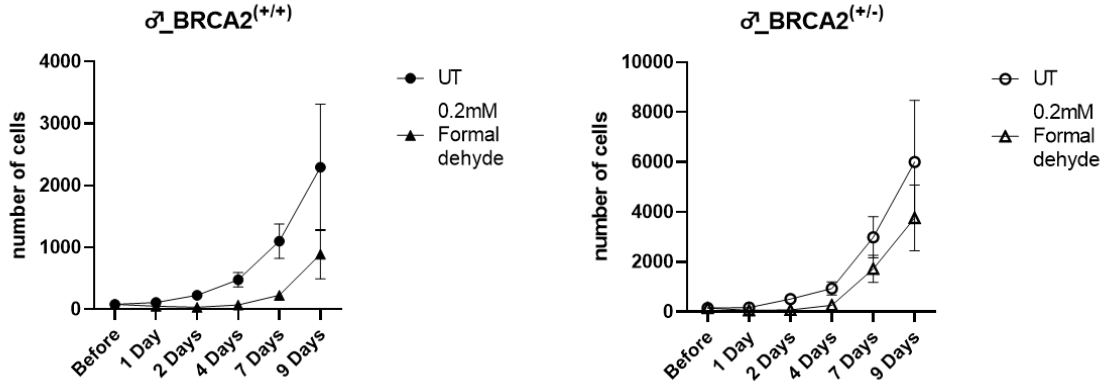

Figure 49 Number of cells over time in ♂_BRCA2(+/-) and ♂_BRCA2(+/+) samples untreated and formaldehyde-treated (0.2mM). The number of cells was manually counted with a counting chamber right before and after (0h) treatment and on four following days. Three biological replicates per sample were used. Mean ± SD. In both cell lines, ♂*_BRCA2(+/+)* and ♂*_BRCA2(+/-)* the number of cells in both samples, untreated and formaldehyde-treated, increased over time, already starting at Day 2 in the untreated samples, while only starting at Day 7 in the treated samples.

To analyze the influence of formaldehyde on cell numbers, cell numbers were taken into relation: at each of the six time points, the cell numbers of the treated samples were divided by the cell numbers of the untreated samples. With this approach it is possible to implement the formaldehyde treatment in the data and compare both cell lines.
It could be seen that for both cell lines, the number of cells decreased after treatment, stayed low until day 4, and increased again at 7 and 9 days after treatment. Furthermore, there was no significant difference between ♂_*BRCA2*$^{(+/+)}$ and ♂_*BRCA2*$^{(+/-)}$ NPCs. Therefore, formaldehyde did not differ in its effect on both cell lines.

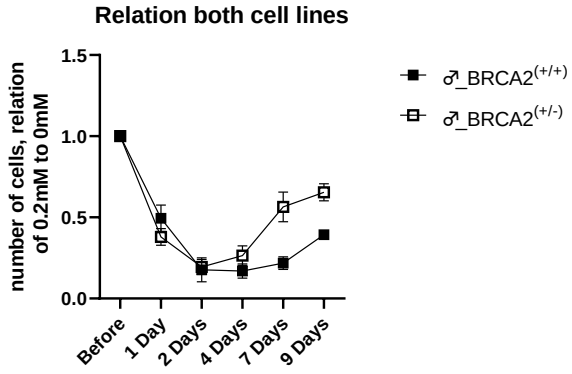

Figure 50 Relation of number of cells of treated to untreated samples in both cell lines. Mean ± SD. Formaldehyde did not affect the cell lines differently.

Proliferation was consistently ongoing in all cell lines. Treatment with formaldehyde decreased the number of cells in both isogenic pairs, but the cells recovered and started to grow again. There was no different effect of formaldehyde on the ♂_*BRCA2*$^{(+/+)}$ and ♂_*BRCA2*$^{(+/-)}$ cell lines.

4.5 Experiments in 3D culture

Besides the analysis in 2D culture, 3D culture experiments were also performed. They were performed to see if subtle changes, due to a *BRCA2* mutation or a treatment with formaldehyde, were detectable in brain-like structures.
Neurospheres are 3D structures that are generated from NPCs. With these neurospheres it is possible to analyze two parameters: cellular proliferation and migration.
Both parameters were analyzed within one batch of neurospheres. One quarter of the neurospheres was used for migration analysis and three quarters for proliferation analysis. Regarding the exact protocol, please refer to the methods section.
First, neurospheres were observed over a period of 10 days to see if the neurospheres proliferated and cells migrated out of the neurospheres regularly and increasingly over time. Second, neurospheres were treated with 0.2mM formaldehyde for 5h, to see if formaldehyde has any influence on proliferation or migration over a period of 10 days. As no effect of formaldehyde could be observed, the incubation time with formaldehyde was increased to 24 hours with an analysis on Day 5. There was no effect of the extended treatment on either proliferation or migration. As cells carrying a *BRCA2* mutation might accumulate more DNA damage over time and be more susceptible to a formaldehyde treatment compared to wildtype cells, older cells (with a passage higher than 15) were used to generate neurospheres, and the experiment with a 24h incubation of formaldehyde was repeated. An effect on proliferation could be observed.

Which isogenic pair, male or female, was used for the exact experiment is indicated in each chapter. For the last experiment all male isogenic cell lines were used.

4.5.1 Neurospheres - proliferation

For proliferation analysis, neurospheres were cultured up to 10 days in low-attachment, round-bottom-shaped 96-well plates, and pictures were taken on day 5, day 8, and day 10. The Feret diameter of each neurosphere was determined with a script from [redacted], a PhD student in the lab. Outliers in the data (ROUT Q=1%) had been identified and removed. The data, if necessary, was analyzed with a one-way ANOVA and multiple comparisons.

4.5.1.1 Proliferation over time

Proliferation of neurospheres generated from the male and female isogenic NPC pairs was measured over time by analyzing pictures taken on day 5, day 8, and day 10; compare Figure 51. For the analysis, the Feret diameter of each neurosphere was automatically determined.

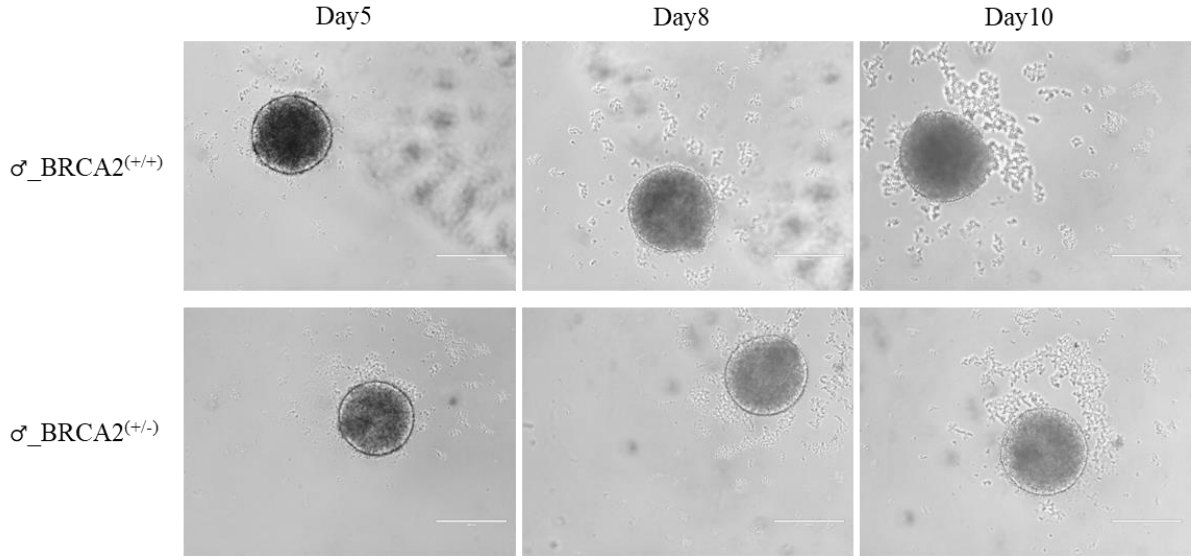

Figure 51 Representative white-light pictures of neurospheres growing over time. Representative pictures of neurospheres of ♂_BRCA2$^{(+/+)}$ and ♂_BRCA2$^{(+/-)}$ cells were taken on Day 5, Day 8, and Day 10. The scale bar is 1000µm.

The neurospheres of all cell lines grew continuously over time (Figure 52). Neurospheres were not treated with formaldehyde in this experiment.

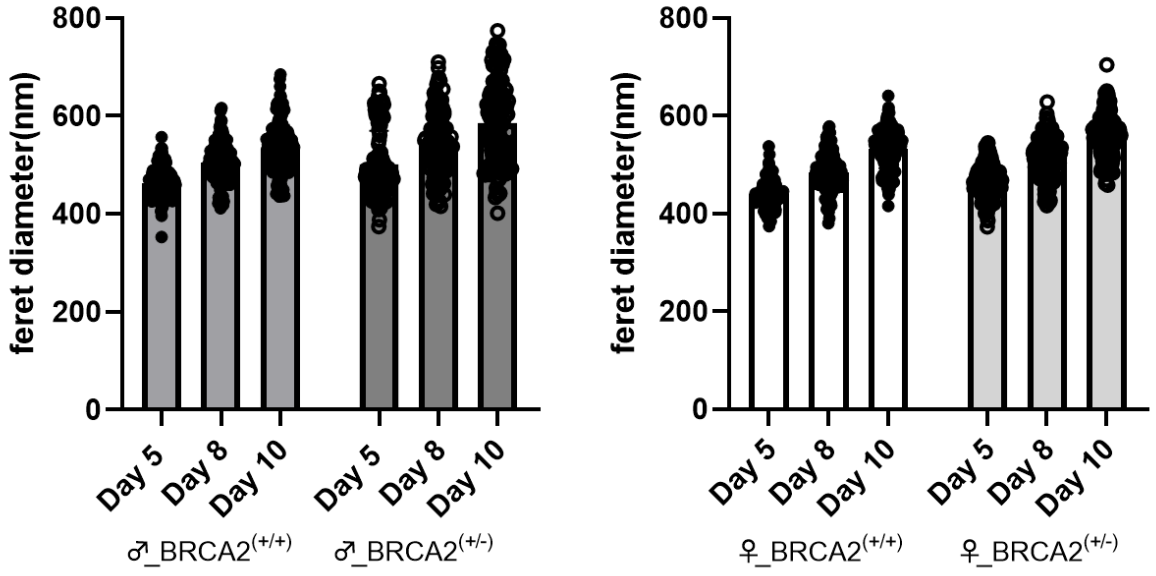

Figure 52 Proliferation of neurospheres over time. In male and female BRCA2$^{(+/+)}$ and BRCA2$^{(+/-)}$ neurospheres, the Feret diameter increased over time, being measured on day 5, day 8, and day 10.

4.5.1.2 Proliferation after 5h formaldehyde treatment

For this experiment, neurospheres were treated with 0.2mM of formaldehyde for 5h at 37°C on day 3. Afterwards they were left to grow and were analyzed again on day 5, day 8, and day 10. The female isogenic pair (♀_*BRCA2*$^{(+/+)}$ and ♀_*BRCA2*$^{(+/-)}$) was used for the experiment.
It could be observed that the neurospheres grew steadily over time, as in the previous experiment; see 4.5.1.1. No significant difference between the untreated and the treated sample in any of the cell lines, nor at any time point (Figure 53), could be observed.

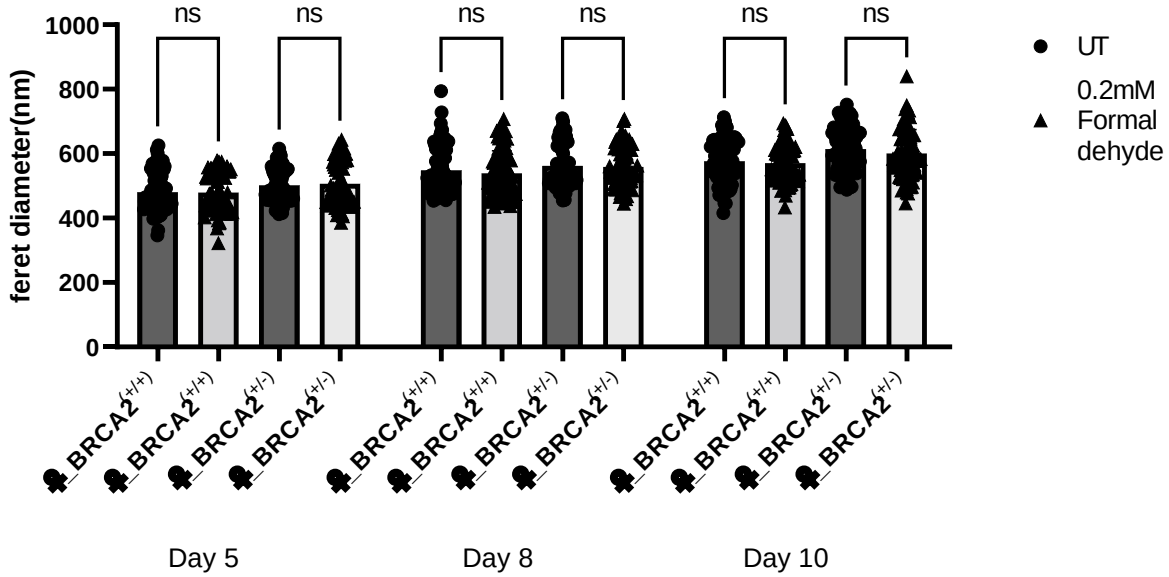

Figure 53 Proliferation of untreated and 5hour formaldehyde (0.2mM)-treated neurospheres. Each dot and arrow represents one neurosphere. Mean ± SD, one-way ANOVA with multiple comparisons. There was no significant difference between the untreated and treated samples in both cell lines at any time point.

4.5.1.3 Proliferation after 24h formaldehyde treatment

No significant differences could be found between untreated and formaldehyde-treated samples after five hours of treatment. Therefore, the incubation time with formaldehyde was increased to 24h. The treatment started on day 3 of the assay and was stopped on day 4. Analysis was again performed on Day 5.

4.5.1.3.1 Neurospheres generated from NPCs with a passage < 15

The male isogenic pair (♂*_BRCA2*$^{(+/+)}$ and ♂*_BRCA2*$^{(+/-)}$) was used for this experiment, and neurospheres were generated of NPCs that had a passage lower than 15.

No significant differences in treated compared to untreated neurospheres could be found on day 5. As the results did not differ between untreated and treated samples on day 5, the later time points, day 8 and day 10, were not analyzed.

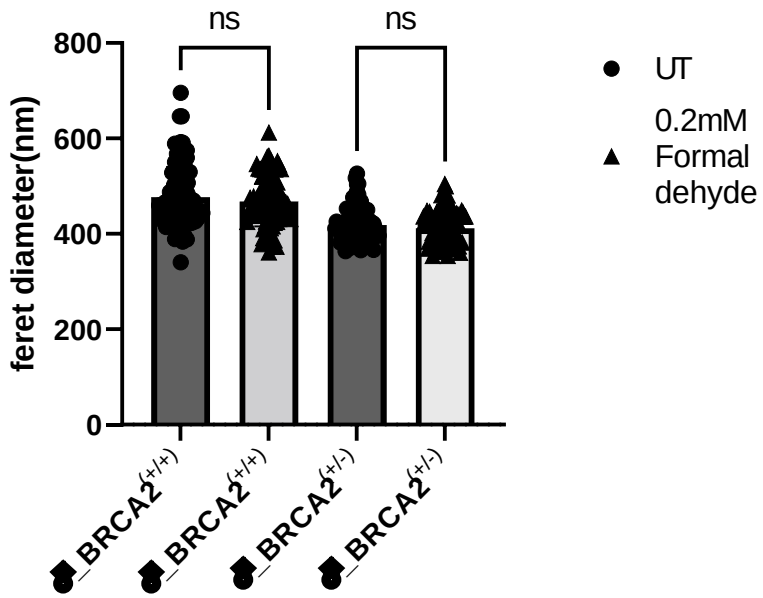

Figure 54 Proliferation of untreated and 24h formaldehyde (0.2mM)-treated neurospheres on day 5. Each dot and arrow represents one neurosphere. Mean ± SD, one-way ANOVA with multiple comparisons. Neurospheres were generated from NPCs with a passage lower than 15 and did not show any significant differences between treated and untreated samples in regard to Feret diameter.

4.5.1.3.2 Neurospheres generated from NPCs with a passage > 15

This 24h formaldehyde treatment was performed in neurospheres generated from NPCs with a passage between 15 and 20.

As significant differences between untreated and formaldehyde-treated samples could be seen in the ♂*_BRCA2*$^{(+/-)}$ cell line on day 5, day 8 and day 10 were also analyzed.

The mean Feret diameter of the neurospheres of all samples can be found in Table 26.

On day 5, a difference could be found in Feret diameter between untreated ♂*_BRCA2*$^{(+/+)}$ and ♂*_BRCA2*$^{(+/-)}$ neurospheres, with ♂*_BRCA2*$^{(+/-)}$ neurospheres being significantly ($p=0.0025$) smaller in diameter. Furthermore, formaldehyde treatment caused an even smaller Feret diameter in *BRCA2*$^{(+/-)}$ treated neurospheres. The p-value for the comparison between treated and untreated ♂*_BRCA2*$^{(+/-)}$ neurospheres was $p=0.0042$. Compared to treated ♂*_BRCA2*$^{(+/+)}$ neurospheres, treated ♂*_BRCA2*$^{(+/-)}$ neurospheres were significantly ($p<0.0001$) smaller.

On day 8 the difference in Feret diameter between both untreated neurosphere batches was not visible anymore, whereas a difference between untreated and treated wildtype samples could

be detected (p=0.021). The difference between both treated neurosphere samples remained (p<0.0001).
On day 10, the effect of formaldehyde on both cell lines continued to be present (p=0.0175 for ♂*_BRCA2*$^{(+/+)}$ samples and p=0.0225 for ♂*_BRCA2*$^{(+/-)}$ sample), while there was no difference between both untreated and both treated samples anymore.

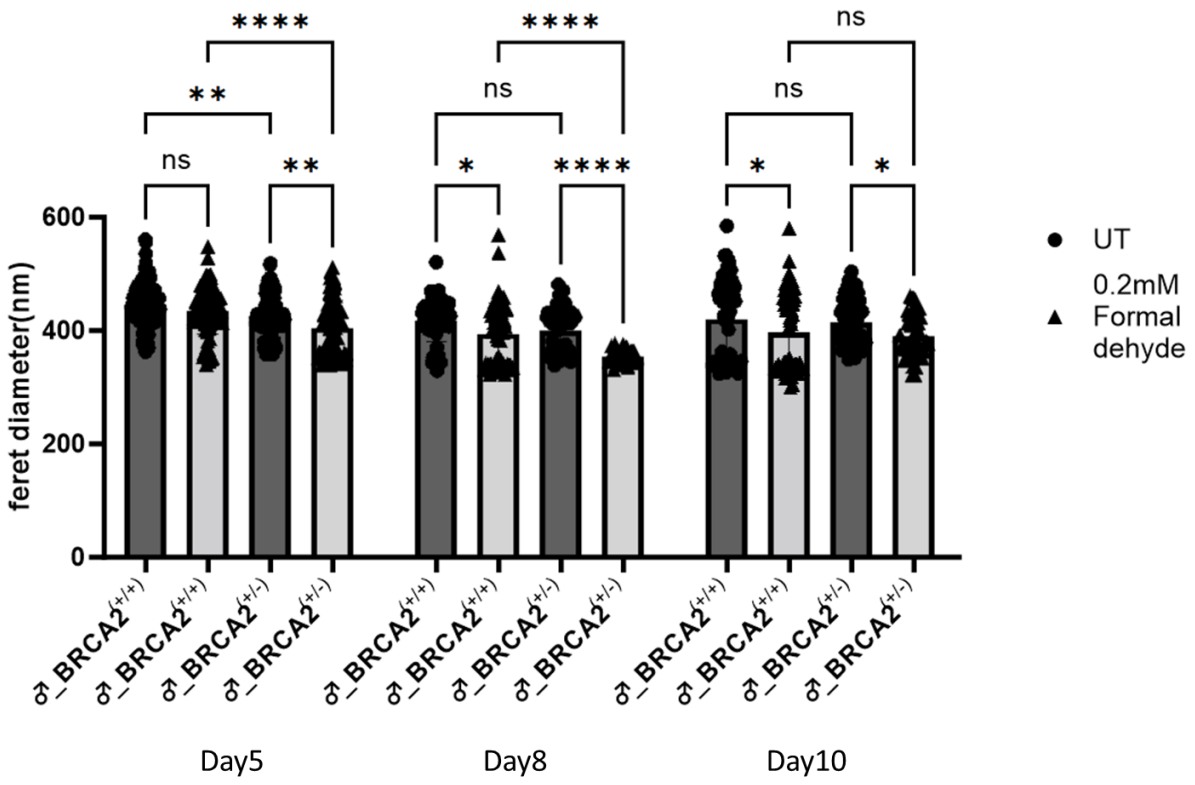

Figure 55 Proliferation of untreated and 24h formaldehyde (0.2mM)-treated neurospheres with >15 passages on days 5, 8, and 10. Neurospheres were generated from NPCs with a passage higher than 15. Each dot and arrow represents one neurosphere. Mean ± SD, one-way ANOVA with multiple comparisons, *p<0.05, **p<0.01, ****p<0.0001. Formaldehyde seemed to affect the neurospheres differently depending on the cell line and day of analysis.

When comparing the values between day 5, day 8, and day 10, no increase in Feret diameter over time could be observed. Usually, it would have been expected that the Feret diameter would increase from day 5 to day 8 to day 10 due to proliferation of the neurospheres. Also similar to the results observed in neurospheres generated from young NPCs, compare 4.5.1.1.. The cells, which were used for this experiment, had a passage higher than 15 and were frozen and thawed between the generation of cells and the experiment.

In addition to the male isogenic pair ♂*_BRCA2*$^{(+/+)}$ and ♂*_BRCA2*$^{(+/-)}$, the experiment was also performed in neurospheres generated from ♂*_BRCA2*$^{(-/-)}$ and ♂*_BRCA1*$^{(+/-)}$ NPCs with a passage higher than 15.
As can be observed in Figure 56, also the other cell lines did not show a continuous, high proliferation from day 5 until day 10.

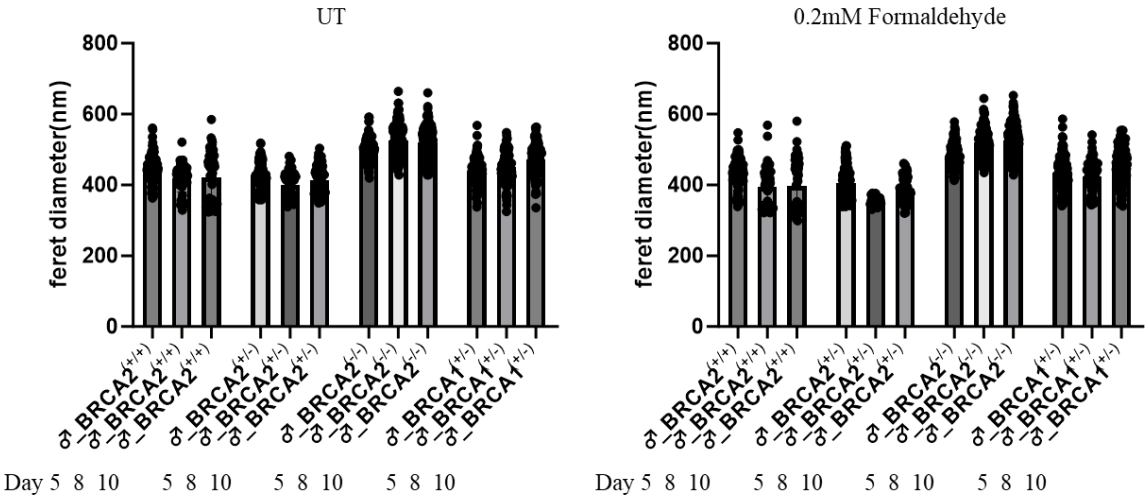

Figure 56 Proliferation in all neurospheres generated from old NPCs on days 5, 8, and 10. The graphs showed proliferation of all neurospheres, either untreated or treated with formaldehyde. The increase of Feret diameter was not as high as in the experiment over time in neurospheres generated from young NPCs; compare Figure 52.

In order to compare continuous proliferation between old and young neurospheres, proliferation over time was calculate; see Table 26. For this analysis, proliferation of neurospheres from experiment one (4.5.1.1 Proliferation over time) and four (4.5.1.3.2 Neurospheres generated from NPCs with a passage > 15) were examined.
To do so, the means of the Feret diameter of all neurospheres on each day were listed, and the difference between day 5 and day 10 was calculated. This difference was subsequently presented as a percentage from the mean on day 10; compare Table 26. As an example: in the ♂*_BRCA2*$^{(+/+)}$ neurospheres generated from young NPCs, the increase/change from day 5 to day 10 is 70.31µm. Those 70.31µm are 13.18% of 533.39µm, which is the Feret diameter on day 10.
Regarding the untreated samples from the fourth experiment: in ♂*_BRCA2*$^{(+/+)}$ and ♂*_BRCA2*$^{(+/-)}$ neurospheres, proliferation was not visible; instead, a reduction over time could be detected. The reduction was 5.79% in ♂*_BRCA2*$^{(+/+)}$ from day 5 to day 10 and 2.55% in ♂*_BRCA2*$^{(+/-)}$. In ♂*_BRCA2*$^{(-/-)}$ and ♂*_BRCA1*$^{(+/-)}$ samples, neurospheres showed an increase of 4.44% and 7.05% respectively. Also, in the treated samples, the change is not consistent: increases in diameter of up to 8.01% (♂*_BRCA2*$^{(-/-)}$) were visible, while also a reduction of up to 9.45% (♂*_BRCA2*$^{(+/+)}$) was visible.
All cells, which were used for this experiment, had a passage higher than 15. But only ♂*_BRCA2*$^{(+/+)}$ and ♂*_BRCA2*$^{(+/-)}$ cells were frozen and thawed between the generation of cells and the experiment, while ♂*_BRCA2*$^{(-/-)}$ and the ♂*_BRCA1*$^{(+/-)}$ samples were continuously cultured after differentiation into NPCs to quickly reach a passage higher than 15 and had not been frozen between the generation of cells and the experiment.

In neurospheres generated during the first experiment, the increase was 70µm for ♂*_BRCA2*$^{(+/+)}$ and 83µm for ♂*_BRCA2*$^{(+/-)}$, which was an increase of 13% and 14% of Feret diameter.

Therefore, it can be concluded that the increase in neurospheres generated from NPCs with a passage higher than 15 is not as regular as in neurospheres generated from NPCs with a lower passage.

Table 26 Calculation of Feret diameter over time in neurospheres generated from old and young NPCs

Experiment		24h formaldehyde treatment, generated from old NPCs				over time, from young NPCs	
Cell line		♂_BRCA2$^{(+/+)}$	♂_BRCA2$^{(+/-)}$	♂_BRCA2$^{(-/-)}$	♂_BRCA1$^{(+/-)}$	♂_BRCA2$^{(+/+)}$	♂_BRCA2$^{(+/-)}$
Treatment condition		UT	UT	UT	UT	UT	UT
Mean of Neurospheres	Day 5	444,76	424,67	497,28	438,47	463,08	501,82
	Day 8	417,50	399,36	526,44	450,07	504,60	544,04
	Day 10	420,43	414,10	520,39	471,71	533,39	585,37
change from Day 5 to Day 10		-24,33	-10,57	23,11	33,24	70,31	83,54
change to Day 10 [%]		-5,79	-2,55	4,44	7,05	13,18	14,27
Treatment condition		0.2mM Formaldehyde	0.2mM Formaldehyde	0.2mM Formaldehyde	0.2mM Formaldehyde		
Mean of Neurospheres	Day 5	433,70	404,86	483,38	434,36		
	Day 8	393,56	354,63	519,96	425,25		
	Day 10	396,25	389,91	525,46	454,97		
change from Day 5 to Day 10		-37,45	-14,95	42,08	20,61		
change to Day 10 [%]		-9,45	-3,83	8,01	4,53		

When comparing neurospheres only within each day, the following can be observed:
On day 5, a significant difference between untreated and treated conditions in both *BRCA2*-mutated samples could be observed. Treated cells in the ♂*_BRCA2*$^{(+/-)}$ sample showed significantly smaller ferret diameters compared to untreated neurospheres with a p-value of p=0.0001. Accordingly, the treated neurospheres in the ♂*_BRCA2*$^{(-/-)}$ sample also showed significantly lower ferret diameters due to formaldehyde treatment compared to untreated neurospheres with a p-value of p=0.0098. ♂*_BRCA2*$^{(+/+)}$ and ♂*_BRCA1*$^{(+/-)}$ neurospheres did not show any differences due to treatment.

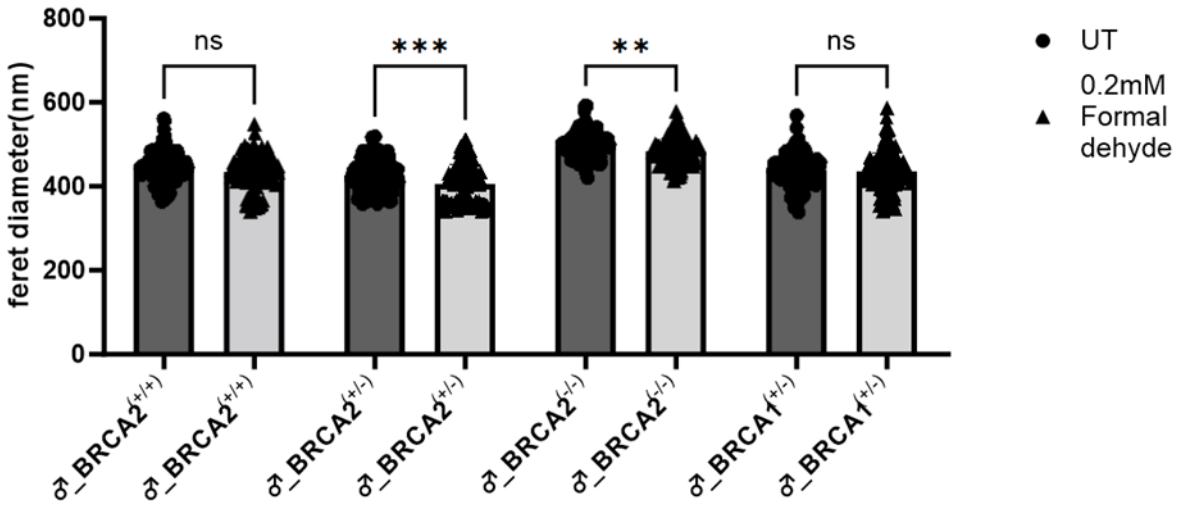

Figure 57 Proliferation of untreated and 24h formaldehyde (0.2mM)-treated neurospheres with >15 passages on day 5 . Neurospheres were generated from NPCs with a passage higher than 15. Each dot and arrow represents one neurosphere. Mean ± SD, one-way ANOVA with multiple comparisons, **p<0.01, ***p<0.001. Neurospheres showed significant differences between treated and untreated samples in regard to Feret diameter in mutated *BRCA2* cells.

On day 8, the effect of formaldehyde was visible in three of the four samples (not in the ♂*_BRCA2*$^{(-/-)}$ sample), with the Feret diameter having been smaller in treated compared to untreated samples. The p-values of those comparisons were p=0.0026 for the ♂*_BRCA2*$^{(+/+)}$, p<0.0001 for the ♂*_BRCA2*$^{(+/-)}$, and p<0.0001 for the ♂*_BRCA1*$^{(+/-)}$ sample.

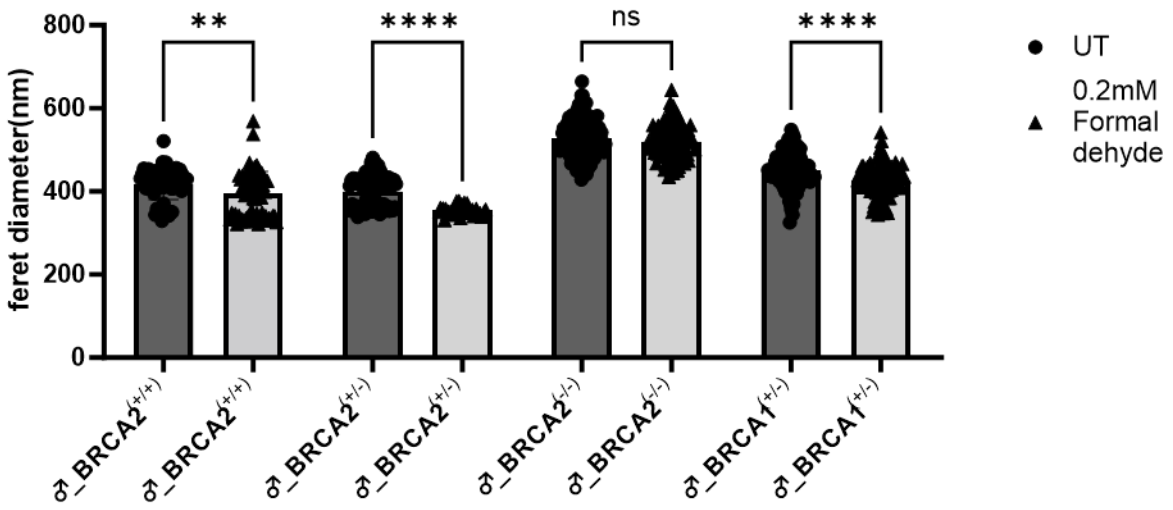

Figure 58 Proliferation of untreated and 24h formaldehyde (0.2mM)-treated neurospheres with >15 passages on day 8. Neurospheres were generated from NPCs with a passage higher than 15. Each dot and arrowhead represents one neurosphere. Mean ± SD, one-way ANOVA with multiple comparisons, **p<0.01, ****p<0.0001. The neurospheres showed significant differences between treated and untreated samples in regard to Feret diameter in all samples besides BRCA2$^{(-/-)}$.

On day 10, the effect of formaldehyde also disappeared in the ♂*_BRCA1$^{(+/-)}$* sample and was only visible in ♂*_BRCA2$^{(+/+)}$* (p=0.0171) and ♂*_BRCA2$^{(+/-)}$* (p=0.0211) samples comparing untreated and treated samples.

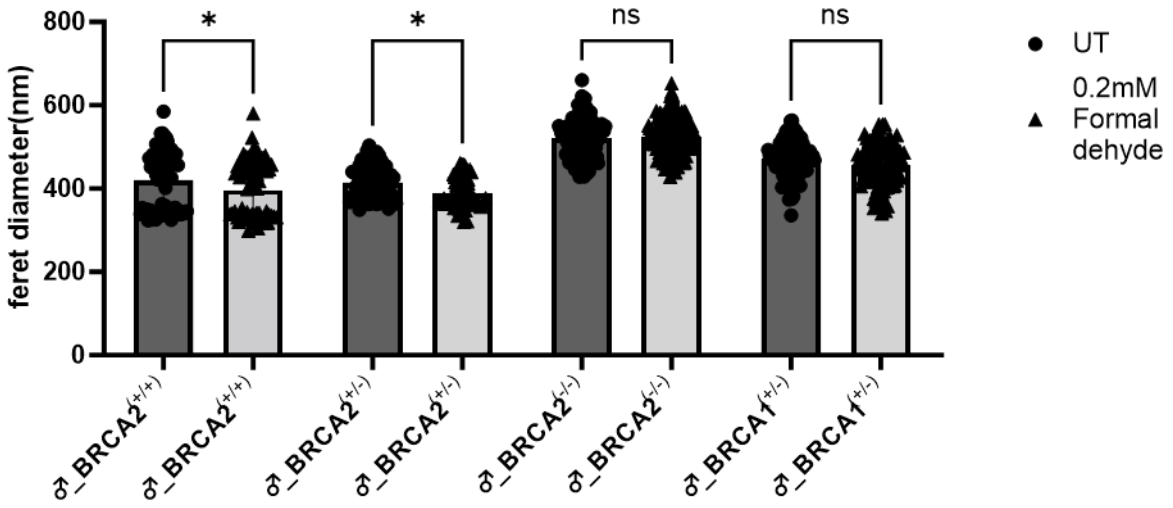

Figure 59 Proliferation of untreated and 24h formaldehyde (0.2mM)-treated neurospheres with >15 passages on day 10. Neurospheres were generated from NPCs with a passage higher than 15. Each dot and arrow represents one neurosphere. Mean ± SD, one-way ANOVA with multiple comparisons, *p>0.05. They showed significant differences between treated and untreated samples in regard to Feret diameter in wildtype and ♂_BRCA2$^{(+/-)}$ samples.

4.5.2 Neurospheres - migration

Not only can proliferation be investigated with the neurosphere assay, but also migration of cells from the neurospheres into the periphery. The same experimental setup regarding time schedules and analysis method as for the proliferation analysis was performed; compare 4.5.1. In the following experiments migration was analyzed: over time, after 5h formaldehyde treatment, after 24h formaldehyde treatment, and after 24h formaldehyde treatment in neurospheres generated from NPCs with a passage >15.

To analyze migration, neurospheres were placed into PL-coated 6-well plates on day 3 of the assay, only slightly covered with neuronal media, and cultured at 37°C with 8% CO_2. After a 24h treatment with formaldehyde, cells were transferred into 6-well plates on Day 4, right after the end of the incubation with formaldehyde. Being attached to the ground, cells could migrate out of the neurospheres, and pictures were taken on day 5, day 8, and day 10. The Feret diameter of each neurosphere was determined, and a second circle was manually drawn around the outer ends of the migrating cells. From those two circles the Feret diameter was calculated, and it was possible to subtract the Feret diameter of the inner circle from the Feret diameter of the outer circle, and therefore the average migrated distance of the cells could be determined. Outliers in the data (ROUT Q=1%) had been identified and removed. The data, if necessary, was analyzed with a one-way ANOVA and multiple comparisons.

4.5.2.1 Migration over time

Migration of cells of neurospheres generated from the male and female isogenic NPC pairs was measured over time by analyzing pictures taken on day 5, day 8, and day 10, compare Figure 60.

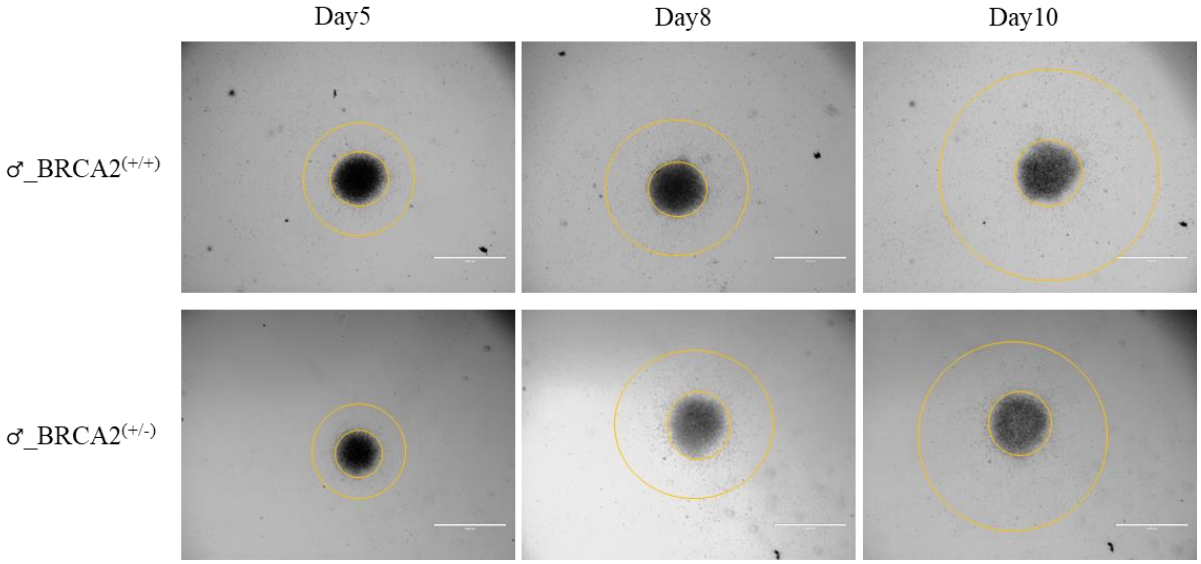

Figure 60 Representative white light pictures of neurospheres migrating over time. Representative pictures of neurospheres of ♂_BRCA2$^{(+/+)}$ and ♂_BRCA2$^{(+/-)}$ cells taken on day 5, day 8, and day 10. The inner circle covered the neurospheres, while the outer circle involved the migrated cells. The scale bar is 1000µm.

In all cell lines, the cells continuously migrated out of the neurospheres over time; compare Figure 61. Neurospheres were not treated with formaldehyde in this experiment.

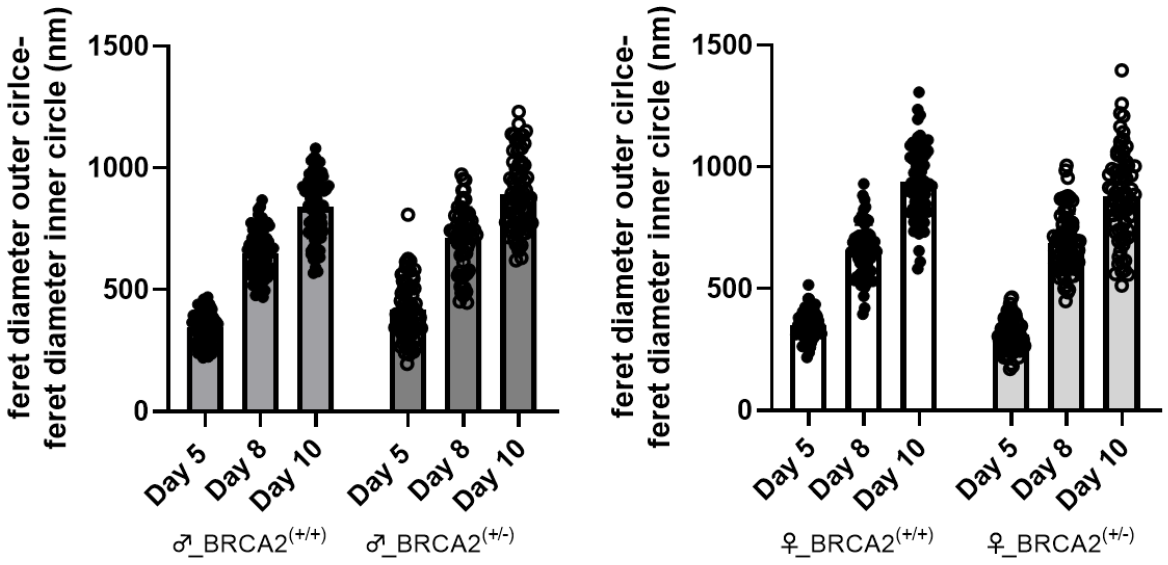

Figure 61 Migration of cells out of neurospheres over time. In male and female BRCA2$^{(+/+)}$ and BRCA2$^{(+/-)}$ neurospheres, migration increased over time, being measured on day 5, day 8, and day 10. Migration distance was calculated by subtracting the Feret diameter of the inner circle from the Feret diameter of the outer circle.

4.5.2.2 Migration after 5h formaldehyde treatment

For this experiment, neurospheres were treated with 0.2mM formaldehyde for 5h at 37°C on day 3. Afterwards they were placed into the PL-coated six-well plate, media was changed, and they were allowed to grow and migrate. Analysis was performed on day 5, day 8, and day 10. The female isogenic pair ♀_*BRCA2*$^{(+/+)}$ and ♀_*BRCA2*$^{(+/-)}$ was used for this experiment.

It could be observed that cells migrated out of the neurospheres over time as in the previous experiment. There was no significant difference between untreated and treated samples in any of the cell lines at any time point (Figure 62).

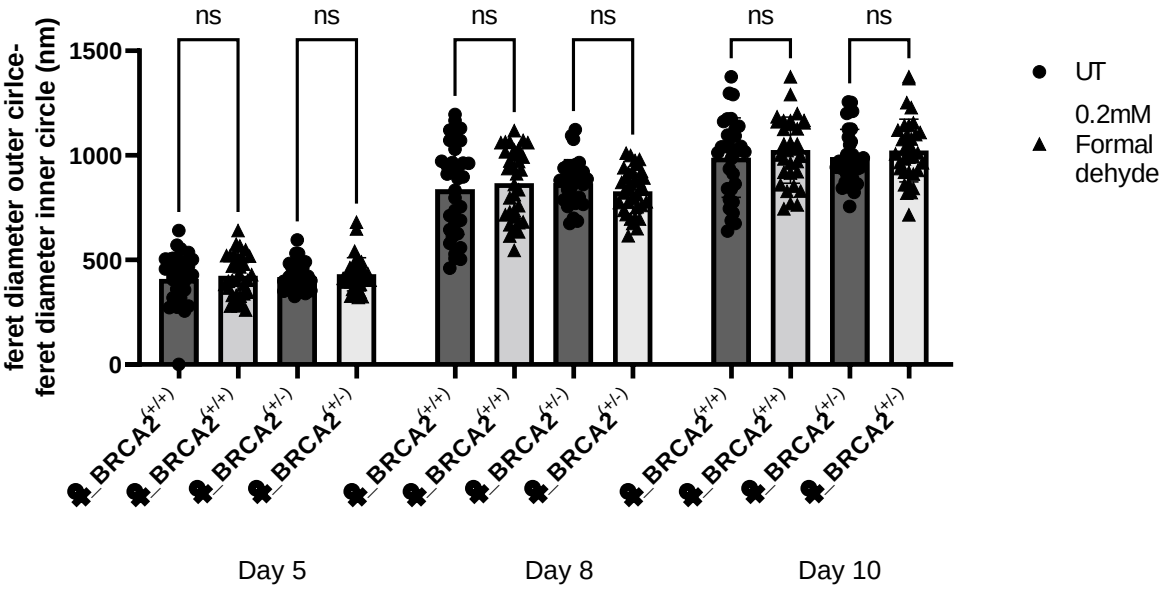

Figure 62 Migration of untreated and 5 hours formaldehyde (0.2mM)-treated neurospheres. Each dot and arrow represents one neurosphere. Mean ± SD, one-way ANOVA with multiple comparisons. There was no significant difference in the migrated distance between the untreated and the treated sample in both cell lines at any time point.

4.5.2.3 Migration after 24h formaldehyde treatment

No significant differences could be found between untreated and formaldehyde-treated samples when the treatment lasted for five hours. Therefore, the incubation time of formaldehyde was increased to 24h. Treatment started on day 3 of the assay and was stopped on day 4. Immediately after the treatment was over, neurospheres were placed into PL-coated 6-well plates.

4.5.2.3.1 Neurospheres generated from NPCs with a passage < 15

Analysis was again performed on day 5, but as the results did not differ between untreated and treated samples, day 8 and day 10 were not analyzed. The male isogenic pair (♂_*BRCA2*$^{(+/+)}$ and ♂_*BRCA2*$^{(+/-)}$) was used for this experiment, and neurospheres were generated of NPCs that had a passage lower than 15.

No significant differences in treated compared to untreated neurospheres could be found.

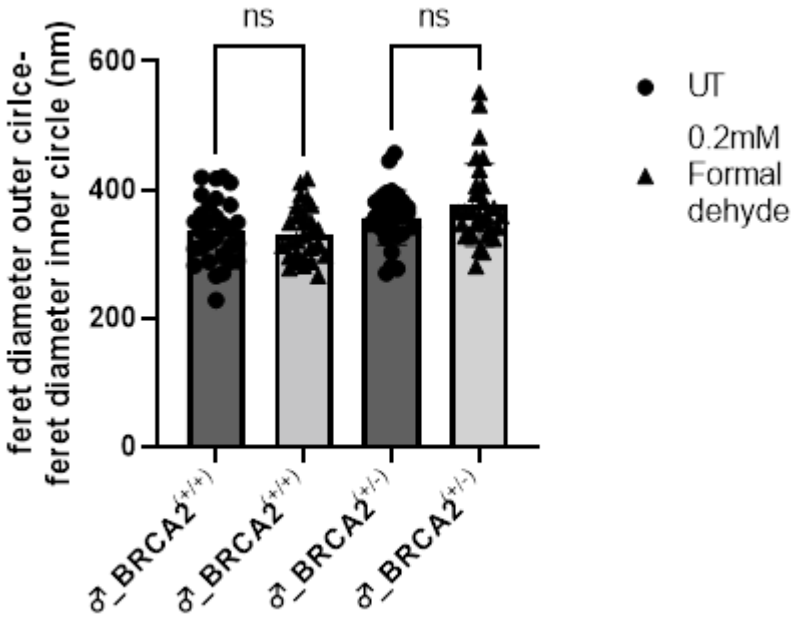

Figure 63 Migration of untreated and 24h formaldehyde (0.2mM)-treated neurospheres on day 5. Neurospheres were generated from NPCs with a passage lower than 15. Each dot and arrow represents one neurosphere. Mean ± SD, one-way ANOVA with multiple comparisons. There were no significant differences between treated and untreated samples in regard to migrated distances.

4.5.2.3.2 Neurospheres generated from NPCs with a passage > 15

As the proliferation assay was performed in neurospheres generated from NPCs with a passage higher than 15, migration was also analyzed in these older NPC cultures.

On day 5, the migrated distance did not differ between any of the samples.

On day 8, a significant difference ($p=0.0474$) between both untreated samples could be observed, with ♂_*BRCA2*$^{(+/-)}$ neurospheres having migrated less compared to ♂_*BRCA2*$^{(+/+)}$ neurospheres.

On day 10, this difference even increased in significance ($p<0.0001$), while additionally a significant difference ($p=0.0221$) between the untreated and treated ♂_*BRCA2*$^{(+/+)}$ samples could be observed. The data points on day 10 showed a high standard deviation, and especially in the ♂_*BRCA2*$^{(+/+)}$ samples, there seem to be two subgroups in the data set.

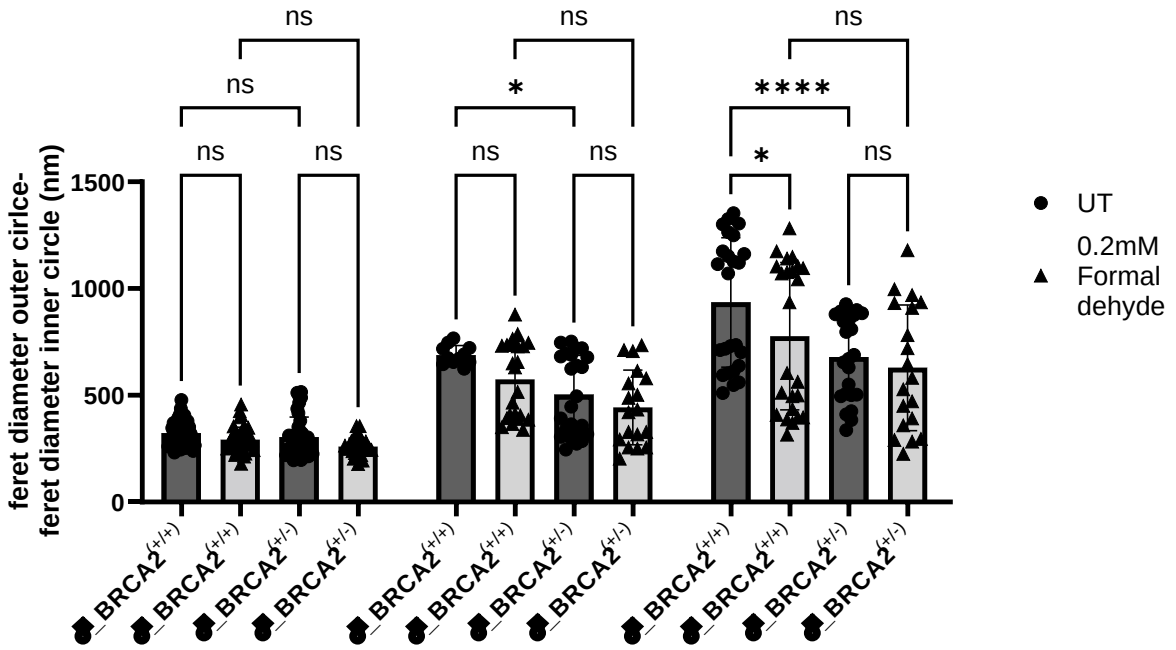

Figure 64 Migration of untreated and 24h formaldehyde (0.2mM)-treated neurospheres on days 5, 8, and 10. Neurospheres were generated from NPCs with a passage higher than 15. Each dot and arrow represents one neurosphere. Mean ± SD, one-way ANOVA with multiple comparisons, *p<0.05, ****p<0.0001. There were no significant differences between treated and untreated samples in regard to migrated distances on day 5. Day 8 and day 10 showed differences between samples.

In addition to the ♂*_BRCA2*$^{(+/+)}$ and ♂*_BRCA2*$^{(+/-)}$ isogenic pair, the experiment was also performed in neurospheres generated from ♂*_BRCA2*$^{(-/-)}$ and ♂*_BRCA1*$^{(+/-)}$ NPCs with a passage higher than 15.
On day 5, no differences in the migrated distances between untreated and treated samples in each cell line could be detected.

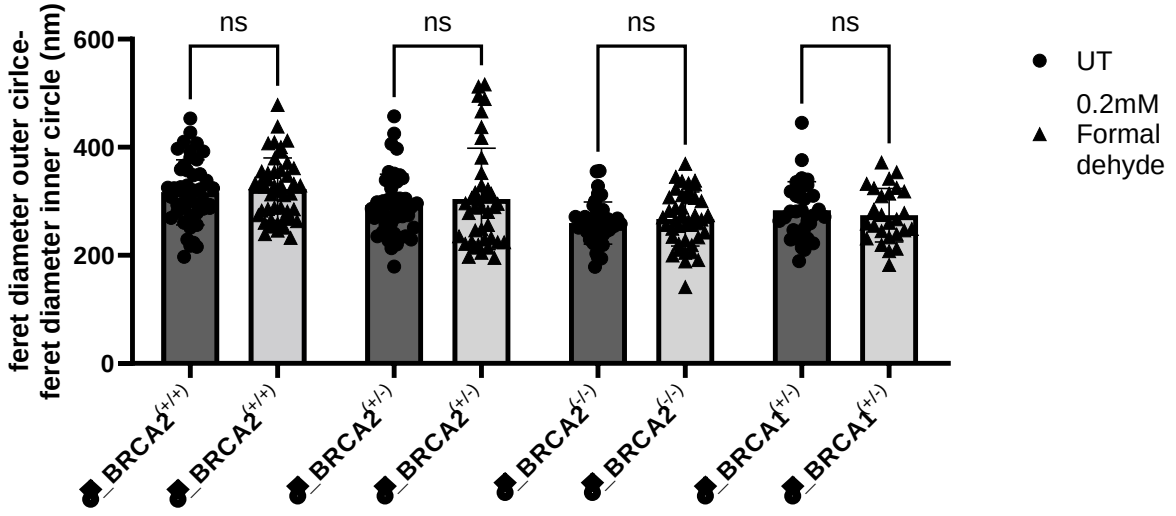

Figure 65 Migration of untreated and 24h formaldehyde (0.2mM)-treated neurospheres on day 5. Neurospheres were generated from NPCs with a passage higher than 15. Each dot and arrow represents one neurosphere. Mean ± SD, one-way ANOVA with multiple comparisons. There were no significant differences between treated and untreated samples in regard to migrated distances in any of the samples.

Similarly, on day 8, no differences between the untreated and the treated samples in each cell line could be detected. The data showed a wider spread in the ♂_*BRCA2*$^{(+/+)}$, ♂_*BRCA2*$^{(+/-)}$ and ♂_*BRCA1*$^{(+/-)}$ samples; compare Figure 66 and Table 27.

Table 27 Overview of samples and their standard deviation in the analysis of migration on day 8 in neurospheres generated from a passage higher than 15

Sample	Treatment condition	Standard deviation
♂_BRCA2$^{(+/+)}$	UT	42,97
♂_BRCA2$^{(+/+)}$	0.2mM Formaldehyde	173,46
♂_BRCA2$^{(+/-)}$	UT	181,64
♂_BRCA2$^{(+/-)}$	0.2mM Formaldehyde	170,51
♂_BRCA2$^{(-/-)}$	UT	46,34
♂_BRCA2$^{(-/-)}$	0.2mM Formaldehyde	43,97
♂_BRCA1$^{(+/-)}$	UT	143,75
♂_BRCA1$^{(+/-)}$	0.2mM Formaldehyde	164,40

The standard deviations were between 42.7 and 181.64 for the samples (compare Table 27) and therefore showed differences of up to 4.5 times between samples.

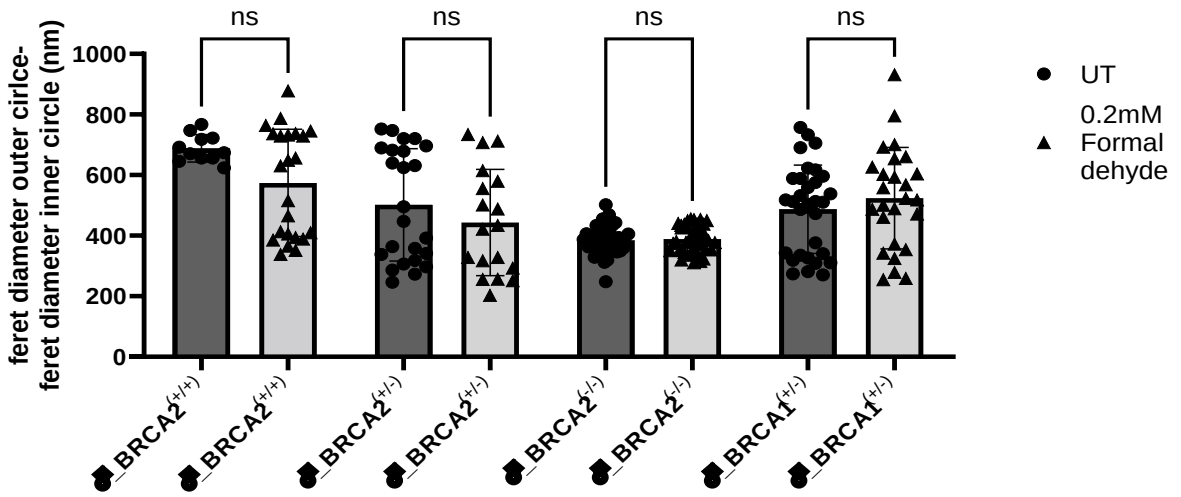

Figure 66 Migration of untreated and 24h formaldehyde (0.2mM)-treated neurospheres on day 8. Neurospheres were generated from NPCs with a passage higher than 15. Each dot and arrow represents one neurosphere. Mean ± SD, one-way ANOVA with multiple comparisons. There were no significant differences between treated and untreated samples in regard to migrated distances in any of the samples.

A significant difference (p=0.027) between untreated and treated samples in ♂_*BRCA2*$^{(+/+)}$ cells could be observed on day 10, as well as two subgroups within both ♂_*BRCA2*$^{(+/+)}$ samples (Figure 67). In the other samples no significant differences between untreated and treated samples could be seen.

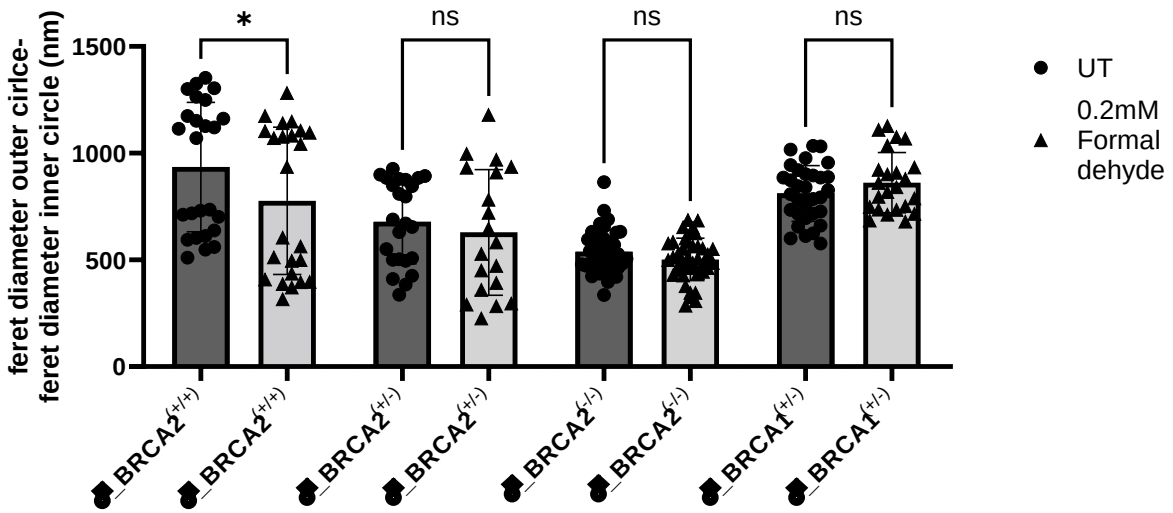

Figure 67 Migration of untreated and 24h formaldehyde (0.2mM)-treated neurospheres on day 10. Neurospheres were generated from NPCs with a passage higher than 15. Each dot and arrow represents one neurosphere. Mean ± SD, one-way ANOVA with multiple comparisons, *p<0.05. There were no significant differences between treated and untreated samples regarding migrated distances in three of the samples. Only in the ♂*_BRCA2*$^{(+/+)}$ sample could a significant difference between untreated and treated samples be detected.

5 Discussion

BRCA2 is a tumor suppressor gene that encodes a protein of 3418 amino acids (Tavtigian et al., 1996). If heterozygously mutated, *BRCA2* leads to an increased risk for the patient to develop HBOC; if homozygously mutated, the patient is suffering from Fanconi Anemia, with symptoms like microcephaly and intellectual disability (Rump et al., 2016; Weinberg-Shukron et al., 2018). *BRCA2* has its main function in the HR repair of DNA damage, namely DSB and ICL (Fradet-Turcotte et al., 2016). It is furthermore involved in the protection of stalled replication forks (Liao et al., 2018; Lomonosov et al., 2003; Schlacher et al., 2011b) and has several additional functions depending on the cell cycle stages (Martinez et al., 2015).

In the brain, *BRCA2* mutations had been associated with decreased cellular proliferation and abnormal brain development in mice (Ludwig et al., 1997; Suzuki, de la Pompa, et al., 1997). It could furthermore be shown that *BRCA2* mutations lead to an increased probability of developing brain metastasis in humans (Ratner et al., 2019). *BRCA2* mutations have also been associated with neuropsychiatric diseases like ASD and bipolar disorder (Neale et al., 2012a; Tesli et al., 2010). Additionally, there is the connection between impaired DNA damage repair and neurodegeneration. Accumulated DSBs in the brain of *BRCA2* mutation carriers have been linked to neurodegeneration (Madabhushi et al., 2014), (neuro-) psychiatric disorders, and intellectual disabilities (Raza et al., 2016; Shiwaku & Okazawa, 2015; Suberbielle et al., 2013).

BRCA2 is influenced by formaldehyde (Tan et al., 2017). Formaldehyde is a highly toxic chemical compound and occurs exogenously and endogenously in the body (Kalapos, 1999). It can accumulate in certain tissues, like the brain, to concentrations of up to 0.4mM (Heck et al., 1982; Tong et al., 2011b; Tong, Han, Luo, Wang, et al., 2013a). It can induce DNA damage (Juarez et al., 2018) and has neurotoxic effects in the brain (Kilburn, Seidman, et al., 1985; Kilburn, Warshaw, et al., 1985; Songur et al., 2008). When accumulated in the brain over time, it has been connected to age-related memory decline (Kilburn et al., 1987; Tong et al., 2011b), as well as brain diseases and tumors (Rana et al., 2021).

In the interaction with *BRCA2,* formaldehyde can stall the replication fork and at the same time inhibit BRCA2. This leads to a haploinsufficiency of BRCA2, where heterozygously mutated *BRCA2* cells are more affected by formaldehyde compared to wildtype cells (Tan et al., 2017). However, the connection between BRCA2 sensitivity to formaldehyde and formaldehyde accumulation in the brain has not been drawn so far.

In the diagnostics of the human genetics department in Mainz, 161 patients presented with developmental delay, mild to moderate intellectual disability, or behavioral anomalies. After sequencing, three patients could be determined to be carrying a heterozygous loss-of-function *BRCA2* mutation. From one patient, it was possible to receive a skin biopsy, which was used for the study. The study aimed at analyzing the effects of formaldehyde on neuronal tissue of *BRCA2* mutation carriers and its effects on cell proliferation and brain function.

5.1 BRCA2 protein and RNA expressions are decreased in cells carrying a *BRCA2* mutation heterozygously or homozygously

In this study protein and RNA expression of BRCA2 in several cell lines were tested to examine basic, untreated expression. Therefore, fibroblasts, iPSCs, and NPCs with or without *BRCA2* mutation were analyzed by RT-qPCR and Western blotting.

Comparing the different expression levels of fibroblasts, iPSCs, and NPCs, it could be observed that fibroblasts always showed the lowest RNA and protein levels of BRCA2 compared to the other two cell types. In the human protein atlas (Karlsson et al., 2021; *The Human Protein Atlas*, 2023) the same results can be observed. TPM (transcripts per million) is the unit in which those

expression levels are given in the protein atlas (Y. Zhao et al., 2021). The RNA expression of BRCA2 in fibroblasts has been reported to be very low (3.8nTPM) and higher in undifferentiated cells (15.6nTPM for *BRCA2*). Observations of this study confirmed the results of a previous study that had examined BRCA2 levels in iPSCs, NPCs, and fibroblasts and found that the expression of BRCA2 is higher in pluripotent cells compared to fibroblasts (Shimada et al., 2019).
BRCA2 is differently expressed in various tissues of the body. The highest expression of BRCA2 can be found in rapidly proliferating cells (Chodosh, 1998; Orii et al., 2006; Rajan et al., 1996) undergoing differentiation (Bernard-Gallon et al., 2001) as well as during brain development (Petryszak et al., 2016). With our results we can support those findings. The reason for higher BRCA2 levels in proliferating cells is its important function in genomic stability during DNA replication and cell cycle progression (Rajan et al., 1996). Proliferating cells require BRCA2's homologous recombination (HR) repair function to resolve DNA double-strand breaks and stalled replication forks (Gorodetska et al., 2019b).

Another aim of these experiments was to find out if a heterozygous or homozygous *BRCA2* mutation has an influence on RNA and protein levels of BRCA2. In fibroblasts, it was found that the heterozygously *BRCA2*-mutated cell line, the patient cell line, always showed a lower expression compared to the wildtype cell line. BRCA2 RNA and protein expression were around 50% expressed in this cell line compared to wildtype. This can be explained by a heterozygous mutation in *BRCA2* in this cell line. A deletion of an adenine leads to a frameshift and is predicted to cause nonsense-mediated decay (NMD) in the cells. NMD is a control system through which mRNAs carrying a premature stop codon can be degraded and do not lead to a truncated or abnormal protein (Lykke-Andersen & Jensen, 2015). The reduction on the RNA, and protein level might be explained by the mutation and the potential NMD. The primers for the RT-qPCR were designed to bind in front of the mutation to additionally test if NMD is happening. As reduced levels of *BRCA2* in the RNA can be detected, it could be assumed that NMD is happening.
The mutation of the heterozygous *BRCA2* cell line is classified as pathogenic by varsome and ClinVar, citing several studies that investigated this mutation (Borg et al., 2010; Kurian et al., 2008; Rebbeck et al., 2018; Turkovic et al., 2010; S. Zhang et al., 2011). If a mutation is classified as pathogenic, this indicates a mutation being strongly associated with disease causation. An example is a mutation leading to a frameshift in a gene where loss of function is disease-associated, as in our samples (The Human Genomics Community, 2023).
The heterozygously mutated *BRCA2* cell line (♂_BRCA2$^{(+/-)}$) also showed lower BRCA2 RNA and protein expression in iPSCs and NPCs compared to wildtype cells. On the protein level, the expression was reduced by 50%, while the reduction on the RNA level was a bit less. The mutation in this cell line is an insertion of an adenine at a very similar position to the patient cell lines. This insertion also leads to a frameshift and is predicted to cause NMD. The mutation itself is classified as likely pathogenic by varsome.
If a *BRCA2* heterozygosity in cells leads to a decrease in BRCA2 RNA and protein, it has also already been investigated before (Tan et al., 2017; Tannenbaum et al., 2007). In 2006 Arnold and colleagues (Arnold et al., 2006a) found that in lymphoblastoid cell lines carrying a heterozygous *BRCA2* mutation, BRCA2 protein levels were reduced by 50%, while RNA levels remained stable. The relationship between heterozygous mutations and RNA levels appears influenced by mutation type (truncating vs. missense) and post-transcriptional regulation (M. Lee et al., 2021; Lima et al., 2025). If a mutation leads to a minor isoform encoding truncated proteins, NMD seems to happen to prevent dysfunctional proteins and is therefore reducing

RNA levels. Also, if certain *BRCA2* mutations produce unstable transcripts with premature termination codons, it can lead to a reduction of functional mRNA through degradation.
The mutations in this study are in exon 11 of the BRCA2 gene, which can be found in the middle of the gene. A frameshift leads to an early stop codon and theoretically, to a truncated protein. Nevertheless, a shortened protein could not be found in our western blot analysis, supporting the hypothesis of NMD.
The compound heterozygously mutated *BRCA2* cell line (♂_BRCA2$^{(-/-)}$) showed, like the heterozygously mutated *BRCA2* cells, a reduction of the BRCA2 RNA and protein expression in iPSCs as well as a reduction of RNA levels in NPCs. Similar to the heterozygously mutated cells, those reductions were also around half. The mutations in these cell lines are two different ones: one allele carries an insertion of an adenine, one base position in front of the mutation of the heterozygously mutated cell lines. The other allele carries a deletion of 6 bases in the same region. The first mutation leads to a frameshift predicting to cause NMD (classified as likely pathogenic by varsome), while the second one is in-frame and therefore classified as a mutation of uncertain significance, as the protein coding length changes in a non-repetitive sequence but not conserved region. As the second mutation is in-frame a protein is probably still produced and only shortened by two amino acids. Therefore, an expression like that found in the heterozygously mutated *BRCA2* cell line would be expected and was also found.

In all its functions and different roles, *BRCA2* is very often closely accompanied by *BRCA1*. Both expression patterns are strikingly similar (Connor et al., 1997). Their spatial and temporal expression patterns are virtually indistinguishable during embryonic development (Chodosh, 1998), and both have been found to be expressed in proliferating cells in mice (Blackshear et al., 1998). They are often co-regulated (Rajan et al., 1996), colocalizing (Garcia-Higuera et al., 2001) and functioning together, as both play a role in HR-directed repair. DSBs can also occur during a replication fork stalling or collapsing and could be repaired by HR, where *BRCA1* is involved. (Ait Saada et al., 2018; Noordermeer & van Attikum, 2019). Different from *BRCA2*, *BRCA1* is additionally involved in NHEJ.
In this study, BRCA1 protein and RNA levels in fibroblasts, iPSCs, and NPCs were also checked, finding that BRCA1 levels, as BRCA2 levels, were lowest in fibroblasts compared to iPSCs and NPCs. In the human protein atlas and two studies (The Human Protein Atlas, 2023 Momcilovic et al., 2010; Shimada et al., 2019) the same results were found with TPMs for BRCA1 of 5.2n TPM for fibroblasts and 21.8nTPM for undifferentiated cells.
Generally, a lower expression of BRCA2 in the brain compared to BRCA1 can be observed in this project, as well as in the database of the GTEx Portal (on November 8th, 2023). TPMs were on average two to three times higher for BRCA1 compared to BRCA2, depending on the exact brain region. *BRCA1* has a broader range of functions compared to *BRCA2*, e.g., in DNA repair it is not only involved in the HR-directed repairs together with *BRCA2*, but also in single-strand annealing and NHEJ after DSB. Furthermore, *BRCA1* is additionally involved in oxidative stress response and transcriptional regulation (De Siervi et al., 2010; Gorodetska et al., 2019b; Mullan et al., 2006; Welcsh et al., 2002; X. Zhang & Li, 2018). *BRCA1* directly influences chromatin structure and remodeling as well as gene silencing through interactions with histone deacetylases and polycomb-repressive complexes. These activities position *BRCA1* as a regulator in a broader ranger compared to *BRCA2*, potentially enabling higher baseline levels (Gorodetska et al., 2019b).
In fibroblasts carrying a heterozygous *BRCA2* mutation, BRCA1 RNA and protein expressions were reduced by half. A study in 1996 found that *BRCA1* and *BRCA2* are often coordinately expressed in mammary epithelial cells (Rajan et al., 1996). As fibroblasts, mammary epithelial

cells are differentiated cells, and the study might give an explanation why also *BRCA1* is downregulated in our fibroblasts.
Different than in fibroblasts, in iPSCs BRCA1 RNA and protein expressions are similar for all cell lines, independent of whether they carry a *BRCA2, BRCA1,* or no mutation. Those results were as expected, as a previous study by Tannenbaum and colleagues could already show that in undifferentiated HT 29 cells carrying a heterozygous BRCA2 mutation, BRCA1 RNA and protein levels were not reduced (Tannenbaum et al., 2007).
In NPCs, *BRCA1* RNA levels were similar for all *BRCA2*-mutated cell lines and the wildtype cell line in NPCs.
The heterozygously *BRCA*- mutated cell line showed a reduction of *BRCA1* RNA in NPCs compared to the wildtype cell line. In this cell line, a deletion of 16 base pairs in one allele of the *BRCA1* gene causes the heterozygosity. This mutation leads to a frameshift and is predicted to cause NMD. Therefore, it is classified as likely pathogenic by varsome. The mutation might be responsible for the reduction of BRCA1 expression in the heterozygously mutated *BRCA1* cell line.

Taken together, fibroblasts showed lower expression of BRCA RNA and protein compared to iPSCs and NPCs, and BRCA1 expression is higher than BRCA2 expression in all cell lines. BRCA2 and BRCA1 RNA and protein levels were reduced in *BRCA2*-mutated cell lines, probably due to NMD and the coregulation of BRCA2 and BRCA1.
(All varsome analyses were done on November 7th, 2023).

5.2 Formaldehyde influences BRCA2 RNA and protein expression

Formaldehyde is an environmental toxin and can be found in every cell of the body (Bernardini et al., 2020; Tyihák et al., 1998). Formaldehyde can be taken up via ingestion, inhalation, and absorption (Tulpule & Dringen, 2013). Additionally, it is also an endogenous product of cellular metabolism, like histone demethylation, methanol oxidation, and the oxidative deamination of methylamine (Cloos et al., 2008; Kou et al., 2022; O'Sullivan et al., 2004; P. H. Yu et al., 2003). Concentrations of both, free and reversibly bound, endogenous formaldehyde in human blood occur between 2–3mg/l (World Health Organization, 2010). In the brain, concentrations of formaldehyde can be up to 0.4mM (Heck et al., 1982; Tong et al., 2011a; Tong, Han, Luo, Wang, et al., 2013a). Formaldehyde can easily enter the brain through the blood-brain barrier (Bernardini et al., 2020), and it has been proposed that formaldehyde is produced locally in the brain, as astrocytes and neurons have the potential to generate and oxidize formaldehyde (Tulpule et al., 2013; Tulpule & Dringen, 2012).

After formaldehyde treatment, *BRCA2* and *BRCA1* RNA were reduced in both fibroblast and NPC lines. A reduction due to formaldehyde on *BRCA2* or *BRCA1* RNA levels had not directly been described before. It has been shown that formaldehyde rather reacts with RNA than DNA (Yamada et al., 2019). As RNA is single stranded and does not show secondary structures, its nucleobases are easier accessible by formaldehyde (McGhee & von Hippel, 1977; Penniston & Doty, 1963). Molecularly formaldehyde reacts with the amino group of the nucleobases and oxidizes RNA (Gonzalez-Rivera et al., 2020b). Gonzalez-Rivera and colleagues could show that formaldehyde can lead to selective RNA oxidation, which altered the expression of many transcripts involved in chromatin modification and p53-mediated DNA-damage responses. In the computational analysis of their data, the *BRCA1* mRNA, among others, was often found to be deregulated after formaldehyde treatment. (Gonzalez-Rivera et al., 2020b) Interestingly, the

oxidation of RNA seems to be a highly selective process, and some mRNA species are more susceptible to oxidation than others. Oxidation of RNA can lead to several cellular processes. One is the impact on protein synthesis by disrupting the translation process, leading to stalling, errors during translation, and a potential production of truncated proteins. Another mechanism induced by RNA oxidation is the activation of cellular surveillance mechanisms like NMD, which degrades damaged RNA to prevent an accumulation of faulty proteins. Other options are the repair of oxidized bases in the RNA and apoptosis of the cell induced by signaling pathways after oxidative RNA modification. (X. Chen et al., 2022; Kong & Lin, 2010; Tanaka & Chock, 2021) In general, oxidized RNA is supposed to be removed by the cell quite fast as it is not tolerable. A working group showed that, after HeLa cells were pulsed with sub-millimolar levels of hydrogen peroxide, which induces oxidation of RNA, their ratio of 8-oxoG/guanosine in total RNA dropped about 50% within 1h (Z. Li et al., 2006). If the exposure lasts longer, as in the experiment of this work, a constant removal of oxidized RNA might happen, leading to the observed low RNA levels.
It would be interesting to investigate if *BRCA2* and *BRCA1* RNA are oxidized after formaldehyde treatment and which cellular process and effect on protein level are induced in the cells.

Taking protein levels after formaldehyde treatment into consideration as well, an interesting picture arises: In fibroblasts and NPCs, a quantification after 0.2mM formaldehyde treatment revealed reduced BRCA2 protein levels in both cell lines compared to untreated cells, while BRCA1 protein levels were not reduced. In 2017 was found that formaldehyde has a direct effect on the BRCA2 protein. It has been shown that it can selectively deplete the BRCA2 protein via proteasomal degradation. The proteolysis of BRCA2 via formaldehyde is a very specific process, as other proteins involved in homologous recombination, the Fanconi anemia repair pathway, or non-homologous end joining, like BRCA1, RAD51, PALB2, XRCC3, FANCI, or FANCD2, KU80, KU70, and XRCC4, were at most modestly affected by formaldehyde. (Tan et al., 2017) The protein results go along with this paper, indicating a posttranslational proteasomal depletion of BRCA2 and not a reduction of BRCA2 due to reduced RNA levels. Also, low *BRCA1* RNA levels but high BRCA1 protein levels support the hypothesis of proteasomal depletion of BRCA2.
The reduction of BRCA2 protein was seen in both cell lines, wildtype and heterozygous *BRCA2* cells. In wildtype fibroblasts and NPCs, those differences were significant as well as in heterozygous *BRCA2* NPCs, while in heterozygous *BRCA2* fibroblasts the decrease was not significant. That the effect in heterozygous BRCA2 fibroblasts is not significant can possibly be explained by the high variability of the data in this sample in the western blot analysis.
The reduction of BRCA2 protein was stronger in heterozygously mutated *BRCA2* cells compared to wildtype cells. Tan and colleagues also observed this and suggested that formaldehyde, together with a heterozygous *BRCA2* mutation status, leads to haploinsufficiency and a loss of function cellular phenotype (Tan et al., 2017). They hypothesize that heterozygous BRCA2 levels are usually enough to maintain cell survival but due to formaldehyde treatment they drop under a certain level leading to a loss of function phenotype.

In this study, observations confirm the hypothesis that indeed, in both cell types, fibroblasts and NPCs, formaldehyde treatment leads to a dramatic reduction of BRCA2 protein levels. These levels are comparable to compound heterozygous or homozygous situations in patients with Fanconi's anemia, suggesting that increased cellular formaldehyde concentrations can

accelerate a heterozygous *BRCA2* mutation into a full loss of protein status. When BRCA2 protein is fully gone, neuronal effects as seen in Fanconi's anemia are to be expected. These include effects on neuronal proliferation and migration (Jarysta et al., 2021; Xie et al., 2024; Zippora E et al., 2020). In an MRI study with Fanconi's anemia patients, it was found that the incidence of abnormalities in size and morphology of the pituitary, as well as the posterior fossa and corpus callosum, is higher in the patient group compared to healthy controls (Stivaros et al., 2015). This hints towards an impact of the disease in the early stage of development of the central nervous system (Stivaros et al., 2015).

5.3 Formaldehyde increases the number of DSBs in cells

DSBs are an intensive harm for the cell, as due to the break of both strands, it is not sure if and how much DNA is missing at the position of the break. There are two ways for cells to repair DSBs. The NHEJ pathway, which leads to potential insertions or deletions at mutation sites, and the error-prone HR-directed repair. HR-directed repair requires a sister chromatid as a template to repair DSBs error-free (X. Zhao et al., 2017). If DSBs are not repaired or falsely repaired, genomic instability with chromosomal aberrations and tumorigenesis can occur (Krenning et al., 2019b). BRCA2 plays a major role in the HR-directed repair, and it has been shown that if BRCA2 is disturbed in its function, chromosomal instability and tumorigenesis are more likely to happen (See et al., 2010).

In this work, it was asked if there are differences in the number of DSBs comparing wildtype and *BRCA2*-mutated cells, if formaldehyde increases DSBs, and if heterozygously mutated cells were more affected by this than wildtype cells.

No differences in the number of DSBs between wildtype and *BRCA2*-mutated cells could be observed. This result is as expected, as BRCA2 does not affect the formation of DSBs but rather the repair of DSBs (C. C. Chen et al., 2018). DSBs occur spontaneously in the cells during normal processes like DNA replication or are induced via exogenous factors like ionized radiation. This happens at similar rates in all cells independent of *BRCA2* mutations. (Vilenchik & Knudson, 2003) Wildtype cells use error-free HR pathways, and cells carrying mutations in the *BRCA2* gene still predominantly rely on the HR pathway but additionally need to rely on error-prone mechanisms like NHEJ or single-strand annealing. This leads to increased genomic instability in those mutated cells but not necessarily to a higher number of DSBs. (Chaudhuri & Nussenzweig, 2017; Tutt et al., 2001)

One could think that cells, like heterozygous *BRCA2* cells, with a mutation in the HR-repair system, might be slower in repairing DSBs and therefore show an accumulation of DSBs. But *BRCA2*-mutated cells rely partially on NHEJ instead of HR (Tutt et al., 2001), and Mao and colleagues could show that NHEJ is a faster way to repair DSBs compared to the HR pathway. They saw that NHEJ takes approximately 30min while HR needs around 7h or longer to complete the DSB repair. (Mao et al., 2008a) Therefore, an accumulation of DSBs and a higher number of DSBs in those cells is unexpected and confirmed with the results in this study.

In the staining and microscopy-based experiments, significantly more DSBs were detected in formaldehyde-treated samples compared to untreated samples. This is plausible, as formaldehyde can induce DSBs. Grafstrom and colleagues found that formaldehyde induces crosslinks between DNA and proteins (Grafstrom et al., 1983), DPCs (DNA-protein crosslinks). Those DPCs can cause stalled replication forks and thereby introduce DSBs. It has been shown that cells from Fanconi anemia patients are hypersensitive to DNA interstrand crosslinking agents, like formaldehyde (Kennedy & D'Andrea, 2005). And it is likely that homologous recombination-deficient cells (e.g., *BRCA2*-deficient cells) are hypersensitive to

formaldehyde because of those DPCs (Ridpath et al., 2007). Another mechanism of how formaldehyde can induce DSBs is via stalling the replication (Kumari et al., 2012; Tan et al., 2017). To analyze stalled replication forks, fiber assays could be performed next.
XPF, *TDP1*, and *EXO1* are DNA repair genes, and it has been described that cells with genomic mutations in those genes show an increase in DSBs, genomic instability, and chromosomal breaks due to formaldehyde treatment. Those results highlight the importance of DNA repair mechanisms towards formaldehyde toxicity. (Gao et al., 2023; Kumari et al., 2011; Nakano et al., 2020)
BRCA2 is also a gene necessary for DNA repair, and it was analyzed if treated *BRCA2* cells show a higher or lower number of DSBs compared to treated wildtype cells. A very small, but significantly lower number of DSBs was detected in formaldehyde-treated mutant samples compared to formaldehyde-treated wildtype samples. This is surprising, since it was expected to see more rather than fewer DSBs in mutant samples.
Formaldehyde leads to more DSBs via stalled replication forks, especially via DNA-protein crosslinks (Blouin & Saini, 2024; Gao et al., 2023; Kumari et al., 2011). Those stalled replication forks lead to DSBs. BRCA2 is responsible for stabilizing stalled replication forks by protecting the nascent strand at those sites and therefore preventing degradation (Rickman et al., 2020).
When there is a mutation in the *BRCA2* gene, the protection of stalled replication forks is deficient, and more DSBs can occur (Schlacher et al., 2011b). Additionally, *BRCA2* cells next to HR also rely on NHEJ. This is more error-prone and leads to more mutations and more genomic instability, which has already been described in 2017 (Chaudhuri & Nussenzweig, 2017). Taken together, it would be expected that in cells carrying a heterozygous *BRCA2* mutation, NHEJ and less protection of stalled replication forks would be seen. Leading to high levels of genomic instability and therefore a higher sensitivity towards DNA-damaging agents like formaldehyde. This higher sensitivity would again lead to more DSBs. In this study those expectations could not be proven. Consequently, it would be interesting to check which repair pathway the cells used after formaldehyde treatment and how much genomic instability could be found.
Other studies have already investigated the number of DSBs in treated wildtype and heterozygous *BRCA2* cells, finding higher numbers of DSBs in *BRCA2* cells. Different from this study, they used γ-irradiation and mitomycin C to induce DSBs (Arnold et al., 2006b) or only γ-irradiation (Baert et al., 2017) for their treatment. γ-irradiation directly induces DSBs, while formaldehyde only induces DPCs and stalled replication forks leading to DSBs in a second step and not directly. Additionally, BRCA2 plays a role in the protection of stalled replication forks, as we have already seen.

Taking statistics into consideration to explain the unexpected differences between treated wildtype and *BRCA2* cells, it can be highlighted that the difference between both samples was highly significant, but the effect itself was small. (Compare 42.79 for the untreated ♂_*BRCA2*$^{(+/+)}$ sample, and 39.69 for the untreated ♂_*BRCA2*$^{(+/-)}$ sample and for the treated ♂_*BRCA2*$^{(+/+)}$ sample it was 63.28, while it was 55.66 for the treated ♂_*BRCA2*$^{(+/-)}$ sample). Both cell lines showed an increase of circa 30% in DSBs due to formaldehyde treatment. The high significance appeared statistically significant because of the high number of cells (n=300) analyzed.
The fact that the effect is subtle might also explain why it could only be detected with microscopy but not via FACS (Forment & Jackson, 2015; Kilgas et al., 2021; Reddig et al.,

2018). The spatial resolution of microscopy is as good as one individual γH2AX focus per cell. γH2AX foci are markers for DSBs. Therefore, as little as one DSB per cell can be visualized, detected, and quantified. FACS-based analyses (flow cytometry), on the other hand, measure the overall fluorescence intensity of cells. This is helpful for cells with a lot of DNA damage, but it is difficult to detect only little DNA damage and differences between samples with little damage. Depending on background fluorescence and gating strategies, even bigger effects might be necessary to detect differences between samples. As in this study only a few DSBs per nuclei could be found, microscopy is the better method for analyzing those small differences.

Summarizing, it was found that formaldehyde leads to an increase of DSBs in wildtype and *BRCA2*-mutated cells. The intensity of the effect of formaldehyde was roughly the same in both cell lines.

Acetaldehyde is the metabolic product of ethanol (C_2H_5OH) and reacts often similarly to formaldehyde, being the metabolic product of methanol (CH_3OH). Tan and colleagues performed their experiments with formaldehyde as well as with acetaldehyde and could show the same results with both components (Tan et al., 2017). In 2017, Tacconi and colleagues could see that cells (carcinoma H1299 cells and colorectal adenocarcinoma DLD1 cells) carrying a *BRCA2* mutation show an increased sensitivity towards acetaldehyde. An accumulation of replication-associated DNA damage led to checkpoint activation, a G2/M arrest, and cell death. In this study the effects of formaldehyde on the cell cycle were analyzed next.

5.4 BRCA2 and formaldehyde have differing effects on the number of cells in each cell cycle stage

It has just been shown that formaldehyde induces DSBs in the cells and hypothesized that this is due to stalled replication forks. Those stalled replication forks occur during the DNA replication process. Consistently, several previous studies could already show that a formaldehyde-induced accumulation of DSB happens, especially during DNA replication (Gao et al., 2023; Kumari et al., 2012; Nakano et al., 2020). DNA replication takes place during the S-phase of the cell cycle.

The cell cycle consists of four different phases: G1-, S-, G2- and M-phase and within one cycle, the cell divides once. In the G1-phase, the cell usually grows and prepares itself for DNA replication in the S-phase. In the G2/ M-phase the cell is also growing, this time with double the amount of DNA, and prepares itself for dividing into two cells in M-phase. Both in the S-phase and in the M-phase it is important for the cell to have intact, repaired DNA without too much harm. Thereby, the cells ensure that no defective DNA is passed on in the cell division. (Schafer, 1998) Before the cell can progress to the next cell cycle step, it needs to pass a checkpoint, which ensures that the DNA and the cell are properly prepared. The cell must pass four main different checkpoints during one cell cycle: the G1/S checkpoint, the G2/M checkpoint, the S/M checkpoint, and the metaphase checkpoint during mitosis (Murray, 1994; Z. Wang, 2022). Depending on the checkpoint, different requirements are necessary for the cell to continue cell cycle progression. The DNA always needs to be undamaged, and for the G2/M checkpoint, all parts of the DNA need to be replicated to pass the checkpoint. Furthermore, the cell size must be sufficient for the cell to pass the G2/M checkpoint. In the metaphase checkpoint, the chromosome spindle attachment is checked, and to pass the G1/S checkpoint, the cells need to have sufficient nutrients and growth factors. (Barnum & O'Connell, 2014) During the S/M checkpoint, the cell makes sure that DNA is undamaged and not too many DNA replication forks are stalled and arrested (Willis & Rhind, 2009).

In this study it was hypothesized that both a *BRCA2* mutation and formaldehyde would influence the cell cycle. With the help of flow cytometry, changes in the number of cells in each cell cycle phase under different conditions could be analyzed. First, the effect of BRCA2 was analyzed by comparing untreated heterozygous *BRCA2* and wildtype cells. Second, the influence of formaldehyde treatment was investigated by comparing treated to untreated cells within one cell line. And third, both effects, *BRCA2* mutation and formaldehyde treatment, were taken into consideration by comparing treated heterozygous *BRCA2* samples to treated wildtype samples.

First, it was found that untreated heterozygous *BRCA2* cells show more cells in S-phase compared to wildtype cells. Cells with less BRCA2 protein usually take longer to repair DNA damage (Leung & Hazrati, 2021) and might accumulate in the S-phase. Mutations in *BRCA2* have been found to influence the usual distribution of cells in the cell cycle. The depletion of BRCA2 has been shown to be associated with senescence of the cell (Carlos et al., 2013) as the efficiency of the DNA repair machinery is reduced (Leung & Hazrati, 2021). A connection between untreated cells carrying a *BRCA2* mutation and an S-phase arrest has not been shown before. However, it had been demonstrated that an increase in DNA damage is slowing down cell cycle progression, especially slowing down S-phase (Kumar & Huberman, 2004). In their study, Kumar and Huberman found that the intra-S-phase checkpoint is responsible for the slowing down in the S-phase. The DNA damage they introduced by methyl methane sulfonate was replication fork pausing. Their experiment was performed in fission yeast, but they could also relate their results to vertebrates, which use similar proteins in their pathway.
BRCA2, as used in this study, plays a major role in the protection of stalled replication forks. In the previous experiment in this study, DNA damage was only checked by analyzing differences in the number of DSB which could not be found. Stalled replication forks themselves were not analyzed but would be an interesting parameter to investigate. An increase in stalled replication forks due to a *BRCA2* mutation could slow down S-phase progression at an intra-S-phase checkpoint. As a next step, it would be interesting to analyze if the intra-S-phase checkpoint is altered in heterozygous *BRCA2* cells.
To broaden the picture, further cell cycle checkpoints could be analyzed, as Willis and Rhind found that an accumulation of arrested DNA replication forks leads to a prevention of mitosis through the S/M checkpoint (Willis & Rhind, 2009).
Next to changes in the number of cells in S-phase, untreated heterozygous *BRCA2* cells also showed a lower number of cells in G1-phase compared to wildtype cells. When discussing this result, a factor in the analysis needs to be taken into consideration: the G1-phase was put together from two sets of cells in G1-phase (compare results). One set of cells without incorporated EdU, so cells in the G1-phase before going through the S-phase. And one set of cells with incorporated EdU, so cells that had gone through the DNA replication once already. Taking both G1-phases together, it was shown that fewer cells could be found in the G1-phase in heterozygous *BRCA2* cells compared to wildtype cells. This might hint towards wildtype cells progressing normally through the cell cycle, not accumulating in the S-phase as heterozygous *BRCA2* cells, and therefore showing more cells in the G1-phase. Heterozygous *BRCA2* cells are probably stuck in S-phase, as seen by the increase of cells there. Proof of this hypothesis could be done by measuring the total cell cycle duration of synchronized cells.
Second, the influence of formaldehyde was analyzed, finding that no differences in the cell cycle phases between untreated and treated wildtype cells could be found. In the heterozygous *BRCA2* samples on the other side, fewer cells in the S-phase in the treated sample compared to the untreated sample could be found.

This partially resembles the results of Nadalutti and colleagues from 2020 and Ortega-Atienza and colleagues from 2015. They found that formaldehyde has substantial effects on the cell cycle, as formaldehyde treatment leads to a reduced time spent in the S-phase (Nadalutti et al., 2020; Ortega-Atienza et al., 2015). Interestingly, both working groups saw changes in the cell cycle in wildtype cells. Nadalutti used primary human fibroblasts, and Ortega-Atienza used human lung epithelial cells. In this experiment, NPCs were used, either wildtype or with a mutation in the *BRCA2* gene. Effects of formaldehyde were only observed in mutated *BRCA2* cells and not in wildtype cells. Referring to those two studies, it would be expected to see differences in cell distribution in the cell cycle in both NPC lines.

The question arose why the wildtype NPCs in this study did not show differences in the cell cycle due to formaldehyde treatment. An idea was whether NPCs might be better prepared in protecting their cell cycle against toxins, compared to fibroblast or epithelial cells, as changes in the cell cycle lead to alterations in brain development (X. Chen et al., 2015; García-García et al., 2012; Homem et al., 2015). Two studies investigated the cell cycle in neural progenitor cells (Nam et al., 2010; Ueno et al., 2006). Nam and Nakayama used etoposide, an anti-tumor agent, to cause DNA damage in murine fetuses. They found that this drug induces S-phase accumulation and G2/M arrest in the mouse fetal brain. The S-phase accumulation happened due to an acceleration of the G1/S transition rather than by inhibition of S-phase progression. (Nam et al., 2010) Ueno and colleagues also investigated the cell cycle in the developing fetal brain of mice. They used 5-azacytidine to induce DNA damage and a deregulation of proliferation and cell death. They found abnormal mitosis, S-phase and G2-phase accumulation, and apoptosis of neural progenitor cells mainly in G1-phase. Their data suggests that G2/M progression was blocked. (Ueno et al., 2006) Therefore, it can be concluded that changes in the cell cycle seem to be possible in NPCs, at least with other toxins than formaldehyde.

Formaldehyde was used by Nadalutti and Ortega-Atienza for their experiments. Their treatment was conducted with 250µM formaldehyde for 24h (Nadalutti et al., 2020) and 100µM for 3h (Ortega-Atienza et al., 2015). Those formaldehyde exposures are higher and lower than in this experiment, where cells were treated with a formaldehyde concentration of 200µM for 5h.

So, it could be assumed that changes in the cell cycle of wildtype NPCs due to formaldehyde are likely, but interestingly not seen here.

Another thought and possible explanation, which has already been proven by Tan and colleagues, is that *BRCA2* cells are more sensitive to formaldehyde compared to wildtype cells (Tan et al., 2017). Therefore, an effect on the cell cycle might be visible faster or stronger than in cells without a *BRCA2* mutation. The effect of formaldehyde might be too subtle to be visible in wildtype cells. Already in the previous experiment analyzing DSBs in NPCs, it was hypothesized that the effect is too subtle to be detected properly.

Additionally, it should be highlighted that Nadalutti, Ortega-Atienza, Nam, and Ueno, and colleagues all found that formaldehyde leads to an arrest of the cell in G2/M. The G2 cell cycle arrest hints towards an increase in DNA damage in the preceding S-phase leading to an activation of the checkpoint when entering the G2-phase (Ortega-Atienza et al., 2015).

Depending on the statistical analysis, more cells in the G2-phase could be observed in this study as well. All analyses were first calculated with one-way ANOVAs, where it is possible to compare two variables within one calculation. The aim was to first analyze the effect of the *BRCA2* mutation (variable a) on all phases of the cell cycle (variable b), second the effect of formaldehyde (variable c) on all phases of the cell cycle (variable b), and third the effect of both (variable a +c) on all phases of the cell cycle (variable b). Furthermore, it was the idea to perform the analysis in an explorative manner; therefore, a t-test for each cell cycle phase individually was performed. With this analysis, it could be found that after formaldehyde

treatment in both cell lines, fewer cells were found in S-phase, but more cells in G2-phase. This goes along with the previous findings that formaldehyde accumulates cells in the G2-phase of the cell cycle and reduces the time spent in the S-phase, independent of genotype (Nadalutti et al., 2020; Nam et al., 2010; Ortega-Atienza et al., 2015; Ueno et al., 2006).
Statistically, it is not surprising that differences between an analysis with a t-test and a one-way ANOVA can be observed. A t-test only compares the mean values of two samples, while a one-way ANOVA takes three or more samples into calculation. The more calculations are performed within one data set with one test, the higher is the likelihood for a Type I error. Therefore, the p-value needs to be adjusted. The more samples are taken into consideration, the more the p-value needs to be adjusted. The higher the p-value is adjusted, the less likely it is to show significantly different results. (Mishra et al., 2019)

Third, the effect of both formaldehyde and *BRCA2* mutation together on the cell cycle was analyzed. When comparing formaldehyde-treated samples, more cells in the S-phase in heterozygous *BRCA2* cells compared to treated wildtype cells could be observed. But the genotype effect, with heterozygous *BRCA2* cells having fewer cells in the G1-phase compared to wildtype cells, was gone. These results resemble observations by Fridlich and colleagues with hydrogen peroxide (Fridlich et al., 2015b). They found that hydrogen peroxide leads to an accumulation of cells in S-phase in *BRCA2*-mutated cells compared to wildtype cells.
They explain their results with hydrogen peroxide being a reduced oxygen species (ROS). ROS can lead to DSBs, which need to be repaired. BRCA2 and BRCA1 are involved in the repair of oxidative DNA damage (Pagano et al., 2003) and can be seen as "caretakers against ROS" (Vurusaner et al., 2012). ROS can furthermore lead to checkpoint activation in the cell cycle. One checkpoint marker is phosphorylated Chk1, which is activated through DNA damage and initiates cell cycle checkpoints, arrest, and DNA repair, and shows elevated levels after formaldehyde treatment (Gao et al., 2023). Tacconi and colleagues could also show that *BRCA2* cells treated with acetaldehyde had an accumulation of toxic replication-associated DNA damage, which led to checkpoint activation, G2/M arrest, and cell death (Tacconi et al., 2017). As formaldehyde leads to the generation and accumulation of ROS (Ungureanu et al., 2024) and increasing formaldehyde concentrations are followed by increasing concentrations of ROS (Ke et al., 2014), this might hint towards an underlying molecular mechanism in the cell cycle in this study. Furthermore, reduced *BRCA2* and *BRCA1* RNA levels after formaldehyde treatment, as already observed and discussed in a previous experiment in this study, also suggest an increase of ROS due to formaldehyde. In a next study, it might be interesting to investigate the ROS levels and checkpoint markers in NPCs and see if those are elevated in the heterozygous *BRCA2* cells and especially under formaldehyde treatment. If ROS levels or checkpoint markers are elevated, this hints towards a potential molecular mechanism responsible for the changes in the cell cycle via cell cycle checkpoint activation.
Summarizing all results from this experiment, two effects play a role in the alteration of the cell cycle within this experiment. One is the *BRCA2* mutation leading to an increase of cells in S-phase as well as a decrease in G1-phase. These results indicate that those cells need longer to repair the DNA damage in the replicating DNA compared to cells with the full amount of BRCA2 protein. The other effect is due to formaldehyde, which leads to a reduction of cells in S-phase and an accumulation of cells in G2-phase. This suggests that cells arrest in the G2-phase and are not going to divide as too much DNA damage occurred with which the cell cannot cope. Taking both effects together, *BRCA2* and formaldehyde show contradicting effects, and formaldehyde seems to revert the effect of the *BRCA2* mutation. The *BRCA2* mutation is increasing the number of cells in S-phase, and formaldehyde is reducing the number of cells in

S-phase. *BRCA2* is the stronger effect compared to formaldehyde, as more cells can still be found in S-phase in formaldehyde-treated heterozygous *BRCA2* cells compared to treated wildtype cells. (Comparing the cells in S-phase within this experiment, most S-phase cells can be found in untreated *BRCA2* cells. Treated *BRCA2* cells showed fewer cells in S-phase, followed by untreated wildtype cells and treated wildtype cells showing the least cells in S-phase.)
The same experiment and calculations were performed for the female isogenic pair, and similar results were obtained. Sometimes the differences were not so prominent, but this might be due to the sample size of n=2.

5.5 Formaldehyde treatment leads to a slowdown of proliferation independent of genotype

Proliferation of cells depends on proper cell cycle progression. Changes in the cell cycle can lead to changes in proliferation. If cell cycle regulators signal for cell growth and division, proliferation increases, while quiescence or cell cycle arrest leads to decreased proliferation. Proliferation was analyzed next.
The regular population doubling time (PDT) for NPCs depends on the subtype and the differentiation method. The PDT is on average between 1.2 and 2.1 days. (M. Zhang et al., 2018) In this study, it could be seen that the PDT was more than one day for both cell lines in the untreated condition confirming those previous results by Zhang and colleagues.
Exogenous factors, like formaldehyde, can influence cell cycle progression, which has already been shown in the cell cycle experiment in this study. The effect of formaldehyde on cells heavily depends on its concentration. Concentrations between 0.1mM and 0.5mM promote cell proliferation (Mo & He, 2017; Nadalutti et al., 2020). While concentrations of about 1mM increase DNA damage in the form of DNA adducts, DPCs, and oxidative stress (Hester et al., 2003). It can even lead to apoptotic cell death (Tyihák et al., 2001). Concentrations higher than 1mM are cytotoxic and lead to necrosis of cells (Kastner et al., 2011; Mo & He, 2017; Tyihák et al., 2001). (Szende & Tyihák, 2010)
Heterozygous *BRCA2* and wildtype cells treated with formaldehyde showed significantly fewer cells in treated conditions compared to untreated three and four days after treatment. Taking the presented studies into regard, it is surprising, as a concentration of 0.2mM formaldehyde has been shown to promote proliferation.
On the other hand, a lower number of cells after formaldehyde treatment goes along with the previous cell cycle results, where also an increased number of cells could be found in the G2-phase after formaldehyde treatment. A possible explanation could be an irreversible G2/M arrest of the cells. Kumari and colleagues (Kumari et al., 2012) investigated the effect of formaldehyde on G2/M arrest in XPF-deficient cells. They found that cells would go into G2/M arrest and not divide anymore depending on the concentration of formaldehyde. A treatment of four hours with 0.2mM formaldehyde was the limit for wildtype cells to overcome the G2/M arrest. Higher concentrations of formaldehyde seem to bring the cells into an irreversible G2/M arrest. Further studies, already presented in the previous chapter (compare 5.4), could show similar results.
In this study, damaged NPCs might go into an irreversible G2/M arrest, so only undamaged or less damaged cells could proliferate, taking a while to increase the cell number. Both genotypes would be affected in a similar manner, therefore reacting similarly. A confirmation that those few cells still proliferate could be seen in the long-term experiment as the number of cells increased again after day 4 in both cell lines.

Another question opens up with these results: why is there no difference between the heterozygous *BRCA2* and the wildtype cell line? In the cell cycle experiment it could be found that the effect of formaldehyde is present in both cell lines but also that the *BRCA2* mutation plays a role. This role, increasing the number of cells in S-phase, is even bigger compared to the effect of formaldehyde, which is reducing the number of cells in S-phase but increasing them in G2-phase. Therefore, it would be expected to potentially see differences in proliferation between both cell lines.
Frappart and colleagues (Frappart et al., 2007a) investigated the effect of BRCA2 on cell cycle and proliferation and found that there is an increase of G2/M cells after Brca2 loss in their mouse line. To analyze if this cell cycle alteration changes proliferation, they performed a BrdU incorporation to quantify proliferation. They could not find differences between mutant and wildtype genotypes and broadened their investigation by analyzing apoptosis. Significant differences in apoptosis could be found between mutant and wildtype genotypes, which they use as an explanation for the microcephaly they also found in the mutant mice. The mutant mouse line they used leads to a homozygous deletion of *Brca2*, which is also present in Fanconi anemia patients. One of the symptoms of Fanconi anemia is microcephaly, and Frappart states that this is due to apoptosis of NPCs and not due to proliferation defects. A direct comparison of this study with heterozygous *BRCA2* cell lines is not possible. But the idea remains to compare apoptosis in heterozygous BRCA2 and wildtype samples in a next step.
Even though the heterozygosity of *BRCA2* leads to more cells in S-phase, the remaining BRCA2 activity in heterozygous cells seems sufficient for most cells to eventually complete DNA replication and continue through the cell cycle. Therefore, the overall proliferation is not significantly impacted. Differences in proliferation speed were not analyzed but could give a hint on a slower cell cycle progression in heterozygous *BRCA2* cells.
While heterozygous *BRCA2* cells progress through the cell cycle and proliferate, they might accumulate subtle genomic instability or DNA damage over time. Therefore, it would be interesting to analyze older NPCs to see if they show increased genomic instability and an altered proliferation behavior.

5.6 Less proliferation in neurospheres generated from aged cells

Regarding the brain, one of the benefits of 3D cultures compared to 2D cultures is the better reflection of the intrinsic spatial development of brain tissue (Bez et al., 2003; Zhou et al., 2016). Further benefits are the polarity of the 3D model, cell-to-cell interactions within the model, and the method of division of cells (Jensen & Teng, 2020; Kapałczyńska et al., 2018), as those characteristics lead to a more detailed and correct reproduction of the brain and can potentially display smaller effects.
As changes in the amount of protein, the number of DSBs, the number of cells in S-, G1-, and G2-phase in the cell cycle, and changes in proliferation were visible in 2D cell culture, neurospheres were generated to investigate those effects in a 3D model. The neurospheres themselves primarily consist of NPCs, which can migrate out of the neurospheres and differentiate into neurons when attached to the ground and supplemented with proper media. (Zhou et al., 2016) With neurospheres it is possible to investigate two parameters within the same experiment: proliferation and migration. All previous results hinted towards a potential deregulation of proliferation in NPCs due to a *BRCA2* mutation and formaldehyde treatment.
In experiments with neurospheres generated from NPCs with young passages (<15), no proliferation effect of either the *BRCA2* mutation or formaldehyde (independent of treatment duration with either 5h or 24h) was seen.

That the *BRCA2* mutation has no effect on the Feret diameter, the characteristic to determine proliferation in neurospheres, is not surprising. Also, in 2D culture the heterozygous *BRCA2* cells did not differ in proliferation compared to wildtype cells. As already elaborated in the previous chapter, the remaining BRCA2 activity in heterozygous cells seems sufficient to complete DNA replication, continue through the cell cycle, and proliferate normally in 2D culture as well as in the 3D model.

As neurospheres are a 3D model, cells grow in a tissue-like structure, and single cells are not, as in 2D monolayers, easily exposed to chemicals. The 3D structure provides more protection and makes penetration and altered cellular metabolism by formaldehyde more difficult. (Duval et al., 2017; Kapałczyńska et al., 2016) This can be an explanation for why an effect of formaldehyde is missing in neurospheres generated from young NPCs, especially as they were treated with the same concentration of formaldehyde as the 2D culture.

In experiments using neurospheres generated from NPCs with a higher passage (> 15), however, differences in Feret diameter of neurospheres were found. This observation had been described before: comparing cells from younger and older individuals, differences in proliferation rate were found (Hara et al., 1987; Tomasetti et al., 2019). Tomasetti and colleagues (Tomasetti et al., 2019) found that there was a significant decrease in stem cell proliferation of human colonic, duodenal, esophageal, and posterior ethmoid sinonasal tissue with age. They compared healthy tissue from individuals between 20-29 years old and 80-89 years old. Hara and colleagues (Hara et al., 1987) found that highly purified B cells from an aged group (70-91 years) proliferated less compared to those cells from a young group (22-29 years).

A possible explanation for the underlying molecular mechanism of the reduced proliferation is genomic instability. More precisely: accumulated DNA damage leading to a slowed division rate in older cells. A proof for a slower cell cycle progression in older cells has already been given in 2019 (Tomasetti et al., 2019). And that accumulated DNA damage could lead to slower cell cycles by cells stopping division, going into a G2/M arrest, or slowing their cell cycle progression was presented by Kumar and Huberman in 2004 (Kumar & Huberman, 2004). The hypothesis of accumulated DNA damage in older cells has also already been investigated in several studies as reviewed by Chen and colleagues in 2007. (J. H. Chen et al., 2007). One paper should be highlighted here: Rübe and colleagues investigated aging and DNA damage in hematopoietic stem/progenitor cells of healthy individuals of different ages. (Rübe et al., 2011) They found an increase of endogenous γH2AX foci, a measurement for DSBs, with advancing donor age, and they discovered that the extent of DNA damage increase seems to be determined by the individual DSB repair capacity. They concluded that age-related DNA damage increase goes along with physiological aging of stem cells and that aging could change the ability of stem cells to repair DNA damage, leading again to an increase of DNA damage.

Pan and colleagues also investigated stem cells, more precisely NPCs, at different passages by determining the susceptibility to viral infections. They found signs of differentiation, increased viral entry, and more efficient production of infectious progeny in NPCs with higher passages, and they stated that the proliferative capacity of NPCs decreased with increasing culture time/number of passages. (Pan et al., 2013) At higher passages, NPCs seem more vulnerable, and a subtle effect of, for example, formaldehyde, is more likely to be seen.

Regarding formaldehyde, it was also described before that formaldehyde has an age-related effect impairing adult neurogenesis. It has been shown that formaldehyde gradually accumulates in the brains of mice and rats in their aging process from six to 24 months (Kou et al., 2022; Tong, Han, Luo, Wang, et al., 2013b) and leads to cognitive decline during aging in rats (Heck et al., 1982; Tong, Han, Luo, Li, et al., 2013). If formaldehyde is injected

intraperitoneally or intrahippocampally into healthy rats, it resembles the age-related memory decline in old rats (Tong, Han, Luo, Li, et al., 2013). In humans, formaldehyde levels in urine, which are highly elevated among the 70-year-old probands, can be associated with cognitive decline (Tong et al., 2017; J. Yu et al., 2014).

It is hypothesized that NPCs with a higher passage accumulate more DNA damage, show changes in the cell cycle like a slowdown of S-phase or a G2/M lead to arrest, and therefore have less proliferative capacity. It is hypothesized that neurospheres generated from old NPCs show smaller Feret diameters compared to neurospheres generated from young NPCs. Furthermore, *BRCA2*-mutated neurospheres might even be more affected, and formaldehyde could also lead to a decrease in Feret diameter.

Therefore, neurospheres from four different cell lines (wildtype/with heterozygous *BRCA2* mutation/with compound heterozygous *BRCA2* mutation/with *BRCA1* mutation) were generated from NPCs with a passage higher than 15. All neurospheres grew slower compared to neurospheres generated from young NPCs, which fits into the picture of less proliferation in aged cells, probably due to an increase in DNA damage.

The slower growth was more prominent in wildtype and heterozygous *BRCA2*-mutated neurospheres compared to compound heterozygous *BRCA2* and heterozygous *BRCA1* neurospheres. Before those two NPC lines (wildtype and heterozygous *BRCA2*) were used for neurosphere generation, both cell lines, due to regular cell culture and the previous experiments, were often frozen and thawed, which might lead to high levels of genomic instability. Intensive freeze and thaw cycles lead to membrane ruptures, reduced viability and function, oxidative stress, and altered cell properties, which often result in cells dying or showing less proliferative capacity (Cottle et al., 2022; McGann et al., 1988; Serra et al., 2022). (Compound heterozygous *BRCA2* and heterozygous *BRCA1* NPCs were explicitly generated for this experiment and therefore cultured and passaged straightforwardly without many freeze and thaw cycles in between.)

Until day 10, instable growth could be observed in wildtype and heterozygous *BRCA2*-mutated, independent of formaldehyde treatment. Formaldehyde furthermore, led to a decrease in Feret diameter in both neurosphere lines and they did not recover until day 10 after formaldehyde treatment, as shown by persisting significant differences in Feret diameter due to treatment until day 10.

Mechanistically, formaldehyde probably leads to an irreversible G2/M arrest of the cells, as was already seen and discussed in the cell cycle and proliferation experiments of this study.

Interestingly, heterozygous *BRCA2* neurospheres were already affected on day 5, while wildtype neurospheres only showed an effect of formaldehyde from day 8 on. A stronger effect of heterozygous *BRCA2* neurospheres is expected, as *BRCA2* had been associated with proliferation previously: It is important for the cell proliferation during embryogenesis (Suzuki, De La Pompa, et al., 1997). High expression of BRCA2 was associated with high proliferation in breast cancer (Satyananda et al., 2021), but also in proliferating tissue in general (Marmorstein et al., 2001; Rajan et al., 1996). If *BRCA2* is depleted due to (compound) heterozygous mutations, proliferation might also be impaired in the old cells. In 1998 it was described that cells carrying a truncated BRCA2 show a proliferation impediment that worsens with successive passaging (Patel et al., 1998a). In this study, different from younger cells, older cells with already accumulated DNA damage could not cope with more DNA damage coming from formaldehyde. And *BRCA2* cells were even more affected, which is supported by our finding that also compound heterozygous *BRCA2* neurospheres differ significantly due to formaldehyde treatment already on day 5. On day 5, the immediate toxic effect of formaldehyde

plays a role. Probably the cell cycle was slowed down, and cells were not dividing due to the formaldehyde treatment, which has already been seen in the 2D culture in this work.
Interestingly, the effect of formaldehyde on day 5 could not be observed in either the wildtype neurospheres or in the *BRCA1*-mutated neurospheres. In both cell lines, the effect only appeared on day 8 after treatment with smaller Feret diameters in treated neurospheres. As already previously explained, both cell lines, wildtype and heterozygous *BRCA1*, are not as sensitive to formaldehyde as cell lines with mutations in the *BRCA2* gene. Therefore, only a progressive effect of formaldehyde might hit them. In 2013, Lai and colleagues investigated the effects of formaldehyde until 7 days after exposure on rabbit corneal epithelial cells. (Lai et al., 2013) They exposed those cells to concentrations between 5 and 600ppm formaldehyde. This is equivalent to 0.17 to 19.99mM formaldehyde, and 0.2mM that was used in this study is close to their lower limit. Among other things, they investigated cell count and survival rate after formaldehyde exposure. To determine the survival rate of cells, they exposed them to different concentrations (5-600ppm) of formaldehyde for 3min and evaluated cell viability with an MTT assay. After all treatments, the survival rate was decreased, significantly decreased after exposure to concentrations of 20-600ppm formaldehyde. To measure cell count, they exposed the cells to 100ppm formaldehyde for various times (0-30min) and examined cell count 1 to 7 days after exposure. They found that after 3min and 5min exposure, cells continue to grow as untreated cells in the first three days but then slow down their growth. An exposure of 10, 15, 20, and 30min led to significantly fewer cells on day 1 after exposure compared to untreated cells. After 10 and 15min exposure, the number of cells stayed approximately stable until day 7, and in the 20 and 30min treatment conditions, the cell count decreased continuously. This shows that formaldehyde leads to acute and progressive effects even at low concentrations of formaldehyde.
It can be concluded that already low concentrations of formaldehyde, like 5ppm, lead to a decrease in survival rate, and the longer the exposure to formaldehyde lasts, the lower the cell count is, already on day 1. The long-term effect of formaldehyde seems to depend on the exposure time and then again on the ability of cells to deal with the harshness of the treatment. The longer the incubation time, the harsher the treatment for the cells is. In this study an incubation duration of 5h with a concentration of 0.2mM formaldehyde was conducted. As already mentioned, *BRCA2*-mutated neurospheres seem to be able to cope worse with this formaldehyde exposure compared to wildtype or *BRCA1*-mutated neurospheres, already showing an effect on day 5 after treatment. Wildtype and *BRCA1*-mutated neurospheres on the other side only show an effect by day 8 after treatment.
Cells that can continue to grow after formaldehyde treatment are only undamaged or less damaged cells, which are not stuck in a G2/M arrest and take a while to increase the cell number again. By day 10 neurospheres seem to have overcome the effect of formaldehyde, as the means of the Feret diameters increased from day 8 to day 10. The difference between untreated and treated neurospheres is lower in the wildtype and heterozygously mutated *BRCA2* neurospheres and disappeared in the *BRCA1*-mutated neurospheres and compound heterozygous *BRCA2* neurospheres (here already on day 8).
That the effect stays longer in wildtype and heterozygously mutated *BRCA2* neurospheres compared to *BRCA1*-mutated and compound heterozygous *BRCA2*-mutated neurospheres is as expected due to their repetitive freeze and thaw history.
Taken together, the effects of the *BRCA2* mutation and formaldehyde are only visible in neurospheres generated from old NPCs. Wildtype and heterozygously mutated *BRCA2* neurospheres are more strongly affected due to their freeze and thaw history compared to compound heterozygous *BRCA2* and *BRCA1* mutated neurospheres. Formaldehyde decreases

the Feret diameter in neurospheres, and neurospheres carrying any *BRCA2* mutation show earlier effects compared to wildtype and *BRCA1*-mutated neurospheres.
Next experiments would be interesting to prove the hypothesis of an interaction between formaldehyde, BRCA2, and aging. The hypothesis is that in *BRCA2*-mutated old cells formaldehyde leads to an unbearable increase in DNA damage, which delays the cell cycle with a slowdown of the S-phase or a G2 arrest, leading to less proliferative capacity. Next to an analysis of genomic instability, it would be helpful to perform the DSB, cell cycle, and proliferation experiments with old NPCs with heterozygous, homozygous, and without *BRCA2* mutations.

5.7 No differences in migration, neither due to *BRCA2* mutation nor due to formaldehyde treatment

Within the neurospheres assay, it was also possible to check the influences of *BRCA2* mutations and formaldehyde on the migration of cells. A connection to migration has already been observed in other proteins of the Fanconi anemia pathway, like FANCD2 (Xie et al., 2024) and Fancg (Jarysta et al., 2021).
In this study there are no differences in migration due to *BRCA2* mutations or formaldehyde treatment.
A connection between *BRCA2* and migration has only sparsely been drawn before in literature. Arbini and colleagues found that a loss of *BCRA2* inhibits migration during the development of prostate tumors (Arbini et al., 2011). Furthermore, it was found that a deletion of *BRCA2* promotes migration on the extracellular matrix, while a *BRCA2* overexpression inhibits cancer cell migration and invasion (Moro et al., 2008). Also, formaldehyde has been linked to cell migration before in tumor cells. The difference in this study compared to our study is that internal formaldehyde levels were elevated or decreased by promoting or inhibiting cell migration (Quan et al., 2023). An external application with formaldehyde on migrating cells was not analyzed before.
All three studies focus on the work with cancer cells, while the cells in this study were neuronal cells, where no information due to migration is currently available.

6 Conclusion

The study aimed at analyzing the effects of formaldehyde on the neuronal tissue of *BRCA2* mutation carriers and its effects on cell proliferation and brain function.

The hypothesis of this study was that formaldehyde, given as an exogenous factor to neural progenitor cells, would deplete BRCA2 protein levels. In wildtype cells, this would decrease BRCA2 concentrations to levels of BRCA2 expression of heterozygous *BRCA2* cells, while in heterozygous *BRCA2* cells, the concentrations would be so low that normal functioning would not be possible anymore. As BRCA2 is involved in DNA damage repair and the cell cycle, both influencing proliferation, those characteristics would be altered after formaldehyde treatment.

The experiments were mainly performed in wildtype and heterozygous *BRCA2* NPCs differentiated from genome-edited iPSCs. It could be shown that BRCA2 protein and RNA expressions were decreased in fibroblasts and NPCs carrying a *BRCA2* mutation heterozygously or compound homozygously. Additionally, formaldehyde decreased BRCA2 protein and RNA levels in wildtype as well as heterozygous *BRCA2* NPCs, while, regarding BRCA1, only RNA levels were decreased after formaldehyde treatment in both cell lines. Mechanistically, formaldehyde led to an increase in the number of DSBs in both NPC lines. The number of cells in the G1-, S-, and G2-phase of the cell cycle was contrarily influenced by the *BRCA2* mutation and formaldehyde. The *BRCA2* mutation led to an increase of cells in S-phase as well as a decrease in G1-phase, while formaldehyde reduced the cells in S-phase and accumulated the cells in G2-phase, which suggests that cells arrest in G2- phase. It was found that *BRCA2* has a stronger effect compared to formaldehyde. Nevertheless, a formaldehyde treatment led to a slowdown of proliferation independent of genotype in 2D culture. In 3D culture, the effect of both a heterozygous mutation in *BRCA2* and formaldehyde, less proliferation, is visible in neurospheres generated from aged NPCs.

The presented results partly confirm previously published data, but beyond that, they are pointing towards a link between *BRCA2*, formaldehyde, ROS, and aging, which has not been investigated before.

In order to strengthen the results and investigate the link further, several experiments might be beneficial. The investigation of the dose-dependent effects of formaldehyde and experiments with another aldehyde like acetaldehyde and cells with homozygous deletions of *BRCA2* would strengthen basic assumptions behind the results. An analysis of ROS levels, stalled replication forks, genomic instability, and total cell cycle duration of synchronized cells would shed light on the molecular mechanism behind the effect of formaldehyde. And to prove the link between *BRCA2*, formaldehyde, and aging, it would be helpful to repeat the experiments with old NPCs and study apoptosis and proliferation speed in all cells. An inclusion of a heterozygous *BRCA1* mutated cell line could support the starting hypothesis following Tan and colleagues (Tan et al., 2017), that only *BRCA2* is influenced by formaldehyde via proteasomal degradation and not *BRCA1*. Additionally, in vitro analysis with brain organoids and in vivo experiments in mice with a *Brca2* knockout might round off the story, and questionnaires with *BRCA2* and *BRCA1* patients could complement the picture.

Taking together with this work, it could be shown that formaldehyde has a specific effect on *BRCA2* mutation carriers by alternating proliferation-relevant parameters in neural progenitor cells. An important fundament is laid for proof of the hypothesis, and at the end, genetic counseling of patients with *BRCA2* mutation might need to be adapted.

7 References

Acedo, A., Sanz, D. J., Durán, M., Infante, M., Pérez-Cabornero, L., Miner, C., & Velasco, E. A. (2012). Comprehensive splicing functional analysis of DNA variants of the BRCA2 gene by hybrid minigenes. *Breast Cancer Research*, *14*(3), R87. https://doi.org/10.1186/bcr3202

Adusumilli, V. S., Walker, T. L., Overall, R. W., Klatt, G. M., Zeidan, S. A., Zocher, S., Kirova, D. G., Ntitsias, K., Fischer, T. J., Sykes, A. M., Reinhardt, S., Dahl, A., Mansfeld, J., Rünker, A. E., & Kempermann, G. (2021). ROS Dynamics Delineate Functional States of Hippocampal Neural Stem Cells and Link to Their Activity-Dependent Exit from Quiescence. *Cell Stem Cell*, *28*(2), 300-314.e6. https://doi.org/https://doi.org/10.1016/j.stem.2020.10.019

Ahmad, A., Nay, S. L., & O'Connor, T. R. (2015). *Direct Reversal Repair in Mammalian Cells* (C. C. Chen, Ed.; p. Ch. 4). IntechOpen. https://doi.org/10.5772/60037

Ai, L., Tan, T., Tang, Y., Yang, J., Cui, D., Wang, R., Wang, A., Fei, X., Di, Y., Wang, X., Yu, Y., Zhao, S., Wang, W., Bai, S., Yang, X., He, R., Lin, W., Han, H., Cai, X., & Tong, Z. (2019). Endogenous formaldehyde is a memory-related molecule in mice and humans. *Communications Biology*, *2*(1). https://doi.org/10.1038/s42003-019-0694-x

Ait Saada, A., Lambert, S. A. E., & Carr, A. M. (2018). Preserving replication fork integrity and competence via the homologous recombination pathway. *DNA Repair*, *71*, 135–147. https://doi.org/10.1016/j.dnarep.2018.08.017

Alt, F. W., & Schwer, B. (2018). DNA double-strand breaks as drivers of neural genomic change, function, and disease. *DNA Repair*, *71*, 158–163. https://doi.org/10.1016/j.dnarep.2018.08.019

Alt, F. W., Wei, P.-C., & Schwer, B. (2017). *Recurrently Breaking Genes in Neural Progenitors: Potential Roles of DNA Breaks in Neuronal Function, Degeneration and Cancer*. (R. Jaenisch, F. Zhang, & F. Gage, Eds.; pp. 63–72). https://doi.org/10.1007/978-3-319-60192-2_6

Alter, B. P., Rosenberg, P. S., & Brody, L. C. (2007). Clinical and molecular features associated with biallelic mutations in FANCD1/BRCA2. In *Journal of Medical Genetics* (Vol. 44, Number 1, pp. 1–9). BMJ Publishing Group Ltd. https://doi.org/10.1136/jmg.2006.043257

Ambjørn, S. M., Duxin, J. P., Hertz, E. P. T., Nasa, I., Duro, J., Kruse, T., Lopez-Mendez, B., Rymarczyk, B., Cressey, L. E., van Overeem Hansen, T., Kettenbach, A. N., Oestergaard, V. H., Lisby, M., & Nilsson, J. (2021). A complex of BRCA2 and PP2A-B56 is required for DNA repair by homologous recombination. *Nature Communications*, *12*(1). https://doi.org/10.1038/s41467-021-26079-0

Andreassen, P. R., Seo, J., Wiek, C., & Hanenberg, H. (2021). Understanding BRCA2 function as a tumor suppressor based on domain-specific activities in DNA damage responses. In *Genes* (Vol. 12, Number 7). https://doi.org/10.3390/genes12071034

Andrews, M. G., & Kriegstein, A. R. (2022). Challenges of Organoid Research. In *Annual Review of Neuroscience* (Vol. 45, pp. 23–39). https://doi.org/10.1146/annurev-neuro-111020-090812

Arbini, A. A., Greco, M., Yao, J. L., Bourne, P., Marra, E., Hsieh, J.-T., di Sant'agnese, P. A., & Moro, L. (2011). Skp2 overexpression is associated with loss of BRCA2 protein in human prostate cancer. *The American Journal of Pathology*, *178*(5), 2367–2376. https://doi.org/10.1016/j.ajpath.2011.01.050

Arnold, K., Kim, M. K., Frerk, K., Edler, L., Savelyeva, L., Schmezer, P., & Wiedemeyer, R. (2006a). Lower level of BRCA2 protein in heterozygous mutation carriers is correlated

with an increase in DNA double strand breaks and an impaired DSB repair. *Cancer Letters*, *243*(1), 90–100. https://doi.org/10.1016/J.CANLET.2005.11.041

Arnold, K., Kim, M. K., Frerk, K., Edler, L., Savelyeva, L., Schmezer, P., & Wiedemeyer, R. (2006b). Lower level of BRCA2 protein in heterozygous mutation carriers is correlated with an increase in DNA double strand breaks and an impaired DSB repair. *Cancer Letters*, *243*(1), 90–100. https://doi.org/10.1016/J.CANLET.2005.11.041

Avilion, A. A., Nicolis, S. K., Pevny, L. H., Perez, L., Vivian, N., & Lovell-Badge, R. (2003). Multipotent cell lineages in early mouse development depend on SOX2 function. *Genes and Development*, *17*(1), 126–140. https://doi.org/10.1101/gad.224503

Baert, A., Depuydt, J., Van Maerken, T., Poppe, B., Malfait, F., Van Damme, T., De Nobele, S., Perletti, G., De Leeneer, K., Claes, K. B. M., & Vral, A. (2017). Analysis of chromosomal radiosensitivity of healthy BRCA2 mutation carriers and non-carriers in BRCA families with the G2 micronucleus assay. *Oncology Reports*, *37*(3), 1379–1386. https://doi.org/10.3892/OR.2017.5407

Barnum, K. J., & O'Connell, M. J. (2014). Cell cycle regulation by checkpoints. *Methods in Molecular Biology*, *1170*, 29–40. https://doi.org/10.1007/978-1-4939-0888-2_2

Bernard-Gallon, D. J., De Latour, M. P., Sylvain, V., Vissac, C., Aunoble, B., Chassagne, J., & Bignon, Y. J. (2001). Brca1 and Brca2 protein expression patterns in different tissues of murine origin. *International Journal of Oncology*, *18*(2), 271–280. https://doi.org/10.3892/IJO.18.2.271/HTML

Bernardini, L., Barbosa, E., Charão, M. F., & Brucker, N. (2020). Formaldehyde toxicity reports from in vitro and in vivo studies: a review and updated data. *Https://Doi.Org/10.1080/01480545.2020.1795190*, 1–13. https://doi.org/10.1080/01480545.2020.1795190

Bez, A., Corsini, E., Curti, D., Biggiogera, M., Colombo, A., Nicosia, R. F., Pagano, S. F., & Parati, E. A. (2003). Neurosphere and neurosphere-forming cells: morphological and ultrastructural characterization. *Brain Research*, *993*(1–2), 18–29. https://doi.org/10.1016/j.brainres.2003.08.061

Bhatia, V., Barroso, S. I., García-Rubio, M. L., Tumini, E., Herrera-Moyano, E., & Aguilera, A. (2014). BRCA2 prevents R-loop accumulation and associates with TREX-2 mRNA export factor PCID2. *Nature*, *511*(7509), 362–365. https://doi.org/10.1038/nature13374

Biswas, K., Alexander, K., & Francis, M. M. (2022). Reactive Oxygen Species: Angels and Demons in the Life of a Neuron. *NeuroSci*, *3*(1), 130–145. https://doi.org/10.3390/neurosci3010011

Blackshear, P. E., Goldsworthy, S. M., Foley, J. F., McAllister, K. A., Bennett, L. M., Collins, N. K., Bunch, D. O., Brown, P., Wiseman, R. W., & Davis, B. J. (1998). Brca1 and Brca2 expression patterns in mitotic and meiotic cells of mice. *Oncogene*, *16*(1), 61–68. https://doi.org/10.1038/sj.onc.1201506

Blouin, T., & Saini, N. (2024). Aldehyde-induced DNA-protein crosslinks- DNA damage, repair and mutagenesis. *Frontiers in Oncology*, *14*. https://doi.org/10.3389/FONC.2024.1478373

Borg, Å., Haile, R. W., Malone, K. E., Capanu, M., Diep, A., Törngren, T., Teraoka, S., Begg, C. B., Thomas, D. C., Concannon, P., Mellemkjaer, L., Bernstein, L., Tellhed, L., Xue, S., Olson, E. R., Liang, X., Dolle, J., Børresen-Dale, A.-L., & Bernstein, J. L. (2010). HUMAN MUTATION MUTATION IN BRIEF Characterization of BRCA1 and BRCA2 Deleterious Mutations and Variants of Unknown Clinical Significance in Unilateral and Bilateral Breast Cancer: The WECARE Study. *HUMAN MUTATION Mutation in Brief*, *31*, Online. https://doi.org/10.1002/humu.21202

Bott, C. J., Johnson, C. G., Yap, C. C., Dwyer, N. D., Litwa, K. A., & Winckler, B. (2019). Nestin in immature embryonic neurons affects axon growth cone morphology and Semaphorin3a sensitivity. *Molecular Biology of the Cell*, *30*(10), 1214–1229. https://doi.org/10.1091/mbc.E18-06-0361

Braun, S. M. G., & Jessberger, S. (2014). Adult neurogenesis: mechanisms and functional significance. *Development*, *141*(10), 1983–1986. https://doi.org/10.1242/dev.104596

Breast Cancer Study Group, A. (2000). *Prevalence and penetrance of BRCA1and BRCA2 mutations in a population-based series of breast cancer cases*. https://doi.org/10.1054/bjoc.2000.1407

Burgio, E., Piscitelli, P., & Migliore, L. (2018). Ionizing radiation and human health: Reviewing models of exposure and mechanisms of cellular damage. an epigenetic perspective. In *International Journal of Environmental Research and Public Health* (Vol. 15, Number 9). https://doi.org/10.3390/ijerph15091971

Cakir, B., & Park, I.-H. (2022). Getting the right cells. *ELife*, *11*. https://doi.org/10.7554/eLife.80373

Caputo, S. M., Léone, M., Damiola, F., Ehlen, A., Carreira, A., Gaidrat, P., Martins, A., Brandão, R. D., Peixoto, A., Vega, A., Houdayer, C., Delnatte, C., Bronner, M., Muller, D., Castera, L., Guillaud-Bataille, M., Søkilde, I., Uhrhammer, N., Demontety, S., … Rouleau, E. (2018). Full in-frame exon 3 skipping of BRCA2 confers high risk of breast and/or ovarian cancer. *Oncotarget*, *9*(25), 17334–17348. https://doi.org/10.18632/oncotarget.24671

Carlos, A. R., Escandell, J. M., Kotsantis, P., Suwaki, N., Bouwman, P., Badie, S., Folio, C., Benitez, J., Gomez-Lopez, G., Pisano, D. G., Jonkers, J., & Tarsounas, M. (2013). ARF triggers senescence in Brca2-deficient cells by altering the spectrum of p53 transcriptional targets. *Nature Communications*, *4*. https://doi.org/10.1038/ncomms3697

Chatterjee, N., & Walker, G. C. (2017). Mechanisms of DNA damage, repair, and mutagenesis. In *Environmental and Molecular Mutagenesis* (Vol. 58, Number 5, pp. 235–263). https://doi.org/10.1002/em.22087

Chaudhuri, A. R., & Nussenzweig, A. (2017). Thwarting endogenous stress: BRCA protects against aldehyde toxicity . *EMBO Molecular Medicine*, *9*(10), 1331–1333. https://doi.org/10.15252/emmm.201708194

Chaw, Y. F., Crane, L. E., Lange, P., & Shapiro, R. (1980). Isolation and Identification of Cross-Links from Formaldehyde-Treated Nucleic Acids"1". In *Biochemistry* (Vol. 19). https://pubs.acs.org/sharingguidelines

Chen, C. C., Feng, W., Lim, P. X., Kass, E. M., & Jasin, M. (2018). Homology-Directed Repair and the Role of BRCA1, BRCA2, and Related Proteins in Genome Integrity and Cancer. *Annual Review of Cancer Biology*, *2*(Volume 2, 2018), 313–336. https://doi.org/10.1146/ANNUREV-CANCERBIO-030617-050502/CITE/REFWORKS

Chen, D., Fang, L., Mei, S., Li, H., Xu, X., Des Marais, T. L., Lu, K., Liu, X. S., & Jin, C. (2017). Regulation of Chromatin Assembly and Cell Transformation by Formaldehyde Exposure in Human Cells. *Environmental Health Perspectives*, *125*(9). https://doi.org/10.1289/EHP1275

Chen, J. H., Hales, C. N., & Ozanne, S. E. (2007). DNA damage, cellular senescence and organismal ageing: Causal or correlative? In *Nucleic Acids Research* (Vol. 35, Number 22, pp. 7417–7428). https://doi.org/10.1093/nar/gkm681

Chen, X., Hartman, A., & Guo, S. (2015). Choosing Cell Fate Through a Dynamic Cell Cycle. *Current Stem Cell Reports*, *1*(3), 129. https://doi.org/10.1007/S40778-015-0018-0

Chen, X., Yu, H., Li, Z., Ye, W., Liu, Z., Gao, J., Wang, Y., Li, X., Zhang, L., Alenina, N., Bader, M., Ding, H., Li, P., Htet, L., & Aung, H. (2022). *Oxidative RNA Damage in the Pathogenesis and Treatment of Type 2 Diabetes*. https://doi.org/10.3389/fphys.2022.725919

Cheng, G., Shi, Y., Sturla, S. J., Jalas, J. R., McIntee, E. J., Villalta, P. W., Wang, M., & Hecht, S. S. (2003). Reactions of formaldehyde plus acetaldehyde with deoxyguanosine and DNA: Formation of cyclic deoxyguanosine adducts and formaldehyde cross-links. *Chemical Research in Toxicology*, *16*(2), 145–152. https://doi.org/10.1021/TX025614R/ASSET/IMAGES/LARGE/TX025614RF6.JPEG

Chernoff, J. (2021). The two-hit theory hits 50. *Molecular Biology of the Cell*, *32*(22). https://doi.org/10.1091/MBC.E21-08-0407

Cheung, A. M. Y., Hande, M. P., Jalali, F., Tsao, M.-S., Skinnider, B., Hirao, A., McPherson, J. P., Karaskova, J., Suzuki, A., Wakeham, A., You-Ten, A., Elia, A., Squire, J., Bristow, R., Hakem, R., & Mak, T. W. (2002). Loss of Brca2 and p53 synergistically promotes genomic instability and deregulation of T-cell apoptosis. *Cancer Research*, *62*(21), 6194–6204.

Chian, J. S., Xu, W., & Wang, M. (2023). Pancreatic cancer cluster region identified in BRCA2. *J Med Genet*, *0*, 1–5. https://doi.org/10.1136/jmg-2022-109111

Chodosh, L. A. (1998). Expression of BRCA1 and BRCA2 in Normal and Neoplastic Cells. *Journal of Mammary Gland Biology and Neoplasia*, *3*(4), 389–402. https://doi.org/10.1023/A:1018784031651/METRICS

Choi, Y. E., Pan, Y., Park, E., Konstantinopoulos, P., De, S., D'Andrea, A., & Chowdhury, D. (2014). MicroRNAs down-regulate homologous recombination in the G1 phase of cycling cells to maintain genomic stability. *ELife*, *3*, e02445. https://doi.org/10.7554/eLife.02445

Cloos, P. A. C., Christensen, J., Agger, K., & Helin, K. (2008). Erasing the methyl mark: histone demethylases at the center of cellular differentiation and disease. *Genes & Development*, *22*(9), 1115–1140. https://doi.org/10.1101/GAD.1652908

Connor, F., Bertwistle, D., Joseph Mee, P., Ross, G. M., Swift, S., Grigorieva, E., Tybulewicz, V. L. J., & Ashworth, A. (1997). Tumorigenesis and a DNA repair defect in mice with a truncating Brca2 mutation. *Nature Genetics*, *17*(4), 423–431. https://doi.org/10.1038/ng1297-423

Costa, L. G., Cole, T. B., Coburn, J., Chang, Y. C., Dao, K., & Roqué, P. J. (2017). Neurotoxicity of traffic-related air pollution. *Neurotoxicology*, *59*, 133–139. https://doi.org/10.1016/J.NEURO.2015.11.008

Cottle, C., Porter, A. P., Lipat, A., Turner-Lyles, C., Nguyen, J., Moll, G., & Chinnadurai, R. (2022). Impact of Cryopreservation and Freeze-Thawing on Therapeutic Properties of Mesenchymal Stromal/Stem Cells and Other Common Cellular Therapeutics. *Current Stem Cell Reports*, *8*(2), 72. https://doi.org/10.1007/S40778-022-00212-1

Daniels, M. J., Wang, Y., Lee, M., & Venkitaraman, A. R. (2004). Abnormal cytokinesis in cells deficient in the breast cancer susceptibility protein BRCA2. *Science (New York, N.Y.)*, *306*(5697), 876–879. https://doi.org/10.1126/science.1102574

De Siervi, A., De Luca, P., Byun, J. S., Di, L. J., Fufa, T., Haggerty, C. M., Vazquez, E., Moiola, C., Longo, D. L., & Gardner, K. (2010). Transcriptional autoregulation by BRCA1. *Cancer Research*, *70*(2), 532. https://doi.org/10.1158/0008-5472.CAN-09-1477

De Toni, E. N., Ziesch, A., Rizzani, A., Török, H.-P., Hocke, S., Lü, S., Wang, S.-C., Hucl, T., Göke, B., Bruns, C., & Gallmeier, E. (2016). Inactivation of BRCA2 in human cancer cells identifies a subset of tumors with enhanced sensitivity towards death receptor-mediated apoptosis. *Oncotarget*, *7*(8), 9477–9490. https://doi.org/10.18632/oncotarget.7053

Denny, L. A., Coles, S., & Blitz, R. (2017). Fetal Alcohol Syndrome and Fetal Alcohol Spectrum Disorders. *American Family Physician*, *96*(8), 515–522. https://doi.org/10.1002/0471695998.mgs020

Drake, D. M., & Wells, P. G. (2021). Novel mechanisms in alcohol neurodevelopmental disorders via BRCA1 depletion and BRCA1-dependent NADPH oxidase regulation. *Redox Biology*, *48*. https://doi.org/10.1016/J.REDOX.2021.102148

Duong, A., Steinmaus, C., McHale, C. M., Vaughan, C. P., & Zhang, L. (2011). Reproductive and developmental toxicity of formaldehyde: a systematic review. *Mutation Research*, *728*(3), 118–138. https://doi.org/10.1016/J.MRREV.2011.07.003

Duque, A., Arellano, J. I., & Rakic, P. (2021). An assessment of the existence of adult neurogenesis in humans and value of its rodent models for neuropsychiatric diseases. *Molecular Psychiatry*. https://doi.org/10.1038/s41380-021-01314-8

Durdik, M., Kosik, P., Lukas Jakl, |, Kozackova, M., Markova, | Eva, Katarina Vigasova, |, Katarina Beresova, |, Jakubikova, J., Horvathova, | Eva, Zastko, L., Fekete, M., Zavacka, I., Pobijakova, M., & Belyaev, I. (2021). Imaging flow cytometry and fluorescence microscopy in assessing radiation response in lymphocytes from umbilical cord blood and cancer patients. *Cytometry*, 99. https://doi.org/10.1002/cyto.a.24468

Duval, K., Grover, H., Han, L. H., Mou, Y., Pegoraro, A. F., Fredberg, J., & Chen, Z. (2017). Modeling Physiological Events in 2D vs. 3D Cell Culture. *Physiology*, *32*(4), 266. https://doi.org/10.1152/PHYSIOL.00036.2016

Easton, D. F., Deffenbaugh, A. M., Pruss, D., Frye, C., Wenstrup, R. J., Allen-Brady, K., Tavtigian, S. V, Monteiro, A. N. A., Iversen, E. S., Couch, F. J., & Goldgar, D. E. (2007). A systematic genetic assessment of 1,433 sequence variants of unknown clinical significance in the BRCA1 and BRCA2 breast cancer-predisposition genes. *American Journal of Human Genetics*, *81*(5), 873–883. https://doi.org/10.1086/521032

Edwards, S. M., Kote-Jarai, Z., Meitz, J., Hamoudi, R., Hope, Q., Osin, P., Jackson, R., Southgate, C., Singh, R., Falconer, A., Dearnaley, D. P., Ardern-Jones, A., Murkin, A., Dowe, A., Kelly, J., Williams, S., Oram, R., Stevens, M., Teare, D. M., … Eeles, R. A. (2003). Two percent of men with early-onset prostate cancer harbor germline mutations in the BRCA2 gene. *American Journal of Human Genetics*, *72*(1), 1–12. https://doi.org/10.1086/345310

Esashi, F., Christ, N., Gannon, J., Liu, Y., Hunt, T., Jasin, M., & West, S. C. (2005). CDK-dependent phosphorylation of BRCA2 as a regulatory mechanism for recombinational repair. *Nature*, *434*(7033), 598–604. https://doi.org/10.1038/nature03404

Esteras, N., Kopach, O., Maiolino, M., Lariccia, V., Amoroso, S., Qamar, S., Wray, S., Rusakov, D. A., Jaganjac, M., & Abramov, A. Y. (2022). Mitochondrial ROS control neuronal excitability and cell fate in frontotemporal dementia. *Alzheimer's and Dementia*, *18*(2), 318–338. https://doi.org/10.1002/alz.12394

Evans, D. G., Shenton, A., Woodward, E., Lalloo, F., Howell, A., & Maher, E. R. (2008). Penetrance estimates for BRCA1 and BRCA2based on genetic testing in a Clinical Cancer Genetics service setting: Risks of breast/ovarian cancer quoted should reflect the cancer burden in the family. *BMC Cancer*, *8*(1), 155. https://doi.org/10.1186/1471-2407-8-155

Fackenthal, J. D., Cartegni, L., Krainer, A. R., & Olopade, O. I. (2002). BRCA2 T2722R is a deleterious allele that causes exon skipping. *American Journal of Human Genetics*, *71*(3), 625–631. https://doi.org/10.1086/342192

Fackenthal, J. D., Yoshimatsu, T., Zhang, B., de Garibay, G. R., Colombo, M., Vecchi, G. De, Ayoub, S. C., Lal, K., Olopade, O. I., Vega, A., Santamariña, M., Blanco, A., Wappenschmidt, B., Becker, A., Houdayer, C., Walker, L. C., López-Perolio, I.,

Thomassen, M., Parsons, M., … kConFaB Investigators. (2016). Naturally occurring BRCA2 alternative mRNA splicing events in clinically relevant samples. *Journal of Medical Genetics*, *53*(8), 548–558. https://doi.org/10.1136/jmedgenet-2015-103570

Farahani, R., Rezaei-Lotfi, S., Simonian, M., & Hunter, N. (2019). Bi-modal reprogramming of cell cycle by MiRNA-4673 amplifies human neurogenic capacity. *Cell Cycle (Georgetown, Tex.)*, *18*(8), 848–868. https://doi.org/10.1080/15384101.2019.1595873

Flint, M. S., & Bovbjerg, D. H. (2012). DNA damage as a result of psychological stress: implications for breast cancer. In *Breast cancer research : BCR* (Vol. 14, Number 5, p. 320). https://doi.org/10.1186/bcr3189

Forment, J. V., & Jackson, S. P. (2015). A flow cytometry-based method to simplify the analysis and quantification of protein association to chromatin in mammalian cells. *Nature Protocols*, *10*(9), 1297–1307. https://doi.org/10.1038/NPROT.2015.066

Fradet-Turcotte, A., Sitz, J., Grapton, D., & Orthwein, A. (2016). BRCA2 functions: from DNA repair to replication fork stabilization. *Endocrine-Related Cancer*, *23*(10), T1–T17. https://doi.org/10.1530/ERC-16-0297

Frappart, P. O., Lee, Y., Lamont, J., & McKinnon, P. J. (2007a). BRCA2 is required for neurogenesis and suppression of medulloblastoma. *EMBO Journal*, *26*(11), 2732–2742. https://doi.org/10.1038/sj.emboj.7601703

Frappart, P. O., Lee, Y., Lamont, J., & McKinnon, P. J. (2007b). BRCA2 is required for neurogenesis and suppression of medulloblastoma. *EMBO Journal*, *26*(11), 2732–2742. https://doi.org/10.1038/sj.emboj.7601703

Frappart, P. O., & McKinnon, P. J. (2007). BRCA2 function and the central nervous system. *Cell Cycle (Georgetown, Tex.)*, *6*(20), 2453–2457. https://doi.org/10.4161/CC.6.20.4785

Fridlich, R., Annamalai, D., Roy, R., Bernheim, G., & Powell, S. N. (2015a). BRCA1 and BRCA2 protect against oxidative DNA damage converted into double-strand breaks during DNA replication. *DNA Repair*, *30*, 11. https://doi.org/10.1016/J.DNAREP.2015.03.002

Fridlich, R., Annamalai, D., Roy, R., Bernheim, G., & Powell, S. N. (2015b). BRCA1 and BRCA2 protect against oxidative DNA damage converted into double-strand breaks during DNA replication. *DNA Repair*, *30*, 11. https://doi.org/10.1016/J.DNAREP.2015.03.002

Friedenson, B. (2011). A common environmental carcinogen unduly affects carriers of cancer mutations: carriers of genetic mutations in a specific protective response are more susceptible to an environmental carcinogen. *Medical Hypotheses*, *77*(5), 791–797. https://doi.org/10.1016/J.MEHY.2011.07.039

Friedman, L. S., Gayther, S. A., Kurosaki, T., Gordon, D., Noble, B., Casey, G., Ponder, B. A., & Anton-Culver, H. (1997). Mutation analysis of BRCA1 and BRCA2 in a male breast cancer population. *American Journal of Human Genetics*, *60*(2), 313–319.

Futamura, M., Arakawa, H., Matsuda, K., Katagiri, T., Saji, S., Miki, Y., & Nakamura, Y. (2000). Potential role of BRCA2 in a mitotic checkpoint after phosphorylation by hBUBR1. *Cancer Research*, *60*(6), 1531–1535. https://pubmed.ncbi.nlm.nih.gov/10749118/

Galano, A., Tan, D. X., & Reiter, R. J. (2018). Melatonin: A versatile protector against oxidative DNA damage. In *Molecules* (Vol. 23, Number 3). https://doi.org/10.3390/molecules23030530

Galkin, V. E., Esashi, F., Yu, X., Yang, S., West, S. C., & Egelman, E. H. (2005). BRCA2 BRC motifs bind RAD51-DNA filaments. *Proceedings of the National Academy of Sciences of*

the United States of America, *102*(24), 8537–8542. https://doi.org/10.1073/pnas.0407266102

Gao, Y., Guitton-Sert, L., Dessapt, J., Coulombe, Y., Rodrigue, A., Milano, L., Blondeau, A., Larsen, N. B., Duxin, J. P., Hussein, S., Fradet-Turcotte, A., & Masson, J.-Y. (2023). *A CRISPR-Cas9 screen identifies EXO1 as a formaldehyde resistance gene*. https://doi.org/10.1038/s41467-023-35802-y

Garaycoechea, J. I., Crossan, G. P., Langevin, F., Mulderrig, L., Louzada, S., Yang, F., Guilbaud, G., Park, N., Roerink, S., Nik-Zainal, S., Stratton, M. R., & Patel, K. J. (2018). Alcohol and endogenous aldehydes damage chromosomes and mutate stem cells. *Nature*, *553*(7687), 171–177. https://doi.org/10.1038/NATURE25154

García-García, E., Pino-Barrio, M. J., Lopez-Medina, L., & Martiñez-Serrano, A. (2012). Intermediate progenitors are increased by lengthening of the cell cycle through calcium signaling and p53 expression in human neural progenitors. *Molecular Biology of the Cell*, *23*(7), 1167–1180. https://doi.org/10.1091/MBC.E11-06-0524/ASSET/IMAGES/LARGE/1167FIG9.JPEG

Garcia-Higuera, I., Taniguchi, T., Ganesan, S., Meyn, M. S., Timmers, C., Hejna, J., Grompe, M., & D'Andrea, A. D. (2001). Interaction of the Fanconi anemia proteins and BRCA1 in a common pathway. *Molecular Cell*, *7*(2), 249–262. https://doi.org/10.1016/s1097-2765(01)00173-3

Gayther, S. A., Mangion, J., Russell, P., Seal, S., Barfoot, R., Ponder, B. A., Stratton, M. R., & Easton, D. (1997). Variation of risks of breast and ovarian cancer associated with different germline mutations of the BRCA2 gene. *Nature Genetics*, *15*(1), 103–105. https://doi.org/10.1038/ng0197-103

Gemma, C., & Bachstetter, A. D. (2013). The role of microglia in adult hippocampal neurogenesis. In *Frontiers in Cellular Neuroscience* (Vol. 7, Number NOV). https://doi.org/10.3389/fncel.2013.00229

Gire, V., & Dulić, V. (2015). Senescence from G2 arrest, revisited. *Cell Cycle*, *14*(3), 297–304. https://doi.org/10.1080/15384101.2014.1000134

Giusti, R. M., Rutter, J. L., Duray, P. H., Freedman, L. S., Konichezky, M., Fisher-Fischbein, J., Greene, M. H., Maslansky, B., Fischbein, A., Gruber, S. B., Rennert, G., Ronchetti, R. D., Hewitt, S. M., Struewing, J. P., & Iscovich, J. (2003). A twofold increase in BRCA mutation related prostate cancer among Ashkenazi Israelis is not associated with distinctive histopathology. In *Journal of medical genetics* (Vol. 40, Number 10, pp. 787–792). https://doi.org/10.1136/jmg.40.10.787

Gong, S., Li, Q., Jeter, C. R., Fan, Q., Tang, D. G., & Liu, B. (2015). Regulation of NANOG in cancer cells. *Molecular Carcinogenesis*, *54*(9), 679–687. https://doi.org/10.1002/mc.22340

Gonzalez-Rivera, J. C., Sherman, M. W., Wang, D. S., Chuvalo-Abraham, J. C. L., Hildebrandt Ruiz, L., & Contreras, L. M. (2020a). RNA oxidation in chromatin modification and DNA-damage response following exposure to formaldehyde. *Scientific Reports*, *10*(1), 16545. https://doi.org/10.1038/S41598-020-73376-7

Gonzalez-Rivera, J. C., Sherman, M. W., Wang, D. S., Chuvalo-Abraham, J. C. L., Hildebrandt Ruiz, L., & Contreras, L. M. (2020b). RNA oxidation in chromatin modification and DNA-damage response following exposure to formaldehyde. *Scientific Reports 2020 10:1*, *10*(1), 1–16. https://doi.org/10.1038/s41598-020-73376-7

Gorodetska, I., Kozeretska, I., & Dubrovska, A. (2019a). BRCA Genes: The Role in Genome Stability, Cancer Stemness and Therapy Resistance. *Journal of Cancer*, *10*. https://doi.org/10.7150/jca.30410

Gorodetska, I., Kozeretska, I., & Dubrovska, A. (2019b). BRCA Genes: The Role in Genome Stability, Cancer Stemness and Therapy Resistance. *Journal of Cancer*, *10*(9), 2109–2127. https://doi.org/10.7150/JCA.30410

Grafstrom, R. C., Fornace, A. J., Autrup, H., Lechner, J. F., & Harris, C. C. (1983). Formaldehyde damage to DNA and inhibition of DNA repair in human bronchial cells. *Science*, *220*(4593), 216–218. https://doi.org/10.1126/science.6828890

Gretarsdottir, S., Thorlacius, S., Gudlaugsdottir, S., Sigurdsson, S., Steinarsdottir, M., Jonasson, J. G., Anamthawat-Jonsson, K., & Eyfjã, J. E. (1998). BRCA2 and p53 Mutations in Primary Breast Cancer in Relation to Genetic Instability1. *CANCER RESEARCH*, *58*, 859–862. http://aacrjournals.org/cancerres/article-pdf/58/5/859/2468546/cr0580050859.pdf

Gupta, M. K., Guy, C. P., Yeeles, J. T. P., Atkinson, J., Bell, H., Lloyd, R. G., Marians, K. J., & McGlynn, P. (2013). Protein-DNA complexes are the primary sources of replication fork pausing in Escherichia coli. *Proceedings of the National Academy of Sciences of the United States of America*, *110*(18), 7252–7257. https://doi.org/10.1073/pnas.1303890110

Hakem, R. (2008). DNA-damage repair; the good, the bad, and the ugly. *The EMBO Journal*, *27*(4), 589–605. https://doi.org/https://doi.org/10.1038/emboj.2008.15

Hakem, R., De La Pompa, J. L., & Mak, T. W. (1998). Developmental Studies of Brca1 and Brca2 Knock-Out Mice. *Journal of Mammary Gland Biology and Neoplasia*, *3*(4), 431–445. https://doi.org/10.1023/A:1018792200700

Hara, H., Negoro, S., Miyata, S., Saiki, O., Yoshizaki, K., Tanaka, T., Igarashi, T., & Kishimoto, S. (1987). Age-associated changes in proliferative and differentiative response of human B cells and production of T cell-derived factors regulating B cell functions. *Mechanisms of Ageing and Development*, *38*(3), 245–258. https://doi.org/https://doi.org/10.1016/0047-6374(87)90093-5

Harman, D. (1981). The aging process. *Proceedings of the National Academy of Sciences*, *78*(11), 7124–7128. https://doi.org/10.1073/pnas.78.11.7124

Harris, C., Wang, S. W., Lauchu, J. J., & Hansen, J. M. (2003). Methanol metabolism and embryotoxicity in rat and mouse conceptuses: comparisons of alcohol dehydrogenase (ADH1), formaldehyde dehydrogenase (ADH3), and catalase. *Reproductive Toxicology*, *17*(3), 349–357. https://doi.org/10.1016/S0890-6238(03)00013-3

Hashimoto, S., Anai, H., & Hanada, K. (2016). Mechanisms of interstrand DNA crosslink repair and human disorders. *Genes and Environment*, *38*(1), 9. https://doi.org/10.1186/s41021-016-0037-9

Heck, H., White, E. L., & Casanova-Schmitz, M. (1982). Determination of formaldehyde in biological tissues by gas chromatography/mass spectrometry. *Biological Mass Spectrometry*, *9*(8), 347–353. https://doi.org/10.1002/bms.1200090808

Heijink, A. M., Talens, F., Jae, L. T., van Gijn, S. E., Fehrmann, R. S. N., Brummelkamp, T. R., & van Vugt, M. A. T. M. (2019). BRCA2 deficiency instigates cGAS-mediated inflammatory signaling and confers sensitivity to tumor necrosis factor-alpha-mediated cytotoxicity. *Nature Communications*, *10*(1). https://doi.org/10.1038/s41467-018-07927-y

Hester, S. D., Benavides, G. B., Yoon, L., Morgan, K. T., Zou, F., Barry, W., & Wolf, D. C. (2003). Formaldehyde-induced gene expression in F344 rat nasal respiratory epithelium. *Toxicology*, *187*(1), 13—24. https://doi.org/10.1016/s0300-483x(03)00008-8

Hollis, R. L., Churchman, M., & Gourley, C. (2017). Distinct implications of different BRCA mutations: Efficacy of cytotoxic chemotherapy, PARP inhibition and clinical outcome in

ovarian cancer. *OncoTargets and Therapy*, *10*, 2539–2551. https://doi.org/10.2147/OTT.S102569

Homem, C. C. F., Repic, M., & Knoblich, J. A. (2015). Proliferation control in neural stem and progenitor cells. *Nature Reviews. Neuroscience*, *16*(11), 647. https://doi.org/10.1038/NRN4021

Howlett, N. G., Taniguchi, T., Olson, S., Cox, B., Waisfisz, Q., De Die-Smulders, C., Persky, N., Grompe, M., Joenje, H., Pals, G., Ikeda, H., Fox, E. A., & D'Andrea, A. D. (2002). Biallelic inactivation of BRCA2 in Fanconi anemia. *Science (New York, N.Y.)*, *297*(5581), 606–609. https://doi.org/10.1126/science.1073834

Huang, Y. Y., Lu, H., Liu, S., Droz-Rosario, R., & Shen, Z. (2012). Requirement of Mouse BCCIP for Neural Development and Progenitor Proliferation. *PLoS ONE*, *7*(1). https://doi.org/10.1371/JOURNAL.PONE.0030638

Jarysta, A., Riou, L., Firlej, V., Lapoujade, C., Kortulewski, T., Barroca, V., Gille, A.-S., Dumont, F., Jacques, S., Letourneur, F., Rosselli, F., Allemand, I., & Fouchet, P. (2021). Abnormal migration behavior linked to Rac1 signaling contributes to primordial germ cell exhaustion in Fanconi anemia pathway-deficient Fancg-/- embryos. *Human Molecular Genetics*, *31*(1), 97–110. https://doi.org/10.1093/hmg/ddab222

Jensen, C., & Teng, Y. (2020). Is It Time to Start Transitioning From 2D to 3D Cell Culture? *Frontiers in Molecular Biosciences*, *7*, 513823. https://doi.org/10.3389/FMOLB.2020.00033/BIBTEX

Juarez, E., Chambwe, N., Tang, W., Mitchell, A. D., Owen, N., Kumari, A., Monnat, R. J., & McCullough, A. K. (2018). An RNAi screen in human cell lines reveals conserved DNA damage repair pathways that mitigate formaldehyde sensitivity. *DNA Repair*, *72*, 1–9. https://doi.org/10.1016/j.dnarep.2018.10.002

Kalapos, M. P. (1999). A possible evolutionary role of formaldehyde. In *Experimental and Molecular Medicine* (Vol. 31, Number 1, pp. 1–4). https://doi.org/10.1038/emm.1999.1

Kalász, H. (2003). Biological role of formaldehyde, and cycles related to methylation, demethylation, and formaldehyde production. *Mini Reviews in Medicinal Chemistry*, *3*(3), 175–192. https://doi.org/10.2174/1389557033488187

Kapałczyńska, M., Kolenda, T., Przybyła, W., Zajączkowska, M., Teresiak, A., Filas, V., Ibbs, M., Bliźniak, R., Łuczewski, Ł., & Lamperska, K. (2016). 2D and 3D cell cultures – a comparison of different types of cancer cell cultures. *Archives of Medical Science : AMS*, *14*(4), 910. https://doi.org/10.5114/AOMS.2016.63743

Kapałczyńska, M., Kolenda, T., Przybyła, W., Zajączkowska, M., Teresiak, A., Filas, V., Ibbs, M., Bliźniak, R., Łuczewski, Ł., & Lamperska, K. (2018). 2D and 3D cell cultures – a comparison of different types of cancer cell cultures. *Archives of Medical Science*, *14*(4), 910–919. https://doi.org/10.5114/aoms.2016.63743

Karaayvaz-Yildirim, M., Silberman, R. E., Langenbucher, A., Saladi, S. V., Ross, K. N., Zarcaro, E., Desmond, A., Yildirim, M., Vivekanandan, V., Ravichandran, H., Mylavagnanam, R., Specht, M. C., Ramaswamy, S., Lawrence, M., Amon, A., & Ellisen, L. W. (2020). Aneuploidy and a deregulated DNA damage response suggest haploinsufficiency in breast tissues of BRCA2 mutation carriers. *Science Advances*, *6*(5), 1–11. https://doi.org/10.1126/sciadv.aay2611

Karlsson, M., Zhang, C., Méar, L., Zhong, W., Digre, A., Katona, B., Sjöstedt, E., Butler, L., Odeberg, J., Dusart, P., Edfors, F., Oksvold, P., von Feilitzen, K., Zwahlen, M., Arif, M., Altay, O., Li, X., Ozcan, M., Mardinoglu, A., … Lindskog, C. (2021). A single-cell type transcriptomics map of human tissues. In *Sci. Adv* (Vol. 7). www.proteinatlas.org

Käseberg, S. (2023). *Mechanisms of clinical variability: gain vs. loss of function : X-chromosomal reactivation underlying female resilience = Mechanismen der klinischen Variabilität: Funktionsgewinn gegen Funktionsverlust : X-chromosomale Reaktivierung der Grundlage der weib*. https://doi.org/http://doi.org/10.25358/openscience-8622

Kastner, P. E., Casset, A., & Pons, F. (2011). Formaldehyde interferes with airway epithelium integrity and functions in a dose- and time-dependent manner. *Toxicology Letters*, *200*(1–2), 109–116. https://doi.org/10.1016/j.toxlet.2010.11.003

Ke, Y. J., Qin, X. D., Zhang, Y. C., Li, H., Li, R., Yuan, J. L., Yang, X., & Ding, S. M. (2014). In vitro study on cytotoxicity and intracellular formaldehyde concentration changes after exposure to formaldehyde and its derivatives. *Human and Experimental Toxicology*, *33*(8), 822–830. https://doi.org/10.1177/0960327113510538/ASSET/187BBB12-A1B9-4ACB-A283-A01E83EB2C21/ASSETS/IMAGES/LARGE/10.1177_0960327113510538-FIG7.JPG

Keil, J. M., Doyle, D. Z., Qalieh, A., Lam, M. M., Funk, O. H., Qalieh, Y., Shi, L., Mohan, N., Sorel, A., & Kwan, K. Y. (2020). Symmetric neural progenitor divisions require chromatin-mediated homologous recombination DNA repair by Ino80. *Nature Communications*, *11*(1). https://doi.org/10.1038/S41467-020-17551-4

Kempermann, G., Gage, F. H., Aigner, L., Song, H., Curtis, M. A., Thuret, S., Kuhn, H. G., Jessberger, S., Frankland, P. W., Cameron, H. A., Gould, E., Hen, R., Abrous, D. N., Toni, N., Schinder, A. F., Zhao, X., Lucassen, P. J., & Frisén, J. (2018). Human Adult Neurogenesis: Evidence and Remaining Questions. *Cell Stem Cell*, *23*(1), 25–30. https://doi.org/10.1016/j.stem.2018.04.004

Kennedy, R. D., & D'Andrea, A. D. (2005). The Fanconi Anemia/BRCA pathway: new faces in the crowd. *Genes & Development*, *19*(24), 2925–2940. https://doi.org/10.1101/GAD.1370505

Kilburn, K. H., Seidman, B. C., & Warshaw, R. (1985). Neurobehavioral and Respiratory Symptoms of Formaldehyde and Xylene Exposure in Histology Technicians. *Archives of Environmental Health: An International Journal*, *40*(4), 229–233. https://doi.org/10.1080/00039896.1985.10545924

Kilburn, K. H., Warshaw, R., Boylen, C. T., Johnson, S. J., Seidman, B., Sinclair, R., & Takaro, T. J. (1985). Pulmonary and neurobehavioral effects of formaldehyde exposure. *Archives of Environmental Health*, *40*(5), 254–260. https://doi.org/10.1080/00039896.1985.10545928

Kilburn, K. H., Warshaw, R., & Thornton, J. C. (1987). Formaldehyde Impairs Memory, Equilibrium, and Dexterity in Histology Technicians: Effects Which Persist for Days after Exposure. *Archives of Environmental Health: An International Journal*, *42*(2), 117–120. https://doi.org/10.1080/00039896.1987.9935806

Kilgas, S., Kiltie, A. E., & Ramadan, K. (2021). Immunofluorescence microscopy-based detection of ssDNA foci by BrdU in mammalian cells. *STAR Protocols*, *2*(4). https://doi.org/10.1016/J.XPRO.2021.100978

Knudson, A. G. J. (1971). Mutation and cancer: statistical study of retinoblastoma. *Proceedings of the National Academy of Sciences of the United States of America*, *68*(4), 820–823. https://doi.org/10.1073/pnas.68.4.820

Kong, Q., & Lin, C. L. G. (2010). Oxidative damage to RNA: mechanisms, consequences, and diseases. *Cellular and Molecular Life Sciences: CMLS*, *67*(11), 1817. https://doi.org/10.1007/S00018-010-0277-Y

Kotsopoulos, J., Kim, S. J., Armel, S., Bordeleau, L., Foulkes, W. D., McKinnon, W., Panchal, S., Cohen, S. A., Sun, S., Sun, P., McKetton, L., Troyer, A. K., & Narod, S. A. (2021). An

evaluation of memory and attention in BRCA mutation carriers using an online cognitive assessment tool. *Cancer*, *127*(17), 3183–3193. https://doi.org/10.1002/CNCR.33654

Kou, Y., Zhao, H., Cui, D., Han, H., & Tong, Z. (2022). Formaldehyde toxicity in age-related neurological dementia. *Ageing Research Reviews*, *73*, 101512. https://doi.org/10.1016/J.ARR.2021.101512

Krenning, L., van den Berg, J., & Medema, R. H. (2019a). Life or Death after a Break: What Determines the Choice? *Molecular Cell*, *76*(2), 346–358. https://doi.org/10.1016/J.MOLCEL.2019.08.023

Krenning, L., van den Berg, J., & Medema, R. H. (2019b). Life or Death after a Break: What Determines the Choice? In *Molecular Cell* (Vol. 76, Number 2, pp. 346–358). Cell Press. https://doi.org/10.1016/j.molcel.2019.08.023

Kumar, S., & Huberman, J. A. (2004). On the slowing of S phase in response to DNA damage in fission yeast. *Journal of Biological Chemistry*, *279*(42), 43574–43580. https://doi.org/10.1074/jbc.M407819200

Kumari, A., Lim, Y. X., Newell, A. H., Olson, S. B., & McCullough, A. K. (2011). Formaldehyde-Induced Genome Instability is Suppressed by an XPF-dependent Pathway. *DNA Repair*, *11*(3), 236. https://doi.org/10.1016/J.DNAREP.2011.11.001

Kumari, A., Lim, Y. X., Newell, A. H., Olson, S. B., & McCullough, A. K. (2012). Formaldehyde-induced genome instability is suppressed by an XPF-dependent pathway. *DNA Repair*, *11*(3), 236–246. https://doi.org/10.1016/j.dnarep.2011.11.001

Kunkel, T. A., & Erie, D. A. (2015). Eukaryotic Mismatch Repair in Relation to DNA Replication. *Annual Review of Genetics*, *49*, 291–313. https://doi.org/10.1146/annurev-genet-112414-054722

Kurian, A. W., Gong, G. D., Chun, N. M., Mills, M. A., Staton, A. D., Kingham, K. E., Crawford, B. B., Lee, R., Chan, S., Donlon, S. S., Ridge, Y., Panabaker, K., West, D. W., Whittemore, A. S., & Ford, J. M. (2008). Performance of BRCA1/2 mutation prediction models in Asian Americans. *Journal of Clinical Oncology*, *26*(29), 4752–4758. https://doi.org/10.1200/JCO.2008.16.8310

Kurian, A. W., Hughes, E., Handorf, E. A., Gutin, A., Allen, B., Hartman, A.-R., & Hall, M. J. (2017). Breast and Ovarian Cancer Penetrance Estimates Derived From Germline Multiple-Gene Sequencing Results in Women. *JCO Precision Oncology*, (1), 1–12. https://doi.org/10.1200/PO.16.00066

Kyrousi, C., O'Neill, A. C., Brazovskaja, A., He, Z., Kielkowski, P., Coquand, L., Di Giaimo, R., D' Andrea, P., Belka, A., Forero Echeverry, A., Mei, D., Lenge, M., Cruceanu, C., Buchsbaum, I. Y., Khattak, S., Fabien, G., Binder, E., Elmslie, F., Guerrini, R., … Cappello, S. (2021). Extracellular LGALS3BP regulates neural progenitor position and relates to human cortical complexity. *Nature Communications 2021 12:1*, *12*(1), 1–22. https://doi.org/10.1038/s41467-021-26447-w

Lai, L. J., Hsu, W. H., Wu, A. M., & Wu, J. H. (2013). Ocular Injury by Transient Formaldehyde Exposure in a Rabbit Eye Model. *PLOS ONE*, *8*(6), e66649. https://doi.org/10.1371/JOURNAL.PONE.0066649

Lee, C. T., Bendriem, R. M., Wu, W. W., & Shen, R. F. (2017). 3D brain Organoids derived from pluripotent stem cells: promising experimental models for brain development and neurodegenerative disorders. *Journal of Biomedical Science 2017 24:1*, *24*(1), 1–12. https://doi.org/10.1186/S12929-017-0362-8

Lee, M., Daniels, M. J., & Venkitaraman, A. R. (2004). Phosphorylation of BRCA2 by the Polo-like kinase Plk1 is regulated by DNA damage and mitotic progression. *Oncogene*, *23*, 865–872. https://doi.org/10.1038/sj.onc.1207223

Lee, M., Shorthouse, D., Mahen, R., Hall, B. A., & Venkitaraman, A. R. (2021). Cancer-causing BRCA2 missense mutations disrupt an intracellular protein assembly mechanism to disable genome maintenance. *Nucleic Acids Research*, *49*(10), 5588–5604. https://doi.org/10.1093/nar/gkab308

Lees-Murdock, D. J., & Walsh, C. P. (2008). DNA methylation reprogramming in the germ line. *Epigenetics*, *3*(1), 5–13. https://doi.org/10.4161/epi.3.1.5553

Leng, J., Liu, C.-W., Hartwell, H. J., Yu, R., Lai, Y., Bodnar, W. M., Lu, K., & Swenberg, J. A. (2019). Evaluation of inhaled low-dose formaldehyde-induced DNA adducts and DNA-protein cross-links by liquid chromatography-tandem mass spectrometry. *Archives of Toxicology*, *93*, 763–773. https://doi.org/10.1007/s00204-019-02393-x

Leung, E., & Hazrati, L. N. (2021). Breast cancer type 1 and neurodegeneration: Consequences of deficient DNA repair. In *Brain Communications* (Vol. 3, Number 2). https://doi.org/10.1093/braincomms/fcab117

Levine, D. A., Federici, M. G., Reuter, V. E., & Boyd, J. (2002). Cell proliferation and apoptosis in BRCA-associated hereditary ovarian cancer. *Gynecologic Oncology*, *85*(3), 431–434. https://doi.org/10.1006/gyno.2002.6646

Li, M., Hale, J. S., Rich, J. N., Ransohoff, R. M., & Lathia, J. D. (2012). Chemokine CXCL12 in neurodegenerative diseases: an SOS signal for stem cell-based repair. *Trends in Neurosciences*, *35*(10), 619–628. https://doi.org/10.1016/j.tins.2012.06.003

Li, Y.-P., Wang, Y.-T., Wang, W., Zhang, X., Shen, R.-J., Jin, K., Jin, L.-W., & Jin, Z.-B. (2022). Second hit impels oncogenesis of retinoblastoma in patient-induced pluripotent stem cell-derived retinal organoids: direct evidence for Knudson's theory. *PNAS Nexus*, *1*(4), pgac162. https://doi.org/10.1093/pnasnexus/pgac162

Li, Z., Wu, J., & DeLeo, C. J. (2006). RNA damage and surveillance under oxidative stress. *IUBMB Life*, *58*(10), 581–588. https://doi.org/10.1080/15216540600946456

Liao, H., Ji, F., Helleday, T., & Ying, S. (2018). Mechanisms for stalled replication fork stabilization: new targets for synthetic lethality strategies in cancer treatments. *EMBO Reports*, *19*(9), e46263. https://doi.org/https://doi.org/10.15252/embr.201846263

Lima, B. A., Pais, A. C., Dupont, J., Dias, P., Custódio, N., Sousa, A. B., Carmo-Fonseca, M., & Carvalho, C. (2025). Genetic modulation of RNA splicing rescues BRCA2 function in mutant cells. *Life Science Alliance*, *8*(3). https://doi.org/10.26508/LSA.202402845

Liu, H., & Song, N. (2016). Molecular Mechanism of Adult Neurogenesis and its Association with Human Brain Diseases. *Journal of Central Nervous System Disease*, *8*, 5–11. https://doi.org/10.4137/JCNSD.S32204

Liu, Q., Zhou, D., Lv, M., Ge, P., Li, Y., & Wang, S. (2018). Formaldehyde inhalation triggers autophagy in rat lung tissues. *Toxicology and Industrial Health*, *34*(12), 834–841. https://doi.org/10.1177/0748233718796347

Lomonosov, M., Anand, S., Sangrithi, M., Davies, R., & Venkitaraman, A. R. (2003). Stabilization of stalled DNA replication forks by the BRCA2 breast cancer susceptibility protein. *Genes & Development*, *17*(24), 3017–3022. https://doi.org/10.1101/gad.279003

Ludwig, T., Chapman, D. L., Papaioannou, V. E., & Efstratiadis, A. (1997). Targeted mutations of breast cancer susceptibility gene homologs in mice: Lethal phenotypes of Brca1, Brca2, Brca1/Brca2, Brca1/p53, and Brca2/p53 nullizygous embryos. *Genes and Development*, *11*(10), 1226–1241. https://doi.org/10.1101/gad.11.10.1226

Lui, S., Jones, R. L., Robinson, N. J., Greenwood, S. L., Aplin, J. D., & Tower, C. L. (2014). Detrimental effects of ethanol and its metabolite acetaldehyde, on first trimester human placental cell turnover and function. *PloS One*, *9*(2). https://doi.org/10.1371/JOURNAL.PONE.0087328

Lykke-Andersen, S., & Jensen, T. H. (2015). Nonsense-mediated mRNA decay: an intricate machinery that shapes transcriptomes. *NATURE REVIEWS | MOLECULAR CELL BIOLOGY*, *16*, 665. https://doi.org/10.1038/nrm4063

MacAllister, S. L., Choi, J., Dedina, L., & O'Brien, P. J. (2011). Metabolic mechanisms of methanol/formaldehyde in isolated rat hepatocytes: Carbonyl-metabolizing enzymes versus oxidative stress. *Chemico-Biological Interactions*, *191*(1–3), 308–314. https://doi.org/10.1016/J.CBI.2011.01.017

Madabhushi, R., Pan, L., & Tsai, L. H. (2014). DNA damage and its links to neurodegeneration. *Neuron*, *83*(2), 266–282. https://doi.org/10.1016/J.NEURON.2014.06.034

Maiellaro, M., Correa-Costa, M., Vitoretti, L. B., Gimenes Júnior, J. A., Câmara, N. O. S., Tavares-de-Lima, W., Farsky, S. H. P., & Lino-dos-Santos-Franco, A. (2014). Exposure to low doses of formaldehyde during pregnancy suppresses the development of allergic lung inflammation in offspring. *Toxicology and Applied Pharmacology*, *278*(3), 266–274. https://doi.org/10.1016/j.taap.2014.05.003

Mano, T., Nagata, K., Nonaka, T., Tarutani, A., Imamura, T., Hashimoto, T., Bannai, T., Koshi-Mano, K., Tsuchida, T., Ohtomo, R., Takahashi-Fujigasaki, J., Yamashita, S., Ohyagi, Y., Yamasaki, R., Tsuji, S., Tamaoka, A., Ikeuchi, T., Saido, T. C., Iwatsubo, T., … Iwata, A. (2017). Neuron-specific methylome analysis reveals epigenetic regulation and tau-related dysfunction of BRCA1 in Alzheimer's disease. *Proceedings of the National Academy of Sciences*, *114*(45), E9645–E9654. https://doi.org/10.1073/pnas.1707151114

Mao, Z., Bozzella, M., Seluanov, A., & Gorbunova, V. (2008a). Comparison of nonhomologous end joining and homologous recombination in human cells. *DNA Repair*, *7*(10), 1765. https://doi.org/10.1016/J.DNAREP.2008.06.018

Mao, Z., Bozzella, M., Seluanov, A., & Gorbunova, V. (2008b). DNA repair by nonhomologous end joining and homologous recombination during cell cycle in human cells. *Cell Cycle (Georgetown, Tex.)*, *7*(18), 2902–2906. https://doi.org/10.4161/cc.7.18.6679

Marmorstein, L. Y., Kinev, A. V., Chan, G. K. T., Bochar, D. A., Beniya, H., Epstein, J. A., Yen, T. J., & Shiekhattar, R. (2001). A human BRCA2 complex containing a structural DNA binding component influences cell cycle progression. *Cell*, *104*(2), 247–257. https://doi.org/10.1016/S0092-8674(01)00209-4

Martinez, J. S., Baldeyron, C., & Carreira, A. (2015). Molding BRCA2 function through its interacting partners. In *Cell Cycle* (Vol. 14, Number 21, pp. 3389–3395). Taylor and Francis Inc. https://doi.org/10.1080/15384101.2015.1093702

Massaad, C. A., & Klann, E. (2011). COMPREHENSIVE INVITED REVIEW Reactive Oxygen Species in the Regulation of Synaptic Plasticity and Memory. In *Antioxid. Redox Signal* (Vol. 14).

Mattson, S. N., Bernes, G. A., & Doyle, L. R. (2019). Fetal Alcohol Spectrum Disorders: A Review of the Neurobehavioral Deficits Associated With Prenatal Alcohol Exposure. *Alcoholism, Clinical and Experimental Research*, *43*(6), 1046–1062. https://doi.org/10.1111/ACER.14040

Maxwell, K. N., Domchek, S. M., Nathanson, K. L., & Robson, M. E. (2016). Population frequency of germline BRCA1/2 mutations. *Journal of Clinical Oncology*, *34*(34), 4183–4185. https://doi.org/10.1200/JCO.2016.67.0554

McGann, L. E., Yang, H., & Walterson, M. (1988). Manifestations of cell damage after freezing and thawing. *Cryobiology*, *25*(3), 178–185. https://doi.org/10.1016/0011-2240(88)90024-7

McGhee, J. D., & von Hippel, P. H. (1977). Formaldehyde as a Probe of DNA Structure. 4. Mechanism of the Initial Reaction of Formaldehyde with DNA. *Biochemistry*, *16*(15), 3276–3293. https://doi.org/10.1021/BI00634A002/ASSET/BI00634A002.FP.PNG_V03

Mckinnon, P. J. (2013). Maintaining genome stability in the nervous system. *Nature Neuroscience*, *16*(11), 1523–1529. https://doi.org/10.1038/NN.3537

McKinnon, P. J. (2017). Genome integrity and disease prevention in the nervous system. *Genes & Development*, *31*(12), 1180–1194. https://doi.org/10.1101/GAD.301325.117

Menzel, T., Nähse-Kumpf, V., Kousholt, A. N., Klein, D. K., Lund-Andersen, C., Lees, M., Johansen, J. V., Syljuåsen, R. G., & Sørensen, C. S. (2011). A genetic screen identifies BRCA2 and PALB2 as key regulators of G2 checkpoint maintenance. *EMBO Reports*, *12*(7), 705–712. https://doi.org/https://doi.org/10.1038/embor.2011.99

Miki, Y., Katagiri, T., Kasumi, F., Yoshimoto, T., & Nakamura, Y. (1996). Mutation analysis in the BRCA2 gene in primary breast cancers. *Nature Genetics*, *13*(2), 245–247. https://doi.org/10.1038/ng0696-245

Milner, J., Ponder, B., Hughes-Davies, L., Seltmann, M., & Kouzarides, T. (1997). Transcriptional activation functions in BRCA2. In *Nature* (Vol. 386, Number 6627, pp. 772–773). https://doi.org/10.1038/386772a0

Mira, H., & Morante, J. (2020). Neurogenesis From Embryo to Adult – Lessons From Flies and Mice. In *Frontiers in Cell and Developmental Biology* (Vol. 8, p. 533). https://doi.org/10.3389/fcell.2020.00533

Mishra, P., Singh, U., Pandey, C., Mishra, P., & Pandey, G. (2019). Application of student's t-test, analysis of variance, and covariance. *Annals of Cardiac Anaesthesia*, *22*(4), 407. https://doi.org/10.4103/aca.aca_94_19

Mo, W., & He, R. (2017). *The Role of Formaldehyde in Cell Proliferation and Death BT - Formaldehyde and Cognition* (R. He, Ed.; pp. 79–97). Springer Netherlands. https://doi.org/10.1007/978-94-024-1177-5_5

Momcilovic, O., Knobloch, L., Fornsaglio, J., Varum, S., Easley, C., & Schatten, G. (2010). DNA damage responses in human induced pluripotent stem cells and embryonic stem cells. *PLoS ONE*, *5*(10). https://doi.org/10.1371/journal.pone.0013410

Moreno-Jiménez, E. P., Terreros-Roncal, J., Flor-García, M., Rábano, A., & Llorens-Martín, M. (2021). Evidences for adult hippocampal neurogenesis in humans. *Journal of Neuroscience*, *41*(12), 2541–2553. https://doi.org/10.1523/JNEUROSCI.0675-20.2020

Morimoto, S., Tsuda, M., Bunch, H., Sasanuma, H., Austin, C., & Takeda, S. (2019). Type II DNA topoisomerases cause spontaneous double-strand breaks in genomic DNA. In *Genes* (Vol. 10, Number 11). https://doi.org/10.3390/genes10110868

Moro, L., Arbini, A. A., Yao, J. L., di Sant'Agnese, P. A., Marra, E., & Greco, M. (2008). Loss of BRCA2 promotes prostate cancer cell invasion through up-regulation of matrix metalloproteinase-9. *Cancer Science*, *99*(3), 553–563. https://doi.org/10.1111/j.1349-7006.2007.00719.x

Moynahan, M. E., Pierce, A. J., & Jasin, M. (2001). BRCA2 is required for homology-directed repair of chromosomal breaks. *Molecular Cell*, *7*(2), 263–272. https://doi.org/10.1016/s1097-2765(01)00174-5

Mulderrig, L., Garaycoechea, J. I., Tuong, Z. K., Millington, C. L., Dingler, F. A., Ferdinand, J. R., Gaul, L., Tadross, J. A., Arends, M. J., O'Rahilly, S., Crossan, G. P., Clatworthy, M. R., & Patel, K. J. (2021). Aldehyde-driven transcriptional stress triggers an anorexic DNA damage response. *Nature 2021 600:7887*, *600*(7887), 158–163. https://doi.org/10.1038/s41586-021-04133-7

Mullan, P. B., Quinn, J. E., & Harkin, D. P. (2006). The role of BRCA1 in transcriptional regulation and cell cycle control. *Oncogene*, *25*, 5854–5863. https://doi.org/10.1038/sj.onc.1209872

Murray, A. (1994). Cell cycle checkpoints. *Current Opinion in Cell Biology*, *6*(6), 872–876. https://doi.org/10.1016/0955-0674(94)90059-0

Nadalutti, C. A., Stefanick, D. F., Zhao, M. L., Horton, J. K., Prasad, R., Brooks, A. M., Griffith, J. D., & Wilson, S. H. (2020). Mitochondrial dysfunction and DNA damage accompany enhanced levels of formaldehyde in cultured primary human fibroblasts. *Scientific Reports*, *10*(1). https://doi.org/10.1038/s41598-020-61477-2

Nakamura, M., Kaneko, S., Dickson, D. W., & Kusaka, H. (2020). Aberrant accumulation of BRCA1 in Alzheimer disease and other tauopathies. *Journal of Neuropathology and Experimental Neurology*, *79*(1), 22–33. https://doi.org/10.1093/jnen/nlz107

Nakano, T., Shoulkamy, M. I., Tsuda, M., Sasanuma, H., Hirota, K., Takata, M., Masunaga, S. I., Takeda, S., Ide, H., Bessho, T., & Tano, K. (2020). Participation of TDP1 in the repair of formaldehyde-induced DNA-protein cross-links in chicken DT40 cells. *PloS One*, *15*(6). https://doi.org/10.1371/JOURNAL.PONE.0234859

Nam, C., Doi, K., & Nakayama, H. (2010). Etoposide induces G2/M arrest and apoptosis in neural progenitor cells via DNA damage and an ATM/p53-related pathway. *Histology and Histopathology*, *25*(4), 485–493. https://doi.org/10.14670/HH-25.485

Neale, B. M., Kou, Y., Liu, L., Ma'ayan, A., Samocha, K. E., Sabo, A., Lin, C. F., Stevens, C., Wang, L. S., Makarov, V., Polak, P., Yoon, S., Maguire, J., Crawford, E. L., Campbell, N. G., Geller, E. T., Valladares, O., Schafer, C., Liu, H., … Daly, M. J. (2012a). Patterns and rates of exonic de novo mutations in autism spectrum disorders. *Nature*, *485*(7397), 242–246. https://doi.org/10.1038/NATURE11011

Neale, B. M., Kou, Y., Liu, L., Ma'ayan, A., Samocha, K. E., Sabo, A., Lin, C.-F., Stevens, C., Wang, L.-S., Makarov, V., Polak, P., Yoon, S., Maguire, J., Crawford, E. L., Campbell, N. G., Geller, E. T., Valladares, O., Schafer, C., Liu, H., … Daly, M. J. (2012b). Patterns and rates of exonic de novo mutations in autism spectrum disorders. *Nature*, *485*(7397), 242–245. https://doi.org/10.1038/nature11011

Neganova, I., Shmeleva, E., Munkley, J., Chichagova, V., Anyfantis, G., Anderson, R., Passos, J., Elliott, D. J., Armstrong, L., & Lako, M. (2016). JNK/SAPK Signaling Is Essential for Efficient Reprogramming of Human Fibroblasts to Induced Pluripotent Stem Cells. *Stem Cells*, *34*(5), 1198–1212. https://doi.org/10.1002/stem.2327

Neuhausen, S. L., Godwin, A. K., Gershoni-Baruch, R., Schubert, E., Garber, J., Stoppa-Lyonnet, D., Olah, E., Csokay, B., Serova, O., Lalloo, F., Osorio, A., Stratton, M., Offit, K., Boyd, J., Caligo, M. A., Scott, R. J., Schofield, A., Teugels, E., Schwab, M., … Goldgar, D. (1998). Haplotype and phenotype analysis of nine recurrent BRCA2 mutations in 111 families: results of an international study. *American Journal of Human Genetics*, *62*(6), 1381–1388. https://doi.org/10.1086/301885

Niccols, A. (2007). Fetal alcohol syndrome and the developing socio-emotional brain. *Brain and Cognition*, *65*(1), 135–142. https://doi.org/10.1016/J.BANDC.2007.02.009

Noordermeer, S. M., & van Attikum, H. (2019). PARP Inhibitor Resistance: A Tug-of-War in BRCA-Mutated Cells. In *Trends in Cell Biology* (Vol. 29, Number 10, pp. 820–834). Elsevier Ltd. https://doi.org/10.1016/j.tcb.2019.07.008

Nurul, F. A. B., Siti, A. O., & Nor, Farah Amirah Nor Azman Nurin, S. J. (2019). *IOP Conference Series: Earth and Environmental Science*. https://doi.org/10.1088/1755-1315/268/1/012005

Nutt, D., Hayes, A., Fonville, L., Zafar, R., Palmer, E. O. C., Paterson, L., & Lingford-Hughes, A. (2021). Alcohol and the Brain. *Nutrients*, *13*(11). https://doi.org/10.3390/NU13113938

Nyberg, T., Frost, D., Barrowdale, D., Evans, D. G., Bancroft, E., Adlard, J., Ahmed, M., Barwell, J., Brady, A. F., Brewer, C., Cook, J., Davidson, R., Donaldson, A., Eason, J., Gregory, H., Henderson, A., Izatt, L., Kennedy, M. J., Miller, C., … Antoniou, A. C. (2020). Prostate Cancer Risks for Male BRCA1 and BRCA2 Mutation Carriers: A Prospective Cohort Study. *European Urology*, *77*(1), 24–35. https://doi.org/10.1016/j.eururo.2019.08.025

Ochi, S., Manabe, S., Kikkawa, T., & Osumi, N. (2022). Thirty Years' History since the Discovery of Pax6: From Central Nervous System Development to Neurodevelopmental Disorders. In *International Journal of Molecular Sciences* (Vol. 23, Number 11). https://doi.org/10.3390/ijms23116115

Orii, K. E., Lee, Y., Kondo, N., & McKinnon, P. J. (2006). Selective utilization of nonhomologous end-joining and homologous recombination DNA repair pathways during nervous system development. *Proceedings of the National Academy of Sciences of the United States of America*, *103*(26), 10017–10022. https://doi.org/10.1073/PNAS.0602436103

Ortega-Atienza, S., Green, S. E., & Zhitkovich, A. (2015). Proteasome activity is important for replication recovery, CHK1 phosphorylation and prevention of G2 arrest after low-dose formaldehyde HHS Public Access. *Toxicol Appl Pharmacol*, *286*(2), 135–141. https://doi.org/10.1016/j.taap.2015.03.018

Orthwein, A., Noordermeer, S. M., Wilson, M. D., Landry, S., Enchev, R. I., Sherker, A., Munro, M., Pinder, J., Salsman, J., Dellaire, G., Xia, B., Peter, M., & Durocher, D. (2015). A mechanism for the suppression of homologous recombination in G1 cells. *Nature*, *528*(7582), 422–426. https://doi.org/10.1038/nature16142

O'Sullivan, J., Unzeta, M., Healy, J., O'Sullivan, M. I., Davey, G., & Tipton, K. F. (2004). Semicarbazide-Sensitive Amine Oxidases: Enzymes with Quite a Lot to Do. *NeuroToxicology*, *25*(1–2), 303–315. https://doi.org/10.1016/S0161-813X(03)00117-7

Oswald, M. C. W., Brooks, P. S., Zwart, M. F., Mukherjee, A., West, R. J. H., Giachello, C. N. G., Morarach, K., Baines, R. A., Sweeney, S. T., & Landgraf, M. (2018). Reactive oxygen species regulate activity-dependent neuronal plasticity in Drosophila. *ELife*, *7*, e39393. https://doi.org/10.7554/eLife.39393

Oyama, Y., Sakai, H., Arata, T., Okano, Y., Akaike, N., Sakai, K., & Noda, K. (2002). Cytotoxic effects of methanol, formaldehyde, and formate on dissociated rat thymocytes: A possibility of aspartame toxicity. *Cell Biology and Toxicology*, *18*(1), 43–50. https://doi.org/10.1023/A:1014419229301

Pagano, G., Youssoufian, H., Anak, S. S., Brunk, U. T., Calzone, R., Clarke, A. A., Degan, P., D'Ischia, M., Dunster, C., Giudice, A., Iaccarino, M., Hirsch-Kauffmann, M., Kelly, F. J., Lloret, A., Malorni, W., Manini, P., Masella, R., Nobili, B., Pallardó, F. V., … Zatterale, A. (2003). Fanconi anaemia proteins: major roles in cell protection against oxidative damage. *BioEssays : News and Reviews in Molecular, Cellular and Developmental Biology*, *25*(6), 589–595. https://doi.org/10.1002/BIES.10283

Pan, X., Li, X.-J., Liu, X.-J., Yuan, H., Li, J.-F., Duan, Y.-L., Ye, H.-Q., Fu, Y.-R., Qiao, G.-H., Wu, C.-C., Yang, B., Tian, X.-H., Hu, K.-H., Miao, L.-F., Chen, X.-L., Zheng, J., Rayner, S., Schwartz, P. H., Britt, W. J., … Luo, M.-H. (2013). Later Passages of Neural Progenitor Cells from Neonatal Brain Are More Permissive for Human Cytomegalovirus Infection. *Journal of Virology*, *87*(20), 10968. https://doi.org/10.1128/JVI.01120-13

Pao, G. M., Zhu, Q., Perez-Garcia, C. G., Chou, S.-J., Suh, H., Gage, F. H., O'Leary, D. D. M., & Verma, I. M. (2014). Role of BRCA1 in brain development. *Proceedings of the National Academy of Sciences*, *111*(13), E1240–E1248. https://doi.org/10.1073/pnas.1400783111

Patel, K. J., Yu, V. P. C. C., Lee, H., Corcoran, A., Thistlethwaite, F. C., Evans, M. J., Colledge, W. H., Friedman, L. S., Ponder, B. A. J., & Venkitaraman, A. R. (1998a). Involvement of Brca2 in DNA Repair. *Molecular Cell*, *1*(3), 347–357. https://doi.org/10.1016/S1097-2765(00)80035-0

Patel, K. J., Yu, V. P. C. C., Lee, H., Corcoran, A., Thistlethwaite, F. C., Evans, M. J., Colledge, W. H., Friedman, L. S., Ponder, B. A. J., & Venkitaraman, A. R. (1998b). Involvement of Brca2 in DNA Repair. *Molecular Cell*, *1*(3), 347–357. https://doi.org/10.1016/S1097-2765(00)80035-0

Penniston, J. T., & Doty, P. (1963). Reaction of formaldehyde with soluble ribonucleic acid. *Biopolymers*, *1*(2), 145–164. https://doi.org/10.1002/BIP.360010205

Pensabene, M., Spagnoletti, I., Capuano, I., Condello, C., Pepe, S., Contegiacomo, A., Lombardi, G., Bevilacqua, G., & Caligo, M. A. (2009). Two mutations of BRCA2 gene at exon and splicing site in a woman who underwent oncogenetic counseling. *Annals of Oncology*, *20*(5), 874–878. https://doi.org/10.1093/annonc/mdn724

Petryszak, R., Keays, M., Tang, Y. A., Fonseca, N. A., Barrera, E., Burdett, T., Füllgrabe, A., Fuentes, A. M. P., Jupp, S., Koskinen, S., Mannion, O., Huerta, L., Megy, K., Snow, C., Williams, E., Barzine, M., Hastings, E., Weisser, H., Wright, J., … Brazma, A. (2016). Expression Atlas update - An integrated database of gene and protein expression in humans, animals and plants. *Nucleic Acids Research*, *44*(D1), D746–D752. https://doi.org/10.1093/nar/gkv1045

Pidoux, G., Gerbaud, P., Guibourdenche, J., Thérond, P., Ferreira, F., Simasotchi, C., Evain-Brion, D., & Gil, S. (2015). Formaldehyde crosses the human placenta and affects human trophoblast differentiation and hormonal functions. *PLoS ONE*, *10*(7). https://doi.org/10.1371/journal.pone.0133506

Pizzino, G., Irrera, N., Cucinotta, M., Pallio, G., Mannino, F., Arcoraci, V., Squadrito, F., Altavilla, D., & Bitto, A. (2017). Oxidative Stress: Harms and Benefits for Human Health. In *Oxidative Medicine and Cellular Longevity* (Vol. 2017). https://doi.org/10.1155/2017/8416763

Poetsch, A. R. (2020). The genomics of oxidative DNA damage, repair, and resulting mutagenesis. *Computational and Structural Biotechnology Journal*, *18*, 207–219. https://doi.org/10.1016/J.CSBJ.2019.12.013

Pontel, L. B., Rosado, I. V., Burgos-Barragan, G., Garaycoechea, J. I., Yu, R., Arends, M. J., Chandrasekaran, G., Broecker, V., Wei, W., Liu, L., Swenberg, J. A., Crossan, G. P., & Patel, K. J. (2015). Endogenous Formaldehyde Is a Hematopoietic Stem Cell Genotoxin and Metabolic Carcinogen. *Molecular Cell*, *60*(1), 177–188. https://doi.org/10.1016/J.MOLCEL.2015.08.020

Pulvers, J. N., & Huttner, W. B. (2009). Brca1 is required for embryonic development of the mouse cerebral cortex to normal size by preventing apoptosis of early neural progenitors. *Development (Cambridge, England)*, *136*(11), 1859–1868. https://doi.org/10.1242/DEV.033498

Qian, X., Song, H., & Ming, G. (2019). Brain organoids: advances, applications and challenges. *Development*, *146*(8). https://doi.org/10.1242/dev.166074

Quan, W., Li, Y., Song, W., Li, Z., Zhang, Q., & Lin, W. (2023). Correlation between tumor cell migration and formaldehyde levels revealed by fluorescence imaging. *Chemical Engineering Journal*, *465*. https://doi.org/10.1016/J.CEJ.2023.142814

Radulovic, I., Kuechler, A., Schündeln, M. M., Paulussen, M., von Neuhoff, N., Reinhardt, D., & Hanenberg, H. (2021). A homozygous nonsense mutation early in exon 5 of BRCA2 is associated with very severe Fanconi anemia. *European Journal of Medical Genetics*, *64*(8). https://doi.org/10.1016/J.EJMG.2021.104260

Rajan, J. V., Wang, M., Marquis, S. T., & Chodosh, L. A. (1996). Brca2 is coordinately regulated with Brcal during proliferation and differentiation in mammary epithelial cells. *Proceedings of the National Academy of Sciences of the United States of America*, *93*(23), 13078–13083. https://doi.org/10.1073/pnas.93.23.13078

Rana, I., Rieswijk, L., Steinmaus, C., & Zhang, L. (2021). Formaldehyde and Brain Disorders: A Meta-Analysis and Bioinformatics Approach. In *Neurotoxicity Research* (Vol. 39, Number 3, pp. 924–948). Neurotox Res. https://doi.org/10.1007/s12640-020-00320-y

Ratner, E., Bala, M., Louie-Gao, M., Aydin, E., Hazard, S., & Brastianos, P. K. (2019). Increased risk of brain metastases in ovarian cancer patients with BRCA mutations. *Gynecologic Oncology*, *153*(3), 568–573. https://doi.org/10.1016/J.YGYNO.2019.03.004

Raza, M. U., Tufan, T., Wang, Y., Hill, C., & Zhu, M. Y. (2016). DNA Damage in Major Psychiatric Diseases. In *Neurotoxicity Research* (Vol. 30, Number 2, pp. 251–267). Springer New York LLC. https://doi.org/10.1007/s12640-016-9621-9

Rebbeck, T. R., Friebel, T. M., Friedman, E., Hamann, U., Huo, D., Kwong, A., Olah, E., Olopade, O. I., Solano, A. R., Teo, S.-H., Thomassen, M., Weitzel, J. N., Chan, T., Couch, F. J., Goldgar, D. E., Kruse, T. A., Torres, D., van Rensburg, E. J., Aalfs, C. M., … Isaacs, C. (2018). Mutational spectrum in a worldwide study of 29,700 families with BRCA1 or BRCA2 mutations Miguel de la Hoya 48 Kim De Leeneer 54 Antoine de Pauw 46 Capucine Delnatte 58 Bent Ejlertsen 67 EMBRACE 20 Anne-Marie Gerdes 82 Paul Gesta 83. *Human Mutation*, *39*, 593–620. https://doi.org/10.1002/humu.23406

Reddig, A., Roggenbuck, D., & Reinhold, D. (2018). Comparison of different immunoassays for γH2AX quantification. *Journal of Laboratory and Precision Medicine*, *3*(0), 80–80. https://doi.org/10.21037/JLPM.2018.09.01

Reynolds, B. A., & Weiss, S. (1992). Generation of neurons and astrocytes from isolated cells of the adult mammalian central nervous system. *Science (New York, N.Y.)*, *255*(5052), 1707–1710. https://doi.org/10.1126/SCIENCE.1553558

Richards, L. J., Kilpatrick, T. J., & Bartlett, P. F. (1992). De novo generation of neuronal cells from the adult mouse brain. *Proceedings of the National Academy of Sciences of the United States of America*, *89*(18), 8591–8595. https://doi.org/10.1073/PNAS.89.18.8591

Rickman, K. A., Noonan, R. J., Lach, F. P., Sridhar, S., Wang, A. T., Abhyankar, A., Huang, A., Kelly, M., Auerbach, A. D., & Smogorzewska, A. (2020). *Distinct roles of BRCA2 in replication fork protection in response to hydroxyurea and DNA interstrand cross-links*. https://doi.org/10.1101/gad.336446.120

Ridpath, J. R., Nakamura, A., Tano, K., Luke, A. M., Sonoda, E., Arakawa, H., Buerstedde, J.-M., Gillespie, D. A. F., Sale, J. E., Yamazoe, M., Bishop, D. K., Takata, M., Takeda, S., Watanabe, M., Swenberg, J. A., & Nakamura, J. (2007). Cells Deficient in the FANC/BRCA Pathway Are Hypersensitive to Plasma Levels of Formaldehyde. *Cancer Res*, *67*(23), 11117–11139. https://doi.org/10.1158/0008-5472.CAN-07-3028

Risch, H. A., McLaughlin, J. R., Cole, D. E., Rosen, B., Bradley, L., Kwan, E., Jack, E., Vesprini, D. J., Kuperstein, G., Abrahamson, J. L., Fan, I., Wong, B., & Narod, S. A. (2001). Prevalence and penetrance of germline BRCA1 and BRCA2 mutations in a population series of 649 women with ovarian cancer. *American Journal of Human Genetics*, *68*(3), 700–710. https://doi.org/10.1086/318787

Rothkamm, K., Krüger, I., Thompson, L. H., Löbrich, M., & Biophysik, F. (2003). Pathways of DNA Double-Strand Break Repair during the Mammalian Cell Cycle The induction and repair of individual IR-induced DSBs in * Corresponding author. Mailing address. *MOLECULAR AND CELLULAR BIOLOGY*, *23*(16), 5706–5715. https://doi.org/10.1128/MCB.23.16.5706-5715.2003

Rübe, C. E., Fricke, A., Widmann, T. A., Fürst, T., Madry, H., Pfreundschuh, M., & Rübe, C. (2011). Accumulation of DNA damage in hematopoietic stem and progenitor cells during human aging. *PLoS ONE*, *6*(3). https://doi.org/10.1371/journal.pone.0017487

Rump, P., Jazayeri, O., Van Dijk-Bos, K. K., Johansson, L. F., Van Essen, A. J., Verheij, J. B. G. M., Veenstra-Knol, H. E., Redeker, E. J. W., Mannens, M. M. A. M., Swertz, M. A., Alizadeh, B. Z., Van Ravenswaaij-Arts, C. M. A., Sinke, R. J., & Sikkema-Raddatz, B. (2016). Whole-exome sequencing is a powerful approach for establishing the etiological diagnosis in patients with intellectual disability and microcephaly. *BMC Medical Genomics*, *9*(1), 7. https://doi.org/10.1186/s12920-016-0167-8

Sadeghi, F., Asgari, M., Matloubi, M., Ranjbar, M., Karkhaneh Yousefi, N., Azari, T., & Zaki-Dizaji, M. (2020). Molecular contribution of BRCA1 and BRCA2 to genome instability in breast cancer patients: review of radiosensitivity assays. *Biological Procedures Online*, *22*(1), 23. https://doi.org/10.1186/s12575-020-00133-5

Satyananda, V., Oshi, M., Endo, I., Takabe, K., Takabe, K., & Surg, A. (2021). High BRCA2 Gene Expression is Associated with Aggressive and Highly Proliferative Breast Cancer. *Annals of Surgical Oncology*, *28*, 7356–7365. https://doi.org/10.1245/s10434-021-10063-5

Schafer, K. A. (1998). The cell cycle: a review. *Veterinary Pathology*, *35*(6), 461–478. https://doi.org/10.1177/030098589803500601

Schlacher, K., Christ, N., Siaud, N., Egashira, A., Wu, H., & Jasin, M. (2011a). Double-strand break repair-independent role for BRCA2 in blocking stalled replication fork degradation by MRE11. *Cell*, *145*(4), 529–542. https://doi.org/10.1016/j.cell.2011.03.041

Schlacher, K., Christ, N., Siaud, N., Egashira, A., Wu, H., & Jasin, M. (2011b). Double-strand break repair-independent role for BRCA2 in blocking stalled replication fork degradation by MRE11. *Cell*, *145*(4), 529–542. https://doi.org/10.1016/J.CELL.2011.03.041

Schroeder, T. M., Anschütz, F., & Knopp, A. (1964). Spontane Chromosomenaberrationen bei familiärer Panmyelopathie. *Human Genetics*, *1*(2), 194–196. https://doi.org/10.1007/BF00389636/METRICS

See, W. L., Miller, J. P., Squatrito, M., Holland, E., Resh, M. D., & Koff, A. (2010). Defective DNA double-strand break repair underlies enhanced tumorigenesis and chromosomal instability in p27 deficient mice with growth-factor induced oligodendrogliomas. *Oncogene*, *29*(12), 1720. https://doi.org/10.1038/ONC.2009.465

Serra, V., Fiorillo, E., Cucca, F., & Orrù, V. (2022). Quantifying the Detrimental Effects of Multiple Freeze/Thaw Cycles on Primary Human Lymphocyte Survival and Function. *International Journal of Molecular Sciences*, *24*(1). https://doi.org/10.3390/IJMS24010634

Shahid, T., Soroka, J., Kong, E. H., Malivert, L., McIlwraith, M. J., Pape, T., West, S. C., & Zhang, X. (2014). Structure and mechanism of action of the BRCA2 breast cancer tumor suppressor. *Nature Structural and Molecular Biology*, *21*(11), 962–968. https://doi.org/10.1038/nsmb.2899

Shanbhag, N. M., Evans, M. D., Mao, W., Nana, A. L., Seeley, W. W., Adame, A., Rissman, R. A., Masliah, E., & Mucke, L. (2019). Early neuronal accumulation of DNA double

strand breaks in Alzheimer's disease. *Acta Neuropathologica Communications*, *7*(1). https://doi.org/10.1186/S40478-019-0723-5

Shapiro, A. M., Miller-Pinsler, L., & Wells, P. G. (2016). Breast cancer 1 (BRCA1)-deficient embryos develop normally but are more susceptible to ethanol-initiated DNA damage and embryopathies. *Redox Biology*, *7*, 30–38. https://doi.org/10.1016/J.REDOX.2015.11.005

Sharan, S. K., & Bradley, A. (1997). Murine Brca2: Sequence, map position, and expression pattern. *Genomics*, *40*(2), 234–241. https://doi.org/10.1006/geno.1996.4573

Shibata, A., Conrad, S., Birraux, J., Geuting, V., Barton, O., Ismail, A., Kakarougkas, A., Meek, K., Taucher-Scholz, G., Löbrich, M., & Jeggo, P. A. (2011). Factors determining DNA double-strand break repair pathway choice in G2 phase. *The EMBO Journal*, *30*(6), 1079–1092. https://doi.org/https://doi.org/10.1038/emboj.2011.27

Shimada, M., Tsukada, K., Kagawa, N., & Matsumoto, Y. (2019). Reprogramming and differentiation-dependent transcriptional alteration of DNA damage response and apoptosis genes in human induced pluripotent stem cells. *Journal of Radiation Research*, *60*(6), 719–728. https://doi.org/10.1093/jrr/rrz057

Shiwaku, H., & Okazawa, H. (2015). Impaired DNA Damage Repair as a Common Feature of Neurodegenerative Diseases and Psychiatric Disorders. *Current Molecular Medicine*, *15*(2), 119–128. https://doi.org/10.2174/1566524015666150303002556

Silva Ibrahim, B., Miranda da Silva, C., Barioni, É. D., Correa-Costa, M., Drewes, C. C., Saraiva Câmara, N. O., Tavares-de-Lima, W., Poliselli Farsky, S. H., & Lino-dos-Santos-Franco, A. (2015). Formaldehyde inhalation during pregnancy abolishes the development of acute innate inflammation in offspring. *Toxicology Letters*, *235*(2), 147–154. https://doi.org/10.1016/j.toxlet.2015.04.001

Simhadri, S., Vincelli, G., Huo, Y., Misenko, S., Tzeh, •, Foo, K., Ahlskog, J., Sørensen, C. S., Gregory, •, Oakley, G., Ganesan, • Shridar, Bunting, S. F., & Xia, B. (2018). PALB2 connects BRCA1 and BRCA2 in the G2/M checkpoint response. *Oncogene*. https://doi.org/10.1038/s41388-018-0535-2

Singh, A. K., Gupta, S., Jiang, Y., Younus, M., & Ramzan, M. (2009). In vitro neurogenesis from neural progenitor cells isolated from the hippocampus region of the brain of adult rats exposed to ethanol during early development through their alcohol-drinking mothers. *Alcohol and Alcoholism (Oxford, Oxfordshire)*, *44*(2), 185–198. https://doi.org/10.1093/ALCALC/AGN109

Songur, A., Ozen, O. A., & Sarsilmaz, M. (2010). The toxic effects of formaldehyde on the nervous system. *Reviews of Environmental Contamination and Toxicology*, *203*, 105–118. https://doi.org/10.1007/978-1-4419-1352-4_3

Songur, A., Sarsilmaz, M., Ozen, O., Sahin, S., Aslan Ozen, O., Koken, R., & Zararsiz, I. (2008). The Effects of Inhaled Formaldehyde on Oxidant and Antioxidant Systems of Rat Cerebellum During the Postnatal Development Process. *Toxicology Mechanisms and Methods*, *18*(7), 569–574. https://doi.org/10.1080/15376510701555288

Sorrells, S. F., Paredes, F., Cebrian-Silla, A., Sandoval, K., Qi, D., Kelley, K. W., James, D., Mayer, S., Chang, J., Auguste, K. I., Chang, E. F., Gutierrez, A. J., Kriegstein, A. R., Mathern, G. W., Oldham, M. C., Huang 10, E. J., Manuel Garcia-Verdugo, J., Yang, Z., & Arturo Alvarez-Buylla, &. (2018). Human hippocampal neurogenesis drops sharply in children to undetectable levels in adults. *Nature Publishing Group*. https://doi.org/10.1038/nature25975

Sousa, J. F. de, Serafim, R. B., Freitas, L. M. de, Fontana, C. R., & Valente, V. (2020). DNA repair genes in astrocytoma tumorigenesis, progression and therapy resistance. In *Genetics*

and Molecular Biology (Vol. 43, Number 1). Genet Mol Biol. https://doi.org/10.1590/1678-4685-gmb-2019-0066

Sousa, J. F. de, Torrieri, R., Serafim, R. B., Di Cristofaro, L. F. M., Escanfella, F. D., Ribeiro, R., Zanette, D. L., Paçó-Larson, M. L., da Silva, W. A., Tirapelli, D. P. da C., Neder, L., Carlotti, C. G., & Valente, V. (2017). Expression signatures of DNA repair genes correlate with survival prognosis of astrocytoma patients. *Tumor Biology*, *39*(4). https://doi.org/10.1177/1010428317694552

Spain, B. H., Larson, C. J., Shihabuddin, L. S., Gage, F. H., & Verma, I. M. (1999). Truncated BRCA2 is cytoplasmic: implications for cancer-linked mutations. *Proceedings of the National Academy of Sciences of the United States of America*, *96*(24), 13920–13925. https://doi.org/10.1073/pnas.96.24.13920

Stella, S., Vitale, S., Martorana, F., Massimino, M., Pavone, G., Lanzafame, K., Bianca, S., Barone, C., Gorgone, C., Fichera, M., & Manzella, L. (2022). Mutational Analysis of BRCA1 and BRCA2 Genes in Breast Cancer Patients from Eastern Sicily. *Cancer Management and Research*, *14*, 1341–1352. https://doi.org/10.2147/CMAR.S348529

Stingele, J., Bellelli, R., Alte, F., Hewitt, G., Sarek, G., Maslen, S. L., Tsutakawa, S. E., Borg, A., Kjær, S., Tainer, J. A., Skehel, J. M., Groll, M., & Boulton, S. J. (2016). Mechanism and Regulation of DNA-Protein Crosslink Repair by the DNA-Dependent Metalloprotease SPRTN. *Molecular Cell*, *64*(4), 688–703. https://doi.org/10.1016/j.molcel.2016.09.031

Stivaros, S. M., Alston, R., Wright, N. B., Chandler, K., Bonney, D., Wynn, R. F., Will, A. M., Punekar, M., Loughran, S., Kilday, J. P., Schindler, D., Patel, L., & Meyer, S. (2015). Central nervous system abnormalities in Fanconi anaemia: Patterns and frequency on magnetic resonance imaging. *British Journal of Radiology*, *88*(1056). https://doi.org/10.1259/bjr.20150088

Suberbielle, E., Djukic, B., Evans, M., Kim, D. H., Taneja, P., Wang, X., Finucane, M., Knox, J., Ho, K., Devidze, N., Masliah, E., & Mucke, L. (2015). DNA repair factor BRCA1 depletion occurs in Alzheimer brains and impairs cognitive function in mice. *Nature Communications*, *6*. https://doi.org/10.1038/ncomms9897

Suberbielle, E., Sanchez, P. E., Kravitz, A. V, Wang, X., Ho, K., Eilertson, K., Devidze, N., Kreitzer, A. C., & Mucke, L. (2013). Physiologic brain activity causes DNA double-strand breaks in neurons, with exacerbation by amyloid-β. *Nature Neuroscience*, *16*(5), 613–621. https://doi.org/10.1038/nn.3356

Suzuki, A., De La Pompa, J. L., Hakem, R., Elia, A., Yoshida, R., Mo, K., Nishina, H., Chuang, T., Wakeham, A., Itie, A., Koo, W., Billia, P., Ho, A., Fukumoto, M., Hui, C. C., & Mak, T. W. (1997). Brca2 is required for embryonic cellular proliferation in the mouse. *Genes and Development*, *11*(10), 1242–1252. https://doi.org/10.1101/gad.11.10.1242

Suzuki, A., de la Pompa, J. L., Hakem, R., Elia, A., Yoshida, R., Mo, R., Nishina, H., Chuang, T., Wakeham, A., Itie, A., Koo, W., Billia, P., Ho, A., Fukumoto, M., Hui, C. C., & Mak, T. W. (1997). Brca2 is required for embryonic cellular proliferation in the mouse. *Genes & Development*, *11*(10), 1242–1252. https://doi.org/10.1101/gad.11.10.1242

Szende, B., & Tyihák, E. (2010). Effect of formaldehyde on cell proliferation and death. *Cell Biology International*, *34*(12), 1273–1282. https://doi.org/10.1042/CBI20100532

Tacconi, E. M., Lai, X., Folio, C., Porru, M., Zonderland, G., Badie, S., Michl, J., Sechi, I., Rogier, M., Matía García, V., Batra, A. S., Rueda, O. M., Bouwman, P., Jonkers, J., Ryan, A., Reina-San-Martin, B., Hui, J., Tang, N., Bruna, A., … Tarsounas, M. (2017). BRCA 1 and BRCA 2 tumor suppressors protect against endogenous acetaldehyde toxicity . *EMBO Molecular Medicine*, *9*(10), 1398–1414. https://doi.org/10.15252/emmm.201607446

Tan, S. L. W., Chadha, S., Liu, Y., Gabasova, E., Perera, D., Ahmed, K., Constantinou, S., Renaudin, X., Lee, M. Y., Aebersold, R., & Venkitaraman, A. R. (2017). A Class of Environmental and Endogenous Toxins Induces BRCA2 Haploinsufficiency and Genome Instability. *Cell*, *169*(6), 1105-1118.e15. https://doi.org/10.1016/j.cell.2017.05.010

Tanaka, M., & Chock, P. B. (2021). *Oxidative Modifications of RNA and Its Potential Roles in Biosystem*. https://doi.org/10.3389/fmolb.2021.685331

Tannenbaum, B., Mofunanya, T., & Schoenfeld, A. R. (2007). DNA damage repair is unaffected by mimicked heterozygous levels of BRCA2 in HT-29 cells. *International Journal of Biological Sciences*, *3*(7), 402–407. https://doi.org/10.7150/ijbs.3.402

Tavtigian, S. V, Simard, J., Rommens, J., Couch, F., Shattuck-Eidens, D., Neuhausen, S., Merajver, S., Thorlacius, S., Offit, K., Stoppa-Lyonnet, D., Belanger, C., Bell, R., Berry, S., Bogden, R., Chen, Q., Davis, T., Dumont, M., Frye, C., Hattier, T., … Goldgar, D. E. (1996). The complete BRCA2 gene and mutations in chromosome 13q-linked kindreds. *Nature Genetics*, *12*(3), 333–337. https://doi.org/10.1038/ng0396-333

Tesli, M., Athanasiu, L., Mattingsdal, M., Kähler, A. K., Gustafsson, O., Andreassen, B. K., Werge, T., Hansen, T., Mors, O., Mellerup, E., Koefoed, P., Jönsson, E. G., Agartz, I., Melle, I., Morken, G., Djurovic, S., & Andreassen, O. A. (2010). Association analysis of PALB2 and BRCA2 in bipolar disorder and schizophrenia in a scandinavian case-control sample. *American Journal of Medical Genetics Part B: Neuropsychiatric Genetics*, *153B*(7), 1276–1282. https://doi.org/10.1002/ajmg.b.31098

The Human Genomics Community. (2023). *Varsome*. https://varsome.com/

The Human protein Atlas. (2023). https://www.proteinatlas.org/

The website of the National Cancer Institute. (2023). *The website of the National Cancer Institute*. https://www.cancer.gov

Thompson, D., & Easton, D. (2001). Variation in cancer risks, by mutation position, in BRCA2 mutation carriers. *American Journal of Human Genetics*, *68*(2), 410–419. https://doi.org/10.1086/318181

Thorslund, T., & West, S. C. (2007). BRCA2: A universal recombinase regulator. In *Oncogene* (Vol. 26, Number 56, pp. 7720–7730). Oncogene. https://doi.org/10.1038/sj.onc.1210870

Thrasher, J. D., & Kilburn, K. H. (2001). Embryo Toxicity and Teratogenicity of Formaldehyde. *Archives of Environmental Health: An International Journal*, *56*(4), 300–311. https://doi.org/10.1080/00039890109604460

Tian, X. X., Rai, D., Li, J., Zou, C., Bai, Y., Wazer, D., Band, V., & Gao, Q. (2005). BRCA2 suppresses cell proliferation via stabilizing MAGE-D1. *Cancer Research*, *65*(11), 4747. https://doi.org/10.1158/0008-5472.CAN-05-0018

Tiwari, V., & Wilson, D. M. (2019). DNA Damage and Associated DNA Repair Defects in Disease and Premature Aging. *American Journal of Human Genetics*, *105*(2), 237–257. https://doi.org/10.1016/j.ajhg.2019.06.005

Tomasetti, C., Poling, J., Roberts, N. J., London, N. R., Pittman, M. E., Haffner, M. C., Rizzo, A., Baras, A., Karim, B., Kim, A., Heaphy, C. M., Meeker, A. K., Hruban, R. H., Iacobuzio-Donahue, C. A., & Vogelstein, B. (2019). Cell division rates decrease with age, providing a potential explanation for the age-dependent deceleration in cancer incidence. *Proceedings of the National Academy of Sciences*, *116*(41), 20482–20488. https://doi.org/10.1073/pnas.1905722116

Tong, Z., Han, C., Luo, W., Li, H., Luo, H., Qiang, M., Su, T., Wu, B., Liu, Y., Yang, X., Wan, Y., Cui, D., & He, R. (2013). Aging-associated excess formaldehyde leads to spatial memory deficits. *Scientific Reports*, *3*. https://doi.org/10.1038/srep01807

Tong, Z., Han, C., Luo, W., Wang, X., Li, H., Luo, H., Zhou, J., Qi, J., & He, R. (2013a). Accumulated hippocampal formaldehyde induces age-dependent memory decline. *Age*, *35*(3), 583–596. https://doi.org/10.1007/s11357-012-9388-8

Tong, Z., Han, C., Luo, W., Wang, X., Li, H., Luo, H., Zhou, J., Qi, J., & He, R. (2013b). Accumulated hippocampal formaldehyde induces age-dependent memory decline. *Age*, *35*(3), 583–596. https://doi.org/10.1007/s11357-012-9388-8

Tong, Z., Wang, W., Luo, W., Lv, J., Li, H., Luo, H., Jia, J., & He, R. (2017). Urine Formaldehyde Predicts Cognitive Impairment in Post-Stroke Dementia and Alzheimer's Disease. *Journal of Alzheimer's Disease : JAD*, *55*(3), 1031–1038. https://doi.org/10.3233/JAD-160357

Tong, Z., Zhang, J., Luo, W., Wang, W., Li, F., Li, H., Luo, H., Lu, J., Zhou, J., Wan, Y., & He, R. (2011a). Urine formaldehyde level is inversely correlated to mini mental state examination scores in senile dementia. *Neurobiology of Aging*, *32*(1), 31–41. https://doi.org/10.1016/j.neurobiolaging.2009.07.013

Tong, Z., Zhang, J., Luo, W., Wang, W., Li, F., Li, H., Luo, H., Lu, J., Zhou, J., Wan, Y., & He, R. (2011b). Urine formaldehyde level is inversely correlated to mini mental state examination scores in senile dementia. *Neurobiology of Aging*, *32*(1), 31–41. https://doi.org/10.1016/j.neurobiolaging.2009.07.013

Torres, D., Bermejo, J. L., Rashid, M. U., Briceño, I., Gil, F., Beltran, A., Ariza, V., & Hamann, U. (2017). Prevalence and Penetrance of BRCA1 and BRCA2 Germline Mutations in Colombian Breast Cancer Patients. *Scientific Reports*, *7*(1), 4713. https://doi.org/10.1038/s41598-017-05056-y

Tulpule, K., & Dringen, R. (2012). Formate generated by cellular oxidation of formaldehyde accelerates the glycolytic flux in cultured astrocytes. *Glia*, *60*(4), 582–593. https://doi.org/10.1002/GLIA.22292

Tulpule, K., & Dringen, R. (2013). Formaldehyde in brain: An overlooked player in neurodegeneration? *Journal of Neurochemistry*, *127*(1), 7–21. https://doi.org/10.1111/jnc.12356

Tulpule, K., Hohnholt, M. C., & Dringen, R. (2013). Formaldehyde metabolism and formaldehyde-induced stimulation of lactate production and glutathione export in cultured neurons. *Journal of Neurochemistry*, *125*(2), 260–272. https://doi.org/10.1111/jnc.12170

Turkovic, L., Gurrin, L. C., Bahlo, M., Dite, G. S., Southey, M. C., & Hopper, J. L. (2010). Comparing the frequency of common genetic variants and haplotypes between carriers and non-carriers of BRCA1 and BRCA2 deleterious mutations in Australian women diagnosed with breast cancer before 40 years of age. *BMC Cancer*, *10*. https://doi.org/10.1186/1471-2407-10-466

Tutt, A., Bertwistle, D., Valentine, J., Gabriel, A., Swift, S., Ross, G., Griffin, C., Thacker, J., & Ashworth, A. (2001). Mutation in Brca2 stimulates error-prone homology-directed repair of DNA double-strand breaks occurring between repeated sequences. *The EMBO Journal*, *20*(17), 4704–4716. https://doi.org/10.1093/EMBOJ/20.17.4704

Tutt, A., Gabriel, A., Bertwistle, D., Connor, F., Paterson, H., Peacock, J., Ross, G., & Ashworth, A. (1999). Absence of Brca2 causes genome instability by chromosome breakage and loss associated with centrosome amplification. *Current Biology : CB*, *9*(19), 1107–1110. https://doi.org/10.1016/S0960-9822(99)80479-5

Tyihák, E., Albert, L., Németh, Z. I., Kátay, G., Király-Véghely, Z., & Szende, B. (1998). Formaldehyde cycle and the natural formaldehyde generators and capturers. *Acta Biologica Hungarica*, *49*(2–4), 225–238.

Tyihák, E., Bocsi, J., Timár, F., Rácz, G., & Szende, B. (2001). Formaldehyde promotes and inhibits the proliferation of cultured tumour and endothelial cells. *Cell Proliferation*, *34*(3), 135–141. https://doi.org/10.1046/j.1365-2184.2001.00206.x

Ueno, M., Katayama, K. ichi, Yamauchi, H., Nakayama, H., & Doi, K. (2006). Cell cycle progression is required for nuclear migration of neural progenitor cells. *Brain Research*, *1088*(1), 57–67. https://doi.org/10.1016/J.BRAINRES.2006.03.042

Ungureanu, L. B., Ghiciuc, C. M., Amalinei, C., Ungureanu, C., Petrovici, C. G., & Stănescu, R. Ștefania. (2024). Antioxidants as Protection against Reactive Oxygen Stress Induced by Formaldehyde (FA) Exposure: A Systematic Review. *Biomedicines*, *12*(8), 1820. https://doi.org/10.3390/BIOMEDICINES12081820

Vaisman, A., McDonald, J. P., & Woodgate, R. (2012). Translesion DNA Synthesis. *EcoSal Plus*, *5*(1), 10.1128/ecosalplus.7.2.2. https://doi.org/10.1128/ecosalplus.7.2.2

Vangipuram, M., Ting, D., Kim, S., Diaz, R., & Schüle, B. (2013). Skin punch biopsy explant culture for derivation of primary human fibroblasts. *Journal of Visualized Experiments : JoVE*, (77), e3779. https://doi.org/10.3791/3779

Venkitaraman, A. R. (2003). A growing network of cancer-susceptibility genes. *The New England Journal of Medicine*, *348*(19), 1917–1919. https://doi.org/10.1056/NEJMcibr023150

Vilenchik, M. M., & Knudson, A. G. (2003). Endogenous DNA double-strand breaks: Production, fidelity of repair, and induction of cancer. *Proceedings of the National Academy of Sciences of the United States of America*, *100*(22), 12871–12876. https://doi.org/10.1073/PNAS.2135498100/SUPPL_FILE/5498TABLE3.HTML

Vurusaner, B., Poli, G., & Basaga, H. (2012). Tumor suppressor genes and ROS: complex networks of interactions. *Free Radical Biology and Medicine*, *52*(1), 7–18. https://doi.org/10.1016/J.FREERADBIOMED.2011.09.035

Wang, S.-C., Shao, R., Pao, A. Y., Zhang, S., Hung, M.-C., & Su, L.-K. (2002). Inhibition of cancer cell growth by BRCA2. *Cancer Research*, *62*(5), 1311–1314.

Wang, Z. (2022). Cell Cycle Progression and Synchronization: An Overview. *Methods in Molecular Biology (Clifton, N.J.)*, *2579*, 3–23. https://doi.org/10.1007/978-1-0716-2736-5_1

Warren, M., Lord, C. J., Masabanda, J., Griffin, D., & Ashworth, A. (2003). Phenotypic effects of heterozygosity for a BRCA2 mutation. *Human Molecular Genetics*, *12*(20), 2645–2656. https://doi.org/10.1093/hmg/ddg277

Weber, B. L. (1996). Familial breast cancer. *Recent Results in Cancer Research. Fortschritte Der Krebsforschung. Progres Dans Les Recherches Sur Le Cancer*, *140*, 5–16. https://doi.org/10.1007/978-3-642-79278-6_2

Wei, L., Nakajima, S., Böhm, S., Bernstein, K. A., Shen, Z., Tsang, M., Levine, A. S., & Lan, L. (2015). DNA damage during the G0/G1 phase triggers RNA-templated, Cockayne syndrome B-dependent homologous recombination. *Proceedings of the National Academy of Sciences*, *112*(27), E3495–E3504. https://doi.org/10.1073/pnas.1507105112

Weinberg-Shukron, A., Rachmiel, M., Renbaum, P., Gulsuner, S., Walsh, T., Lobel, O., Dreifuss, A., Ben-Moshe, A., Zeligson, S., Segel, R., Shore, T., Kalifa, R., Goldberg, M., King, M.-C., Gerlitz, O., Levy-Lahad, E., & Zangen, D. (2018). Essential Role of BRCA2 in Ovarian Development and Function. *The New England Journal of Medicine*, *379*(11), 1042–1049. https://doi.org/10.1056/NEJMoa1800024

Welcsh, P. L., Lee, M. K., Gonzalez-Hernandez, R. M., Black, D. J., Mahadevappa, M., Swisher, E. M., Warrington, J. A., & King, M.-C. (2002). *BRCA1 transcriptionally regulates genes involved in breast tumorigenesis*. www.netaffx.comindex2.jsp

Wezyk, M., Szybinska, A., Wojsiat, J., Szczerba, M., Day, K., Ronnholm, H., Kele, M., Berdynski, M., Peplonska, B., Fichna, J. P., Ilkowski, J., Styczynska, M., Barczak, A., Zboch, M., Filipek-Gliszczynska, A., Bojakowski, K., Skrzypczak, M., Ginalski, K., Kabza, M., … Zekanowski, C. (2018). Overactive BRCA1 Affects Presenilin 1 in Induced Pluripotent Stem Cell-Derived Neurons in Alzheimer's Disease. *Journal of Alzheimer's Disease : JAD*, *62*(1), 175–202. https://doi.org/10.3233/JAD-170830

Wezyk, M., & Zekanowski, C. (2018). Role of BRCA1 in Neuronal Death in Alzheimer's Disease. *ACS Chemical Neuroscience*, *9*(5), 870–872. https://doi.org/10.1021/acschemneuro.8b00149

Williams, H. L., Gottesman, M. E., & Gautier, J. (2013). *The differences between ICL repair during and outside of S-Phase*. https://doi.org/10.1016/j.tibs.2013.05.004

Willis, N., & Rhind, N. (2009). Regulation of DNA replication by the S-phase DNA damage checkpoint. In *Cell Division* (Vol. 4). https://doi.org/10.1186/1747-1028-4-13

Wooster, R., Bignell, G., Lancaster, J., Swift, S., Seal, S., Mangion, J., Collins, N., Gregory, S., Gumbs, C., & Micklem, G. (1995). Identification of the breast cancer susceptibility gene BRCA2. *Nature*, *378*(6559), 789–792. https://doi.org/10.1038/378789a0file://///fs02/apabst01$/Downloads/378789a0.pdf

Wooster, R., Neuhausen, S. L., Mangion, J., Quirk, Y., Ford, D., Collins, N., Nguyen, K., Seal, S., Tran, T., & Averill, D. (1994). Localization of a breast cancer susceptibility gene, BRCA2, to chromosome 13q12-13. *Science (New York, N.Y.)*, *265*(5181), 2088–2090. https://doi.org/10.1126/science.8091231

World Health Organization. (2010). WHO guidelines for indoor air quality: selected pollutants. *Bonn, Germany: In Puncto Druck+ Medien GmbH*, 484.

Xia, F., Taghian, D. G., DeFrank, J. S., Zeng, Z. C., Willers, H., Iliakis, G., & Powell, S. N. (2001). Deficiency of human BRCA2 leads to impaired homologous recombination but maintains normal nonhomologous end joining. *Proceedings of the National Academy of Sciences of the United States of America*, *98*(15), 8644–8649. https://doi.org/10.1073/pnas.151253498

Xie, X., Zhao, Y., Du, F., Cai, B., Fang, Z., Liu, Y., Sang, Y., Ma, C., Liu, Z., Yu, X., Zhang, C., Jiang, J., Gao, Z., Liu, Y., Lin, X., Jing, H., Zhong, X., Cong, L., Dai, H., … Shang, L. (2024). Pan-cancer analysis of the tumorigenic role of Fanconi anemia complementation group D2 (FANCD2) in human tumors. *Genomics*, *116*(1), 110762. https://doi.org/10.1016/j.ygeno.2023.110762

Xiping, Z., Qingshan, W., Shuai, Z., Hongjian, Y., & Xiaowen, D. (2017). A summary of relationships between alternative splicing and breast cancer. In *Oncotarget* (Vol. 8, Number 31, pp. 51986–51993). https://doi.org/10.18632/oncotarget.17727

Xu, P., Shi, X., Zhang, X., Liu, Q., Xie, Y., Hong, Y., Li, J., Peng, M., Liu, X., & Xu, G. (2019). Overexpression of BRCA1 in neural stem cells enhances cell survival and functional recovery after transplantation into experimental ischemic stroke. *Oxidative Medicine and Cellular Longevity*, *2019*. https://doi.org/10.1155/2019/8739730

Yamada, M., Funaki, S., & Miki, S. (2019). Formaldehyde interacts with RNA rather than DNA: Accumulation of formaldehyde by the RNA-inorganic hybrid material. *International Journal of Biological Macromolecules*, *122*, 168–173. https://doi.org/10.1016/j.ijbiomac.2018.10.159

Yamaguchi, N. H. (2019). Smoking, immunity, and DNA damage. In *Translational lung cancer research* (Vol. 8, Number Suppl 1, pp. S3–S6). https://doi.org/10.21037/tlcr.2019.03.02

Yang, Q., Hong, Y., Zhao, T., Song, H., & Ming, G. (2022). What Makes Organoids Good Models of Human Neurogenesis? *Frontiers in Neuroscience*, *16*. https://doi.org/10.3389/fnins.2022.872794

Yao, B., Christian, K. M., He, C., Jin, P., Ming, G., & Song, H. (2016). Epigenetic mechanisms in neurogenesis. *Nature Publishing Group*. https://doi.org/10.1038/nrn.2016.70

Yu, J., Su, T., Zhou, T., He, Y., Lu, J., Li, J., & He, R. (2014). Uric formaldehyde levels are negatively correlated with cognitive abilities in healthy older adults. *Neurosci Bull*, *30*(2), 172–184. https://doi.org/10.1007/s12264-013-1416-x

Yu, P. H., Wright, S., Fan, E. H., Lun, Z. R., & Gubisne-Harberle, D. (2003). Physiological and pathological implications of semicarbazide-sensitive amine oxidase. *Biochimica et Biophysica Acta (BBA) - Proteins and Proteomics*, *1647*(1–2), 193–199. https://doi.org/10.1016/S1570-9639(03)00101-8

Zhang, H., Xiong, Y., & Chen, J. (2020). DNA–protein cross-link repair: what do we know now? *Cell & Bioscience*, *10*(1), 3. https://doi.org/10.1186/s13578-019-0366-z

Zhang, M., Ngo, J., Pirozzi, F., Sun, Y. P., & Wynshaw-Boris, A. (2018). Highly efficient methods to obtain homogeneous dorsal neural progenitor cells from human and mouse embryonic stem cells and induced pluripotent stem cells. *Stem Cell Research and Therapy*, *9*(1), 1–13. https://doi.org/10.1186/S13287-018-0812-6/FIGURES/4

Zhang, R., Quan, H., Wang, Y., & Luo, F. (2023). Neurogenesis in Primates versus Rodents and the Value of Non-human Primate Models. *National Science Review*. https://doi.org/10.1093/nsr/nwad248

Zhang, S., Royer, R., Li, S., McLaughlin, J. R., Rosen, B., Risch, H. A., Fan, I., Bradley, L., Shaw, P. A., & Narod, S. A. (2011). Frequencies of BRCA1 and BRCA2 mutations among 1,342 unselected patients with invasive ovarian cancer. *Gynecologic Oncology*, *121*(2), 353–357. https://doi.org/10.1016/j.ygyno.2011.01.020

Zhang, S., Xiong, X., & Sun, Y. (2020). Functional characterization of SOX2 as an anticancer target. In *Signal Transduction and Targeted Therapy* (Vol. 5, Number 1). https://doi.org/10.1038/s41392-020-00242-3

Zhang, X., & Li, R. (2018). BRCA1-Dependent Transcriptional Regulation: Implication in Tissue-Specific Tumor Suppression. *Cancers*, (10). https://doi.org/10.3390/cancers10120513

Zhao, C., Deng, W., & Gage, F. H. (2008). Mechanisms and Functional Implications of Adult Neurogenesis. *Cell*, *132*(4), 645–660. https://doi.org/10.1016/j.cell.2008.01.033

Zhao, X., Wei, C., Li, J., Xing, P., Li, J., Zheng, S., & Chen, X. (2017). Cell cycle-dependent control of homologous recombination. *Acta Biochim Biophys Sin*, (8), 655–668. https://doi.org/10.1093/abbs/gmx055

Zhao, Y., Li, M.-C., Konaté, M. M., Chen, L., Das, B., Karlovich, C., Mickey Williams, P., Evrard, Y. A., Doroshow, J. H., & McShane, L. M. (2021). TPM, FPKM, or Normalized Counts? A Comparative Study of Quantification Measures for the Analysis of RNA-seq Data from the NCI Patient-Derived Models Repository. *J Transl Med*, *19*, 269. https://doi.org/10.1186/s12967-021-02936-w

Zhou, S., Szczesna, K., Ochalek, A., Kobolák, J., Varga, E., Nemes, C., Chandrasekaran, A., Rasmussen, M., Cirera, S., Hyttel, P., Dinnyés, A., Freude, K. K., & Avci, H. X. (2016). Neurosphere based differentiation of human IPSC improves astrocyte differentiation. *Stem Cells International*, *2016*. https://doi.org/10.1155/2016/4937689

Zhu, L., Jacob, D. J., Keutsch, F. N., Mickley, L. J., Scheffe, R., Strum, M., González Abad, G., Chance, K., Yang, K., Rappenglück, B., Millet, D. B., Baasandorj, M., Jaeglé, L., & Shah, V. (2017). Formaldehyde (HCHO) As a Hazardous Air Pollutant: Mapping Surface

Air Concentrations from Satellite and Inferring Cancer Risks in the United States. *Environmental Science and Technology*, *51*(10), 5650–5657. https://doi.org/10.1021/ACS.EST.7B01356/ASSET/IMAGES/LARGE/ES-2017-013564_0007.JPEG

Zippora E, B., Patra, B., Govarthanan, K., Yadav, R., Mohan, S., Shyamsunder, P., & Verma, R. S. (2020). Defective cell proliferation is an attribute of overexpressed Notch1 receptor and impaired autophagy in Fanconi Anemia. *Genomics*, *112*(6), 4628–4639. https://doi.org/10.1016/j.ygeno.2020.08.009

8 Attachment

8.1 List of Abbreviations

Abbreviation	**explanation**
µg	microgram
µl	microliter
AD	Alzheimer's disease
AMPA	α-amino-3-hydroxy-5-methyl- 4-isoxazolepropionic acid
ASD	autism spectrum disorder
ATM	Ataxia-telangiectasia mutated
BBB	blood brain barrier
BER	base excision repair
BO	brain organoids
BRCA1	Breast cancer susceptibility gene 1
BRCA2	Breast cancer susceptibility gene 2
CDK2	Cyclin-dependent kinase 2
CHK2	Checkpoint kinase 2
CO_2	carbon dioxide
CP	cortical plate
CR	Cajal-Retzius
CtIP	CtBP interacting protein
DDR	DNA damage response
DL	deep-layer neuron
DNA	Deoxyribonucleic acid
DPC	DNA-protein crosslink
DSB	Double-strand breaks
EdU	5-Ethynyl-2′-deoxyuridine
FACS	Fluorescence activated cell sorting
FAS	fetal alcohol syndrome
GAPDH	Glyceraldehyde 3-phosphate dehydrogenase
GFP	Green fluorescent protein
GluA1	Glutamate Ionotropic Receptor AMPA
gr	gram
GWAS	a genome-wide association study
h	hour
HR	homology-directed repair
ICL	interstrand crosslink
indel	insertion/ deletion
IPs	intermediate progenitors
iPSCs	induced pluripotent stem cells
ISVZ	inner subventricular zone
IZ	intermediate zone
kDA	kilo Dalton

Abbreviation	**explanation**
KLF4	Krüppel-like factor 4
l	liter
MDC1	Mediator of DNA damage checkpoint protein 1
min	minutes
ml	milliliter
mM	millimolar
MMR	mismatch repair
MRE11	Meiotic Recombination 11
MZ	marginal zone
NANOG	Homeobox protein
NBS1	nibrin
NE	neuroepithelial cells
NER	nucleotide excision repair
NESTIN	neuroepithelial stem cell protein
NGS	next generation sequencing
NHEJ	non homologous end joining
NMDA	N-methyl-D-aspartate
NPCs	neural progenitor cells
NR2B	N-methyl D-aspartate receptor subtype 2B
NSCs	neural stem cells
OCT4	octamer-binding transcription factor 4
oRG	outer radial glial cells
OSVZ	outer subventricular zone
PALB2	Partner and localizer of BRCA2
PAX6	Paired box protein 6
PLK	Polo-like-Kinase
PP	preplate
RAD50	DNA repair protein 50
RAD51	RAD51 recombinase
RAP80	ubiquitin interaction motif containing 1 protein
RG	radial glial cells
RNA	ribonucleic acid
RNF8	E3 ubiquitin-protein ligase
ROS	reactive oxygen species
rpm	rounds per minute
sec	second
SERPINH1	heat shock protein 47
SOX2	sex determining region Y (SRY)- box 2
SP	subplate
SSB	singel-strand breaks
TLS	translesion synthesis
tRG	truncated radial glial cells

Abbreviation	**explanation**
UL	upper-layer neuron
USP21	Ubiquitin specific peptidase 21
vRG	ventricular radial glial cells
VZ	ventricular zone
γH2AX	Histone H2AX

8.2 List of Figures

8.3 List of Tables

8.4 Acknowledgment

Statement of Authorship (Selbstständigkeitserklärung)

Hiermit erkläre ich, Ann-Sophie Pabst (geb. am 01.05.1993 in Freising), an Eides statt, dass ich die vorliegende Arbeit selbst und ohne unerlaubte Hilfe verfasst haben und keine entgeltliche Hilfe Dritter, wie Promotionsberatung oder -vermittlung in Anspruch genommen habe. Die Stellen der Arbeit, die dem Wortlaut oder dem Sinne nach anderen Werken entnommen wurden, wurden unter Angabe der Quelle kenntlich gemacht. KI-Werkzeuge (perplexity.ai und quillbot.com) wurden zur Unterstützung bei der Quellenrecherche und Rechtschreibkorrektur verwendet. Ich versichere außerdem, dass die Arbeit bisher noch nicht veröffentlich wurde oder in einer anderen Form als Prüfungsleistung eingereicht wurde.

_____ _____

Ort, Datum Unterschrift